



University of Kentucky  
UKnowledge

---

Theses and Dissertations--Chemical and  
Materials Engineering

Chemical and Materials Engineering

---

2014

## INFLUENCE OF FERRITE PHASE IN ALITE-CALCIUM SULFOALUMINATE CEMENTS

Tristana Y. Duvallet

University of Kentucky, [tristanaduvallet@gmail.com](mailto:tristanaduvallet@gmail.com)

[Right click to open a feedback form in a new tab to let us know how this document benefits you.](#)

---

### Recommended Citation

Duvallet, Tristana Y., "INFLUENCE OF FERRITE PHASE IN ALITE-CALCIUM SULFOALUMINATE CEMENTS" (2014). *Theses and Dissertations--Chemical and Materials Engineering*. 27.  
[https://uknowledge.uky.edu/cme\\_etds/27](https://uknowledge.uky.edu/cme_etds/27)

This Doctoral Dissertation is brought to you for free and open access by the Chemical and Materials Engineering at UKnowledge. It has been accepted for inclusion in Theses and Dissertations--Chemical and Materials Engineering by an authorized administrator of UKnowledge. For more information, please contact [UKnowledge@lsv.uky.edu](mailto:UKnowledge@lsv.uky.edu).

## **STUDENT AGREEMENT:**

I represent that my thesis or dissertation and abstract are my original work. Proper attribution has been given to all outside sources. I understand that I am solely responsible for obtaining any needed copyright permissions. I have obtained needed written permission statement(s) from the owner(s) of each third-party copyrighted matter to be included in my work, allowing electronic distribution (if such use is not permitted by the fair use doctrine) which will be submitted to UKnowledge as Additional File.

I hereby grant to The University of Kentucky and its agents the irrevocable, non-exclusive, and royalty-free license to archive and make accessible my work in whole or in part in all forms of media, now or hereafter known. I agree that the document mentioned above may be made available immediately for worldwide access unless an embargo applies.

I retain all other ownership rights to the copyright of my work. I also retain the right to use in future works (such as articles or books) all or part of my work. I understand that I am free to register the copyright to my work.

## **REVIEW, APPROVAL AND ACCEPTANCE**

The document mentioned above has been reviewed and accepted by the student's advisor, on behalf of the advisory committee, and by the Director of Graduate Studies (DGS), on behalf of the program; we verify that this is the final, approved version of the student's thesis including all changes required by the advisory committee. The undersigned agree to abide by the statements above.

Tristana Y. Duvallet, Student

Dr. Rodney Andrews, Major Professor

Dr. Fuqian Yang, Director of Graduate Studies

INFLUENCE OF FERRITE PHASE IN ALITE-CALCIUM SULFOALUMINATE  
CEMENTS

---

DISSERTATION

---

A dissertation submitted in partial fulfillment of the requirements for the degree of  
Doctor of Philosophy in the College of Engineering at the University of Kentucky

By

Tristana Yvonne Françoise Duvallat

Lexington, Kentucky

Director: Dr. Rodney Andrews, Associate Professor and Director University of Kentucky  
Center for Applied Energy Research

Lexington, Kentucky

2014

Copyright © Tristana Yvonne Françoise Duvallat 2014

## ABSTRACT OF DISSERTATION

### INFLUENCE OF FERRITE PHASE IN ALITE-CALCIUM SULFOALUMINATE CEMENTS

Since the energy crisis in 1970's, research on low energy cements with low CO<sub>2</sub>-emissions has been increasing. Numerous solutions have been investigated, and the goal of this original research is to create a viable hybrid cement with the components of both Ordinary Portland cement (OPC) and calcium sulfoaluminate cement (CSAC), by forming a material that contains both alite and calcium sulfoaluminate clinker phases. Furthermore, this research focuses on keeping the cost of this material reasonable by reducing aluminum requirements through its substitution with iron. The aim of this work would produce a cement that can use large amounts of red mud, which is a plentiful waste material, in place of bauxite known as an expensive raw material.

Modified Bogue equations were established and tested to formulate this novel cement with different amounts of ferrite, from 5% to 45% by weight. This was followed by the production of cement from reagent chemicals, and from industrial by-products as feedstocks (fly ash, red mud and slag). Hydration processes, as well as the mechanical properties, of these clinker compositions were studied, along with the addition of gypsum and the impact of a ferric iron complexing additive triisopropanolamine (TIPA). To summarize this research, the influence of the addition of 5-45% by weight of ferrite phase, was examined with the goal of introducing as much red mud as possible in the process without negatively attenuate the cement properties.

Based on this PhD dissertation, the production of high-iron alite-calcium sulfoaluminate-ferrite cements was proven possible from the two sources of raw materials. The hydration processes and the mechanical properties seemed negatively affected by the addition of ferrite, as this phase was not hydrated entirely, even after 6 months of curing. The usage of TIPA counteracted this decline in strength by improving the ferrite hydration and increasing the optimum amount of gypsum required in each composition. The mechanical data were equivalent to OPC strengths for some compositions with 25% ferrite.

This preliminary work constitutes the first research phase of this novel cement and requires additional research for its improvement. Topics for additional research are identified in this dissertation.

KEYWORDS: alite, calcium sulfoaluminate, ferrite, low-energy cement, triisopropanolamine



INFLUENCE OF FERRITE PHASE IN ALITE-CALCIUM  
SULFOALUMINATE CEMENTS

By

Tristana Yvonne Françoise Duvallat

Dr. Rodney Andrews

---

Dr. Fuqian Yang

---

04/01/2014

---

To my family

And

To Nicolas,

Who were always there for me

## Acknowledgements

I would not have been able to complete this dissertation without the generous help provided by the following great people.

First of all, I would like to gratefully and sincerely thank Dr. Rodney Andrews and Dr. Thomas Robl for giving me the opportunity to join the Center for Applied Energy Research (CAER) as a PhD student, for mentoring me, guiding me, and letting me scientifically explore on my own. This experience was an eye-opener, I learned so much, and I cannot thank them enough.

I would like to acknowledge Dr. John Balk, Dr. Richard Eitel and Dr. John Selegue for being members of my committee and for their very useful comments through the writing of this dissertation.

I would also like to thank Robert Rathbone for supervising and mentoring me during my internship in 2008 at the Center for Applied Energy Research, allowing me to discover the science of cements, which led me to pursue a degree focusing on this scientific field, and for helping me review my dissertation.

I am very grateful to Dr. Yongmin Zhou, as without him and his preliminary work, I would not have been able to work on this great project.

I also would like to thank the Environmental and Coal Technologies group (ECT) at CAER who helped me so much throughout this work: Robert Jewell, John Wiseman, Dr. Jack Groppo, Dr. James Hower and Anne Oberlink for all their generous help and helpful discussions. Thank you also to Shelley Hopps for her expertise in X-ray fluorescence



analyses, and to Dr. Kevin Henke for his great help with X-ray diffraction and Rietveld analyses and for reviewing my dissertation.

This research would not have been possible without the financial help from the University of Kentucky, Minova, and the National Institute of Hometown Security.

I also want to thank all my family and friends around the world. Despite the distance, they were always there for me and I am really grateful to have all of them in my life. Thank you Nicolas, you are the best support I have and I do not know what I would do without you.

## Table of Contents

Acknowledgements.....	iii
Table of Contents.....	v
List of Tables.....	x
List of Figures.....	xiii
Chapter 1 : Introduction.....	1
1.1. Introduction.....	1
1.2. Research Plan / Purpose and Scope.....	2
1.3. Scope of Dissertation.....	4
1.4. Nomenclature.....	5
1.4.1. Cement Chemistry Notations.....	5
1.4.2. Acronyms.....	7
Chapter 2 : Literature Review / Background.....	8
2.1. Presentation of the most common cement: Ordinary Portland Cement.....	8
2.1.1. Composition, formation and CO <sub>2</sub> -emissions.....	8
2.1.2. Hydration Processes.....	11
2.1.3. Physical Properties.....	13
2.1.4. Advantages and Disadvantages of OPC Concrete.....	14
2.2. Calcium Sulfoaluminate Cements (CSAC).....	15
2.2.1. Composition / Formation.....	15
2.2.2. Hydration.....	16
2.2.3. Physical Properties.....	17
2.2.4. Advantages and Disadvantages of OPC and CSA cement.....	18
2.3. Alite-Calcium Sulfoaluminate cements.....	18
2.3.1. Relevancy of alite-calcium sulfoaluminate cements.....	18
2.3.2. Effects of temperature on the different phases.....	19
2.3.3. Formation / Production – Effects of CaF <sub>2</sub> and CaSO <sub>4</sub> .....	20
2.4. Influence of ferrite phase in Alite-Calcium Sulfoaluminate cements.....	21

2.4.1.	Several interests in this kind of cements .....	21
2.4.2.	High iron cements .....	22
2.4.3.	How to calculate phases – predictions with modulus values .....	22
Chapter 3 :	Materials and Methods .....	28
3.1.	Materials .....	28
3.1.1.	Reagents chemicals (RC) .....	28
3.1.2.	By-Products (BP) .....	28
3.2.	Methods .....	30
3.2.1.	Production and Firing Processes .....	30
3.2.2.	Characterization Instruments.....	33
3.2.2.1.	“Burnability Test” (Free Lime Determination).....	33
3.2.2.2.	X-Ray Diffraction coupled with Rietveld Refinement (XRD/Rietveld).....	34
3.2.2.3.	X-Ray Fluorescence (XRF).....	34
3.2.2.4.	Scanning Electron Microscope coupled with Energy-Dispersive X- Ray Spectroscopy (SEM/EDS).....	35
3.2.2.5.	Particle Size Distribution .....	43
3.2.2.6.	Example of some of these methods on a known clinker sample.....	43
3.2.3.	Studies on Pastes .....	47
3.2.3.1.	Calorimeter Study .....	47
3.2.3.2.	Hydration Paste Study.....	48
3.2.4.	Mechanical Tests.....	50
Chapter 4 :	Preliminary Experiments.....	53
4.1.	Production of small batches of clinker from RC and BP .....	53
4.1.1.	Formulation .....	53
4.1.2.	Synthesis.....	55
4.2.	Characterization Results .....	55
4.2.1.	From Reagent Chemicals .....	55
4.2.2.	From Industrial By-Products.....	62

4.3.	Comparison between small RC and MBP samples .....	72
Chapter 5 : From Reagent Chemicals .....		74
5.1.	Characterization tests.....	74
5.1.1.	XRD/Rietveld.....	74
5.1.2.	Free Lime .....	76
5.1.3.	Particle Size Distribution .....	76
5.2.	Hydration tests.....	77
5.2.1.	Calorimetric tests.....	77
5.2.1.1.	Influence of the clinker composition with the different weight percentages of gypsum.....	77
5.2.1.2.	Influence of gypsum in each batch.....	80
5.2.1.3.	Physical aspect of the inside of the calorimeter samples .....	83
5.2.1.4.	Discussion .....	84
5.2.2.	Hydration pastes for large batches of clinkers #1, #3 and #5 produced from reagent chemicals (RC).....	86
5.2.2.1.	Clinker #3 (25 wt. % C <sub>4</sub> AF).....	86
5.2.2.1.1.	XRD analyses.....	86
5.2.2.1.2.	TGA Analyses .....	87
5.2.2.1.3.	“Stellerite” phase.....	89
5.2.2.1.4.	Summary of all XRD and TGA analyses from the study of hydration pastes of clinker #3 .....	91
5.2.2.2.	Clinker #1 (5% C <sub>4</sub> AF).....	93
5.2.2.3.	Clinker #5 (45% C <sub>4</sub> AF).....	95
5.2.3.	Summary of the findings .....	96
5.3.	Mechanical tests .....	98
5.3.1.	Preparation and testing.....	98
5.3.2.	Results .....	98
5.4.	Summary of the hydration process .....	100
5.5.	Improvement of the mechanical properties with the utilization of triisopropanolamine (TIPA)?.....	101

5.5.1.	Effects of Triisopropanolamine – Literature Review.....	102
5.5.2.	Effect of TIPA on selected compositions.....	103
5.5.2.1.	Calorimeter Tests .....	104
5.5.2.1.1.	Clinker #3 (25% C <sub>4</sub> AF).....	104
5.5.2.1.2.	Clinker #5 (45% C <sub>4</sub> AF).....	106
5.5.2.1.3.	Summary of the calorimetric analyzes .....	110
5.5.2.2.	Hydration Pastes on clinker #5 produced from RC.....	110
5.5.2.3.	Mechanical tests on clinker #5 produced from RC .....	113
5.5.3.	Summary of the influence of TIPA on high-iron alite-calcium sulfoaluminate-ferrite cement .....	114
Chapter 6 : From By-Products Materials .....		115
6.1.	Characterization tests.....	115
6.1.1.	XRD/Rietveld.....	115
6.1.2.	Particle Size Distribution .....	116
6.2.	Calorimetric Analyses .....	117
6.2.1.	Calorimetric tests.....	117
6.2.1.1.	Influence of gypsum.....	117
6.2.1.2.	Influence of TIPA.....	120
6.3.	Mechanical tests .....	122
Chapter 7 : Conclusions and Future Work.....		126
7.1.	Reminder of the general problem .....	126
7.2.	General Conclusions.....	127
7.3.	Future Work.....	128
Appendices.....		130
Appendix A: XRD patterns for clinker and hydrated phases .....		130
Appendix B: XRD diffractograms for batches #1 through #5 produced from reagent chemicals (RC) fired at different temperatures and dwelling times .....		132

Appendix C: XRD diffractograms for batches #1 through #5 produced from by-products (BP), fired at different temperatures and dwelling times.....	135
Appendix D: Calculation of the amount of iron oxide underestimated in red mud (RM) from XRF .....	138
Appendix E: XRD diffractograms for batches #1 to #5 produced from different processes (reagent chemicals (RC), by-products (BP) and modified by-products (MBP)), fired at different temperatures and dwelling times .....	140
Appendix F: All calorimeter data for batches #1 to #5 with 30%, 40% and 50% gypsum, all produced from reagent chemicals (RC) .....	142
Appendix G: Calorimeter data for each batch produced from reagent chemicals (RC) with different amounts of gypsum introduced .....	145
Appendix H: TGA data for all batches produced from Reagent Chemicals (RC).....	150
Appendix I: XRD diffractograms of hydration of cement pastes from batches #1, #3 and #5 produced from reagent chemicals (RC) with different amounts of gypsum, stopped at different times (after 5 hours, 1, 7, 28, 90 and 180 days of hydration) .....	163
Appendix J: Derivation of the theoretical amount of gypsum required to completely react with $C_4A_3\dot{S}$ and $C_4AF$ .....	171
Appendix K: Influence of addition of TIPA to batch #5 produced from RC with 10%, 20% and 30% gypsum by weight.....	172
Appendix L: Influence of addition of gypsum to clinkers #1, #3 and #5 produced from Modified By-Products (MBP) .....	180
References.....	182
Vita.....	190

## List of Tables

Table 1-1: Cement Abbreviations, Chemical Formulae and Scientific Names of cement elements and phases .....	6
Table 1-2: List of acronyms used through this dissertation .....	7
Table 2-1: Bogue equations used to formulate OPC (by weight percentage).....	9
Table 2-2: Minimum compressive strength for different types of OPC in MPa [18, 19].	14
Table 2-3: CO <sub>2</sub> released from manufacture of clinker phases from limestone CaCO <sub>3</sub> [5]	16
Table 2-4: Chemical composition and compressive strength values for SAC and FAC clinkers [21, 23-25].....	16
Table 2-5: Advantages and Disadvantages of OPC and CSAC.....	18
Table 2-6: Typical clinker composition of a C <sub>3</sub> S-C <sub>4</sub> A <sub>3</sub> S cement .....	18
Table 2-7: Description of some cement pastes with percentages by weight (wt. %) of the clinker phases and mechanical properties data .....	21
Table 2-8: Phase composition of samples tested [2].....	24
Table 2-9: Study of free lime while varying all moduli [2], with “S#” meaning sample number (bold and italic numbers are related to a group where only one modulus value varies; green numbers are related to the same sample S#03 as it is a reference sample; and red numbers highlight the lowest free lime content for each group and firing temperature tested).....	26
Table 3-1: Chemical composition of each product in percentage by weight (AO: Acros Organics and SA: Sigma Aldrich) .....	28
Table 3-2: Chemical composition of by-products from XRF analysis in wt. % (*data from Fisher website) .....	30
Table 3-3: Example of a mass fraction calculation.....	43
Table 3-4: Phase composition of samples B1 and B4 by percentage by weight .....	44
Table 3-5: Theoretical, XRD/Rietveld and SEM/EDS data for the composition analyses of B1 and B4 .....	46
Table 4-1: Chemical compositions for the batches produced from reagent chemicals in wt. % .....	53
Table 4-2: Chemical compositions for batches produced from by-products in wt. % .....	53
Table 4-3: Moduli obtained from the actual formulation established in Section 4.1.1. for each composition .....	54
Table 4-4: Clinker phase composition predicted from the actual formulation established earlier by using the modified Bogue equations (in wt. %) for each composition.	54

Table 4-5: Summary of all results for phase composition determination from XRD/Rietveld and SEM/EDS compared to the theoretical data (Fl*=Fluorellestadite) .....	59
Table 4-6: Average of three measurements of particle size distribution (PSD) for each small pellet (10g in shatter box Chrome 40 for 45sec).....	62
Table 4-7: Modification of the Batch #3-BP by adding/removing red mud/bottom ash/gypsum (all the values are in grams – <b><i>bold and italic values</i></b> are the modified values compared to the original Batch #3-BP) .....	66
Table 4-8: Summary of XRD/Rietveld and SEM/EDS data for all modified batches from MBP, all fired at 1250°C for 60min (the minor phases, such as Na <sub>2</sub> O, P <sub>2</sub> O <sub>5</sub> and K <sub>2</sub> O were neglected).....	71
Table 4-9: Average of three measurements of particle size distribution for each small pellet.....	71
Table 5-1: Comparison of the Rietveld values for each small (chapter 4) and large (this chapter) batches of clinker produced from reagent chemicals (Fl*=Fluorellestadite) .....	75
Table 5-2: Particle sizes d(0.1), d(0.5) and d(0.9) for each large batch of clinker produced from RC (in μm) .....	77
Table 5-3: Description of the physical aspect of cement pastes inside the plastic vials after the calorimeter tests were completed (H=hard cement paste, H/S=hard/soft cement paste, Ex=expanded cement paste into powder and a “dome”) of samples produced from reagent chemicals (RC) .....	83
Table 5-4: Temperatures of decomposition for different hydrates observed in TGA analyses [6, 87-89].....	88
Table 5-5: XRD and TGA data showing the clinker phases consumed and the hydrates formed from the hydration paste of clinker #3 with various amounts of gypsum (sign + means that this phase remained in the cement paste even after 180 days of hydration and “time/time” means “formation/consumption”).....	91
Table 5-6: XRD and TGA data presenting the clinker phases consumed and the hydrates formed from the hydration paste of clinker #1 with various amounts of gypsum (sign + means that this phase remained in the cement paste even after 180 days of hydration; and time/time means formation/consumption).....	94
Table 5-7: XRD and TGA data presenting the clinker phases consumed and the hydrates formed from the hydration paste of clinker #5 with various amounts of gypsum (sign + means that this phase remained in the cement pastes even after 180 days of hydration; and time/time means formation/consumption).....	96
Table 5-8: Comparison between the amounts of gypsum required for each clinker to completely react, determined from Lerch method and from the equation of gypsum required with the theoretical and Rietveld results.....	101



Table 5-9: Visual appearance of the cement paste from clinker #3 inside each plastic vials after the end of the calorimeter test (H=hard, S=scratchable, Ex=expanded) ....	106
Table 5-10: Visual aspect of the cement paste from clinker #5 inside each plastic vials after the end of the calorimeter test (H=hard, S=scratchable, Ex=expanded) ....	110
Table 5-11: Pictures of clinker #5 with 30 wt. % gypsum with different additions of TIPA inside plastic vials after the end of the calorimeter test .....	110
Table 5-12: XRD and TGA data presenting the clinker phases consumed and the hydrates formed from the hydration paste of clinker #5 with 20 wt. % and 30 wt. % gypsum with various amounts of TIPA (sign “+” means that this phase remains in the sample after 28 days of hydration).....	112
Table 6-1: Comparison of the Rietveld values for each small (Chapter 4) and large (this Chapter) batches of clinkers produced from modified by-products (MBP) .....	116
Table 6-2: Particle sizes d(0.1), d(0.5) and d(0.9) for each large batch produced from MBP, in $\mu\text{m}$ .....	117

## List of Figures

Figure 1-1: Research Plan followed during this dissertation research [3, 4] .....	4
Figure 2-1: Steps of the manufacture of ordinary Portland cement in weight %. [6].....	8
Figure 2-2: Influence of SEC and QLP modulus on free lime [2].....	25
Figure 3-1: Batches produced from reagent chemicals (RC).....	31
Figure 3-2: Batches produced from by-products (BP).....	31
Figure 3-3: Small pellets for each batch produced from RC and BP before firing .....	31
Figure 3-4: Front view of the arrangement of the pellets in the platinum crucible on the left, and on a thick layer of $ZrO_2$ (1-2 mm) on the right.....	32
Figure 3-5: Top view of the arrangement of the pellets in the platinum crucible .....	32
Figure 3-6: Front view of the Carbolite ® furnace .....	32
Figure 3-7: Firing program followed with the box furnace for the preliminary experiments .....	32
Figure 3-8: Carbolite ® furnace with front opening to facilitate quenching step.....	33
Figure 3-9: Ventilator used to quench the pellets .....	33
Figure 3-10: Front view of prepared epoxy samples .....	36
Figure 3-11: Top view of prepared epoxy samples .....	36
Figure 3-12: SEM images and elemental maps of calcium, silicon, aluminum, iron and sulfur of a clinker sample composed theoretically of 30.6 wt. % $C_3S$ , 13.3% $C_2S$ , 15.3% $C_4A_3S$ , 35.7% $C_4AF$ and 5.1% of $CS$ (861 $\mu m$ width).....	37
Figure 3-13: The different steps processed through ImageJ software for the calcium elemental map from Figure 3-12 (861 $\mu m$ width) .....	38
Figure 3-14: Multispectral image stack of the elemental maps (861 $\mu m$ width).....	39
Figure 3-15: Unsupervised clustering analysis .....	40
Figure 3-16: Cluster analysis of a sample before identification of each cluster .....	41
Figure 3-17: Cluster analysis of a sample after identification of each cluster (black = void/epoxy; blue = silicates; red = ferrite; green = calcium sulfoaluminate; grey = calcium sulfate; the light blue and purple colors help to determine which major elements are present in each cluster) .....	41
Figure 3-18: Final unsupervised clustering analysis (861 $\mu m$ width). Color code: black = void/epoxy; blue = silicates; red = ferrite; green = calcium sulfoaluminate; grey = calcium sulfate. ....	42
Figure 3-19: Comparison of XRD data for batches B1 and B4 made from pure phases..	45
Figure 3-20: SEM picture of sample B1 .....	46
Figure 3-21: SEM picture of sample B4 .....	46

Figure 3-22: Phase mapping of sample B1 .....	46
Figure 3-23: Phase mapping of sample B4 .....	46
Figure 3-24: Calorimeter data of the influence of addition of SO <sub>3</sub> to cements of high C <sub>3</sub> A and low alkali content [77] .....	48
Figure 3-25: Overview of a mortar cube mold preparation .....	51
Figure 3-26: Close-up of one 1-in hollow mortar cube mold .....	51
Figure 3-27: Side of the mold where petroleum is applied to prevent water leak .....	51
Figure 3-28: 1-in mini-mortar cube mold filled with sample .....	52
Figure 3-29: Mini-mortar cubes after demolding step .....	52
Figure 4-1: XRD graphs and free lime determinations (in red) of all batches produced from RC, fired at the reference regime of 1300°C for 30 minutes (the peak encircled in green corresponds to the tricalcium aluminate (C <sub>3</sub> A) peak) .....	55
Figure 4-2: Free lime tests for each small sample produced from reagent chemicals (RC), fired at different temperatures for 30-60 minutes (hatched bars indicate C <sub>3</sub> A was present in this sample) .....	56
Figure 4-3: XRD graphs of small batches #1, 2, 3, 4 and 5 produced from reagent chemicals (RC).....	57
Figure 4-4: XRD/Rietveld approximation of each small batch with the optimum parameters (“Fluoro” = Fluorellestadite) .....	58
Figure 4-5: SEM/EDS pictures showing clinker phases after firing step (blue=C <sub>3</sub> S/C <sub>2</sub> S; red=C <sub>4</sub> AF; green=C <sub>4</sub> A <sub>3</sub> Ŝ; white=Fluorellestadite; pink=C <sub>3</sub> S/C <sub>2</sub> S/C <sub>4</sub> AF; yellow=C <sub>3</sub> S/C <sub>2</sub> S/C <sub>4</sub> AF/C <sub>4</sub> A <sub>3</sub> Ŝ; “/” means combination of clinker phases).....	60
Figure 4-6: Particle Size Distribution of each small batch after 45sec ground in a shatter box.....	62
Figure 4-7: XRD graphs and free lime determinations of all batches from BP fired at the reference regime of 1300°C for 30 minutes (the peak encircled in green corresponds to tricalcium aluminate peak, in blue to calcium sulfoaluminate and values in red to free lime) .....	63
Figure 4-8: Pellets made from industrial by-products (BP) just before firing process .....	64
Figure 4-9: Pellets made from industrial by-products (BP) just after firing at 1300°C and quenching step .....	64
Figure 4-10: Free lime tests for each small sample produced from industrial by-products (BP) and fired at different temperature for 30-60 minutes .....	65
Figure 4-11: XRD data from the different modifications of the amounts of raw materials for the batch #3 made from by-products, fired at 1250°C for 60min (RM=Red Mud; Sp=Spurlock FBC and Gyp=gypsum). The C <sub>4</sub> A <sub>3</sub> Ŝ and C <sub>3</sub> S peaks, respectively close to 24°-2θ and 29°-2θ and circled in red, were both more intense than with all the other modifications. ....	67

Figure 4-12: XRD data of batch #3 from reagent chemicals, from original by-products (BP) and from modified composition of by-products (called MBP) .....	68
Figure 4-13: SEM/EDS pictures showing clinker phases after firing step (blue= $C_3S/C_2S$ ; red= $C_4AF$ ; green= $C_4A_3\dot{S}$ ; white=Fluorellestadite; pink= $C_3S/C_2S/C_4AF$ ; yellow= $C_3S/C_2S/C_4AF/C_4A_3\dot{S}$ ; purple=MgO; cyan= $C\dot{S}$ ; flashy green= $C_3A/C_4F$ )	70
Figure 4-14: Particle Size Distribution of each small batch from modified by-products, after 45sec ground in a shatter box .....	72
Figure 5-1: XRD graphs from the large batches of clinker made from reagent chemicals .....	75
Figure 5-2: Particle Size Distributions of each large batch of clinker produced from reagent chemicals.....	76
Figure 5-3: Calorimeter analyses for every clinker made from RC with different amounts of gypsum. From left to right, and top to bottom: with 0%, 5%, 10%, 12.5%, 15%, 17.5%, 20% and 25% of gypsum by weight.....	78
Figure 5-4: Calorimeter analyses for every large batch with 5% of gypsum by weight for the first 25 hours (zoom of the top right graph in Figure 5-3).....	79
Figure 5-5: Calorimeter data of the power per cement material for the batch #3 from reagent chemicals (RC) with different amounts of gypsum (G) by weight.....	82
Figure 5-6: Calorimeter data of the energy per cement material for the batch #3 from reagent chemicals (RC) with different amounts of gypsum (G) by weight.....	82
Figure 5-7: Images of several cement pastes from the inside of plastic vials, following the end of the calorimetric tests. Left image: B#3-RC+15G defined as hard cement paste (H); middle image: B#5-RC+25G defined as moderately hard/soft cement paste (H/S) and easily “scratchable”; right image: B#3-RC+50G defined as completely expanded cement paste (Ex), turned into powder-like aspect.....	84
Figure 5-8: XRD analyses of the hydration paste of the clinker #3 with 15 wt. % gypsum, halted after 5 hours, 1, 7, 28, 90 and 180 days .....	87
Figure 5-9: TGA graph of the hydrated cement paste of clinker #3 with 15% gypsum stopped after 5 hours, 1, 7, 28, 90 and 180 days.....	89
Figure 5-10: XRD graphs illustrating the evolution of "stellerite" “rounded-peak” (between 10 and 11°-2 $\theta$ ) through sample #3 with addition of gypsum.....	90
Figure 5-11: TGA graphs illustrating the evolution of the "stellerite" peak through sample #3 with addition of gypsum .....	90
Figure 5-12: Calorimeter data of hydration paste of clinker #3 with various amounts of gypsum combined with XRD and TGA results from hydration pastes, halted after 5 hours, 1, 7 and 28 days. The 90 and 180-day measurements are not included in this graph.....	92

Figure 5-13: Calorimeter data of hydration paste of clinker #1 with different amounts of gypsum stopped after 5 hours, 1, 7 and 28 days. The 90 and 180-day measurements are not included in this graph.....	94
Figure 5-14: Calorimeter data of hydration paste of clinker #5 with different amount of gypsum stopped after 5 hours, 1, 7 and 28-day. The 90 and 180-day measurements are not included in this graph.....	96
Figure 5-15: Comparison of compressive strength measurements of OPC with clinkers made from reagent chemicals (RC) with 10% and 15% of gypsum.....	99
Figure 5-16: Chemical structure of triisopropanolamine (TIPA) .....	102
Figure 5-17: Schema displaying the influence of TIPA with ferrite, proposed by Gartner and Myers [94].....	103
Figure 5-18: Calorimeter results of clinker #3 produced from RC with 20 wt.% gypsum (G) and different amounts of TIPA (T) for 145 hours .....	105
Figure 5-19: Calorimeter results of clinker #3 produced from RC with 30 wt. % gypsum (G) and different amounts of TIPA (T) for 145 hours .....	105
Figure 5-20: Calorimeter results of clinker #5 produced from RC with 10 wt. % gypsum (G) and different amounts of TIPA (T) for 35 hours (second peak after 10 hours is present but too weak to be detected here, refer to Figure 5-4) .....	107
Figure 5-21: Calorimeter results of clinker #5 produced from RC with 20 wt. % gypsum (G) and different amounts of TIPA (T) for 145 hours .....	107
Figure 5-22: Calorimeter results of clinker #5 produced from RC with 30 wt. % gypsum (G) and different amounts of TIPA (T) for 300 hours .....	108
Figure 5-23: Calorimeter results of clinker #5 produced from RC with 40 wt. % gypsum (G) and different amounts of TIPA (T) for 300 hours .....	108
Figure 5-24: Calorimeter results of clinker #5 produced from RC with 50 wt. % gypsum (G) and different amounts of TIPA (T) for 300 hours .....	109
Figure 5-25: Calorimeter data of hydration paste of clinker #5 with 20 wt. % gypsum and TIPA stopped after 1, 7 and 28 days. The 28-day measurement is not shown in this graph.....	111
Figure 5-26: Calorimeter data of hydration paste of clinker #5 with 30 wt. % gypsum and TIPA stopped after 24, 30, 48 hours, 7 and 28 days. The 28-day measurement is not shown in this graph.....	112
Figure 5-27: Compressive strength results of clinker #5 with 10, 15 and 20 wt. % gypsum, with addition of TIPA .....	113
Figure 6-1: Comparison of XRD diffractograms of the small batches of clinkers (SB) from Chapter 4, and the large batches of clinkers (LB) from this chapter, made from modified by-products (MBP).....	116
Figure 6-2: Particle size distributions of each large batch of clinker produced from MBP .....	117

Figure 6-3: Calorimeter data from clinker #1 produced from modified by-products (MBP) and reagent chemicals (RC) with addition of gypsum (G) .....	118
Figure 6-4: Calorimeter data from clinker #3 produced from modified by-products (MBP) and reagent chemicals (RC) with addition of gypsum (G) .....	119
Figure 6-5: Calorimeter data from clinker #5 produced from modified by-products (MBP) and reagent chemicals (RC) with addition of gypsum (G) .....	119
Figure 6-6: Calorimeter data of clinker#3-MBP with addition of gypsum (G) and TIPA (T) .....	121
Figure 6-7: Calorimeter data of clinker#5-MBP with addition of gypsum (G) and TIPA (T) .....	121
Figure 6-8: Compressive strength data for clinker#3 produced from RC and MBP with the additions of gypsum (G) and TIPA (T).....	123
Figure 6-9: Mini mortar cube of clinker#3-MBP+15G after 28 days of hydration .....	123
Figure 6-10: Mini mortar cubes of clinker#3-MBP+15G+1.0T, #3-MBP+10G+0.5/1.0T after 28 days of hydration .....	123
Figure 6-11: Compressive strength data for clinker#5 produced from RC and MBP with the additions of gypsum and TIPA .....	124
Figure 6-12: Mortar cubes of clinker#5-MBP+10/15G after 28 days of hydration.....	125
Figure 6-13: Mortar cubes of clinker#5-MBP+10/15G+0.2T after 28 days of hydration .....	125
Figure 6-14: Mortar cubes of clinker-MBP#5+10/15G+0.5/1.0T after 28 days of hydration .....	125

## Chapter 1 : Introduction

### 1.1. Introduction

Ordinary Portland cement (OPC) is the most common and widely used material around the world. It has been studied for decades and a lot of research is still going on to improve its technology. Even though this material is used worldwide and has recognized good properties, some disadvantages are still present. The main disadvantage is the amount of carbon dioxide released, estimated from 5 to 8% of the man-made CO<sub>2</sub>-emissions. [1] The other major disadvantage is the manufacturing process, which consumes a large amount of energy from grinding, using a wet process, and firing at elevated temperature for clinkerization.

Several ideas have been investigated to improve the energy use for cement production such as optimization of cement manufacturing process using a dry process for example. The use of alternative raw materials, such as by-products, can be envisaged to decrease the release of CO<sub>2</sub>-emissions, by using less calcium carbonate (CaCO<sub>3</sub>). Also the use of supplementary cementitious materials (or also called SCMs), which can be added to concrete, can help to reduce the cost and influence its chemical and physical properties. SCM can be fly ash, blast-furnace slag, or silica fume. Another option would be to use low-energy cements which are easier to grind, such as calcium sulfoaluminate cements or also named CSAC, and are produced at about 200°C lower than OPC. Blended cements of OPC and CSAC can also be envisaged. Furthermore, high iron cements have been produced which perform similarly to OPC.

OPC concrete is known to exhibit high long-term compressive strength due to the presence of the alite (C<sub>3</sub>S) phase in the cement, whereas CSAC are known to set and harden quickly due to the presence of the Klein's compound (C<sub>4</sub>A<sub>3</sub>S̄) phase. By combining both of these characteristics, a new kind of cement can be produced having very high early and late strengths. Some researchers have found it possible to produce this novel cement by using fluxes and mineralizers such as calcium fluoride and sulfates. Moreover, the influence of the ferrite phase has not been thoroughly studied yet in the alite-calcium sulfoaluminate cements.

Currently, the rapid development of industries and utilities creates more and more wastes and by-products. They include fly ash, bottom ash, flue gas desulfurization (FGD) gypsum, red mud, and many others with limited landfill space. The beneficial use of these by-products is considered to be a high priority and research will focus on producing high-iron cements.

The objective of this research was to combine the best properties of two kinds of cement, OPC and CSAC, by not mixing or blending them but rather by producing one unique cement that possesses high early strength as well as long-term strength and durability. Initial work focused on production of cement from reagent chemicals followed by the inclusion of by-products as feedstocks. Finally, the influence of the ferrite phase, present in large amounts, was examined with the goal of introducing as much red mud as possible in the process.

## **1.2. Research Plan / Purpose and Scope**

The first phase of this research was to derive modified Bogue (i.e. normative) equations and moduli to predict clinker composition. The final clinker composition was calculated stoichiometrically and was considered a first approximation of the phase composition. Some minor errors can occur due to the possibility of the formation of other minor phases during the firing step, which depends on the heating temperature, or the iron can substitute into other phases. This has been done previously by Zhou [2], who has formulated five moduli which were presented in an internal report on Alite-Calcium Sulfoaluminate cements at the University of Kentucky, and resumed in Section 2.4.3.

In order to study the influence of ferrite in this kind of cement, some moduli were kept constant, such as the ratio alite/belite, as well as the amount of calcium sulfoaluminate (15% by wt.). Thus as the amount of ferrite increased from 5 to 45% by weight and the amount of alite and belite decreased, the influence of the ferrite phase was studied. In total, five clinkers were made from reagent grade chemicals (RC) and five from industrial by-products (BP) both with the same parameters. This approach helped to determine the influence of the minor elements, such as titanium dioxide or magnesium oxide, which are present in the industrial by-products but not in the reagent chemicals.



From these five formulations prepared using RC and BP, the optimum firing temperature and dwelling time were first optimized by “firing” small batches of clinker. Free lime content, powder X-ray diffraction with quantitative Rietveld (XRD/Rietveld) analyses and scanning electron microscopy with energy dispersive X-ray spectroscopy (SEM/EDS) analyses were performed to check the chemical and mineralogical composition of each clinker formulation. When studying the influence of ferrite, the particle size was kept constant for each composition so as not to interfere with the chemical and mechanical properties.

After optimizing the firing procedure for each composition, larger batches were produced of about 500 g from reagent chemicals and 2000 g from industrial by-products. The hydration processes of these clinkers were then studied. The optimum amount of gypsum, added to the clinker to complete the formulation, was determined through calorimetric measurements, and the hydrated phases formed during the hydration process were identified through hydration paste studies, halted at specific times by immersion in isopropanol. These different times were carefully selected after studying the calorimetric data and identifying the main peaks during the hydration process. Several characterization methods were employed to identify the hydrated phases such as XRD and thermogravimetric analyses (TGA). Mechanical tests were performed on the optimum compositions (with gypsum included) such as compressive strength tests. Also, the use of a chemical, triisopropanolamine (TIPA), to improve the mechanical properties of these compositions was tested.

Figure 1-1 presents a summary of the work with the different steps listed and methods employed.

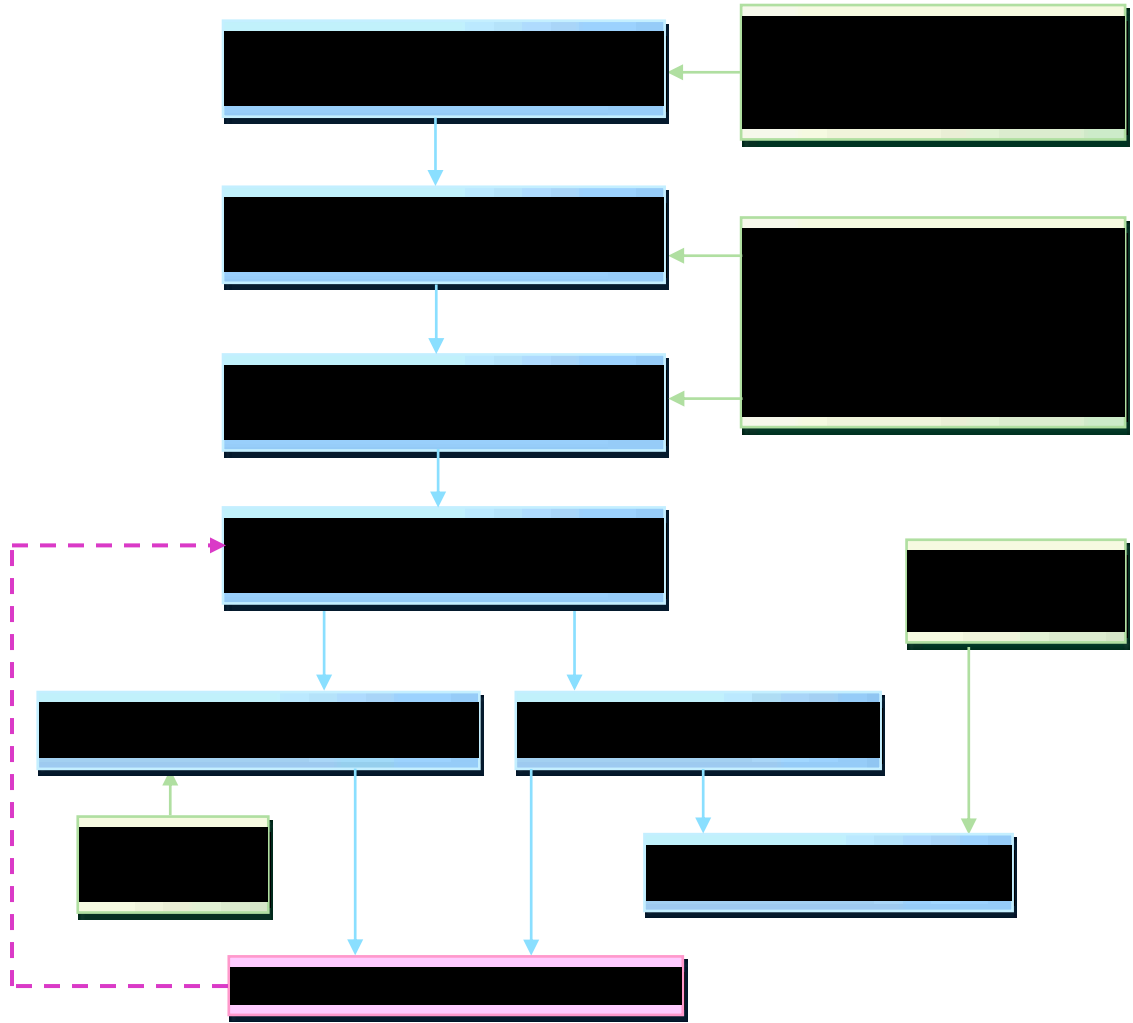


Figure 1-1: Research Plan followed during this dissertation research [3, 4]

### 1.3. Scope of Dissertation

The first chapter introduces the project and the research plan. The second chapter provides a literature background about OPC and CSAC, but also focuses on the alite-calcium sulfoaluminate cements with recent data and the importance of studying the influence of tetracalcium ferroaluminate ( $C_4AF$ ) on alite-calcium sulfoaluminate cements. The third chapter presents the materials and the methods used to complete this work. The fourth chapter includes preliminary experiments on clinkers made from RC and BP and presents the optimum parameters for their production such as firing temperature and dwelling time. The fifth and sixth chapters describe the hydration processes, sulfate optimization and mechanical tests performed on the compositions made

from RC and BP. The effect of a chemical reagent used to improve strength gain and stability is also described. The last chapter discusses the results of these compositions and future research.

#### **1.4. Nomenclature**

Because of the frequent recurrence of the clinker phases and cement components within the text, abbreviations commonly used in the cement industry, as well as acronyms, are used to simplify the reading of this dissertation and are displayed in Sections 1.4.1 and 1.4.2.

##### **1.4.1. Cement Chemistry Notations**

The cement abbreviations, chemical formulae and scientific names for each cement component and hydrated phases are presented in Table 1.1.

Table 1-1: Cement Abbreviations, Chemical Formulae and Scientific Names of cement elements and phases

<b>Cement Abbreviations</b>	<b>Chemical Formulae</b>	<b>Scientific Name (Cement Name)</b>
<b>C</b>	CaO	Calcium Oxide (Lime)
<b>S</b>	SiO <sub>2</sub>	Silicon Dioxide
<b>A</b>	Al <sub>2</sub> O <sub>3</sub>	Aluminum Oxide
<b>F</b>	Fe <sub>2</sub> O <sub>3</sub>	Iron Oxide
<b>H</b>	H <sub>2</sub> O	Water
<b>Ś</b>	SO <sub>3</sub>	Sulfur Trioxide
<b>Ĉ</b>	CO <sub>2</sub>	Carbon Dioxide
<b>M</b>	MgO	Magnesium Oxide (Periclase)
<b>T</b>	TiO <sub>2</sub>	Titanium Dioxide
<b>K</b>	K <sub>2</sub> O	Potassium Oxide
<b>N</b>	Na <sub>2</sub> O	Sodium Oxide
<b>C<sub>3</sub>S</b>	3CaO.SiO <sub>2</sub>	Tricalcium Silicate (Alite)
<b>C<sub>2</sub>S</b>	2CaO.SiO <sub>2</sub>	Dicalcium Silicate (Belite)
<b>C<sub>3</sub>A</b>	3CaO.Al <sub>2</sub> O <sub>3</sub>	Tricalcium Aluminate
<b>C<sub>4</sub>AF</b>	4CaO.Al <sub>2</sub> O <sub>3</sub> .Fe <sub>2</sub> O <sub>3</sub>	Tetracalcium Aluminoferrite (Brownmillerite)
<b>C<sub>4</sub>A<sub>3</sub>Ś</b>	4CaO.3Al <sub>2</sub> O <sub>3</sub> .SO <sub>3</sub>	Calcium Sulfoaluminate or CSA (Yeelimite)
<b>CŚ</b>	CaO.SO <sub>3</sub>	Calcium Sulfate (Anhydrite)
<b>CŚH<sub>0.5</sub></b>	CaO.SO <sub>3</sub> .0.5H <sub>2</sub> O	Calcium Sulfate Hemihydrate (Hemihydrate)
<b>CŚH<sub>2</sub></b>	CaO.SO <sub>3</sub> .2H <sub>2</sub> O	Calcium Sulfate Dihydrate (Gypsum)
<b>C<sub>6</sub>A<sub>3</sub>Ś<sub>3</sub>H<sub>32</sub></b>	6CaO.Al <sub>2</sub> O <sub>3</sub> .3SO <sub>3</sub> .32H <sub>2</sub> O	Ettringite
<b>C<sub>4</sub>AŚH<sub>12</sub></b>	4CaO.Al <sub>2</sub> O <sub>3</sub> .SO <sub>3</sub> .12H <sub>2</sub> O	Monosulfate (Kuzelite)
<b>CH</b>	CaO.H <sub>2</sub> O or Ca(OH) <sub>2</sub>	Calcium Hydroxide (Portlandite)
<b>CAS<sub>7</sub>H<sub>7</sub></b>	CaO.Al <sub>2</sub> O <sub>3</sub> .7SiO <sub>2</sub> .7H <sub>2</sub> O	Stellerite
<b>C<sub>2</sub>ASH<sub>8</sub></b>	2CaO.Al <sub>2</sub> O <sub>3</sub> .SiO <sub>2</sub> .8H <sub>2</sub> O	Strätlingite
<b>C<sub>3</sub>AH<sub>6</sub></b>	3CaO.Al <sub>2</sub> O <sub>3</sub> .6H <sub>2</sub> O	Hydrogarnet
<b>C<sub>4</sub>AĈ<sub>0.5</sub>H<sub>12</sub></b>	4CaO.Al <sub>2</sub> O <sub>3</sub> .0.5CO <sub>2</sub> .12H <sub>2</sub> O	Hemicarboaluminate
<b>C<sub>4</sub>AĈH<sub>11</sub></b>	4CaO.Al <sub>2</sub> O <sub>3</sub> .CO <sub>2</sub> .11H <sub>2</sub> O	Monocarboaluminate
<b>CĈ</b>	CaO.CO <sub>2</sub> or CaCO <sub>3</sub>	Calcite
<b>C-S-H</b>	Detailed structure not completely known	Calcium Silicate Hydrate
<b>C<sub>4</sub>AH<sub>13</sub></b>	4CaO.Al <sub>2</sub> O <sub>3</sub> .13H <sub>2</sub> O	Calcium Aluminum Hydrates
<b>C<sub>4</sub>AH<sub>19</sub></b>	4CaO.Al <sub>2</sub> O <sub>3</sub> .19H <sub>2</sub> O	
<b>C<sub>2</sub>AH<sub>8</sub></b>	2CaO.Al <sub>2</sub> O <sub>3</sub> .8H <sub>2</sub> O	
<b>TIPA</b>	C <sub>9</sub> H <sub>21</sub> NO <sub>3</sub>	Triisopropanolamine

## 1.4.2. Acronyms

Acronyms used through this dissertation are shown in Table 1.2.

Table 1-2: List of acronyms used through this dissertation

<b>Acronyms</b>	<b>Signification</b>
<b>OPC</b>	Ordinary Portland Cement
<b>CSAC</b>	Calcium SulfoAluminate Cement
<b>RC</b>	Reagent Chemicals
<b>FGD Gypsum</b>	Flue Gas Desulfurization Gypsum
<b>BP</b>	By-Products
<b>MBP</b>	Modified By-Products
<b>AFm</b>	Al <sub>2</sub> O <sub>3</sub> -Fe <sub>2</sub> O <sub>3</sub> -mono
<b>AFt</b>	Al <sub>2</sub> O <sub>3</sub> -Fe <sub>2</sub> O <sub>3</sub> -tri
<b>d(0.1), d(0.5), d(0.9)</b>	Volume weighted particle size distributions indicate that 10%, 50% and 90% of a sample are below this particle size
<b>PSD</b>	Particle Size Distribution
<b>XRD/Rietveld</b>	X-Ray Diffraction/Rietveld
<b>SDT</b>	Simultaneous TGA / DSC
<b>TGA</b>	Thermogravimetric analysis
<b>DSC</b>	Differential scanning calorimetry
<b>SEM</b>	Scanning Electron Microscope
<b>EDS</b>	Energy Dispersive Spectroscopy
<b>LSF</b>	Lime Saturation Factor
<b>SR</b>	Silica Ratio
<b>AR</b>	Alumina Ratio
<b>LAD</b>	Lime Adequate Degree
<b>RSA</b>	Ratio of Silicates and Aluminates
<b>RSF</b>	Ratio of Sulfoaluminates and Ferroaluminates
<b>SEC</b>	Sulfur Excessive Coefficient
<b>QLP</b>	Quantity of Liquid Phase
<b>f<sub>CaO</sub></b>	Free Lime
<b>PEG</b>	Polyethylene glycol
<b>rpm</b>	Round per minute
<b>wt. %</b>	Weight percentage

## Chapter 2 : Literature Review / Background

### 2.1. Presentation of the most common cement: Ordinary Portland Cement

#### 2.1.1. Composition, formation and CO<sub>2</sub>-emissions

Portland cement, also called ordinary Portland cement or OPC, is the most common and widely used material in the world [5]. This cement is prepared from ingredients such as limestone (CaCO<sub>3</sub>) and clay (SiO<sub>2</sub>-Al<sub>2</sub>O<sub>3</sub>), which provide the essential components of lime and silica. Other materials can be added to the cement raw mix, for example bauxite, iron oxide or sand, as a flux and/or to adjust the mineralogical composition. The raw materials are then mixed together, ground and heated at a temperature close to 1450-1500°C, producing a hard nodular material called “clinker”. The heating step is referred to as “clinkerization”. From 0 to 10% by weight of calcium sulfate is then substituted to the clinker before being ground again and the final cement is obtained. All the steps can be resumed in Figure 2-1.

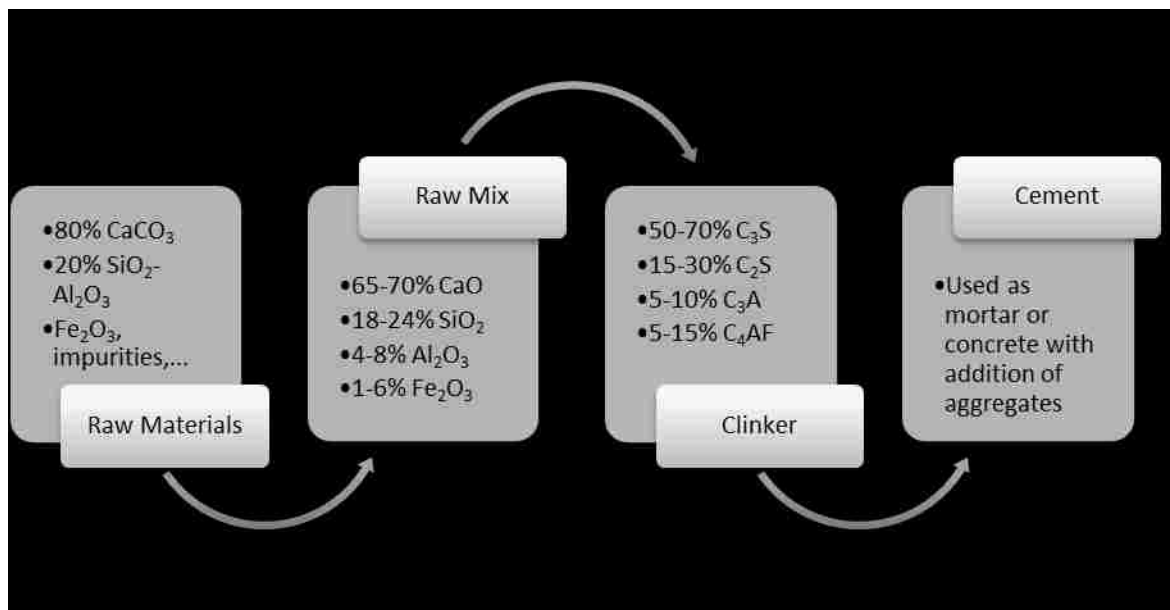


Figure 2-1: Steps of the manufacture of ordinary Portland cement in weight %. [6]

During the heating process, different reactions occur at specific temperatures. The first one is the evaporation of water, if there is any in the raw materials. Then a “preheating step” is usually completed to completely decompose the limestone into lime and carbon dioxide following this equation:  $\text{CaCO}_3 (\text{s}) \rightarrow \text{CaO} (\text{s}) + \text{CO}_2 (\text{g})$ . This reaction is called

calcination and occurs at around 900°C. Largely because of this reaction, it has been estimated that the production of OPC is the source of about 5% of the total annual CO<sub>2</sub>-emissions in the world. Data from 1994 show that 0.815 ton of CO<sub>2</sub> is emitted to produce 1 ton of cement, where 0.425 ton of CO<sub>2</sub> comes from the raw materials and the rest, 0.390 ton, comes from the combustion of the fuels. [7]

Lime is also produced during the calcination process and some clinker phases begin to form, such as belite, ferrite, aluminate phases and some other intermediate phases depending on the raw materials composition.

Between 1300 and 1450°C, clinkerization occurs, different phases form in the clinker (Figure 2-1), and numerous reactions happen quickly at this stage. At this high temperature a melt is formed, mainly composed of the aluminate and ferrite phases, which represents approximately from 20 to 30% by weight of the mixture. This liquid phase helps to promote the formation of alite from the reaction between belite and lime.

After the heating process, slow cooling should be avoided since this increases the belite content by decomposing the alite, and also the formation of large C<sub>3</sub>A crystals is observed which can be detrimental to the properties of cement. [8]

In order to formulate cement and predict its composition, Bogue equations are used as reference. [9] These formulae are designed to predict the final clinker composition depending on the raw materials. They are as follow in Table 2-1, by weight percentage.

Table 2-1: Bogue equations used to formulate OPC (by weight percentage)

<b>If A/F&gt;0.64</b>	<b>If A/F&lt;0.64 (Rare Case)</b>
$C_3S = 4.071 \text{ CaO} - 7.602 \text{ SiO}_2 - 6.719$	$C_3S = 4.071 \text{ CaO} - 7.602 \text{ SiO}_2 - 4.479$
$Al_2O_3 - 1.430 \text{ Fe}_2O_3 - 2.852 \text{ SO}_3$	$Al_2O_3 - 2.859 \text{ Fe}_2O_3 - 2.852 \text{ SO}_3$
$C_2S = 2.867 \text{ SiO}_2 - 0.754 \text{ C}_3S$	$C_2S = 2.867 \text{ SiO}_2 - 0.754 \text{ C}_3S$
$C_3A = 2.650 \text{ Al}_2O_3 - 1.692 \text{ Fe}_2O_3$	$C_3A = 0$
$C_4AF = 3.043 \text{ Fe}_2O_3$	$C_4AF = 2.10 \text{ Al}_2O_3 + 1.702 \text{ Fe}_2O_3$

These equations are based on several assumptions described below:

- 1- Only four phases are considered in the clinker formation,  $C_3S$ ,  $C_2S$ ,  $C_3A$  and  $C_4AF$ ;
- 2- Iron oxide is only present in the ferrite phase;
- 3- Aluminum and iron oxides are present in equivalent amount in the ferrite phase;
- 4- The magnesia is only present as uncombined  $MgO$ ;
- 5- The remaining aluminum oxide occurs in tricalcium aluminate;
- 6- The lime, not engaged in the previous reactions, reacts with silica to form belite and then the remaining lime reacts with belite to form alite. The uncombined lime is then called free lime.

These equations contribute to some errors, since equilibrium is not maintained during the cooling process and the clinker phases are not actually pure. Indeed, some minor oxides are incorporated into the phase structures. [10] Also, the presence of  $MgO$  or  $TiO_2$ , as minor oxides in the mix, can interfere with the chemical reactions and thus the Bogue equations should be modified accordingly.

Other parameters, also called composition parameters or modulus values, are used to predict the feasibility and evaluate the formulation of a cement composition. They are described by the following equations:

$$LSF = \frac{CaO}{2.8 SiO_2 + 1.2 Al_2O_3 + 0.65 Fe_2O_3}$$

$$SR = \frac{SiO_2}{Al_2O_3 + Fe_2O_3}$$

$$AR = \frac{Al_2O_3}{Fe_2O_3}$$

The lime saturation factor (LSF) is actually the ratio of alite to belite and predicts the proportion of free lime in the clinker. If LSF is above 1.0, free lime will remain. For actual clinkers, the ideal value would be between 0.92 and 0.98.

The silica ratio (SR) represents the proportion of silicate phases present in the clinker. It is typically between 2.0 and 3.0. If this modulus is increased, this means that more



silicate than aluminate and/or ferrite phases are present in the clinker, thus less liquid phase forms which makes it difficult for the clinker to “burn” (or in other words “react completely”).

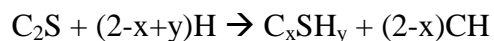
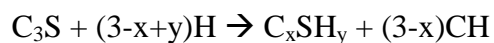
The alumina ratio (AR) is the ratio of aluminate to ferrite phases. It is typically between 1.0 and 4.0.

All of these parameters help to create a cement with a specific composition depending on the required properties.

### **2.1.2. Hydration Processes**

During the hydration of OPC (i.e. setting and hardening of mortar and concrete), different hydrated phases are observed depending on the clinker phases initially present, but also on the preparation of the clinker, the clinkerization conditions, and on the type and amount of foreign ions present in the chemical structure of the clinker phases. The clinker phases presented previously have different properties and hydration processes which make each cement unique.

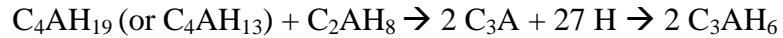
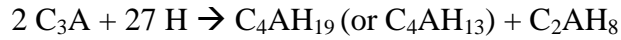
The hydration of the silicate phases ( $C_3S$  and  $C_2S$ ) is quite complex and still not well understood.  $C_3S$  phase is the most important phase in OPC due to its rapid reaction with water and its high contribution to the early strength of hydrated cement. The other silicate phase,  $C_2S$ , reacts slowly with water and contributes to the late strength of cement. The general equations representing their hydration reactions are as follow: [6, 11]



The hydrates formed during the reactions are  $C_xSH_y$ , also called C-S-H phase or “tobermorite” gel, which is a poorly crystalline almost amorphous phase; and CH which is calcium hydroxide, also called portlandite.

The aluminate phase ( $C_3A$ ), reacts quickly with water, but can cause undesirable rapid set unless gypsum is used as a set-controlling agent, which creates another hydrated phase (ettringite) explained later. Also, this phase can cause the cement to expand a lot, which is an undesirable effect. Its hydration reaction depends on the presence of calcium sulfate.

Without it, C<sub>3</sub>A reacts with water to form AFm phases, C<sub>2</sub>AH<sub>8</sub> and C<sub>4</sub>AH<sub>19</sub> (or C<sub>4</sub>AH<sub>13</sub>), and are converted to a hydrogarnet phase (C<sub>3</sub>AH<sub>6</sub>), which is thermodynamically stable at ordinary temperatures. The hydrated phase C<sub>4</sub>AH<sub>13</sub> can be present instead of C<sub>4</sub>AH<sub>19</sub> when the relative humidity is below 88%, this is why this phase is often detected in dried pastes.

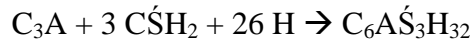


Also, the C<sub>4</sub>AH<sub>x</sub> hydrates react with CO<sub>2</sub> in the air to form hemicarboaluminate, or C<sub>4</sub>AĈ<sub>0.5</sub>H<sub>12</sub>. [12] This phase is then converted to monocarboaluminate (C<sub>4</sub>AĈH<sub>11</sub>) with an increase in the concentration of carbonates. [13-15]

AFm (Al<sub>2</sub>O<sub>3</sub>-Fe<sub>2</sub>O<sub>3</sub> -mono) phases are defined by the following general formula C<sub>3</sub>(A,F).CaX<sub>2</sub>.yH<sub>2</sub>O, where y = 2(x+3). X can represent OH<sup>-</sup>, SO<sub>4</sub><sup>2-</sup> and CO<sub>3</sub><sup>2-</sup>. [6] This group includes hydrated phases such as monosulfate, hemicarboaluminate, monocarboaluminate and strätlingite (C<sub>2</sub>ASH<sub>8</sub>). [16]

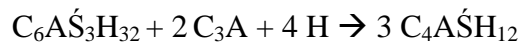
If calcium hydroxide is initially present, only C<sub>4</sub>AH<sub>19</sub> forms and then converts to hydrogarnet.

When calcium sulfate is present during the hydration reaction, ettringite phase (AFt phase) is formed as the main product:

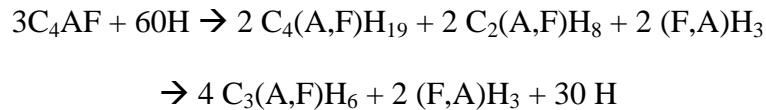


AFt (Al<sub>2</sub>O<sub>3</sub>-Fe<sub>2</sub>O<sub>3</sub>-tri) phases are defined by the following general formula C<sub>3</sub>(A,F).3CX.yH<sub>2</sub>O, where y = x+30 and X can represent OH<sup>-</sup>, SO<sub>4</sub><sup>2-</sup> and CO<sub>3</sub><sup>2-</sup>. [6]

If the entire calcium sulfate is consumed during the hydration and if some C<sub>3</sub>A remains, the ettringite will react with the remaining aluminate phase to form the AFm phase called calcium aluminate monosulfate hydrate, or also “monosulfate”.



The last phase, the ferrite phase ( $C_4AF$ ), reacts similarly to, but slower than the hydration of tricalcium aluminate ( $C_3A$ ). When water is added to  $C_4AF$ , AFm phases form and convert to hydrogarnet in the same way as the hydration of  $C_3A$  as shown below:



When calcium sulfate is added, the same effect as with  $C_3A$  is observed and iron substituted ettringite forms followed by iron substituted AFm phases when sulfate ions become unavailable.

When  $C_3A$  and  $C_4AF$  are present together during the hydration process,  $C_3A$  tends to react more effectively with gypsum, leaving  $C_4AF$  to convert to AFm from the lack of sulfate ions. [17]

### 2.1.3. Physical Properties

The mechanical properties of OPC depend on several variables. First of all, the fineness of a cement can affect its hydration rate and thus its rate of strength gain. This is due to the fact that the small particles have higher surface area to volume ratio which increases the water-cement interactions. The soundness, which is the property of cement to expand after setting, is mainly influenced by the amount of free lime and magnesia. [18, 19] The setting time is another characteristic which depends on factors such as cement fineness, water-cement ratio, chemical composition (especially gypsum content) and admixtures. Three types of strength are usually tested: compressive, tensile and flexural strengths. The dimensional stability is also tested by studying the expansion/shrinkage evolution of mortar and concrete prisms.

Some compressive strength values are presented in Table 2-2 in order to provide an idea of the properties of different types of OPC.

Table 2-2: Minimum compressive strength for different types of OPC in MPa [18, 19]

Types of OPC	ASTM Designation	Composition / Properties	Compressive strength at different curing times (days)			
			1	3	7	28
I	Normal	C <sub>3</sub> S: 55%; C <sub>2</sub> S: 19%; C <sub>3</sub> A: 10%; C <sub>4</sub> AF: 7%; MgO: 2.8%; SO <sub>3</sub> : 2.9%, LOI: 1%; f <sub>CaO</sub> : 1%	-	12.0	19.0	-
II	Moderate sulfate resistance	C <sub>3</sub> A ≤ 8%	-	10.0	17.0	-
III	High early strength	Similar to Type I - Cement ground finer	12.0	24.0	-	-
IV	Low heat of hydration	C <sub>3</sub> S: 28%; C <sub>2</sub> S: 49%; C <sub>3</sub> A: 4%; C <sub>4</sub> AF: 12%; MgO: 1.8%; SO <sub>3</sub> : 1.9%, LOI: 0.9%; f <sub>CaO</sub> : 0.8%	-	-	7.0	17.0
V	High sulfate resistance	C <sub>3</sub> A ≤ 5% and C <sub>4</sub> AF + 2C <sub>3</sub> A ≤ 20%	-	8.0	15.0	21.0

#### 2.1.4. Advantages and Disadvantages of OPC Concrete

The primary advantage of OPC is the large amount of research dedicated to this cement over many decades which makes this cement very well-known and reliable. Its major disadvantage is the pollution aspect. Indeed, 5% of the total annual global carbon dioxide emissions is released from the production of cement (from calcination and combustion processes). [7] These emissions come from a variety of sources: a high firing temperature associated with a long dwelling time, use of high carbon fuel such as coal, and from grinding the hard clinker.

Several solutions for lowering carbon emissions and energy use have been considered, such as improving the production process (switching from wet to dry processing, reducing firing times and temperatures), replacing high carbon with low carbon fuels, using blended cement in concrete (OPC with fly ash,...), mineral polymers (geopolymers) and others. [5, 7]

The research presented in this dissertation is focused on lowering the firing temperature, combining different clinker phases (alite and calcium sulfoaluminate) into one unique

cement, and using industrial by-products as raw materials with the aim of reducing CO<sub>2</sub>-emissions from cement production.

## **2.2. Calcium Sulfoaluminate Cements (CSAC)**

Calcium sulfoaluminate cement, also called CSAC or third cement series, has a different mineral composition and hydration products than OPC, and is defined as a low CO<sub>2</sub>-emitting cement substitute for OPC. [5] More than 50 years ago, the first purpose of the production and use of the CSAC has been as a concrete additive to compensate the shrinkage phenomenon observed in OPC. Since the energy crisis of the mid 1970's, the interest in the development of CSAC has been growing, especially for its potential fuel savings. [5, 20] China was the first country to develop a major calcium sulfoaluminate industry with about 1 million tons per year manufactured, and by designing a series of standards and classifications specifically for CSAC. [21, 22] Currently, CSAC is primarily used instead of OPC when rapid strength gain, self-stressing properties, or sulfate resistance are desired. Even with all the advantages of this cement, the production and use of the CSAC are limited due to its expensive production.

### **2.2.1. Composition / Formation**

The amounts of carbon dioxide released from limestone during the formation of several clinker phases are presented in Table 2-3. As shown in this table, the formation of the C<sub>3</sub>S phase releases the most CO<sub>2</sub>-emissions, followed by C<sub>2</sub>S. Hence, the CSAC do not contain any C<sub>3</sub>S in their mineralogical composition, which reduces carbon dioxide formation but also could negatively affect its early strength. However, another phase called Klein's Compound, or C<sub>4</sub>A<sub>3</sub>S̄, is substituted for alite. Compared to C<sub>3</sub>S, C<sub>4</sub>A<sub>3</sub>S̄ releases more than 2.5 times less CO<sub>2</sub> than C<sub>3</sub>S and forms at lower temperatures of around 1250-1350°C. Furthermore, the clinker is substantially softer and thus easier to grind than OPC due to this phase. Another advantage of CSAC is the potential to use large amounts of by-products, such as fly ash, as raw materials. Its production requires sources of calcium, sulfate and alumina. Calcium and sulfate needs are easily fulfilled, whereas the alumina need requires large amounts of bauxite. But the price of the bauxite is a disadvantage to its production as it is very expensive.

Table 2-3: CO<sub>2</sub> released from manufacture of clinker phases from limestone CaCO<sub>3</sub> [5]

Clinker phase	C <sub>3</sub> S	β-C <sub>2</sub> S	C <sub>3</sub> A	C <sub>4</sub> AF	CA	C <sub>4</sub> A <sub>3</sub> Ŝ
CO <sub>2</sub> released (kg/kg clinker)	0.578	0.511	0.489	0.362	0.279	0.216

In China, two kinds of cements were developed called SAC (sulfoaluminate cement) and FAC (ferroaluminate cement) in which the amount of iron differs between them.

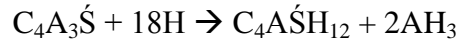
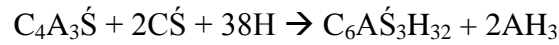
Table 2-4: Chemical composition and compressive strength values for SAC and FAC clinkers [21, 23-25]

Clinker (%)	Chemical Composition by wt. %					Clinker Composition by wt. %				
	CaO	SiO <sub>2</sub>	Al <sub>2</sub> O <sub>3</sub>	Fe <sub>2</sub> O <sub>3</sub>	SO <sub>3</sub>	C <sub>4</sub> A <sub>3</sub> Ŝ	C <sub>2</sub> S	C <sub>4</sub> AF	C <sub>6</sub> AF <sub>2</sub>	
SAC	36-45	3-13	30-40	1-3	8-15	55-75	8-37	3-10	-	
FAC	43-50	5-13	25-35	3-13	7-12	33-63	14-37	-	15-35	
Compressive Strength in MPa										
In water stored 20C 7/28/720 days					In air stored 20C 7/28/720 days					
SAC	40.5/44.0/59					42.5/45.0/38.5				
FAC	46.5/51.5/55.5					51.5/55.5/53.0				

The firing temperature of these cements is typically around 1250-1350°C due to the formation of the C<sub>4</sub>A<sub>3</sub>Ŝ phase starting at 1200°C. Compared to OPC, this temperature is lowered by 100 to 200°C. The formation of this phase occurs by solid state reactions between CaSO<sub>4</sub>, CaO and Al<sub>2</sub>O<sub>3</sub>, and also between CaSO<sub>4</sub> and CaAl<sub>2</sub>O<sub>4</sub> at higher temperatures. [26] Other phases are formed during the heating process, including C<sub>2</sub>S, C<sub>4</sub>AF and CŜ. However no alite is formed due to the low firing temperature used during the process.

### 2.2.2. Hydration

As explained earlier, this cement introduces a new phase, C<sub>4</sub>A<sub>3</sub>Ŝ, which is responsible for the high early strength of CSAC. Its hydration depends on the availability of sulfate. When calcium sulfate is present, C<sub>4</sub>A<sub>3</sub>Ŝ reacts with water and the calcium sulfate to produce ettringite and amorphous Al(OH)<sub>3</sub>. When all of the sulfate is consumed, the ettringite converts into monosulfate, an AFm phase. When not enough sulfate is present, AFm phases form; when too much sulfate is present, undesirable expansion occurs. The chemical reactions are presented below. [27-30]



The type of sulfate used during the hydration process has been studied and the results indicate that the amount and the reactivity of the added calcium sulfate influence the early hydration of the  $C_4A_3\dot{S}$  phase. [31]

Other phases, such as belite and ferrite, hydrate normally. However it has been noticed that when belite is present, C-S-H is not formed, but instead strätlingite,  $C_2ASH_8$ , forms from  $C_4A_3\dot{S}$  and/or  $AH_3$  and a source of silica. [30]

### 2.2.3. Physical Properties

The mechanical properties of these cements depend on the amounts of  $C_4A_3\dot{S}$  and minor phases included in the clinker and also on the sulfate present. Indeed, the addition of 15-25% by weight of calcium sulfate helps to control the setting time, the strength development and the volume stability. [25] CSAC matches OPC in performance [32], as it is capable of achieving similar compressive strength and flexural strength at a shorter time than OPC. Indeed, CSAC attains 75% of its ultimate strength in 24 hours versus about 40% for OPC. The main physical properties of CSAC are its very high early strength (35 MPa after 24 hours and 60 MPa after 28 days [27]), low permeability, good sulfate resistance, good corrosion resistance and controllable expansion. Because of their short working time, the use of set retarding admixtures may be required in order to gain more time for placing and finishing, and also to improve long-term strength, durability and consistency. [21, 23] These kinds of cements can be useful in other applications, as suggested by Péra [33], such as “self-leveling screed, self-leveling topping mortars and high performance glass-fiber-reinforced composites” because of the rapid formation of ettringite, expansion and low alkalinity. CSAC may also be used in hazardous waste encapsulation due to the low pH (compared to OPC), low porosity and the hydrate’s ability to bind heavy metals. [34-36]

### 2.2.4. Advantages and Disadvantages of OPC and CSA cement

Both cements present different properties which are summarized in Table 2-5.

Table 2-5: Advantages and Disadvantages of OPC and CSAC

Type of Cement	Ordinary Portland cement	Calcium sulfoaluminate cement
<b>Advantages</b>	C <sub>3</sub> S phase Processes very well known	C <sub>4</sub> A <sub>3</sub> S̄ phase Low firing temperature of 1250°C Low CO <sub>2</sub> -emissions Low-energy High early strength Use of by-products
<b>Disadvantages</b>	High CO <sub>2</sub> -emission High firing temperature of 1450°C	Expensive Specific Usage Need experts to use it, sets very quickly, Unknown durability

## 2.3. Alite-Calcium Sulfoaluminate cements

### 2.3.1. Relevancy of alite-calcium sulfoaluminate cements

Alite-calcium sulfoaluminate cement is an innovating cement for several reasons. First of all, this cement has the benefit of having both alite and calcium sulfoaluminate phases present in the clinker, which provides early and late strength in concrete. Because of the presence of C<sub>4</sub>A<sub>3</sub>S̄, this cement lowers the CO<sub>2</sub>-emissions compared to OPC. Also, the cement can be produced from by-products, so they would be less expensive to produce. Some researchers have already been able to produce this cement using by-products as raw materials (as further discussed in Section 2.3.3.). This cement is also being studied in China, but access to Chinese papers is limited. As defined in a paper from Tang and Lu, a “typical” C<sub>3</sub>S-C<sub>4</sub>A<sub>3</sub>S̄ cement has the following clinker composition (Table 2-6). [37]

Table 2-6: Typical clinker composition of a C<sub>3</sub>S-C<sub>4</sub>A<sub>3</sub>S̄ cement

Clinker phases	C <sub>3</sub> S	C <sub>2</sub> S	C <sub>4</sub> A <sub>3</sub> S̄	C <sub>4</sub> AF
Typical composition by wt. %	30-50	30-40	5-20	3-10



### 2.3.2. Effects of temperature on the different phases

The production of alite-calcium sulfoaluminate cement is challenged by the temperature formation of the two major clinker phases, alite and calcium sulfoaluminate, which do not form at the same range of temperatures in the clinker. In OPC, alite begins to form at around 1300°C [6], whereas in CSAC,  $C_4A_3\dot{S}$  begins to form at 900-1000°C and decomposes at a temperature close to 1300-1350°C. [38] Several studies demonstrate that the use of appropriate mineralizers and fluxes helps in overcoming this problem. By definition, a flux is an additive lowering the melting point of the first liquid formation [39], and a mineralizer is a minor component that reacts with a phase to lower its free energy ( $\Delta G$ ) via the entropy of mixing. This causes the temperature of formation of a phase to decrease, and so the phase will form at lower temperatures. [40] The combination of additives, containing  $SO_3$  and F, has made possible the production of this kind of cement. The additives used are often calcium sulfates, such as gypsum or anhydrite, combined with  $CaF_2$ . [39, 41-44] Because of these compounds, a liquid phase appears during the heating process at lower temperatures and can improve the formation of alite. [45-47] An intermediate phase, called fluorellestadite ( $3C_2S.3C\dot{S}.CaF_2$ ), forms and is stable up to 1240°C before decomposing into  $C_2S$  and a liquid phase. [39] The presence of this liquid phase at low temperatures enhances the kinetics of alite formation by accelerating the reaction between belite and lime to form alite. Normally, an excess of  $CaSO_4$  prevents the formation of alite [39], but  $CaF_2$  assists the formation of alite. [42] It has also been observed that  $CaSO_4$  and  $CaF_2$  accelerate the decomposition of  $CaCO_3$  at lower temperatures and improve the burnability of clinker (or in other terms the reactivity of the raw materials during the firing process), which is measured by the free lime content following the firing process. [44, 48] In summary, contrary to OPC where  $C_3A$  and  $C_4AF$  form the liquid phase,  $C_4AF$  and fluorellestadite form the liquid phase in alite-CSA cements. They actually interact with each other and decrease the melting point of the liquid phase necessary to form alite at low temperatures. [2] The addition of  $CaF_2$  has other advantages: it improves the mechanical properties, especially the compressive strength (approximately a 20% improvement), in clinker pastes with 0.4% of  $CaF_2$  added; and it also increases the amount of alite in this clinker by 15 wt. %. [42]

### 2.3.3. Formation / Production – Effects of CaF<sub>2</sub> and CaSO<sub>4</sub>

Some researchers have already produced both C<sub>3</sub>S and C<sub>4</sub>A<sub>3</sub>S̄ as the main clinker phases with additions of CaF<sub>2</sub> ranging from 0.5 to 1.0 wt. %, and by firing them from 1250°C to 1300°C. [49-54] An “exceptionally good grindability” of the clinker has been observed. [49] Also, some studies report that a small amount of MgO and TiO<sub>2</sub> influences the formation of important clinker phases. The addition of 2.0 to 5.0 wt. % of MgO assists with the formation of phases and the absorption of free lime [52]; the optimal quantity for TiO<sub>2</sub> is found to be below 1.0 wt. %. [54] The appropriate addition of these impurities can also improve the strength of cement or affect it negatively if an excess quantity is added and therefore delaying the setting time. Furthermore, during the hydration process, the amount of Ca(OH)<sub>2</sub> present is lower than in OPC [51], and the presence of AFt, C-S-H and AFm phases is observed. [53] The mechanical properties depend on the phase composition; hence C<sub>3</sub>S and C<sub>4</sub>A<sub>3</sub>S̄ affect early strength, whereas later strength is influenced by C<sub>4</sub>AF and C<sub>2</sub>S. The presence of C<sub>4</sub>A<sub>3</sub>S̄ also shortens the setting time compared to OPC. [50]

To illustrate the earlier statements, Table 2-7 presents some compressive strength data for different compositions of cement. The strength is thus influenced by the water/cement ratio, the amount of gypsum added and the curing process, which make the comparison of all these cement compositions challenging. However, this table provides a general idea of their characteristics.

Table 2-7: Description of some cement pastes with percentages by weight (wt. %) of the clinker phases and mechanical properties data

<b>Cement Names (from papers)</b>	<b>F-2</b>	<b>SY04</b>	<b>C6/6</b>	<b>M4</b>
<b>C<sub>3</sub>S</b>	23.99	45.19	40	44.4
<b>C<sub>2</sub>S</b>	2.87	22.10	40	28.8
<b>C<sub>4</sub>A<sub>3</sub>S</b>	58.73	13.34	10	14.8
<b>C<sub>4</sub>AF</b>	-	9.28	10	4.4
<b>C<sub>S</sub></b>	-	2.86	-	5.0
<b>Other phases</b>	C <sub>11</sub> A <sub>7</sub> .CaF <sub>2</sub> / C <sub>12</sub> A <sub>7</sub> 14.07%	MgO 3.87%	-	MgO 3.0%
<b>Firing Temp. (°C)</b>	1300	1250 to 1350	1250	1300
<b>Compressive Strength (MPa) at</b>				
1-day	27.3	34.0	15.9	-
3-day	36.0	43.0	36.3	74.1
7-day	45.0	-	-	89.3
28-day	49.1	52.4	79.0	119.5
180-day	-	-	113.6	-
<b>References</b>	[53]	[55]	[49, 50]	[52]
<b>Other Comments</b>	Paste w/c=0.50 Add 6% Gypsum	Paste w/c=0.4 Add 5% Gypsum and 5% Limestone	Paste w/c=0.35 6% SO <sub>3</sub> added	Paste w/c=0.30 Add 5% Gypsum

## 2.4. Influence of ferrite phase in Alite-Calcium Sulfoaluminate cements

### 2.4.1. Several interests in this kind of cements

The alite-calcium sulfoaluminate cement is a promising cement, based on its mechanical properties and low-cost production, and the study of integrating the ferrite phase into it is a novel breakthrough. In fact, this would increase the amount and diversity of useable by-products, especially red mud which is very rich in iron, and still decrease CO<sub>2</sub>-emissions compared to OPC. To summarize, this cement would be less expensive to produce, “greener”, and have better or at least similar mechanical properties compared to OPC and CSAC, by combining the best properties from these cements into one unique cement.

### 2.4.2. High iron cements

Conventional wisdom states that tetracalcium aluminoferrite  $C_4AF$  does not contribute much to the strength of OPC due to its slow reactivity, which is why the concentration of this phase is quite low in clinker. However, it has been demonstrated that a high iron cement paste without alite, had a compressive strength of about 31MPa (actually 4500 psi) after 7 days. [56] Quillin also found the same results with Belite-CSA-Ferrite (BCSAF) cements, where he explains that “the ferrite phase also appears to be somewhat reactive, as reported by Mehta”. [32] He concluded that this cement was behaving the same way as OPC when hydrated, and had similar results for compressive strength and carbonation tests (compared with blended Portland cements). Odler and Zhang studied mortars prepared from alite-calcium sulfoaluminate cements with  $C_4AF$  contents from 0 to 30 wt. %. From their data, C1/4 (70% $C_3S$ -30% $C_4AF$ ) had higher late strength at 28-day of 49.5MPa than C2/4 (70% $C_3S$ -20% $C_4AF$ -10% $C_4A_3\acute{S}$ ) or C3/4 (70% $C_3S$ -10% $C_4AF$ -20% $C_4A_3\acute{S}$ ), and C2/4 had the highest early strength at 1 day of 13.9MPa. When belite is included in the clinker, as for the C6/6 composition (40% $C_3S$ -40% $C_2S$ -10% $C_4AF$ -10% $C_4A_3\acute{S}$ ), the compressive strengths were 9.0, 15.2 and 34.1MPa at 1, 3 and 28 days respectively. [50] These experiments prove that the  $C_4AF$  phase can actually highly contribute to the strength of cement. This idea can be applied to alite-calcium sulfoaluminate-ferrite cements, and this is the research focus of this dissertation.

### 2.4.3. How to calculate phases – predictions with modulus values

The production of high-iron alite-calcium sulfoaluminate-ferrite cement requires the establishment of specific equations to formulate the clinker in appropriate proportions. By using the same method that Bogue used for his equations, the same logic is adopted to derive the “new” equations.

First of all, the following assumptions were made:

- 1- Five clinker phases are considered to form during the firing process of the raw materials:  $C_3S$ ,  $C_2S$ ,  $C_4A_3\acute{S}$ ,  $C_4AF$  and  $C\acute{S}$ ; the minor phases are neglected;
- 2- All of the iron is used to produce the  $C_4AF$  phase;
- 3- The remaining alumina from the step 2 is used to produce the  $C_4A_3\acute{S}$  phase;

- 4- All of the silicon dioxide initially present reacts to produce  $C_2S$ . Following this step, the remaining lime reacts with  $C_2S$  to finally form  $C_3S$ ;
- 5- The main liquid phase present during the formation of clinker phases is provided by the decomposition of the fluorellestadite ( $3C_2S.3C\acute{S}.CaF_2$ ) phase into  $C_2S$  and a liquid phase. The quantity of liquid phase (QLP modulus) depends on the percentage of  $CaF_2$  and  $CaSO_4$  (or  $C\acute{S}$ ) added to the raw materials.  $C_4AF$  can also be a part of the liquid phase depending on the selected firing temperature, as demonstrated by Zhou, which when both of these phases are present decrease their respective melting temperatures [2];
- 6- To ensure that enough  $CaF_2$  is present to form the liquid phase and other minerals, the minimum concentration of  $CaF_2$  in the clinker is related to the amount of fluorellestadite present which is equal to the quantity of liquid phase.

As with OPC, the introduction of moduli helps predict and design cement properties. In this case, new moduli are established from Zhou [2] and are explained below. The first modulus is called lime adequate degree (LAD) describing the ratio between the remaining CaO after reacting to form  $C_4AF$  and  $C_4A_3\acute{S}$  and the CaO required to form  $C_3S$  and  $C_2S$ .

$$LAD = \frac{(CaO - f_{CaO}) - 0.5499 Al_2O_3 - 1.0543 Fe_2O_3 - 0.7004 SO_3}{2.7999 SiO_2}$$

$$= \frac{C_3S + 0.8835 C_2S}{C_3S + 1.3253 C_2S}$$

The second modulus is named ratio of silicates and aluminates (RSA) which by definition defines the ratio between silicates and aluminates.

$$RSA = \frac{(CaO - f_{CaO}) + SiO_2 - 0.5500 Al_2O_3 - 1.0535 Fe_2O_3 - 0.7004 SO_3}{1.9951 Al_2O_3 + 1.7693 Fe_2O_3}$$

$$= \frac{C_3S + C_2S}{C_4A_3\acute{S} + C_4AF}$$

The third modulus describes the ratio of sulfoaluminates and ferroaluminates (RSF).

$$RSF = 0.6556 \frac{Al_2O_3}{Fe_2O_3} - 0.4186 = \frac{C_4A_3\acute{S}}{C_4AF}$$

The fourth modulus, called sulfur excessive coefficient (SEC), corresponds to the ratio of the remaining SO<sub>3</sub> in the clinker after forming the liquid phase and the SO<sub>3</sub> requested for the formation of C<sub>4</sub>A<sub>3</sub>S̄. This ratio exceeds 1.0 in order to have sufficient SO<sub>3</sub>, which explains its name SEC.

$$SEC = \frac{SO_3 - 3.0766 CaF_2}{0.2617 Al_2O_3 - 0.1671 Fe_2O_3} = 1 + 4.4825 * \frac{CaSO_4 - 5.2315 CaF_2}{C_4A_3\bar{S}}$$

The last modulus, named quantity of liquid phase (QLP), represents the percentage of liquid phase in the clinkers during the firing process.

$$QLP = 12.8494 CaF_2$$

The last two moduli, SEC and QLP, were studied by Zhou in order to evaluate the appropriate amount of CaSO<sub>4</sub> and CaF<sub>2</sub> needed for the reactions to be optimal. [2]

First, specific compositions of clinker with fixed modulus values (LAD=0.95, RSA=2.80 and RSF=2.10) and variable SEC and QLP moduli were prepared and tested for free lime content to study the “burnability” of each composition (Table 2-8). The raw materials used for this experiment were reagent materials. They were pressed into pellets and heated at 1300°C for 30 minutes before being quenched with compressed air. The free lime content was then determined and presented in Figure 2-2.

Table 2-8: Phase composition of samples tested [2]

<b>LAD/RSA/RSF 0.95/2.80/2.10</b>	
<b>Clinker Phase</b>	<b>wt. %</b>
<b>C<sub>3</sub>S</b>	58.80-63.52
<b>C<sub>2</sub>S</b>	7.83-8.63
<b>C<sub>4</sub>A<sub>3</sub>S̄</b>	15.93-17.31
<b>C<sub>4</sub>AF</b>	7.59-8.24
<b>CaSO<sub>4</sub></b>	2.03-8.95
<b>CaF<sub>2</sub></b>	0.39-1.17

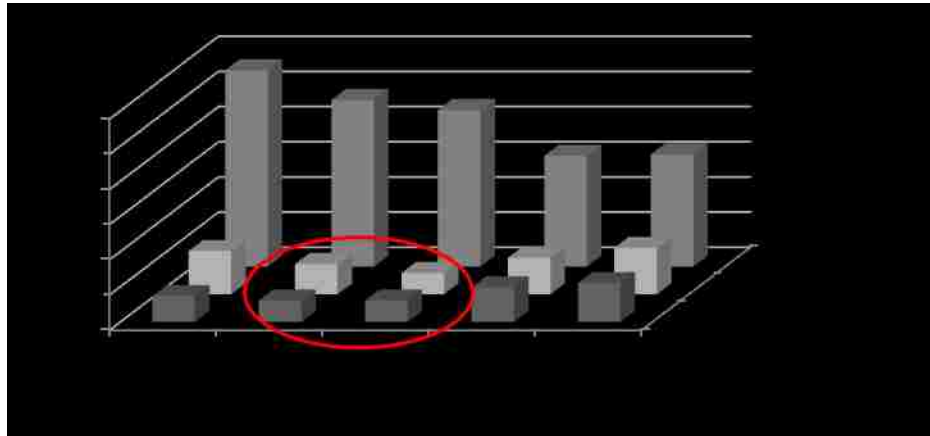


Figure 2-2: Influence of SEC and QLP modulus on free lime [2]

In this case, the optimum SEC and QLP modulus for this composition was 1.20-1.40 and 0.1-0.15 respectively, where the lowest values for free lime were detected.

This test was extended by modifying all the moduli in order to analyze the influence of each modulus on the “burnability” of different clinkers. Eighteen clinkers were produced from reagent chemicals with the same preparation method presented earlier (p.24), and their mineralogical compositions, moduli, and the free lime determinations are presented in Table 2-9. From these experiments, the optimal moduli were found to be SEC=1.20 and QLP=0.10. Regarding the other modulus values, it was determined that low LAD and RSF moduli led to improved burnability. Free lime results were all below 2%, which is the maximum amount allowed for the production of an acceptable clinker, and the use of reagent chemicals helped obtaining low free lime values.

Table 2-9: Study of free lime while varying all moduli [2], with “S#” meaning sample number (bold and italic numbers are related to a group where only one modulus value varies; green numbers are related to the same sample S#03 as it is a reference sample; and red numbers highlight the lowest free lime content for each group and firing temperature tested)

S#	Clinker phases						Modulus Values					Free Lime (%)	
	C <sub>3</sub> S	C <sub>2</sub> S	C <sub>4</sub> A <sub>3</sub> S	C <sub>4</sub> AF	CaSO <sub>4</sub>	CaF <sub>2</sub>	LAD	RSA	RSF	SEC	QLP	1300°C	1350°C
<b>01</b>	49.56	20.96	15.63	7.81	5.46	0.78	<b>0.88</b>	3.00	2.00	1.40	0.10	<b>0.64</b>	<b>0.43</b>
<b>02</b>	53.33	17.18	15.63	7.81	5.46	0.78	<b>0.90</b>	3.00	2.00	1.40	0.10	0.70	0.49
<b>03</b>	56.97	13.54	15.63	7.81	5.47	0.78	<b>0.92</b>	3.00	2.00	1.40	0.10	0.85	0.61
<b>04</b>	60.51	10.01	15.63	7.81	5.47	0.78	<b>0.94</b>	0.50	2.00	1.40	0.10	0.92	0.72
<b>05</b>	24.99	5.89	40.68	20.34	7.70	0.78	0.92	<b>0.50</b>	2.00	1.40	0.10	1.82	1.33
<b>06</b>	37.59	8.91	30.80	15.40	6.82	0.78	0.92	<b>1.00</b>	2.00	1.40	0.10	1.23	0.55
<b>07</b>	50.45	11.98	20.74	10.37	5.92	0.78	0.92	<b>2.00</b>	2.00	1.40	0.10	0.79	0.54
<b>03</b>	56.97	13.54	15.63	7.81	5.47	0.78	<b>0.92</b>	3.00	2.00	1.40	0.10	0.85	0.61
<b>08</b>	60.92	14.48	12.54	6.27	5.19	0.78	0.92	<b>4.00</b>	2.00	1.40	0.10	<b>0.78</b>	<b>0.49</b>
<b>09</b>	76.92	18.31	0.01	0.00	4.07	0.78	0.92	<b>9967</b>	1.91	1.18	0.10	0.96	0.79
<b>10</b>	57.35	13.63	7.87	15.74	4.77	0.78	0.92	3.00	<b>0.50</b>	1.40	0.10	<b>0.42</b>	<b>0.30</b>
<b>11</b>	57.16	13.59	11.76	11.76	5.12	0.78	0.92	3.00	<b>1.00</b>	1.40	0.10	0.61	0.31
<b>03</b>	56.97	13.54	15.63	7.81	5.47	0.78	<b>0.92</b>	3.00	2.00	1.40	0.10	0.85	0.61
<b>12</b>	56.83	13.50	18.70	4.67	5.74	0.78	0.92	3.00	<b>4.00</b>	1.40	0.10	0.98	0.49
<b>13</b>	57.79	13.74	15.86	7.93	4.07	0.78	0.92	3.00	2.00	<b>1.00</b>	0.10	<b>0.43</b>	<b>0.43</b>
<b>14</b>	57.38	13.64	15.74	7.87	4.77	0.78	0.92	3.00	2.00	<b>1.20</b>	0.10	0.79	0.49
<b>03</b>	56.97	13.54	15.63	7.81	5.47	0.78	<b>0.92</b>	3.00	2.00	<b>1.40</b>	0.10	0.85	0.61
<b>15</b>	56.58	13.44	15.51	7.76	6.15	0.78	0.92	3.00	2.00	<b>1.60</b>	0.10	0.97	0.61
<b>16</b>	58.10	13.82	15.95	7.97	3.86	0.47	0.92	3.00	2.00	1.40	<b>0.06</b>	1.53	0.86
<b>17</b>	57.54	13.67	15.79	7.89	4.66	0.62	0.92	3.00	2.00	1.40	<b>0.08</b>	1.16	<b>0.49</b>
<b>03</b>	56.97	13.54	15.63	7.81	5.47	0.78	<b>0.92</b>	3.00	2.00	1.40	<b>0.10</b>	0.85	0.61
<b>18</b>	56.42	13.39	15.47	7.73	6.26	0.94	0.92	3.00	2.00	1.40	<b>0.12</b>	<b>0.61</b>	0.55

The XRD scans for each sample showed clearly the presence of each phase which demonstrated the possibility of producing alite-calcium sulfoaluminate-ferrite cement. When QLP increased, the C<sub>4</sub>A<sub>3</sub>S peak was higher and more well-defined, as was the alite peak. This behavior is explained by the increase of liquid phase in the clinker, which, as in OPC, contributes to the formation of alite (C and C<sub>2</sub>S react more efficiently when a liquid phase is present).

By following this logic for this dissertation research, three moduli were kept constant for the production of the clinkers to obtain the optimum composition. Consequently, LAD, SEC and QLP were kept constant at 0.88, 1.20 and 0.10 respectively. The other moduli varied to observe the influence of the amount of ferrite on the clinker composition.

Because of the presence of “impurity” elements other than Ca, Al, Fe, Si and S in the industrial by-products, care was taken when by-products were used as raw materials for the production of these compositions.





## Chapter 3 : Materials and Methods

### 3.1. Materials

#### 3.1.1. Reagents chemicals (RC)

Reagent grade chemicals were obtained from Acros Organics and Sigma Aldrich. The purity of chemical reagents was confirmed by contacting each company and inquiring as to the exact purity of each chemical. Table 3-1 presents the information provided by the companies. Anhydrite was obtained by drying Hemihydrate at 500°C for 4 hours and the purity of the product was controlled by XRD analysis.

Table 3-1: Chemical composition of each product in percentage by weight (AO: Acros Organics and SA: Sigma Aldrich)

Chemicals	Ca(OH) <sub>2</sub>	SiO <sub>2</sub>	Al(OH) <sub>3</sub>	Fe <sub>2</sub> O <sub>3</sub>	CaSO <sub>4</sub> .1/2H <sub>2</sub> O	CaF <sub>2</sub>	CaSO <sub>4</sub>
<b>Brands</b>	AO - 98+% extra pure	SA – 99.6 %	AO – extra pure powder	SA – 99%	AO – 97%+	SA –	CaSO <sub>4</sub> .1/2H <sub>2</sub> O, dried
<b>Purity (%)</b>	97.6	99.6	-	99.0	100.0	99.5	100.0
<b>CaO</b>	73.8	-	-	-	39.21	-	41.19
<b>SiO<sub>2</sub></b>	-	99.60	-	-	-	-	-
<b>Al<sub>2</sub>O<sub>3</sub></b>	-	-	65.00	-	-	-	-
<b>Fe<sub>2</sub>O<sub>3</sub></b>	-	-	-	99.00	-	-	-
<b>SO<sub>3</sub></b>	-	-	-	-	55.99	-	58.81
<b>LOI</b>	23.73	0.50	34.45	-	4.80	0.30	-
<b>CaF<sub>2</sub></b>	-	-	-	-	-	99.50	-
<b>Sum</b>	97.60	100.1	99.45	99.00	100.00	99.80	100.00

#### 3.1.2. By-Products (BP)

Several by-products were used during this research work and are described below:

- Agricultural hydrated lime from South States is a natural “alternative” insecticide, essentially composed of calcium hydroxide.

- Bottom ash is a by-product from the combustion of coal. Both bottom and fly ashes are produced from a circulating fluidized bed combustor (CFBC). This process burns coal with limestone, which absorbs sulfur dioxide SO<sub>2</sub>, to form anhydrite CaSO<sub>4</sub>.

- Class C fly ash is a by-product of coal combustion at electric utility plants, and is generally composed of aluminosilicate glass, quartz, mullite and unburned carbon. There are actually two types of fly ashes classified as Class F (low calcium) and Class C (high calcium).

- Bauxite, which is largely aluminum hydroxide, is the principal aluminum ore, and is very expensive.

- Red mud is a by-product of the Bayer process, which refines bauxite to produce alumina. As a low-cost waste material, this by-product is generally disposed as a slurry with a solid concentration range of 20-40 wt. %, and essentially composed of iron. Their composition actually depends on the bauxite source. [57]

- Blast furnace slag fines is an air cooled blast furnace slag (BFS). This by-product is a glassy and granular material produced from quenching molten iron slag (by-product of iron and steel-making), from a blast furnace, in water or steam. This glassy material is then dried and ground into a fine powder before utilization.

The chemical composition of these by-products performed by X-ray fluorescence (XRF) is presented in Table 3-2. The particle size  $d(0.5)$  in  $\mu\text{m}$ , representing the volume median diameter where 50% of the distribution is above and 50% below this value, is also included in Table 3-2.

Table 3-2: Chemical composition of by-products from XRF analysis in wt. % (\*data from Fisher website)

	<b>Hydrated Lime</b>	<b>Bottom Ash</b>	<b>Red Mud</b>	<b>Bauxite</b>	<b>BFS</b>	<b>Class C Fly Ash</b>	<b>Fluorite</b>
<b>CaO</b>	65.27	45.91	6.96	0.16	38.34	26.28	-
<b>SiO<sub>2</sub></b>	1.96	15.30	9.41	6.64	37.03	35.24	-
<b>Al<sub>2</sub>O<sub>3</sub></b>	1.56	5.95	15.33	58.54	10.25	20.47	-
<b>Fe<sub>2</sub>O<sub>3</sub></b>	0.42	3.44	41.81	6.28	1.13	5.13	-
<b>SO<sub>3</sub></b>	0.07	23.14	0.44	0.24	0.80	1.83	-
<b>LOI</b>	29.83	4.61	12.81	27.60	0.54	0.38	0.30
<b>MgO</b>	2.11	1.99	0.45	0.20	10.99	5.04	-
<b>K<sub>2</sub>O</b>	0.07	0.47	0.18	0.01	0.39	0.46	-
<b>Na<sub>2</sub>O</b>	0.11	0.11	1.59	0.01	0.30	1.47	-
<b>P<sub>2</sub>O<sub>5</sub></b>	0.01	0.11	0.74	0.22	0.01	1.43	-
<b>TiO<sub>2</sub></b>	0.07	0.30	5.70	2.18	0.49	1.24	-
<b>CaF<sub>2</sub></b>	-	-	-	-	-	-	100.00
<b>Sum</b>	101.48	101.33	95.42	102.08	100.27	98.97	100.00
<b>d(0.5)</b>	9.6235	25.214	14.706	17.462	14.792	9.0715	1.82*

## 3.2. Methods

### 3.2.1. Production and Firing Processes

The preparation was the same for both raw materials, RC and BP. The only differences came from the size of the batch, small at 50g or large at 500-2000g.

The raw materials were proportioned by weight (see Figures 3-1 and 3-2), and mixed in a mortar and pestle (for small batches), or in a bar mill (for large batches), until a complete homogenization of the powder was obtained. This was observed when all the iron had uniformly colored the entire batch and all the hydrated lime was crushed (no more white fragments present). The mixtures for the small batches were then placed in a glass jar and “rolled” (like for a ball mill) for approximately 15 minutes. This step was not necessary for the production of the large batches as they were already mixed in a bar mill for 15 minutes. The samples were finally mixed with 10% by weight of deionized water and pressed into 28x7mm pellets for the small pellets, or 57x7mm for the large pellets, as shown in Figure 3-3.



Figure 3-1: Batches produced from reagent chemicals (RC)



Figure 3-2: Batches produced from by-products (BP)



Figure 3-3: Small pellets for each batch produced from RC and BP before firing

The samples were placed either in a platinum crucible (for small pellets) or on an alumina plate covered by a thick layer (1-2mm) of zirconium dioxide (for large pellets), to ensure the non-contamination of the samples with the ceramic plate. Pictures of the disposition of the pellets are displayed in Figures 3-4 and 3-5.

A specific furnace, as shown in Figure 3-6, was used with a front door opening to facilitate the rapid removal of the pellets for the quenching procedure. This Carbolite ® furnace can generate heat up to 1500°C. The firing program followed is displayed in Figure 3-7. The only difference was that the clinkerization temperature varied depending on the clinker studies performed during the preliminary experiments, presented in Chapter 4. The firing temperature for each batch composition was then settled when the production of large batches started.



Figure 3-4: Front view of the arrangement of the pellets in the platinum crucible on the left, and on a thick layer of ZrO<sub>2</sub> (1-2 mm) on the right



Figure 3-5: Top view of the arrangement of the pellets in the platinum crucible



Figure 3-6: Front view of the Carbolite ® furnace

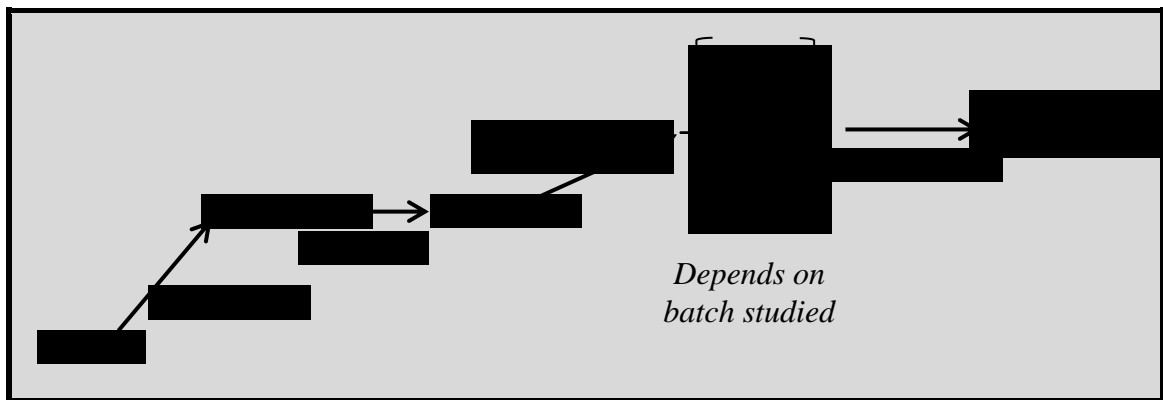


Figure 3-7: Firing program followed with the box furnace for the preliminary experiments

Quenching of the hot clinker was completed by rapidly removing the clinker from the hot furnace (Figure 3-8) and immediately placing it beneath an arrangement of powerful fans, as seen in Figure 3-9.

Following quenching, each batch was crushed in a shatter box for 45 seconds (for each small pellet), or until  $d(0.5)$  was approximately  $15\mu\text{m}$  (for large pellets). The samples were then analyzed by XRD/Rietveld, SEM/EDS and free lime analyses. The parameters used for the analyses are described in Section 3.2.2.



Figure 3-8: Carbolite ® furnace with front opening to facilitate quenching step



Figure 3-9: Ventilator used to quench the pellets

### 3.2.2. Characterization Instruments

Following the firing step, characterization tests were performed on the finely ground clinker to determine and confirm the chemical and mineralogical composition of the samples.

#### 3.2.2.1. “Burnability Test” (Free Lime Determination)

A “burnability test” was first carried out by determining the free lime content in the clinker after the firing step by following ASTM C 114-06, called “Rapid  $\text{Sr}(\text{NO}_3)_2$  Method”, or also “Alternative Test Method B”. [58] This procedure gives an approximation of the free lime as uncombined  $\text{CaO}$ , and thus the extent of the clinkering reactions. If more than 3.0% of free lime was present, which is generally the maximum allowed (preferably below 2%) [8], firing parameters were modified to minimize the free lime content. Low free lime cements show higher late strength than cement with high

level of free lime. Therefore the maximum free lime allowed in this work was targeted to be 1.0 wt. % or less.

#### **3.2.2.2. *X-Ray Diffraction coupled with Rietveld Refinement (XRD/Rietveld)***

The next characterization method used was powder X-ray Diffraction (XRD) with Rietveld refinement. XRD is a non-destructive analytical method able to determine the crystal structure, chemical composition and physical properties of materials; here the determination of the different phases in the clinker and hydrated cement pastes is its primary purpose. Rietveld refinement was developed by H. M. Rietveld to first refine neutron diffraction data [59] and then adapted for XRD by Malmros and Thomas and by Young. [60, 61] The appropriate description of the method is as follows: “The principal of the method is that the intensities calculated from a model of the crystalline structure are fitted to the observed X-ray powder pattern by a least squares refinement”. [62] In order to fit both patterns as close as possible, parameters are modified such as crystal structure and peak profiles parameters. A semi-automatic analysis is performed first, and then different parameters are modified until the GOF (goodness of fit) is acceptable (usually  $1.20 \pm 0.05$ ).

The XRD software was X’Pert HighScore Plus from PanAlytical and the XRD results were obtained with a Philips X’Pert diffractometer (PW3040-PRO X’Pert) operating at 45 kV and 40 mA. The samples were ground by hand in a ceramic mortar and pestle, dry mounted in aluminum holders, and scanned at  $8-60^\circ 2\theta$  with Cu K- $\alpha$  radiation for a simple XRD, or at  $8-90^\circ 2\theta$  for a Rietveld analysis. All pattern diffraction files (PDF) used for the identification of clinker and hydrated phases are shown in Appendix A. [63]

#### **3.2.2.3. *X-Ray Fluorescence (XRF)***

X-ray fluorescence (XRF) analyses were performed to determine the chemical composition of samples in term of major oxides and trace elements. All XRF analyses were conducted following ASTM D 4327-97 [64] and performed in a PW 2404 x-ray spectrometer, from Thermo Scientific Philips. XRF analyses were only performed on industrial by-products as it was noticed that the determination of the chemical



composition of samples with a high iron content was inaccurate. Further explanations are presented in Appendix D.

#### ***3.2.2.4. Scanning Electron Microscope coupled with Energy-Dispersive X-Ray Spectroscopy (SEM/EDS)***

Sample preparation is a very critical step to the study of clinkers using scanning electron microscopy with energy-dispersive X-ray spectroscopy (SEM/EDS). The sample requires a very flat and finely polished surface. Furthermore, due to the small amount of each batch (about 10g) produced in this research for the preliminary experiments, small epoxy pellets were prepared. The method selected consisted of drilling a hole of about 5mm diameter into a standard size pellet of 2.5cm diameter so as to reduce the quantity of sample necessary for their analysis. The clinker : epoxy ratio by mass was kept at 2:1 at all times, as it was necessary to have enough particles to obtain sufficient information, but not to have a too viscous mixture which would contain a lot of voids. The clinker was then gently mixed with the ultrathin epoxy with a glass rod to avoid any air entrapment. This mixture was then poured into the drilling hole of a previously made epoxy pellet. The sample pellet was cured for 24 hours in an oven at 40°C, followed by another 24 hours in a vacuum desiccator to prevent hydration.

The appropriate polishing method for this work was carefully selected by comparing methods developed by different researchers [65-69]. The most appropriate method for polishing these specific clinkers was designed to not result in clinker hydration or disintegration during the polishing step. Once the samples were ready, six of them were loaded into an automatic grinder/polisher. When there were not enough samples to completely load the machine, blank epoxy samples were used to homogenize the force provided from the grinder/polisher. Silicon-carbide paper #60 was first used to obtain a flat surface. The next papers were #240, #400 and #600 for 1 to 3 minutes, or until the scratches caused by the previous paper were replaced by the uniform scratches from the new paper. During each grinding step, no solvent was used.

Following the grinding step, each sample was polished with different diamond pastes: 5µm, 1µm and 0.25µm. The diamond paste is composed of diamond particles (less than

15%) in a non-aqueous solution, more specifically in polyethylene glycol (PEG-more than 90%). The paste was applied on a TekMet® C cloth with some propylene glycol drops. Several minutes were required to remove all the scratches and produce a nice polished surface.

The speed for both steps, grinding and polishing, was kept at a constant 150 rpm. For grinding steps, the mechanical grinder/polisher rotated to the left; and polishing was done in the opposite direction. The applied force of approximately 50N was the same in all steps. Between each grinding and polishing step, the samples were washed with isopropanol to prevent them from hydrating. Finally, when all samples were polished, they were placed in an ultrasonic bath of isopropanol to eliminate any inclusions of impurities at the surface. The final samples, as shown in Figures 3-10 and 3-11, were then kept in a vacuum desiccator until SEM/EDS analyses were performed.



Figure 3-10: Front view of prepared epoxy samples



Figure 3-11: Top view of prepared epoxy samples

SEM/EDS is used to identify clinker phases through elemental mapping and hence confirm the results from the previous methods, such as XRD/Rietveld and free lime tests. The optimum parameters were identified through an iterative process, based upon the materials framework of the study. The investigated parameters included the number of frames required to obtain an image which can be worked with easily, the quality of the images (number of pixels), the working distance, the current and ampere used.

When ready for SEM/EDS analyses, the samples were removed from the desiccator and coated with carbon to obtain a conductive surface. The coating process was done at least two times, by turning the sample 45° between the two coatings to get an uniform layer of carbon. Carbon coating was chosen because this material does not interfere with EDS analyses. The sample was then loaded into the Hitachi S-4800 SEM, and different parameters were adjusted to have an optimal image for EDS analyses. First, the largest

aperture available of 100 $\mu$ m was used. The working distance was chosen as 15.0mm, with a voltage of 15kV and a current of 20 $\mu$ A. The magnification was actually very low, from 100 to 150x, to obtain a large sampling of particles without zooming on a specific area. The area studied was then “locked”, meaning that the sample was unable to move which was very decisive during the collecting of 50 frames of the same area. After selecting the area to be analyzed and adjusted all the SEM parameters, the EDS instrument (Oxford Instruments X-Max-50mm<sup>2</sup> - Inca Energy software) was turned on. The quality of all of the images was set at 512 by 512 pixels. In the quest of getting the most information as possible, 50 frames were taken for the same area with a dwell time of 200 $\mu$ s. The dead time was kept below 10% and the x-ray count rate between 3.0 and 6.0 kcps with a process time set at 4.

Elemental maps were obtained for Ca, Si, Al, Fe, S, Mg and Ti and saved in a \*.tif file as seen on Figure 3-12. These images were then analyzed with the utilization of two software packages called ImageJ and MultiSpec. These software packages were previously used in several studies and demonstrated accurate results. [65, 70]

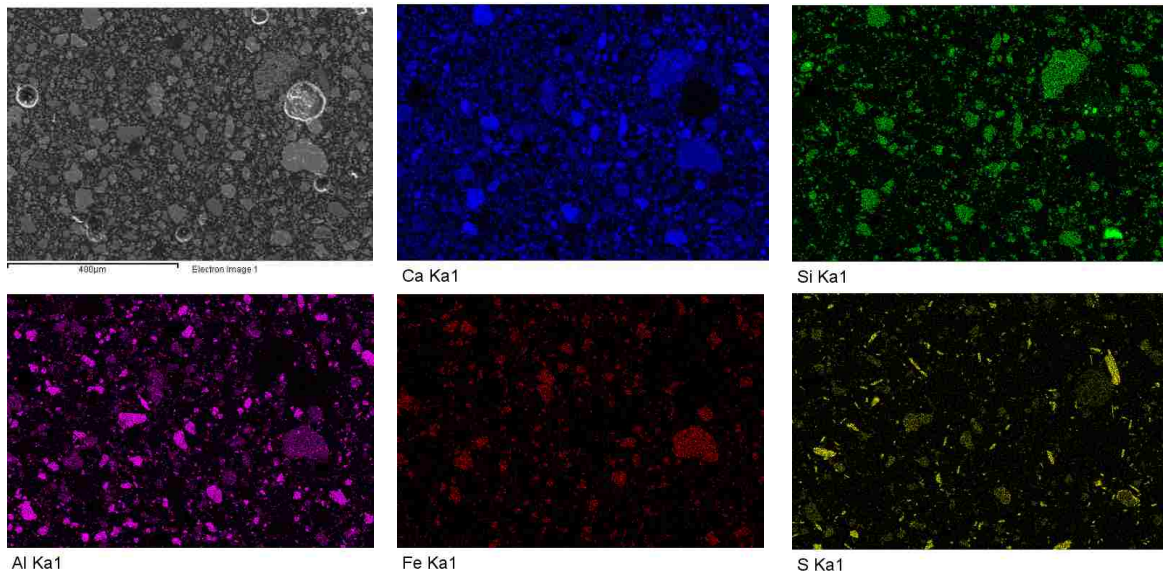


Figure 3-12: SEM images and elemental maps of calcium, silicon, aluminum, iron and sulfur of a clinker sample composed theoretically of 30.6 wt. %  $C_3S$ , 13.3%  $C_2S$ , 15.3%  $C_4A_3S$ , 35.7%  $C_4AF$  and 5.1% of  $CS$  (861 $\mu$ m width)

ImageJ [71] is specially used for displaying, editing, analyzing and processing the “raw” images extracted from the EDS instrument program. Each elemental map was first individually processed through ImageJ. The first step was to crop the pictures to remove the caption below each image, and make them all of identical size for superimposition. The images were then modified to black and white 8-bit. The brightness/contrast was first adjusted automatically and then manually depending on the image, especially for minor elements, such as iron, where noise was often present. A median filter of radius 1.0 was finally used to obtain the final image of the elemental map.

As an example, a sample was composed of 30.6%  $C_3S$ , 13.3%  $C_2S$ , 15.3%  $C_4A_3\dot{S}$  and 5.1%  $C\dot{S}$  by weight. This sample was prepared from mixing pure clinker phases, previously produced separately and confirmed as pure clinker phases by XRD. The EDS images were first extracted as \*.tif files as seen on Figure 3-12. Each elemental map was individually cropped (Figure 3-13-a) to remove the caption and modified to an 8-bit type greyscale to be processed through the MultiSpec software. An automatic adjustment of the brightness and contrast (Figure 3-13-b) was applied to optimize the quality of each image and a median filter of radius 1.0 was applied to reduce the noise (Figure 3-13-c). All these images were saved for the MultiSpec software.

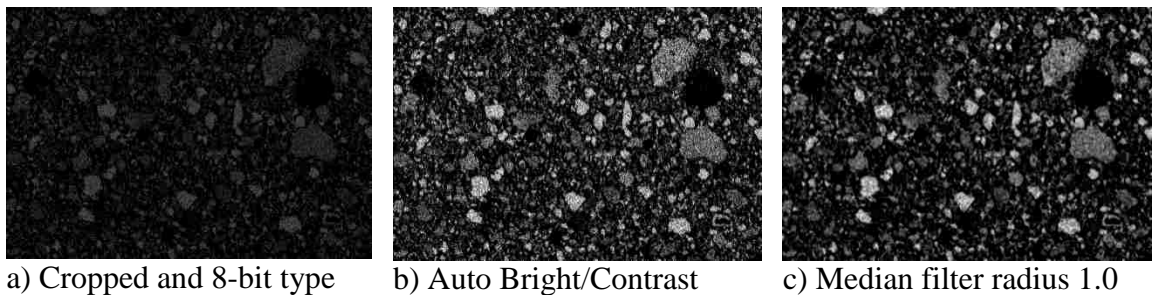


Figure 3-13: The different steps processed through ImageJ software for the calcium elemental map from Figure 3-12 (861  $\mu\text{m}$  width)

MultiSpec [72] is a software program that is capable of displaying different information of the same area. It is especially useful as the program is able to link all elemental maps in one image and thus the quantification of each clinker phase can be determined. Greyscale images of 512x512 pixels, as X-ray maps saved in .tif files, were required for the MultiSpec software to analyze them. The individual elemental maps of the same area

were then linked to each other and the clinker phases were identified and quantified using the “unsupervised cluster analysis” procedure from Lydon. [73] Forty clusters were selected to identify as many phases as possible and each cluster was assign to a specific clinker phase.

The detailed procedure followed here is described below:

- 1- First the elemental maps (Ca, Si, Al, Fe, S and Mg for by-products compositions) were linked together with the MultiSpec software, producing a multispectral image stack (Figure 3-14);
- 2- Because of the difficulty in analyzing the multispectral image stack, Lydon’s method was used [73]. His procedure consists of the quantification of the clinker phases through an unsupervised clustering analysis. The 40 clusters were applied to assure that all clinker phases, even minor ones, were detected (Figure 3-15);

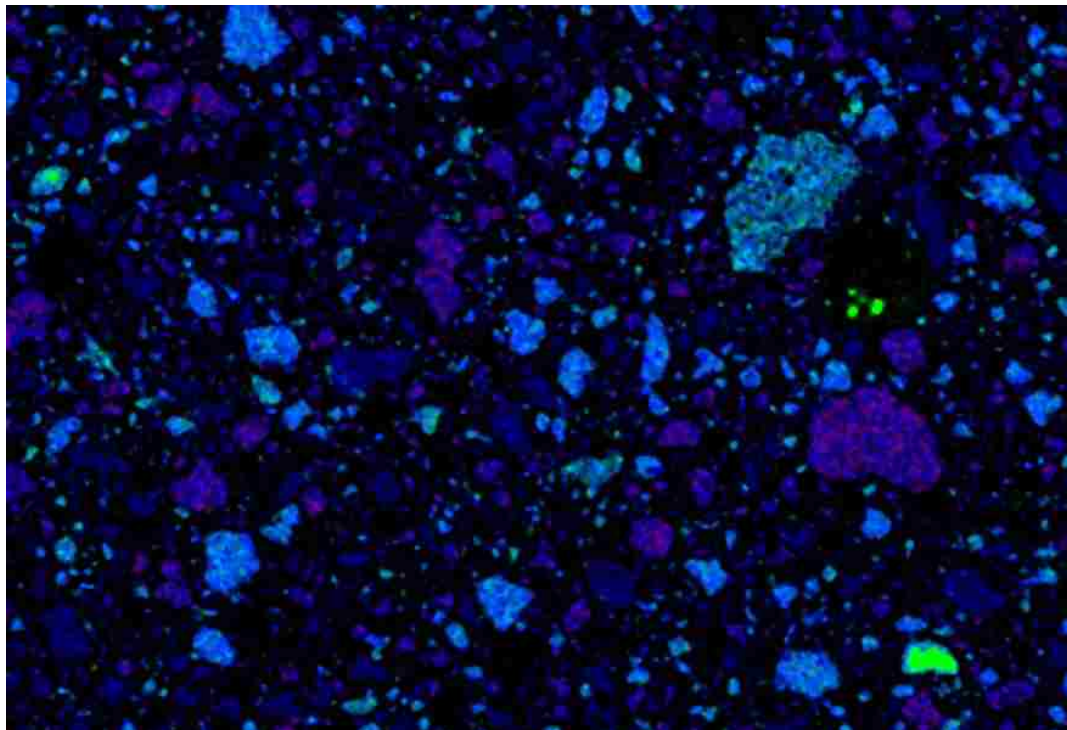


Figure 3-14: Multispectral image stack of the elemental maps (861 $\mu$ m width)

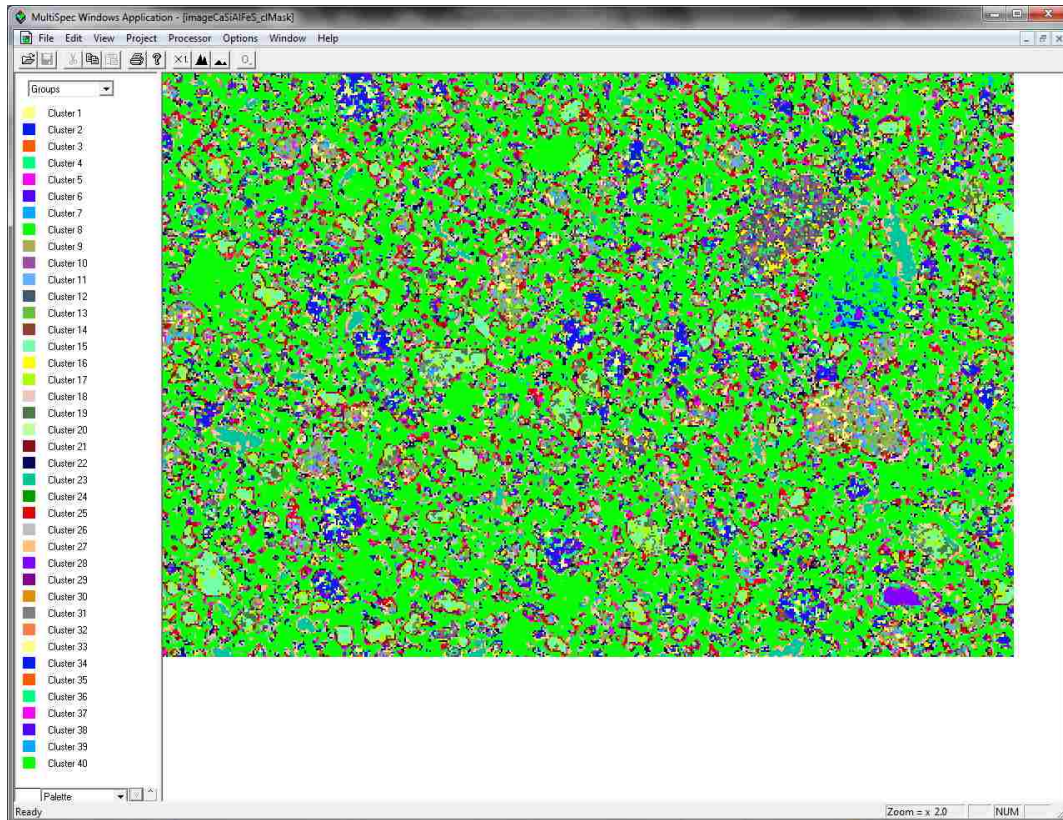


Figure 3-15: Unsupervised clustering analysis

- 3- This unsupervised clustering analysis provides a table including the number of pixels assigned to each cluster, which also represents the percentage of the surface occupancy of each cluster as seen in Figure 3-16.

The next part of the procedure is dependent on the scientist judgment, who by his/her own choices, decides the assignment of a cluster to a specific clinker phase. The general method follows Lydon's procedure. [73] The first step was to identify the main elements present in each cluster, which was represented by the light blue and purple colors in Figure 3-17. Once decided, the assignment of each cluster to a clinker phase was processed. For example in Figure 3-17, the cluster #11 is composed of calcium, aluminum and iron which matches with the composition of ferrite. This step also depends on the greyscale value for each element which is proportional to its amount in the clinker phase. It was decided not to independently differentiate alite from belite in order not to introduce

additional error because the differentiation between the two silicate phases was very difficult.

Final cluster class statistics.								
Cluster	Pixels	%	Channel Means					
			Ca	Si	Al	Fe	S	
1	1,400	0.8	243.9	123.7		1	0	0.5
2	2,553	1.4	244.4	71.3		0.9	0	0.5
3	877		194.3	17		1.3	0.1	0.6
4	1,765	1	199.1	136.8		0.9	0	0.4
5	561	0.3	171.2	0		73.3	70.8	0.5
6	3,349	1.9	198.9	64.8		0.8	0	0.5
7	875	0.5	168.7	0.2		40	18.4	1.5
8	2,102	1.2	180	95.2		0.7	0	0.4
9	2,083	1.2	136.7	0		56	71.8	0.7
10	2,690	1.5	144.1	107.6		0.8	0	0.6
11	1,432	0.8	158.6	0.3		75	17.9	1.6
12	3,658	2	131.3	63.9		1	0	0.5
13	4,590	2.6	112.8	0.1		74.3	16.2	1.3
14	3,872		134.1	8.6		10.5	5.9	0.7
15	4,040	2.3	89	0		209.3	0.1	40.4
16	3,136	1.8	91.2	40		0.7	0	0.6
17	3,721	2.1	69.2	0		158.9	1.1	19.9
18	3,897	2.2	99	1.6		15.8	7.4	0.9
19	787	0.4	100.2	0.1		166.8	0	112
20	301	0.2	88.4	4		9.9	0.1	75.2
21	2,434		49.4	0.1		102.7	3.2	7
22	6,844		70	5.6		3.5	1.8	1.1
23	1,961	1.1	69.3	0		0.9	0	242.2
24	1,267		46	1.8		3.9	0.6	13
25	6,103		57.1	0.2		41.5	6.9	2.2
26	11,265		46	3.3		3.7	1.2	0
27	1,790	1	42.4	0		2	0	146.2
28	269		19.8	248.3		1	0	0.6
29	2,258		11	0		69.2	1	5.5
30	990	0.6	54.5	73.7		1.3	0	0.7
31	963	0.5	61.4	0.5		109.5	0	69.5
32	920	0.5	28.7	0.1		3.5	0	65
33	1,432	0.8	89.8	0		54.9	70.5	0.6
34	2,376		10.5	20		1.4	0	1.8
35	962		9.4	0.1		33	0.4	13
36	403		10.2	60.1		1.4	0	2.9
37	3,515		9.5	0.1		33	1.5	0
38	938		12.1	0.1		6.1	21.9	0.4
39	788		0	1.8		2.1	0	65
40	83,683		4	0		2.1	0	1.1
		100.2						

Figure 3-16: Cluster analysis of a sample before identification of each cluster

Final cluster class statistics.								
Cluster	Pixels	%	Channel Means					
			Ca	Si	Al	Fe	S	
1	1,400	0.8	243.9	123.7		1	0	0.5
2	2,553	1.4	244.4	71.3		0.9	0	0.5
3	877	0.5	194.3	17		1.3	0.1	0.6
4	1,765	1	199.1	136.8		0.9	0	0.4
5	561	0.3	171.2	0		73.3	70.8	0.5
6	3,349	1.9	198.9	64.8		0.8	0	0.5
7	875	0.5	168.7	0.2		40	18.4	1.5
8	2,102	1.2	180	95.2		0.7	0	0.4
9	2,083	1.2	136.7	0		56	71.8	0.7
10	2,690	1.5	144.1	107.6		0.8	0	0.6
11	1,432	0.8	158.6	0.3		75	17.9	1.6
12	3,658	2	131.3	63.9		1	0	0.5
13	4,590	2.6	112.8	0.1		74.3	16.2	1.3
14	3,872	2.2	134.1	8.6		10.5	5.9	0.7
15	4,040	2.3	89	0		209.3	0.1	40.4
16	3,136	1.8	91.2	40		0.7	0	0.6
17	3,721	2.1	69.2	0		158.9	1.1	19.9
18	3,897	2.2	99	1.6		15.8	7.4	0.9
19	787	0.4	100.2	0.1		166.8	0	112
20	301	0.2	88.4	4		9.9	0.1	75.2
21	2,434	1.4	49.4	0.1		102.7	3.2	7
22	6,844	3.8	70	5.6		3.5	1.8	1.1
23	1,961	1.1	69.3	0		0.9	0	242.2
24	1,267	0.7	46	1.8		3.9	0.6	13
25	6,103	3.4	57.1	0.2		41.5	6.9	2.2
26	11,265	6.3	46	3.3		3.7	1.2	0
27	1,790	1	42.4	0		2	0	146.2
28	269	0.2	19.8	248.3		1	0	0.6
29	2,258	1.3	11	0		69.2	1	5.5
30	990	0.6	54.5	73.7		1.3	0	0.7
31	963	0.5	61.4	0.5		109.5	0	69.5
32	920	0.5	28.7	0.1		3.5	0	65
33	1,432	0.8	89.8	0		54.9	70.5	0.6
34	2,376	1.3	10.5	20		1.4	0	1.8
35	962	0.5	9.4	0.1		33	0.4	13
36	403	0.2	10.2	60.1		1.4	0	2.9
37	3,515	2	9.5	0.1		33	1.5	0
38	938	0.5	12.1	0.1		6.1	21.9	0.4
39	788	0.4	0	1.8		2.1	0	65
40	83,683	46.8	4	0		2.1	0	1.1
		100.2						

Figure 3-17: Cluster analysis of a sample after identification of each cluster (black = void/epoxy; blue = silicates; red = ferrite; green = calcium sulfoaluminate; grey = calcium sulfate; the light blue and purple colors help to determine which major elements are present in each cluster)

- 4- After identifying each cluster, the same color scheme, used in Figure 3-17, was employed to modify the unsupervised clustering analysis and obtain the final cluster analysis as shown in Figure 3-18.

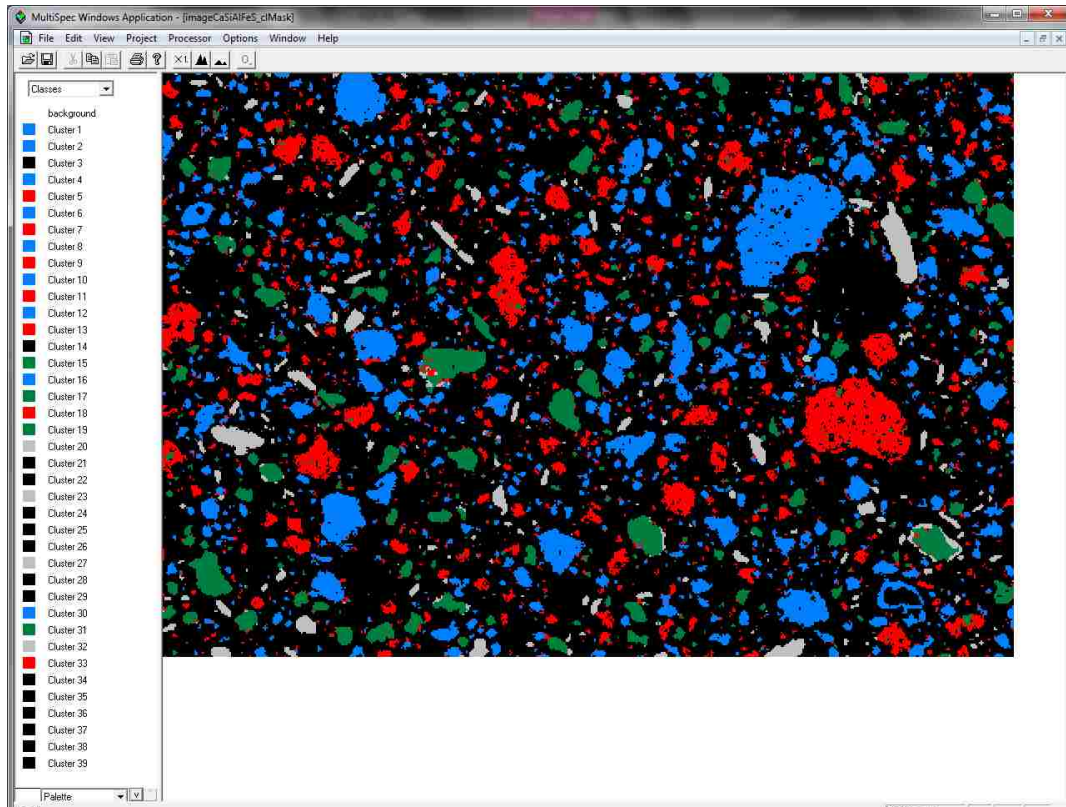


Figure 3-18: Final unsupervised clustering analysis (861  $\mu\text{m}$  width). Color code: black = void/epoxy; blue = silicates; red = ferrite; green = calcium sulfoaluminate; grey = calcium sulfate.

- 5- The final step of this method was to convert the surface percentages of each previously identified cluster into weight percentages and compare these data with the data obtained from the other characterization methods, such as XRD/Rietveld. The area fraction was normalized, without voids, and assimilated to a volume fraction  $V$  with the simplifying assumption that the shape of the clinker particles was approximately spherical ( $\text{Area} = V$ ). This volume fraction  $V$  was finally multiplied by the density  $D$  of each corresponding phase to obtain the mass fraction and then the normalized mass of each clinker phase. The results are shown in Table 3-3. Section 3.2.2.6. will compare the XRD/Rietveld results with the SEM/EDS results of this sample, later referred as B4.



Table 3-3: Example of a mass fraction calculation

	Area %	Area % Normalized (no void)	Densities D (kg.m <sup>-3</sup> )	D*Volume	Mass % normalized
<b>Silicates</b>	12.2	42.81	3.23 [74]	138.28	<b>42.28</b>
<b>CSA</b>	5.3	18.60	2.61 [6]	48.55	<b>14.85</b>
<b>C<sub>4</sub>AF</b>	8.4	29.47	3.77 [74]	111.10	<b>33.97</b>
<b>CS</b>	2.8	9.83	2.96 [6]	29.10	<b>8.90</b>
<b>FI*</b>	0	0	3.05 [75]	0	<b>0</b>
<b>MgO</b>	0	0	3.61 [76]	0	<b>0</b>
<b>C<sub>3</sub>A</b>	0	0	3.06 [6]	0	<b>0</b>
<b>Void</b>	71.5	0	0	0	<b>0</b>
<b>Sum</b>	100.2	100.71	-	327.03	<b>100</b>

### 3.2.2.5. Particle Size Distribution

Following synthesis and characterization, each clinker was ground in a shatter box to a median particle size  $d(0.5)$  of approximately 15 $\mu\text{m}$ . The particle size distributions, or PSD, were determined with a Malvern Mastersizer 2000, having a size range detection from 0.02 to 2000 $\mu\text{m}$ . Measurements were performed in isopropanol, so the cement would not react during the analysis.

The MIE calculations were used instead of Fraunhofer's as the solvent and particle sizes were relevant in the measurement. The refractive index (RI) of the tested materials was 1.66 and isopropanol was 1.39, whereas the absorption index was 0.5. Ultrasounds were employed for 40 seconds before the measurement to disperse the sample particles thoroughly in the solvent.

### 3.2.2.6. Example of some of these methods on a known clinker sample

Preliminary analyses were conducted beforehand to validate the characterization methods. Some reference samples were produced by mixing pure clinker phases (C<sub>3</sub>S, C<sub>2</sub>S, C<sub>4</sub>A<sub>3</sub>S, C<sub>4</sub>AF and CS) and analyzed with XRD/Rietveld and SEM/EDS.

The composition of samples B1 and B4 were similar to the mineralogical composition of the clinkers #1 and #4, respectively, presented in Section 4.1.1.1. These compositions

were chosen to prove the effectiveness of the XRD/Rietveld and SEM/EDS, methods in determining the phase compositions.

The pure clinker phases,  $C_3S$ ,  $C_2S$ ,  $C_4A_3\acute{S}$ ,  $C_4AF$  and  $C\acute{S}$ , were made in the laboratory and their purities were confirmed by XRD. They were blended together thoroughly in a mortar and pestle in order to match the targeted phase composition presented in Table 3-4.

Table 3-4: Phase composition of samples B1 and B4 by percentage by weight

<b>Reference Samples</b>	<b><math>C_3S</math></b>	<b><math>C_2S</math></b>	<b><math>C_4A_3\acute{S}</math></b>	<b><math>C_4AF</math></b>	<b><math>C\acute{S}</math></b>	<b>Sum</b>
<b>B1</b>	52.1	22.4	15.3	5.1	5.1	100
<b>B4</b>	30.6	13.3	15.3	35.7	5.1	100

The first approach to analyze the phase composition of these samples was through the XRD/Rietveld method. The sample preparation for the samples B1 and B4 was described in Section 3.2.2.2.

The XRD diffractograms are displayed in Figure 3-19. The ferrite peak is well defined in B4, whereas a small peak is seen in B1. This matches their phase compositions with 5.1% and 35.7 wt. % of  $C_4AF$ , respectively, in B1 and B4. Concerning the other peaks,  $C_4A_3\acute{S}$  and  $C\acute{S}$  peaks present almost the same shape and height in both samples which is consistent with their similar content in Table 3-4. The silicate peaks, where  $C_2S$  and  $C_3S$  often overlap with each other, are generally smaller in the sample B4 than in the sample B1, which is consistent with their phase compositions in Table 3-4.

The phase composition data obtained from the Rietveld refinement from both samples are presented in Table 3-5. The data are very close to the known values. The maximum difference observed between the experiment and theoretical values is for the amount of alite in the sample B1 where 46.1% of alite has been identified while actually 52.1% is present. Overall, this method is very useful and reliable for our work.

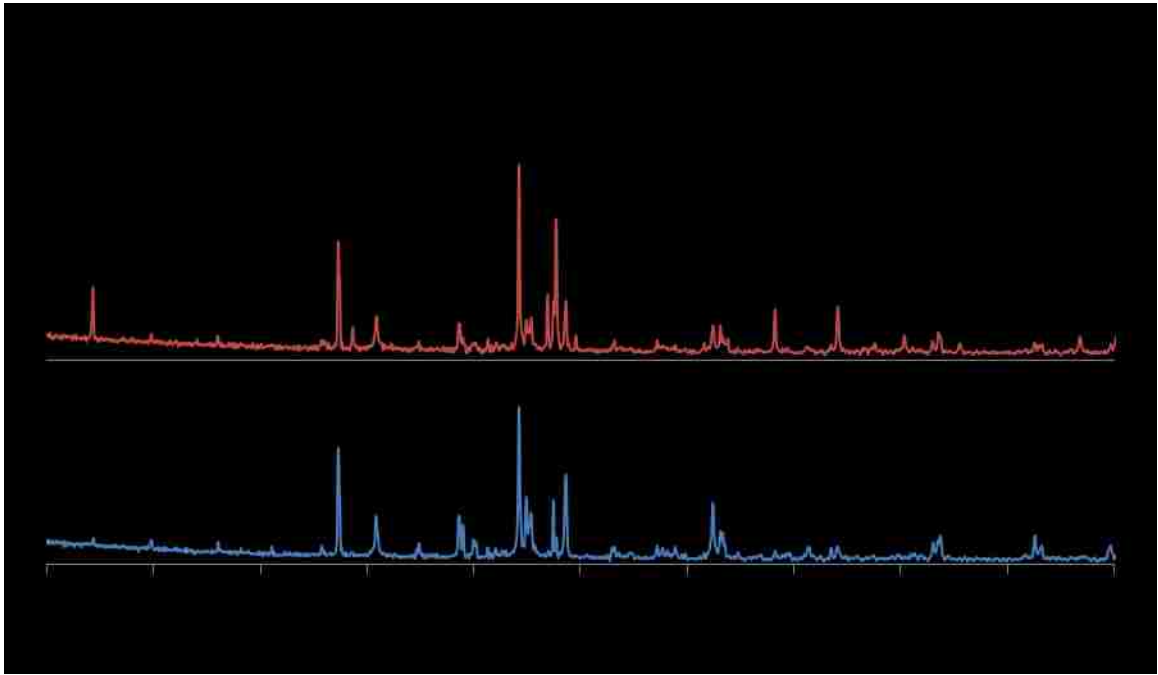


Figure 3-19: Comparison of XRD data for batches B1 and B4 made from pure phases

The XRD/Rietveld results were compared with SEM/EDS results. The final SEM/EDS images are displayed in Figures 3-20 and 3-21. Different colors were assigned to each clinker phase as displayed in Figures 3-22 and 3-23. Blue, green, red, grey and black were respectively related to the silicates phases ( $C_3S$  and  $C_2S$ ),  $C_4A_3S$ ,  $C_4AF$ ,  $C_3S$  and the epoxy material.

All the results for the two samples B1 and B4 obtained from the different characterization methods (XRD/Rietveld and SEM/EDS) are displayed in Table 3-5.

To summarize when comparing these two methods, XRD/Rietveld and SEM/EDS, the results are close to each other, and both methods can be used together to confirm the composition of any clinker.

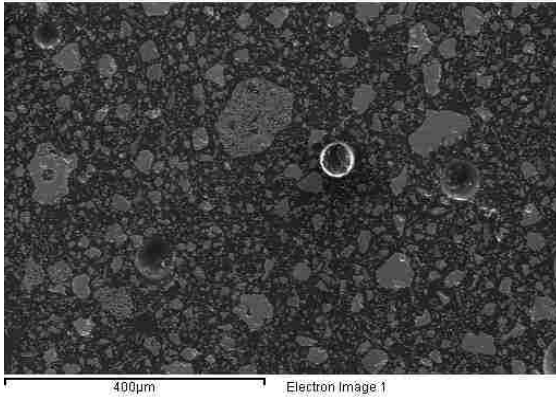


Figure 3-20: SEM picture of sample B1

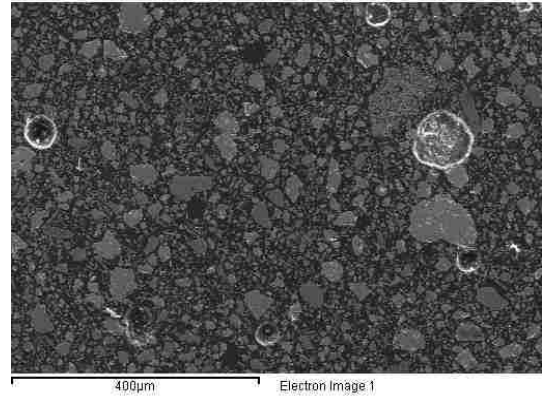


Figure 3-21: SEM picture of sample B4

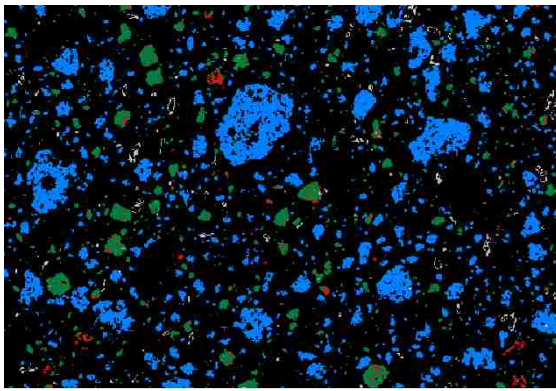


Figure 3-22: Phase mapping of sample B1

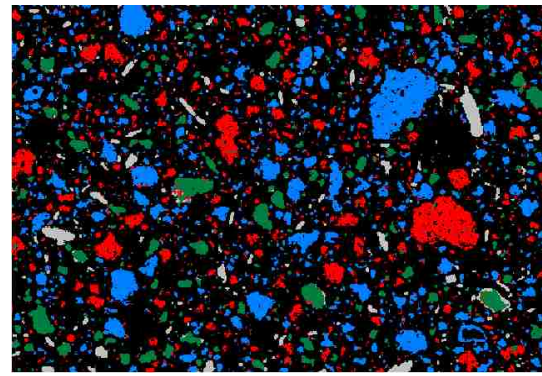


Figure 3-23: Phase mapping of sample B4

Table 3-5: Theoretical, XRD/Rietveld and SEM/EDS data for the composition analyses of B1 and B4

Reference Samples	B1			B4		
	Characterization Methods			Characterization Methods		
	Theory	Rietveld	SEM/EDS	Theory	Rietveld	SEM/EDS
<b>C<sub>3</sub>S</b>	52.1	46.1	75.5	30.6	29.5	42.3
<b>C<sub>2</sub>S</b>	22.4	23.3		13.3	12.2	
<b>C<sub>4</sub>A<sub>3</sub>S</b>	15.3	18.6	14.4	15.3	19.2	14.8
<b>C<sub>4</sub>AF</b>	5.1	5.5	6.7	35.7	30.0	34.0
<b>C<sub>S</sub></b>	5.1	5.0	3.4	5.1	4.7	8.9
<b>C<sub>3</sub>A</b>	-	0.0	-	-	0.1	-
<b>CaO</b>	-	0.1	-	-	0.4	-
<b>Fluorellestadite</b>	-	-	-	-	2.0	-
<b>MgO</b>	-	0.5	-	-	0.5	-
<b>Others</b>	-	0.8	-	-	1.6	-
<b>Sum</b>	100	99.9	100	100	100.2	100

### **3.2.3. Studies on Pastes**

Two types of experiments are based on hydration pastes: calorimeter study and hydration paste study. Both studies involve the hydration of only the cement paste without any addition of aggregates. This way, TGA and XRD analyses could be performed without any interference from other materials. For these experiments, cement material was produced by blending clinker with gypsum and the water:cement material ratio was kept constant at 0.45. The hydration process was then studied, first by calorimeter to identify the time range of some hydration reactions, and then by hydration paste study with hydration process stopped at some specified periods of times based on analyses of the calorimetric data to identify the formed hydrates. These two methods are described in Sections 3.2.3.1 and 3.2.3.2.

#### **3.2.3.1. Calorimeter Study**

Prior to the analyses of the hydration pastes, the hydration process had to be identified and comprehended. The calorimeter is very useful for accomplishing this work, as the hydration reactions occur during the cement hydration at different times depending on the present clinker phases, additives, water/cement ratio, and other parameters.

Cement studies involve the study of the optimization of gypsum addition to clinker. Lerch described the optimization of the amount of gypsum in OPC as follows: “A properly retarded cement is defined on the basis of the shape of the heat-liberation curve during the first 30 [hours] of hydration. A properly retarded cement is one that contains the minimum quantity of gypsum required to give a heat-liberation curve that shows two cycles of ascending and descending rates and that shows no appreciable change with larger additions of gypsum. The results of the physical tests show that when considering cements ground from a given clinker, those containing the proper amount of gypsum to give this type of curve will develop the highest strength and the lowest contraction.” [77] From his definition and for easy comprehension of his explanation, the optimum amount of gypsum is defined when the sulfate depletion peak, or when all the sulfate is consumed, occurs after the silicate hydration peak, and the peaks do not overlap.

An example of the determination of the optimum gypsum concentration is displayed in Figure 3-24. From this graph, the optimum amount of gypsum is between 3.0 and 3.5% because the silicate peak occurring at around 5 hours remained constant with the addition of more gypsum, and the sulfate depletion peak occurred around 30 hours.

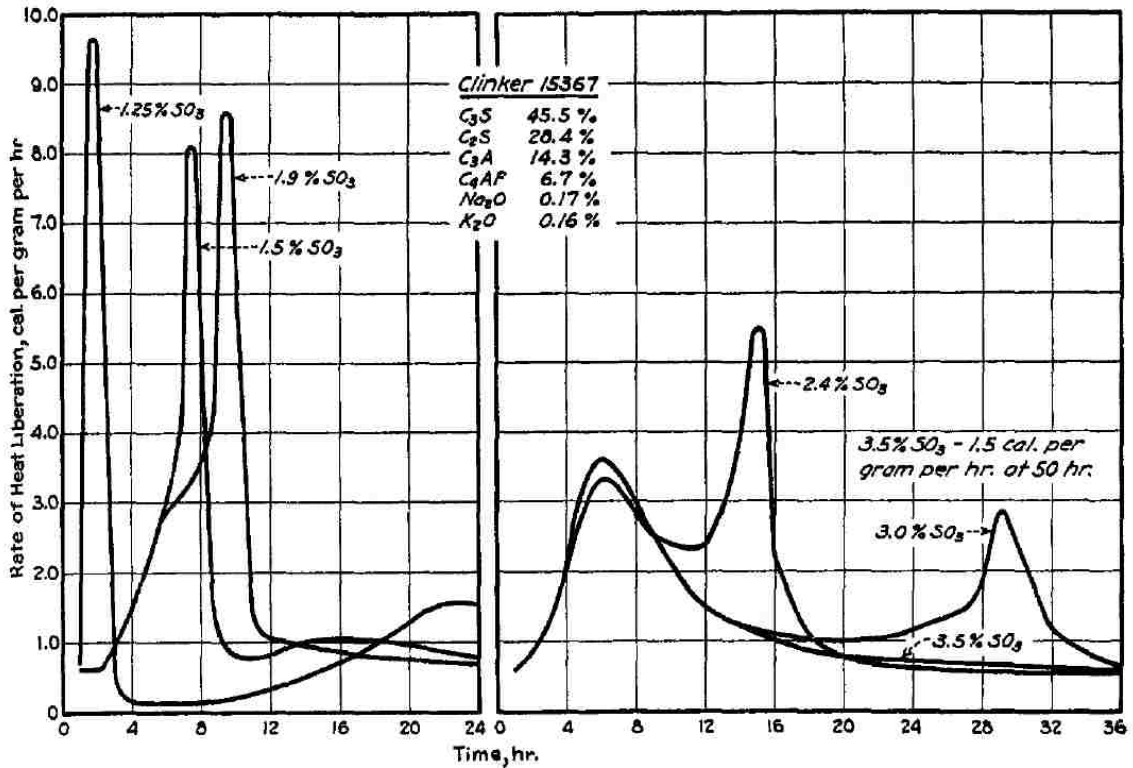


Figure 3-24: Calorimeter data of the influence of addition of SO<sub>3</sub> to cements of high C<sub>3</sub>A and low alkali content [77]

A TAM Air isothermal calorimeter was used to study the hydration evolution of each composition for the first 300 hours at 23°C. Two grams of cement material (clinker and gypsum) were introduced into a plastic container, and 0.9 grams of deionized water was added and mixed for 30 seconds with the cement material, at room temperature.

### 3.2.3.2. Hydration Paste Study

Following the calorimeter studies, hydration pastes studies were performed. As with the calorimeter, only the cement paste was studied. The hydration process was stopped at specific times for each sample, determined from the calorimeter data, and the phases

formed during the hydration were identified from XRD and thermogravimetric analyzer (TGA) analyses.

For the hydration paste study, different methods were available to stop the hydration process, such as freeze drying, solvent replacement, oven drying, vacuum drying, and others. Depending on the characterization methods employed for the subsequent step, these methods may or may not be adequate for the purpose of the upcoming experiments. Several papers have been published about the influence of the water removal techniques on the cement composition and hydration. [78-80] Zhang stated, “complete drying without any chemical and/or physical effects is not possible in practice” [79]. Every method has its own advantages and disadvantages.

The purpose of this hydration paste study is the characterization of the hydrates formed during the hydration process at a specific time interval. The microstructure of a sample is then not a priority here, consequently the appropriate method adopted here to halt the hydration process was chosen to best conserve the chemical structure of the products formed during hydration. Solvent replacement with isopropanol has been identified as the best method for this work because of the non-interaction of isopropanol with cement and the rapidity of the method. As explained by Zhang, isopropanol can be trapped into the cement microstructure and TGA analysis can be affected with appearance of a few undesired peaks from the presence of impurities. Zhang used pieces of cement of 3mm size which is not the case in this work, where the cement paste was crushed into a fine powder in a mortar and pestle, and hence no isopropanol was trapped. [79]

In this dissertation, 10g of cement material were mixed with 4.5g of deionized water for about 30 seconds in a closed tight plastic vessel. A wet paper towel was introduced into the plastic container after the paste hardened to keep a high relative humidity. When the time of testing was attained, a piece of the cement paste sample was first crushed in a mortar and pestle and immersed in isopropanol for several minutes. The alcohol was then removed and another wash with isopropanol was completed for several minutes. The sample was then placed in an oven at 45°C until completely dried. Afterward, the sample was moved to a desiccator in wait for XRD and TGA analyses. Both methods were complementary as minor phases cannot be readily detected with only XRD. Basic XRD

analyses, without Rietveld analyses, were performed as explained earlier in Section 3.2.2.2. TGA analyses were performed through a TA Instruments SDT Q600. Approximately 10mg of sample was placed into an alumina sample pan, and fired from 50°C to 1000°C at a heating rate of 20°C/min, under a flow of nitrogen of 100mL/min.

#### **3.2.4. Mechanical Tests**

Mechanical tests were performed depending on the paste study results from the calorimeter and hydration paste experiments for each formulation chosen. If enough material is available, mechanical tests could include: compressive, flexural, tensile strength tests and length change tests (to study expansion and shrinkage). Because this is a research study, only compressive strength measurements were performed. The batches were produced in low amounts, and hence 5cm mortar cubes could not be produced. Small 2.5cm mortar cubes were produced and tested, and due to this size reduction, the ratio cement material:sand was modified from 1:2.75 [4] to 1:2 to have enough strength to test the “mini-cubes.”

For this experiment, molds used to produce length change tests were employed as molds for the production of the mini-mortar cubes. Steel separators of 0.95cm (exactly 3/8-in) were placed, and fixed with duct tape, every inch to obtain cubes of regular size. All of the surfaces having any contact with the mortar material were first covered with petroleum and TaegaSeal PTFE tape (commercial grade – 2.54cm wide), which allows for the easy removal of the mini-cubes from the molds (Figure 3-26). Petroleum gel was also applied into the joints between the side and the bottom plates to prevent any water leakage, as this would modify the actual water/cement ratio (Figure 3-27). Nine mini mortar cubes could be produced in one expansion bar mold as seen in Figure 3-25, hence two to three cubes were tested at 1, 7 and 28 days, depending on the compositions.



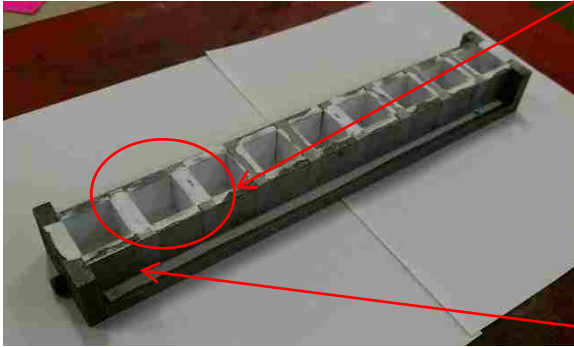


Figure 3-25: Overview of a mortar cube mold preparation



Figure 3-26: Close-up of one 1-in hollow mortar cube mold



Figure 3-27: Side of the mold where petroleum is applied to prevent water leak

The mortar cubes were prepared by hand, by mixing 100g of cement material with 45g of deionized water. For each mix, 200g of graded sand was then added until a homogeneous mixture was obtained. The mortar cement material was placed into the molds, as seen in Figure 3-28, in two layers tamped with index fingers copying the same procedure than with the 2.5cm cubes with a tamper. The molds were then placed in a chamber at 25°C and 100% relative humidity. The mini-cubes were then removed from the molds 24 hours later and placed back into the same humidity chamber until the compressive strength was measured. Figure 3-29 shows mini-cubes just before being measured and tested.



Figure 3-28: 1-in mini-mortar cube mold filled with sample



Figure 3-29: Mini-mortar cubes after demolding step

## Chapter 4 : Preliminary Experiments

This chapter is dedicated to the investigation of the optimal firing parameters to produce clinkers from both reagent chemicals (RC) and industrial by-products (BP). The formulations, synthesis and characterization methods performed are described in this chapter. Also, the definition of the optimal parameters and the choice of the optimal firing parameters are explained.

### 4.1. Production of small batches of clinker from RC and BP

#### 4.1.1. Formulation

Depending on the raw materials used, reagent chemicals (RC) or by-products (BP), the chemical compositions were slightly different. The amounts of each reagent chemical and industrial by-product for each batch are displayed in Tables 4-1 and 4-2.

Table 4-1: Chemical compositions for the batches produced from reagent chemicals in wt. %

	Batch #1	Batch #2	Batch #3	Batch #4	Batch #5
<b>Ca(OH)<sub>2</sub></b>	63.725	60.85	58.015	55.18	52.32
<b>SiO<sub>2</sub></b>	17.06	14.67	12.31	9.96	7.6
<b>Al(OH)<sub>3</sub></b>	10.68	13.27	15.83	18.38	20.95
<b>Fe<sub>2</sub>O<sub>3</sub></b>	1.34	4.025	6.695	9.34	12
<b>CaSO<sub>4</sub></b>	6.56	6.55	6.52	6.51	6.5
<b>CaF<sub>2</sub></b>	0.635	0.635	0.63	0.63	0.63
<b>Sum</b>	100	100	100	100	100

Table 4-2: Chemical compositions for batches produced from by-products in wt. %

	Batch #1	Batch #2	Batch #3	Batch #4	Batch #5
<b>Hydrated Lime</b>	46.3	46.3	46.3	46.3	45.8
<b>Bottom Ash</b>	15.236	15.364	15.353	15.3	15.285
<b>Red Mud</b>	-	5.551	11.7	18	23.8
<b>Bauxite</b>	1	4	7	10	13
<b>Blast Furnace Slag Fines</b>	24.102	17.62	10.139	3	-
<b>Class C Fly Ash</b>	12.7	10.515	8.87	6.774	1.5
<b>CaF<sub>2</sub></b>	0.662	0.65	0.638	0.626	0.615
<b>Sum</b>	100	100	100	100	100

All the moduli and clinker phase compositions are summarized in Tables 4-3 and 4-4. Table 4-3 shows that all batches, whether produced from reagent chemicals (RC) or industrial by-products (BP), presented the same, or as close as possible, LAD, SEC and QLP moduli, as explained in Section 2.4.3. Only RSA and RSF moduli varied resulting from the increasing amount of C<sub>4</sub>AF from 5 to 45 wt. % and by keeping the amount of C<sub>4</sub>A<sub>3</sub>S̄ and the ratio of C<sub>3</sub>S to C<sub>2</sub>S constant.

Table 4-3: Moduli obtained from the actual formulation established in Section 4.1.1. for each composition

	Batch #1		Batch #2		Batch #3		Batch #4		Batch #5	
	RC	BP	RC	BP	RC	BP	RC	BP	RC	BP
<b>LAD</b>	0.88	0.88	0.88	0.88	0.880	0.88	0.88	0.88	0.88	0.88
<b>RSA</b>	3.63	3.30	2.09	2.01	1.317	1.25	0.86	0.78	0.54	0.51
<b>RSF</b>	3.01	2.38	1.00	1.01	0.599	0.61	0.43	0.43	0.33	0.33
<b>SEC</b>	1.20	1.20	1.20	1.20	1.202	1.20	1.20	1.20	1.20	1.21
<b>QLP</b>	0.10	0.10	0.10	0.10	0.100	0.10	0.10	0.10	0.10	0.10

Table 4-4 presents the theoretical mineralogical compositions of each batch predicted from the modified Bogue equations displayed in Section 2.4.3. Due to the presence of impurities in the industrial by-products, the compositions of each of the batches from RC and BP were not exactly the same.

Table 4-4: Clinker phase composition predicted from the actual formulation established earlier by using the modified Bogue equations (in wt. %) for each composition

	Batch #1		Batch #2		Batch #3		Batch #4		Batch #5	
	RC	BP	RC	BP	RC	BP	RC	BP	RC	BP
<b>C<sub>3</sub>S</b>	50.90	47.97	43.95	42.34	36.96	35.04	30.00	27.63	22.88	21.22
<b>C<sub>2</sub>S</b>	21.65	21.12	18.61	17.05	15.66	14.49	12.69	11.62	9.75	8.91
<b>C<sub>4</sub>A<sub>3</sub>S̄</b>	14.99	14.54	15.00	14.84	14.97	14.98	14.97	14.98	14.98	14.67
<b>C<sub>4</sub>AF</b>	4.98	6.11	14.99	14.7	24.99	24.6	34.95	35.05	45.01	44.54
<b>C<sub>S</sub></b>	4.74	4.73	4.75	4.74	4.74	4.74	4.74	4.75	4.75	4.76
<b>CaF<sub>2</sub></b>	0.78	0.78	0.78	0.78	0.78	0.78	0.78	0.78	0.78	0.78
<b>MgO</b>	-	5.37	-	4.53	-	3.55	-	2.55	-	1.87
<b>TiO<sub>2</sub></b>	-	0.44	-	0.84	-	1.29	-	1.77	-	2.2
<b>K<sub>2</sub>O</b>	-	0.3	-	0.28	-	0.25	-	0.22	-	0.2
<b>Na<sub>2</sub>O</b>	-	0.386	-	0.437	-	0.51	-	0.58	-	0.59
<b>P<sub>2</sub>O<sub>5</sub></b>	-	0.24	-	0.26	-	0.3	-	0.34	-	0.31
<b>Sum</b>	98.05	100.99	98.07	100.80	98.1	100.53	98.13	100.27	98.15	100.05

### 4.1.2. Synthesis

The sample preparation of small batches from RC and BP was presented in Section 3.2.1.

## 4.2. Characterization Results

### 4.2.1. From Reagent Chemicals

The first firing temperature tested on all samples was 1300°C for 30 minutes, and was defined as the reference firing regime. XRD and free lime analyses were then performed for each of those samples. The results are displayed in Figure 4-1, and showed that this firing regime was not high enough for the batch #1 as free lime content exceeded 1.0% by weight, actually 1.50 wt. %. On the other hand, this temperature regime seemed too high for the other batches, as C<sub>3</sub>A peaks were detected on the XRD graphs.

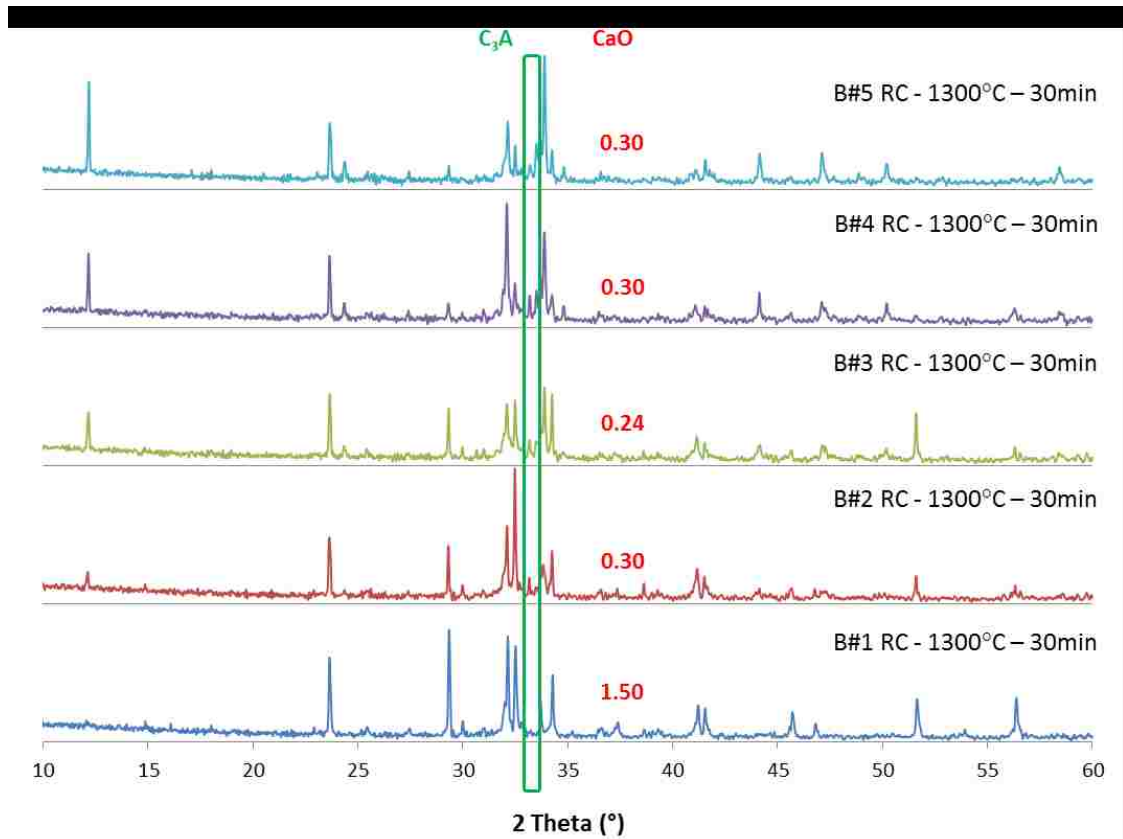


Figure 4-1: XRD graphs and free lime determinations (in red) of all batches produced from RC, fired at the reference regime of 1300°C for 30 minutes (the peak encircled in green corresponds to the tricalcium aluminate (C<sub>3</sub>A) peak)

Different firing regimes were then tested: high temperatures from 1300 to 1350°C were tested for the batch #1; and low temperatures from 1250°C to 1300°C for all the other batches. All the XRD analyses performed for each batch are gathered in Appendix B. To simplify all the information retrieved from these experiments, Figure 4-2 includes all the free lime contents and the presence of tricalcium aluminate is represented by hatched bars.

Two parameters were considered for the optimization of the firing regime of every batch. If  $C_3A$  was present in a sample, or if free lime exceeded 1.0 wt. %, the temperature and dwelling time used for this sample were rejected. Consequently, by using this information, the firing temperatures of 1350°C for batch#1 and 1300°C for the other batches were eliminated due to a large amount of  $C_3A$  present. Also, the dwelling time of 30 minutes for all the batches was not enough for the clinkers to consume all the free lime as it exceeded 1.0 wt. %.

Finally, the firing temperature of 1325°C for 60 minutes for batch #1 was selected due to the low free lime present. The firing temperature of 1300°C for 60 minutes could have been selected as well.

For batches #2 through #5, the optimum firing regime was 1275°C for 60 minutes as the 1250°C for 60 minutes had too much free lime detected in them.

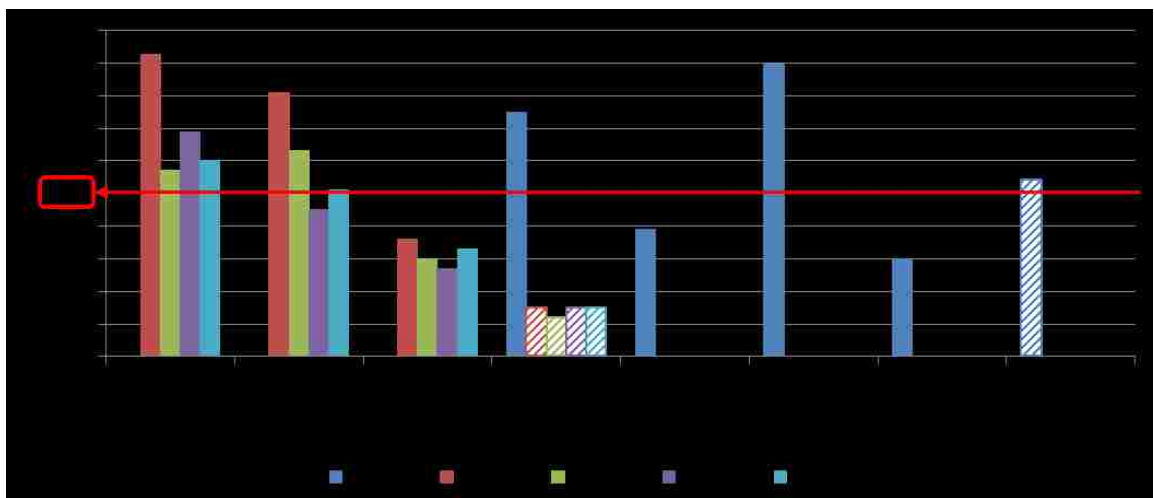


Figure 4-2: Free lime tests for each small sample produced from reagent chemicals (RC), fired at different temperatures for 30-60 minutes (hatched bars indicate  $C_3A$  was present in this sample)

The XRD graphs corresponding to the firing parameters selected for each batch are presented in Figure 4-3. More tests were performed on these optimal batches in order to completely characterize them, such as Rietveld approximation, SEM/EDS scans and particle size analyses.

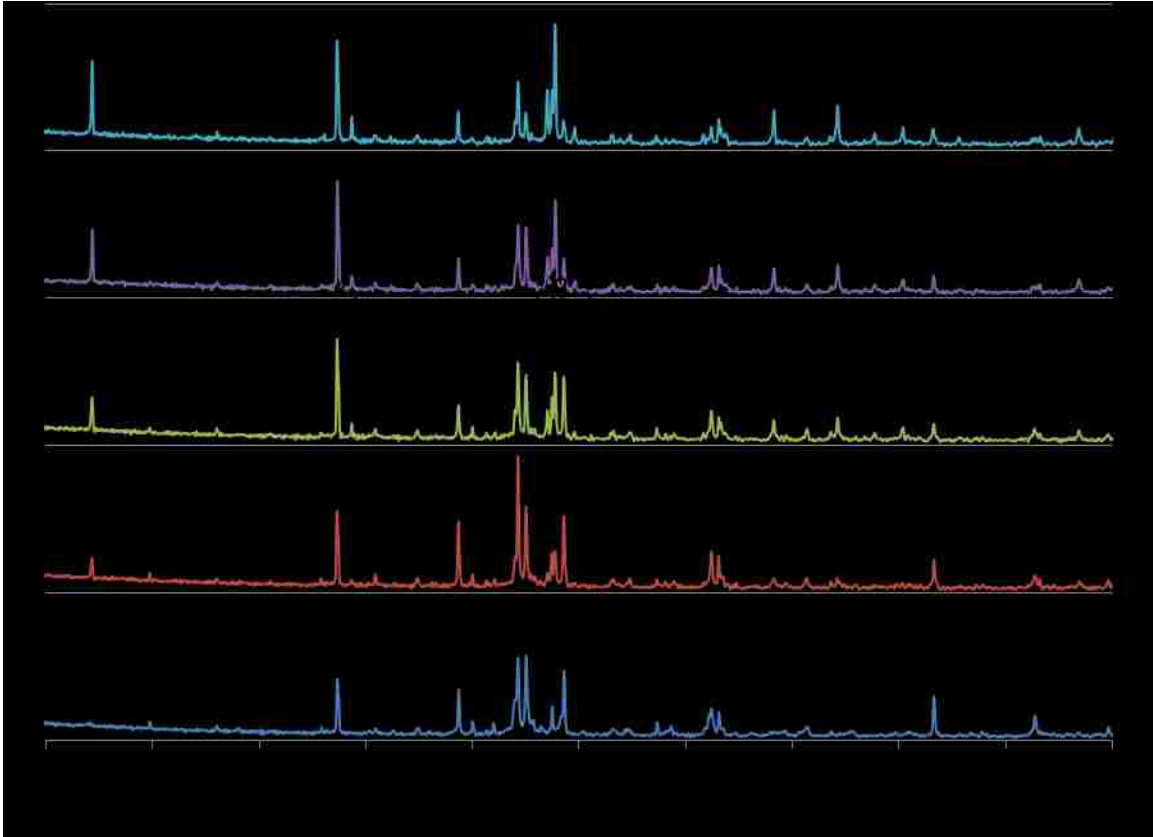


Figure 4-3: XRD graphs of small batches #1, 2, 3, 4 and 5 produced from reagent chemicals (RC)

The Rietveld approximation performed on these samples were slightly different from the data expected. Figure 4-4 shows that the amounts of alite and ferrite were lower than expected in theory. The opposite was observed for the amounts of belite and calcium sulfoaluminate. The amorphous content was not taken into account, and these tests were performed to give an estimation of the phase composition.

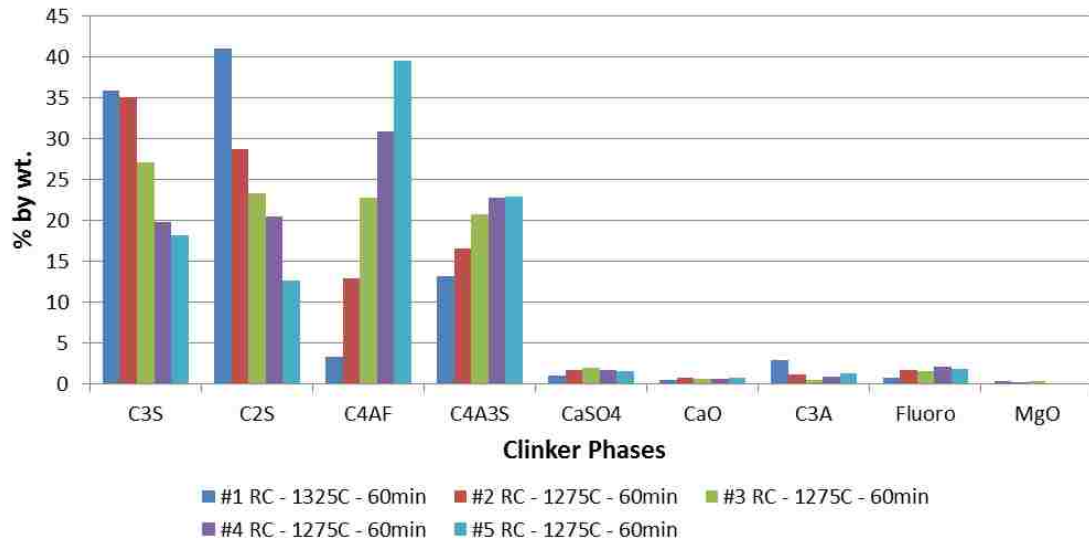


Figure 4-4: XRD/Rietveld approximation of each small batch with the optimum parameters (“Fluoro” = Fluorellestadite)

SEM/EDS scans were performed to compare the subsequent results with the Rietveld approximation and the theoretical data. During the analyses of the SEM/EDS scans, the alite and belite phases were too difficult to differentiate, thus the amounts of both of them were gathered and compared with the theoretical values. As shown in Table 4-5, the XRD/Rietveld approximation provided values very close to the values expected theoretically if one considers the alite plus belite content; the amount of alite was lower and belite was higher than the theoretical values. The calcium sulfoaluminate and ferrite amounts were quite close to the theoretical data too, while the other minor phases, such as calcium sulfate and fluorellestadite were troublesome to detect using SEM/EDS.



Table 4-5: Summary of all results for phase composition determination from XRD/Rietveld and SEM/EDS compared to the theoretical data (Fl\*=Fluorellestadite)

<b>Batches</b>	<b>Methods</b>	<b>C<sub>3</sub>S</b>	<b>C<sub>2</sub>S</b>	<b>C<sub>4</sub>A<sub>3</sub>S</b>	<b>C<sub>4</sub>AF</b>	<b>C<sub>S</sub></b>	<b>CaF<sub>2</sub></b>	<b>Fl*</b>	<b>C<sub>3</sub>A</b>	<b>f<sub>CaO</sub></b>	<b>MgO</b>	
<b>B#1 RC</b>	Theory	50.90	21.65	14.99	4.98	4.74	0.78	-	-	-	-	
	<b>1325°C</b>	Rietveld	35.9	41	13.1	3.3	1.0	-	0.8	2.9	0.5	0.3
	<b>60min</b>	SEM/EDS	86.7		9.4	3.5	-	-	0.4	-	-	-
<b>B#2 RC</b>	Theory	43.95	18.61	15.00	14.99	4.75	0.78	-	-	-	-	
	<b>1275°C</b>	Rietveld	35.0	28.7	16.6	12.9	1.7	-	1.7	1.1	0.8	0.2
	<b>60min</b>	SEM/EDS	68.3		17.2	12.2	-	-	2.3	-	-	-
<b>B#3 RC</b>	Theory	36.96	15.66	14.97	24.99	4.74	0.78	-	-	-	-	
	<b>1275°C</b>	Rietveld	27.1	23.3	20.7	22.8	1.9	-	1.5	0.5	0.6	0.4
	<b>60min</b>	SEM/EDS	58.7		17.2	23.1	-	-	1.0	-	-	-
<b>B#4 RC</b>	Theory	30.00	12.69	14.97	34.95	4.74	0.78	-	-	-	-	
	<b>1275°C</b>	Rietveld	19.8	20.4	22.7	30.8	1.7	-	2.1	0.9	0.6	0
	<b>60min</b>	SEM/EDS	43.8		21.6	32.8	-	-	1.9	-	-	-
<b>B#5 RC</b>	Theory	22.88	9.75	14.98	45.01	4.75	0.78	-	-	-	-	
	<b>1275°C</b>	Rietveld	18.2	12.6	22.9	39.5	1.6	-	1.8	1.3	0.7	0.1
	<b>60min</b>	SEM/EDS	33.1		27.9	39.1	-	-	-	-	-	-

The images from the SEM/EDS analyses are displayed in Figure 4-5, and show the dispersion of the mineralogical phases inside the clinker.

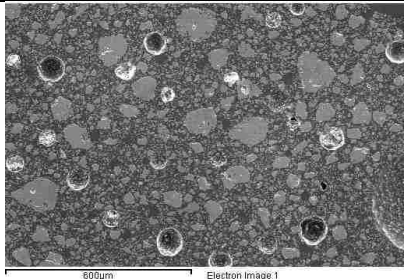
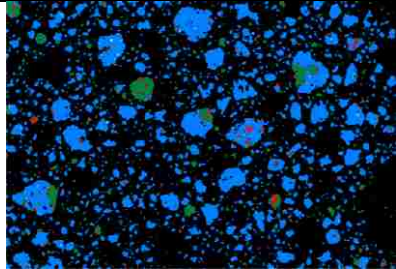
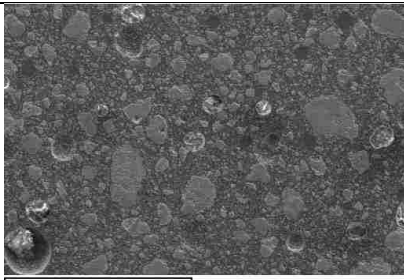
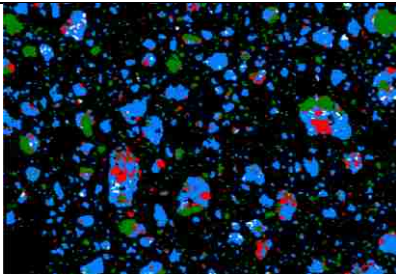
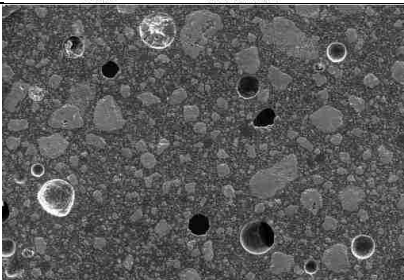
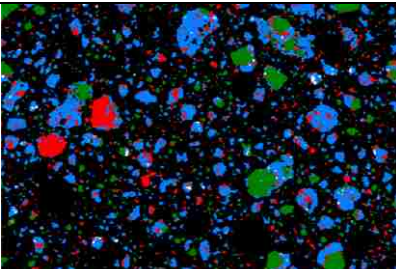
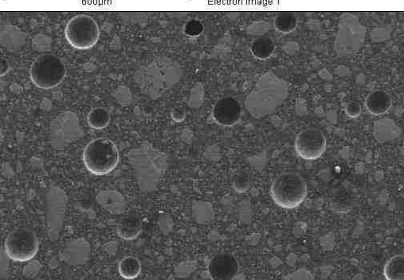
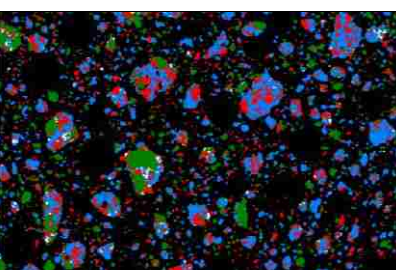
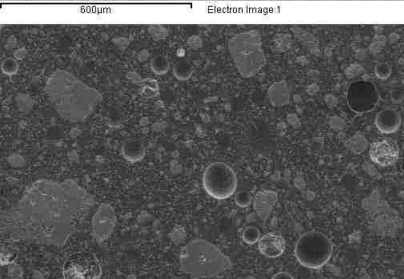
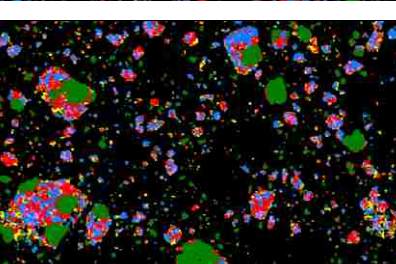
	Original SEM/EDS Pictures	Pictures modified with software
B #1 RC 1325°C 60min		
B #2 RC 1275°C 60min		
B #3 RC 1275°C 60min		
B #4 RC 1275°C 60min		
B #5 RC 1275°C 60min		

Figure 4-5: SEM/EDS pictures showing clinker phases after firing step (blue= $C_3S/C_2S$ ; red= $C_4AF$ ; green= $C_4A_3\dot{S}$ ; white=Fluorellestadite; pink= $C_3S/C_2S/C_4AF$ ; yellow= $C_3S/C_2S/C_4AF/C_4A_3\dot{S}$ ; “/” means combination of clinker phases)

The last characterization test performed was the particle size determination. Each clinker batch of the same quantity was ground for 45 seconds in a shatter box and analyzed with a Malvern Particle Size Analyzer at least three times. The averages of these three measurements are displayed in Table 4-6 and Figure 4-6, and showed differences between the batches.

Before describing the particle size distribution in the different batches, the hardness of each clinker phase is discussed. Several researches focused on the determination of the hardness of each clinker phase, through Vickers micro-indenter [81, 82] or by nanoindentation testing. [83] From the Vickers experiment, the brittleness index of the clinker phases varies.  $C_3S$  has the highest brittleness index of 4.9, which means that this phase is the easiest to grind.  $C_3A$  is harder to grind than  $C_3S$  with a value of 2.9, and  $C_2S$  and  $C_4AF$  have the smallest brittleness index of 2.0 which makes them the hardest clinker phases to grind. By nanoindentation testing, the results differ slightly. The hardness is the smallest for both silicate phases  $C_3S$  and  $C_2S$ , respectively 8.7 and 8.0 GPa. Then ferrite (9.5GPa) is slightly harder than the silicate phases; whereas the  $C_3A$  phase (10.8GPa) is the hardest clinker phase to grind. As there is no tricalcium aluminate phase in any of the produced clinkers, results from both methods are consistent with each other, as the ferrite phase is the hardest clinker phase to grind, and the silicates the easiest. The hardness value was not available for the  $C_4A_3\dot{S}$  phase, but it is known that this phase is very easy to grind, as CSAC are easily ground. [11] Even if this value was known, it is not of significance here, as the quantity of  $C_4A_3\dot{S}$  is supposed to be constant in all batches, at 15 wt. %.

Table 4-6 shows that the particle size  $d(0.5)$  decreased from batches #1 to #5. Figure 4-6 shows also some differences between the batches. Batch #1, containing almost no ferrite, showed one large peak at 20-30  $\mu\text{m}$ , whereas the other batches presented two large peaks centered at around 7 and 50  $\mu\text{m}$ . Furthermore, the peak situated at 7  $\mu\text{m}$  became higher and the other peak at 50  $\mu\text{m}$  weaker as the amount of ferrite increased and silicate decreased. The silicate phases may be easier to grind than the ferrite phase, but they may be larger at the beginning of the grinding process, which would explain the trend observed in Figure 4-6.

Table 4-6: Average of three measurements of particle size distribution (PSD) for each small pellet (10g in shatter box Chrome 40 for 45sec)

	Particle Size in $\mu\text{m}$				
Batch	1	2	3	4	5
<b>d(0.1)</b>	1.42	1.22	1.44	1.53	1.65
<b>d(0.5)</b>	14.12	11.81	10.54	9.76	9.82
<b>d(0.9)</b>	60.58	66.64	61.73	70.97	75.83

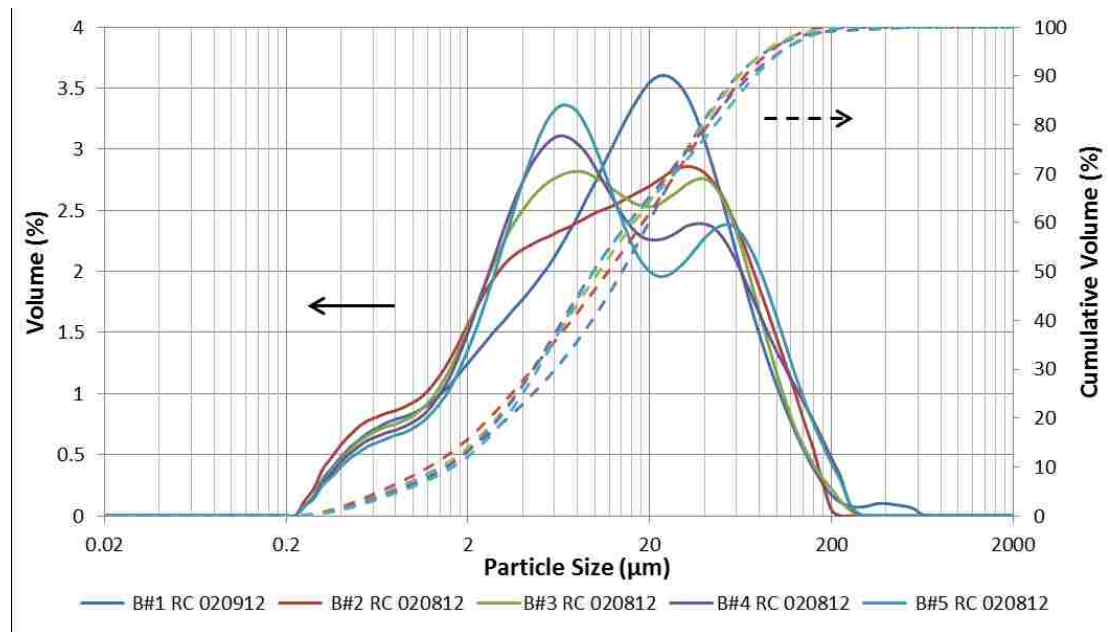


Figure 4-6: Particle Size Distribution of each small batch after 45sec ground in a shatter box

#### 4.2.2. From Industrial By-Products

The purpose of reproducing the same compositions obtained from RC but this time with BP is to compare and analyze the differences introduced by the industrial by-products as raw materials. The same analysis procedure used to optimize the firing regime of RC samples was followed for the BP samples. The firing temperature and dwelling time of 1300°C for 30 minutes thus served as a reference firing regime to determine the parameters to be modified.

As observed in Figure 4-7, this reference regime was unsuitable as the  $\text{C}_4\text{A}_3\text{S}$  phase was almost not present in all the XRD diffractograms. Furthermore,  $\text{C}_3\text{A}$  was detected which

means that the calcium sulfoaluminate was actually decomposing into tricalcium aluminate and calcium sulfate. In addition to these observations, Figures 4-8 and 4-9 show that the pellets were stuck to each other after the firing regime of 1300°C for 30 minutes.

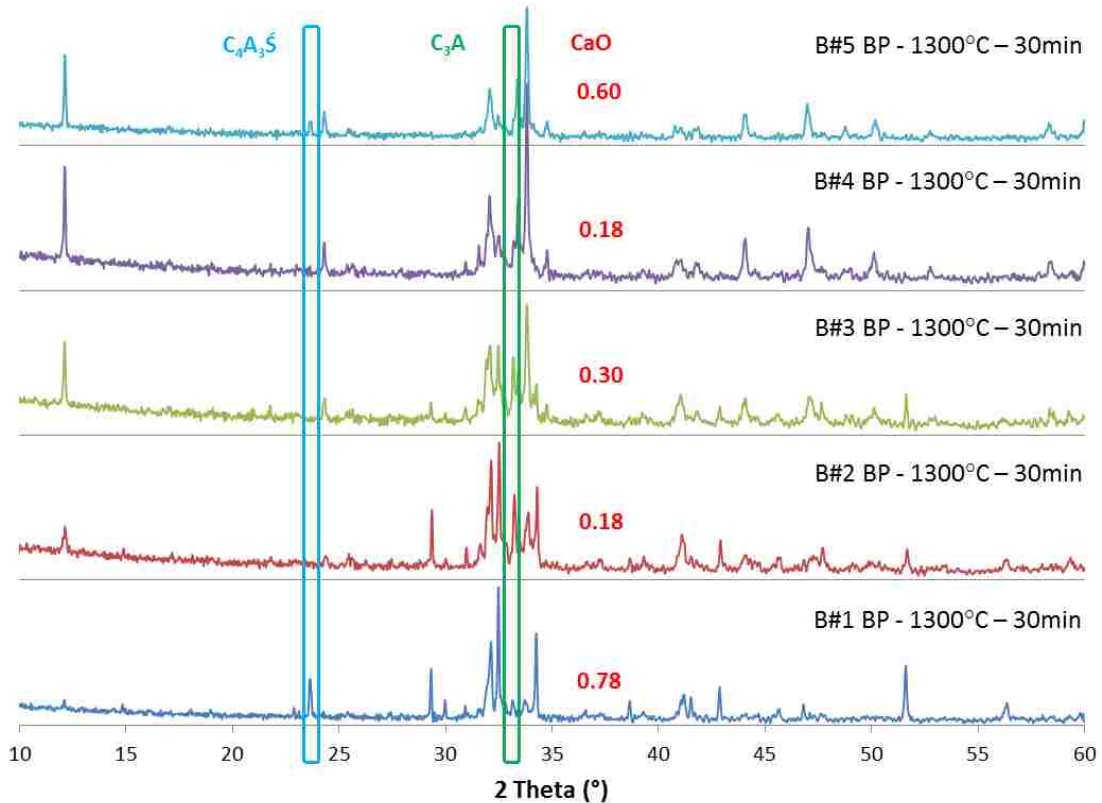


Figure 4-7: XRD graphs and free lime determinations of all batches from BP fired at the reference regime of 1300°C for 30 minutes (the peak encircled in green corresponds to tricalcium aluminate peak, in blue to calcium sulfoaluminate and values in red to free lime)



Figure 4-8: Pellets made from industrial by-products (BP) just before firing process



Figure 4-9: Pellets made from industrial by-products (BP) just after firing at 1300°C and quenching step

The next approach of this work was similar to the one employed with the samples produced from RC. All the batches were fired at temperatures lower than 1300°C (1250°C and 1275°C) with a dwelling time of 30 or 60 minutes. All the XRD data are gathered in Appendix C. To simplify the analysis of the data, all the information, such as the amount of free lime and the presence of tricalcium aluminate, are combined in Figure 4-10.

The firing regimes of 1250°C and 1275°C for 30 minutes for every batch presented a low amount of alite in the XRD diffractograms. The firing regime of 1250°C for 60 minutes was selected for the optimum firing regime as the amount of free lime was low enough, no  $C_3A$  was present, and enough alite and calcium sulfoaluminate formed. The optimum firing regime of 1250°C for 60 minutes for batch #1 from BP was selected, even though the free lime was 2.0%, no substantial peak of CaO was present on the XRD diffractogram.

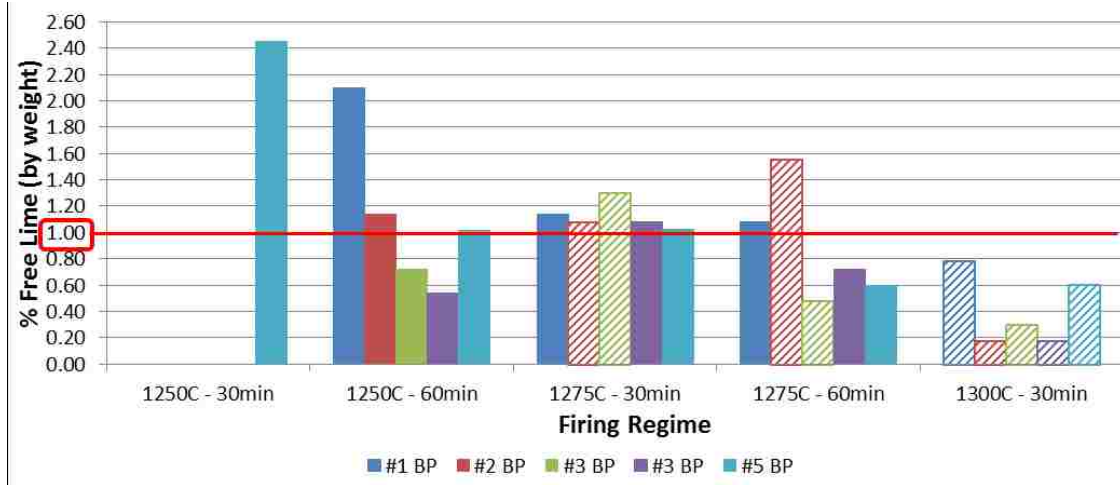


Figure 4-10: Free lime tests for each small sample produced from industrial by-products (BP) and fired at different temperature for 30-60 minutes

To summarize the results, the best combination temperature/dwelling time was 1250°C for 60min, with low free lime and low C<sub>3</sub>A content. With these parameters, the amount of ferrite phase in every batch was higher than expected: instead of having 5-15-25-35-45% by weight of C<sub>4</sub>AF for batches #1-2-3-4-5, the XRD/Rietveld values were respectively approximately 9-17-30-43-55% by weight.

These differences in the quantities of ferrite may be due to the XRF instrument, which provides higher errors when too much iron is present. An experiment determining the error caused from the XRF instrument was performed and is displayed in Appendix D. Consequently, the amount of iron oxide was underestimated due to the XRF analysis, which means that there was actually more iron present in the samples than expected from the XRF data.

To decrease the iron content of the clinkers, the source of the by-products was changed. Instead of using bottom ash and blast furnace slag as raw materials, they were replaced with gypsum and river sand following the same modified Bogue equations established earlier. The results were actually neither better, nor worse, than with the original by-products.

The next approach to decrease the iron content was to decrease the amount of red mud, which is the main source of iron for the production of  $C_4AF$ , and replace it with bottom ash or gypsum as a source of sulfate in order to produce more  $C_4A_3\dot{S}$ . By evaluating the excess of  $C_4AF$  in each batch, which was around 20 wt. % of the theoretical value, 20% by weight of red mud was removed from its initial amount, which corresponds to 2.34g for batch #3-BP. Instead of removing this exact value, 1.5g and 3.0g were chosen and tested. This means that for sample “#3BP -1.5RM +1.5Sp”, 1.5g of red mud was subtracted from the 11.7g and 1.5g of bottom ash was added to the original value. Six samples of 10g each were then prepared and their compositions are presented in Table 4-7.

Table 4-7: Modification of the Batch #3-BP by adding/removing red mud/bottom ash/gypsum (all the values are in grams – ***bold and italic values*** are the modified values compared to the original Batch #3-BP)

	#3 BP Original	#3BP - 1.5RM +1.5Sp	#3BP -1.5RM +1.5Sp	#3BP -1.5RM +1.5Gyp	#3BP - 3.0RM +3.0Sp	#3BP -3.0RM +3.0Gyp	#3BP -3.0RM +3.0Gyp
<b>Hydrated Lime</b>	46.3	46.3	46.3	46.3	46.3	46.3	46.3
<b>FGD Gypsum</b>	-	-	-	<b><i>0.15</i></b>	-	-	<b><i>0.30</i></b>
<b>Fluorite</b>	0.638	0.638	0.638	0.638	0.638	0.638	0.638
<b>Bottom Ash</b>	15.353	15.353	<b><i>16.853</i></b>	15.353	-	<b><i>18.353</i></b>	-
<b>Red Mud</b>	11.7	<b><i>10.2</i></b>	<b><i>10.2</i></b>	<b><i>10.2</i></b>	<b><i>8.7</i></b>	<b><i>8.7</i></b>	<b><i>8.7</i></b>
<b>Bauxite</b>	7.0	7.0	7.0	7.0	7.0	7.0	7.0
<b>BF slag fines</b>	10.139	10.139	10.139	10.139	10.139	10.139	10.139
<b>Class C Fly Ash</b>	8.87	8.87	8.87	8.87	8.87	8.87	8.87
<b>TOTAL</b>	100	<b><i>98.5</i></b>	100	100	<b><i>97</i></b>	100	100



The XRD results obtained from these compositions are presented in Figure 4-11. All the XRD scans looked similar, but the Rietveld data presented several differences. From all these results, the best composition was the modified batch #3 where 3.0g red mud was subtracted and 3.0g bottom ash was added. With this configuration, the  $C_4A_3\dot{S}$  and  $C_3S$  peaks, respectively close to  $24^\circ-2\theta$  and  $29^\circ-2\theta$  and circled in red, were both more intense than with all the other modifications. Also the amount of  $C_4AF$  from Rietveld was the lowest for this composition.

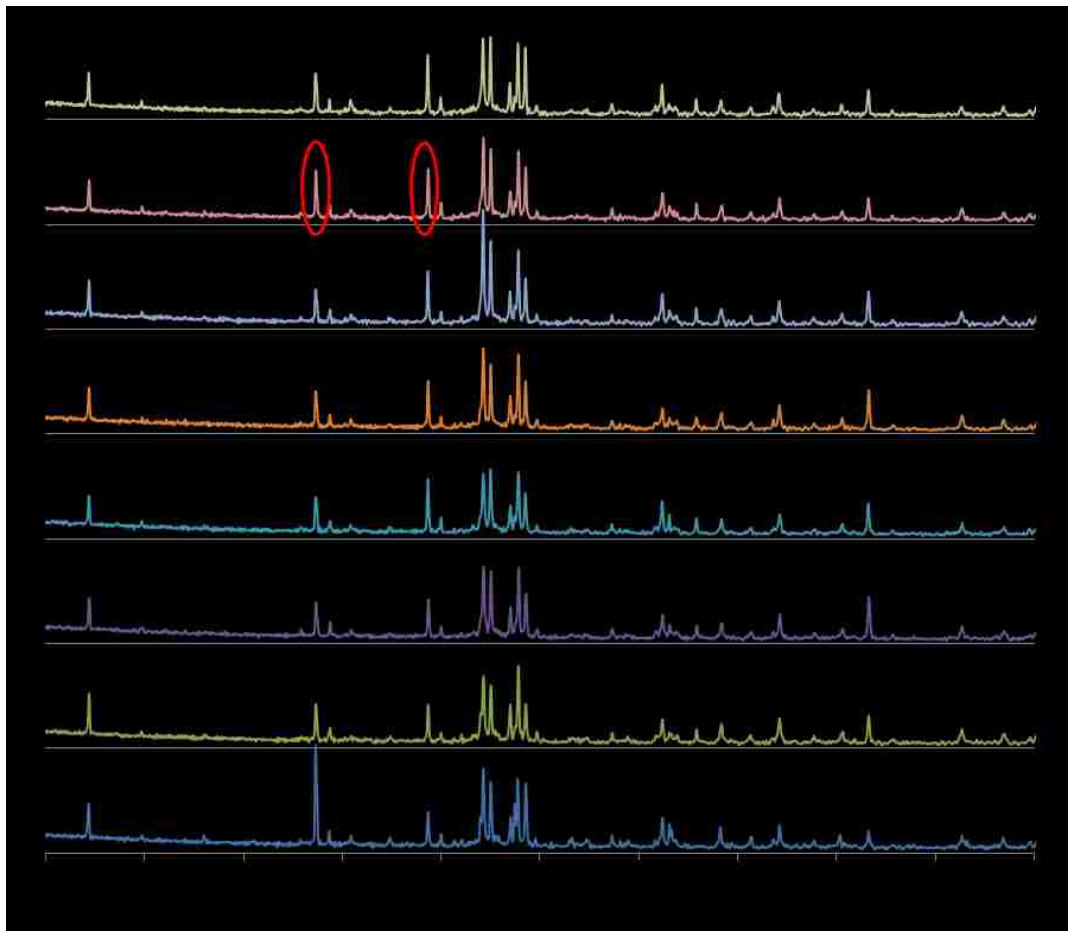


Figure 4-11: XRD data from the different modifications of the amounts of raw materials for the batch #3 made from by-products, fired at  $1250^\circ\text{C}$  for 60min (RM=Red Mud; Sp=Spurlock FBC and Gyp=gypsum). The  $C_4A_3\dot{S}$  and  $C_3S$  peaks, respectively close to  $24^\circ-2\theta$  and  $29^\circ-2\theta$  and circled in red, were both more intense than with all the other modifications.

This modification of the composition was performed on all the other batches to reduce the amount of ferrite and free lime and have a composition as close as possible to the batches made from reagent chemicals. As the composition of the Batch #1-BP did not include any red mud, Class C fly ash was subjected to the same method as red mud because this raw material was the only one to contain a substantial amount of iron oxide in its composition.

As shown in Figure 4-12, the XRD diffractograms of batches #3 indicated that the modified composition from industrial by-products (called MBP to differentiate from BP) better matches the XRD diffractograms of the batch made from reagent chemicals than does the original batch #3. For example the  $C_4A_3\dot{S}$  and  $C_3S$  peaks from the diffractogram (1), at around  $24^\circ-2\theta$  and  $29^\circ-2\theta$  respectively, are higher than the ones from the diffractogram (2). Furthermore the presence of the MgO peak at  $43^\circ$  for diffractograms (1) and (2) is noticeable.

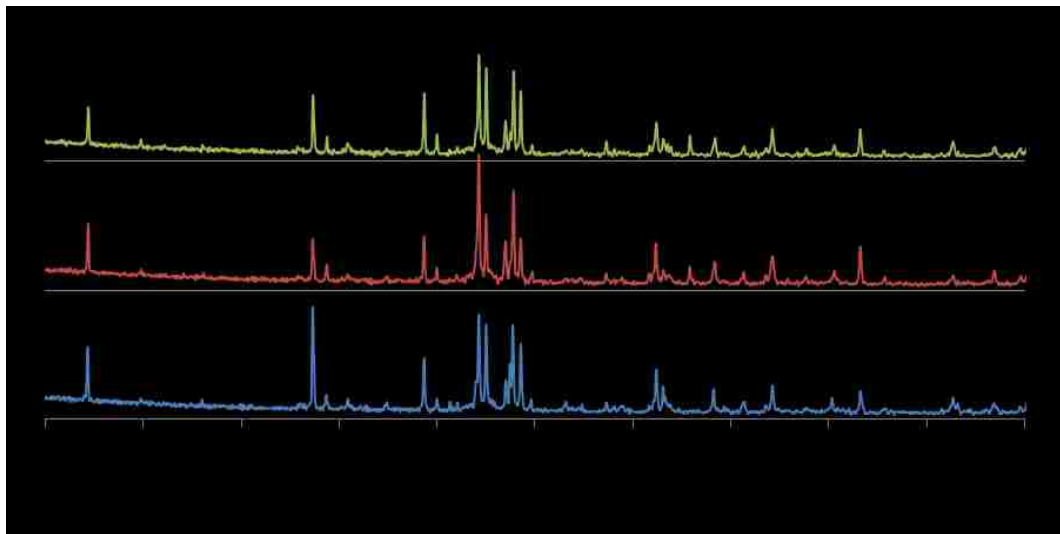


Figure 4-12: XRD data of batch #3 from reagent chemicals, from original by-products (BP) and from modified composition of by-products (called MBP)

The XRD data for the other batches are presented in Appendix E and showed similar results with batch #3. It was also determined that the firing temperature was different depending on the raw materials used. Batches made from MBP (modified by-products) required a lower firing temperature than the ones made from reagent chemicals. This can be explained by the presence of minor phases such as MgO or TiO<sub>2</sub> for example, which can influence the firing process.

In addition to these XRD analyses, free lime tests were performed to confirm the low amount of free lime shown in the XRD diffractograms. The free lime data for the modified batches #1, 2, 3, 4 and 5 from MBP were respectively 0.72%, 0.66%, 0.72%, 0.48% and 0.78%; and were all below 1.0% by weight, which meant that the raw materials had almost completely reacted.

As with the reagent chemicals, SEM/EDS analyses were performed to have more information on the phase composition of the different batches made from MBP and to compare them with the XRD/Rietveld data, which are displayed in Figure 4-13.

All XRD/Rietveld and SEM/EDS data are summarized in Table 4-8. As observed for the previous section with the reagent chemicals, the data were similar. Because the identification of minor phases, such as C<sub>3</sub>A, C<sub>2</sub>S or Fluorellestadite, as well as the differentiation between alite and belite with the SEM/EDS method were very difficult, the sum of both phases, alite and belite, was compared to the other data.

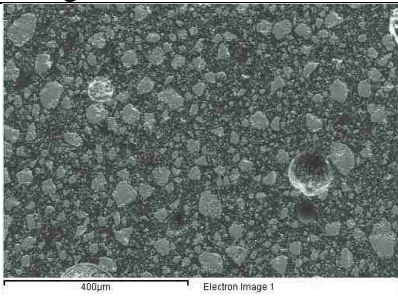
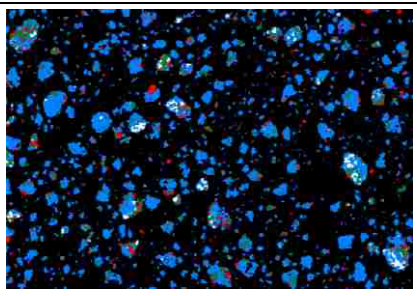
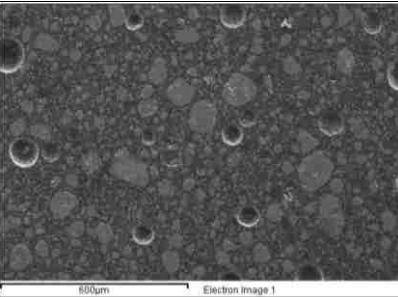
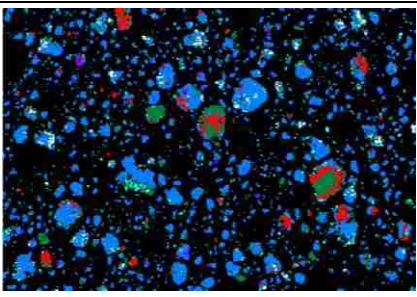
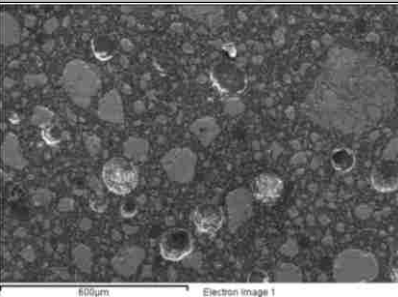
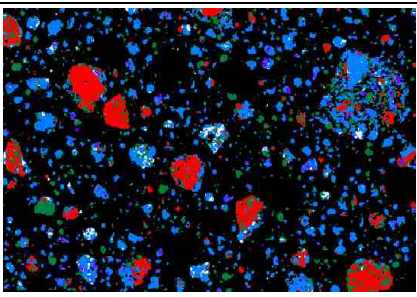
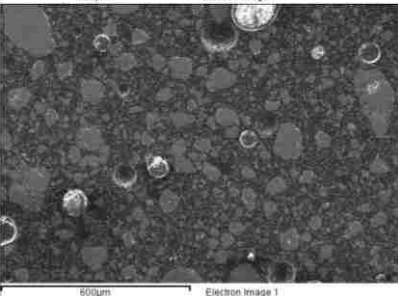
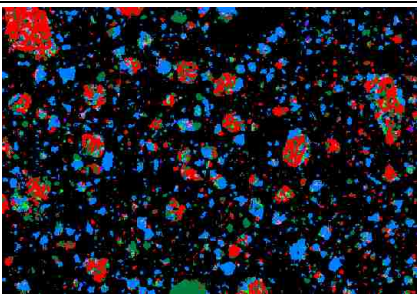
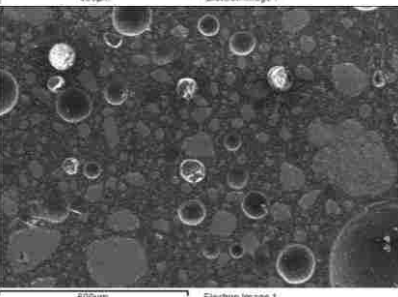
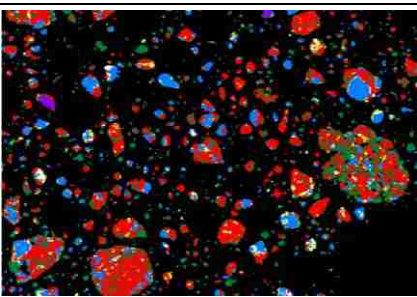
	Original SEM/EDS Pictures	Pictures modified with software
Batch #1 – MBP 1250°C - 60min		
Batch #2 – MBP 1250°C - 60min		
Batch #3 – MBP 1250°C - 60min		
Batch #4 – MBP 1250°C - 60min		
Batch #5 – MBP 1250°C - 60min		

Figure 4-13: SEM/EDS pictures showing clinker phases after firing step (blue= $C_3S/C_2S$ ; red= $C_4AF$ ; green= $C_4A_3S$ ; white=Fluorellestadite; pink= $C_3S/C_2S/C_4AF$ ; yellow= $C_3S/C_2S/C_4AF/C_4A_3S$ ; purple= $MgO$ ; cyan= $CS$ ; flashy green= $C_3A/C_4F$ )

Table 4-8: Summary of XRD/Rietveld and SEM/EDS data for all modified batches from MBP, all fired at 1250°C for 60min (the minor phases, such as Na<sub>2</sub>O, P<sub>2</sub>O<sub>5</sub> and K<sub>2</sub>O were neglected)

Batches	Methods	C <sub>3</sub> S	C <sub>2</sub> S	C <sub>4</sub> A <sub>3</sub> S	C <sub>4</sub> AF	C <sub>S</sub>	CaF <sub>2</sub>	FI*	C <sub>3</sub> A	f <sub>CaO</sub>	MgO	TiO <sub>2</sub>
#1 - MBP	Initial Theory	47.97	20.12	14.54	6.11	4.73	0.78	-	-	-	5.37	0.44
1250°C	Rietveld	50.4	20.5	8.0	7.8	2.9	-	1.4	0.0	0.3	5.9	0
60min	SEM/EDS	73.2		10.7	10.1	-	-	3.0	-	-	3.0	-
#2 - MBP	Initial Theory	42.34	17.05	14.84	14.7	4.74	0.78	-	-	-	4.53	0.84
1250°C	Rietveld	48.02	18.2	10.3	11.3	2.4	-	2.3	0.2	0.2	4.6	0
60min	SEM/EDS	67.3		11.2	11.7	2.7	-	3.2	-	-	3.8	-
#3 - MBP	Initial Theory	35.04	14.49	14.98	24.6	4.74	0.78	-	-	-	3.55	1.29
1250°C	Rietveld	37.0	17.7	10.5	22.2	1.9	-	2.4	1.2	0.3	3.7	0
60min	SEM/EDS	50.3		14.6	28.1	-	-	2.8	-	-	4.2	-
#4 - MBP	Initial Theory	27.63	11.62	14.98	35.05	4.75	0.78	-	-	-	2.55	1.77
1250°C	Rietveld	24.3	14.8	11.7	38.5	1.9	-	4.4	0.5	0.3	1.9	0
60min	SEM/EDS	43.4		13.3	40.9	-	-	-	1.6	-	0.8	-
#5 - MBP	Initial Theory	21.22	8.91	14.67	44.54	4.76	0.78	-	-	-	1.87	2.2
1250°C	Rietveld	15.4	11.5	9.4	53.0	2.2	-	4.3	1.1	0.4	0.4	0
60min	SEM/EDS	23.5		20.4	52.8	-	-	2.4	-	-	0.8	-

The grinding process followed for the samples produced from RC was also followed for the samples made from modified by-products (or MBP). Table 4-9 and Figure 4-14 show that the particle size distribution of the MBP batches gave an opposite trend as the particle sizes increased through the batches #1 to #5. Hence, this suggests that batch #5 was harder to grind than batch #1. This can be explained by the introduction of additional impurities, such as MgO or TiO<sub>2</sub>, which influence the grinding process producing harder clinkers.

Table 4-9: Average of three measurements of particle size distribution for each small pellet

Batches from MBP	Particle Size in μm				
	1	2	3	4	5
d(0.1)	0.92	1.14	1.23	1.22	1.50
d(0.5)	8.91	11.05	11.10	12.26	14.37
d(0.9)	35.29	42.43	46.48	61.49	74.92

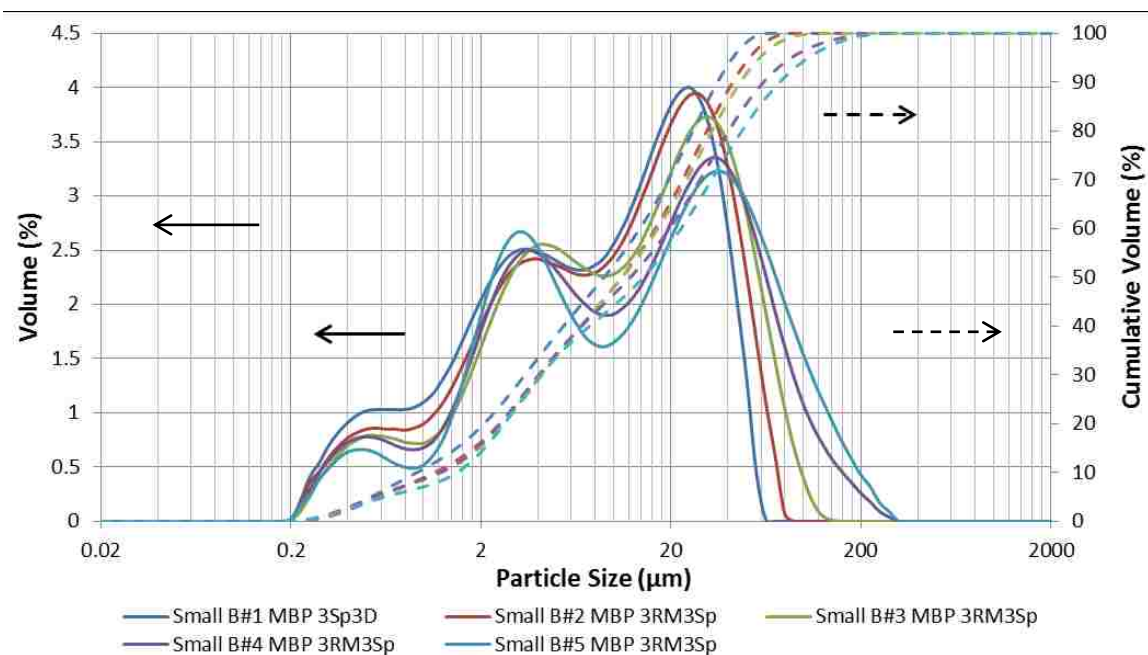


Figure 4-14: Particle Size Distribution of each small batch from modified by-products, after 45sec ground in a shatter box

#### 4.3. Comparison between small RC and MBP samples

Some differences can already be discerned from the production of the compositions from reagent chemicals and industrial by-products. First of all, the firing regime varies with the sources of the raw materials. Compositions produced from RC need a higher firing temperature of 1275-1325°C than the ones made from MBP, which require a firing temperature of 1250°C. The firing temperature may be influenced by impurities introduced from the industrial by-products. A suitable amount of magnesium oxide, MgO, can actually influence and lower the clinkering temperature of both  $C_3S$  and  $C_4A_3\dot{S}$  in a cement. [84] Titanium dioxide can also promote the formation of both  $C_3S$  and  $C_4A_3\dot{S}$ . [54] Both of these observations can explain the lower firing regime required for the samples produced from MBP.

The other difference between the two sources of raw materials is the particle size distribution of the milled compositions. Opposite trends are observed depending on the raw materials used. Milled clinkers from RC tend to decrease in overall particle size through batches #1 to #5, whereas the opposite occurs for the clinkers from MBP. This

phenomenon may also be due to the impurities present in the industrial by-products. It has been demonstrated that the addition of titanium and titanium dioxide affects the crystallographic structure of the ferrite phase [85, 86], and hence this modification can cause the grinding process to differ. Bhatti also confirmed that the addition of 0.25% and 0.5% by weight of titanium into Type I clinker makes this clinker harder to grind as the grindability indices of this clinker decrease. [85]

Even though the clinker composition of batches #1 through #5 were not exactly the same when they were produced from RC or MBP, they were considered close enough to observe the influence introduced from the raw material sources.

## **Chapter 5 : From Reagent Chemicals**

This chapter is dedicated to the chemical and physical studies of clinkers made from reagent chemicals (RC). Large batches of clinker (500g), with similar mineralogical compositions with the small batches of clinker in Chapter 4, were produced. The fabrication process was identical, except for the use of a large pellet mold with a diameter of 5.7 cm and different grinding times, as some of them were easier to grind than others.

The studies presented in Chapter 5 were performed to identify and understand the hydration processes occurring in high-iron alite-calcium sulfoaluminate-ferrite cements. Mechanical tests were conducted to identify the relationships between the chemical and physical properties of these materials. In addition, the influence of triisopropanolamine (TIPA), a chemical which is described later in this chapter, was tested at different concentrations to enhance the material properties.

### **5.1. Characterization tests**

Characterization tests were performed to ensure that the mineralogical compositions of the large batches of clinker were not different from the small batches of clinker previously discussed in Chapter 4.

#### **5.1.1. XRD/Rietveld**

As before, Rietveld analyses were performed to determine the clinker composition of each batch. XRD diffractograms and Rietveld analyses are displayed in Figure 5-1 and Table 5-1. The results show that the reproduction of the small batches from Chapter 4 into large batches was successful, which was confirmed by the almost identical Rietveld values between the small and large batches of clinker in Table 5-1. As a consequence, no SEM/EDS analyses were performed.



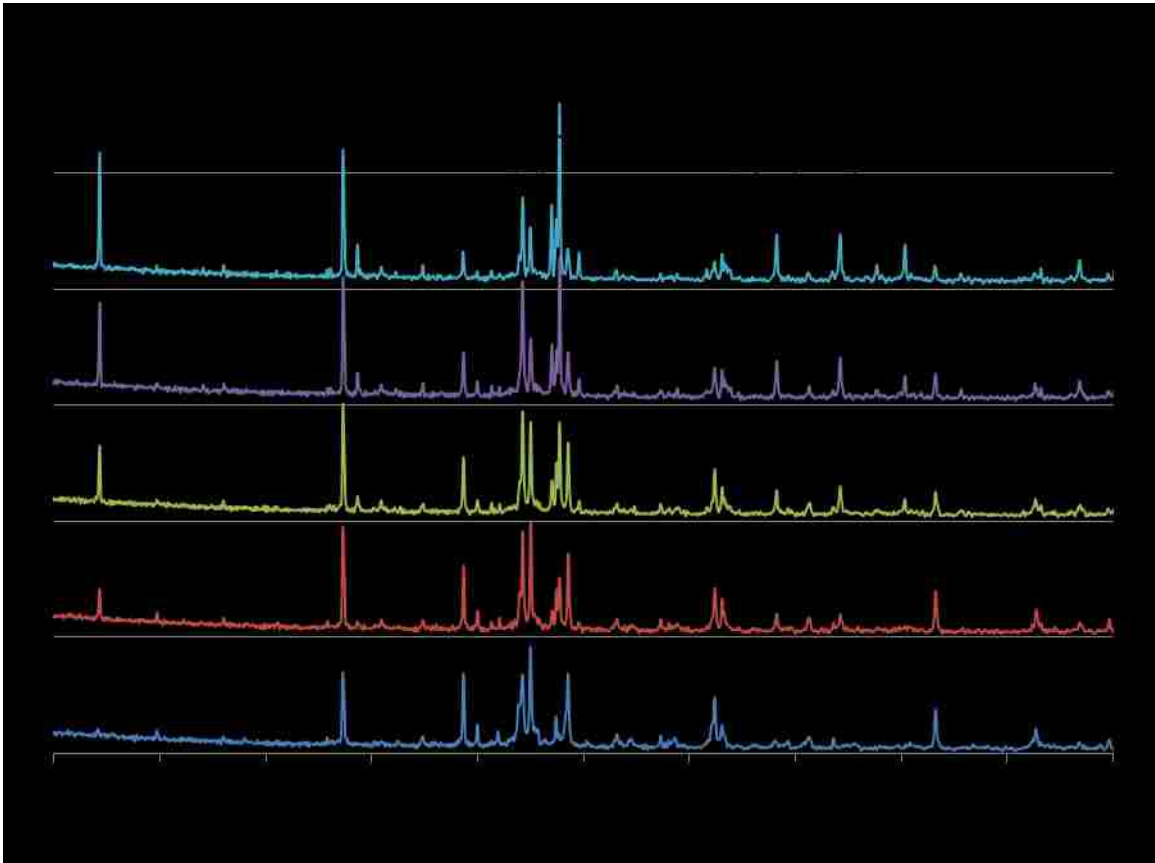


Figure 5-1: XRD graphs from the large batches of clinker made from reagent chemicals

Table 5-1: Comparison of the Rietveld values for each small (chapter 4) and large (this chapter) batches of clinker produced from reagent chemicals (FI\*=Fluorellestadite)

<b>Batches</b>		<b>C<sub>3</sub>S</b>	<b>C<sub>2</sub>S</b>	<b>C<sub>4</sub>A<sub>3</sub>S̄</b>	<b>C<sub>4</sub>AF</b>	<b>C<sub>2</sub>S̄</b>	<b>FI*</b>	<b>C<sub>3</sub>A</b>	<b>f<sub>CaO</sub></b>	<b>MgO</b>
<b>#1 RC</b>	Small Ch4	35.9	41	13.1	3.3	1.0	0.8	2.9	0.5	0.3
	Large Ch5	36.7	39.8	13.8	4	0.8	1.3	1.8	0.3	0.1
<b>#2 RC</b>	Small Ch4	35.0	28.7	16.6	12.9	1.7	1.7	1.1	0.8	0.2
	Large Ch5	34.7	26.5	17.4	15.7	1.3	1.5	0	0	0.5
<b>#3 RC</b>	Small Ch4	27.1	23.3	20.7	22.8	1.9	1.5	0.5	0.6	0.4
	Large Ch5	27.2	25.4	17.9	23.4	1.6	2.4	0.7	0	0.1
<b>#4 RC</b>	Small Ch4	19.8	20.4	22.7	30.8	1.7	2.1	0.9	0.6	0
	Large Ch5	21.6	19.5	19.6	30.9	1.7	2.7	1.2	0	0.5
<b>#5 RC</b>	Small Ch4	18.2	12.6	22.9	39.5	1.6	1.8	1.3	0.7	0.1
	Large Ch5	16.2	14	22.3	41	1.3	3.3	0.5	0	0.2

### 5.1.2. Free Lime

The free lime content was determined for all large batches of clinker #1 to #5, and was respectively 0.6%, 0.5%, 0.3%, 0.4% and 0.2% by weight for each clinker. All compositions included a small amount of free lime below 1.0 wt. %, which validated and confirmed their mineralogical compositions for the following experiments.

### 5.1.3. Particle Size Distribution

As explained earlier, the grinding process varied with the clinker compositions, as some of them required longer grinding times than others to attain a median particle size  $d(0.5)$  close to  $15\mu\text{m}$ , or at least in the same size range for all clinkers.

As displayed in Figure 5-2 and Table 5-2, both data confirmed that the particle size distributions of each batch were close to each other. Indeed, all the  $d(0.5)$  were close to  $8\text{--}14\mu\text{m}$ , and so the particle size should not significantly influence the hydration process for the next steps of this work.

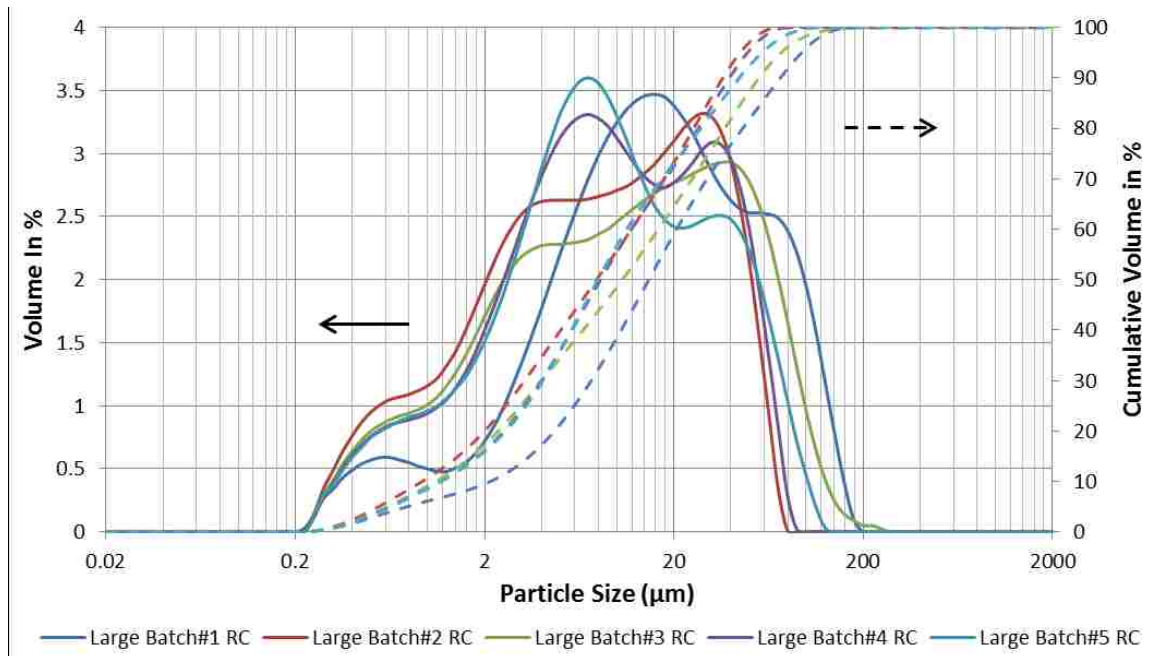


Figure 5-2: Particle Size Distributions of each large batch of clinker produced from reagent chemicals

Table 5-2: Particle sizes d(0.1), d(0.5) and d(0.9) for each large batch of clinker produced from RC (in  $\mu\text{m}$ )

<b>Large Batches #</b>	<b>1</b>	<b>2</b>	<b>3</b>	<b>4</b>	<b>5</b>
<b>d(0.1)</b>	2.15	0.94	1.10	1.18	1.17
<b>d(0.5)</b>	14.73	7.81	10.68	8.19	7.93
<b>d(0.9)</b>	72.91	36.23	56.19	39.24	44.15

## 5.2. Hydration tests

### 5.2.1. Calorimetric tests

As explained in Section 3.2.3.1., calorimeter studies were performed to monitor the hydration processes and identify the optimum amount of gypsum for each clinker produced from reagent chemicals. This study was divided into two parts: to first study the influence of the clinker compositions for a given amount of gypsum; and then to study the influence of gypsum for a given clinker composition. These first analyses provide crucial information for subsequent research, as the hydration pastes would need to be halted at specific times to identify the formed hydrates, and hence the hydration processes.

#### 5.2.1.1. *Influence of the clinker composition with the different weight percentages of gypsum*

In this section, the amount of gypsum included in each clinker was kept constant and only the influence of the clinker composition was studied. All the calorimeter data are displayed in Figure 5-3.

When no gypsum was incorporated into the clinkers (top left graph in Figure 5-3), only two main peaks were observable. The first peak occurred in the first few minutes of the hydration process and could be related to the dissolution of the clinker phases, and also probably to ettringite formation. A second peak occurred after 100 hours, appearing within the clinker #1 at around 120 hours and within the clinkers #2 and #3 at 250 hours. The second peak for the clinkers #4 and #5 may have appeared after 75-150 hours as their total energy curve suggested a slightly increase during this time range.

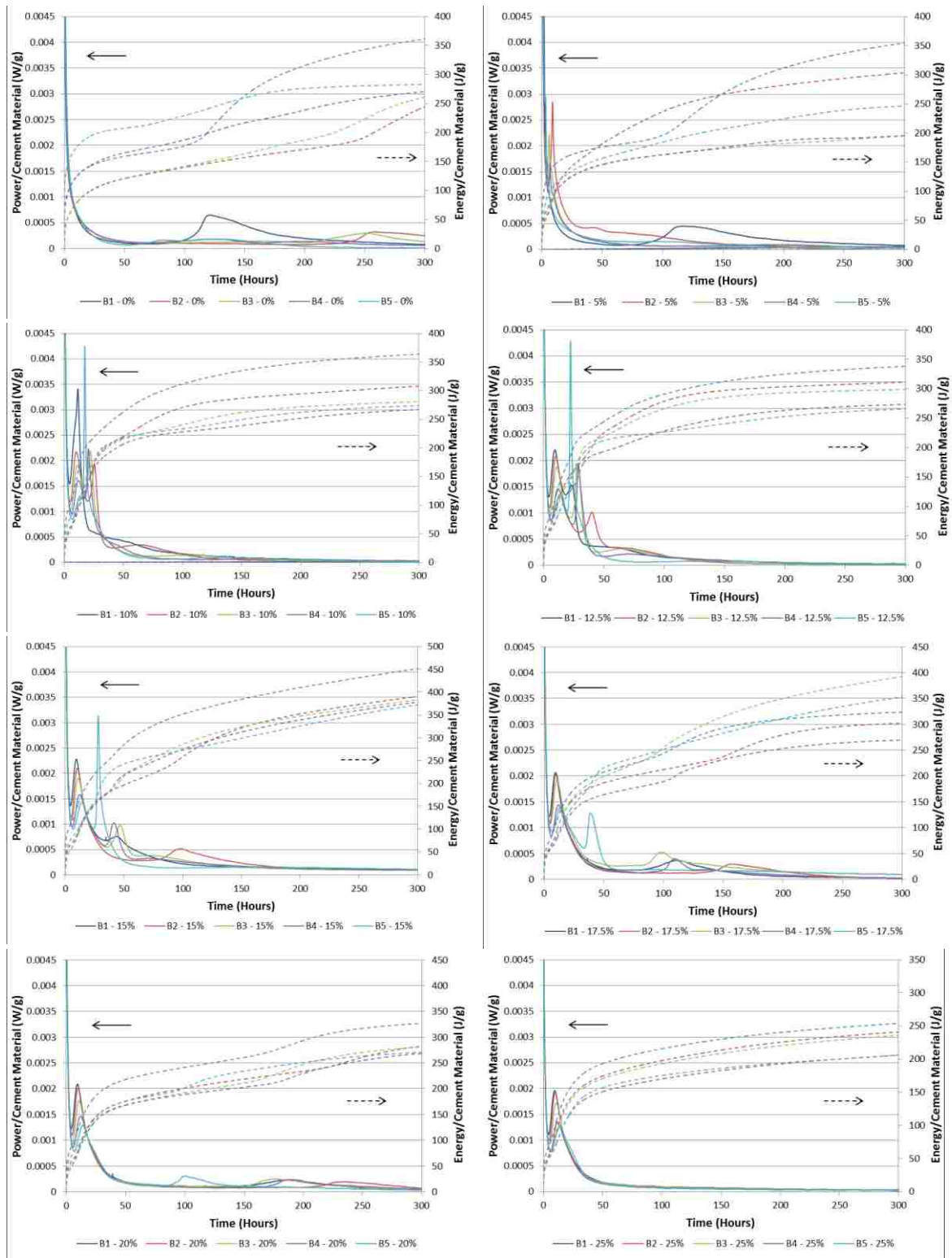


Figure 5-3: Calorimeter analyses for every clinker made from RC with different amounts of gypsum. From left to right, and top to bottom: with 0%, 5%, 10%, 12.5%, 15%, 17.5%, 20% and 25% of gypsum by weight

When 5 % by weight of gypsum was incorporated in each clinker (top right graph in Figure 5-3), two peaks were still visible but occurred at different times. The first peak was still present within the first few minutes of the hydration process in all clinkers, while the second peak occurred at around 110 hours for clinker #1, and between 3 and 9 hours for clinkers #5, #3, #4 and #2 in that order, as shown in a magnification of the top right graph of Figure 5-3 in Figure 5-4. Weak peaks or plateaux could also be discerned in Figure 5-4, as a weak peak around 9 hours was visible just following the second peak of the batch #4 at around 7 hours. As weak as they are, these peaks, or plateaux, are not considered as high hydration reactions unlike the other observed peaks.

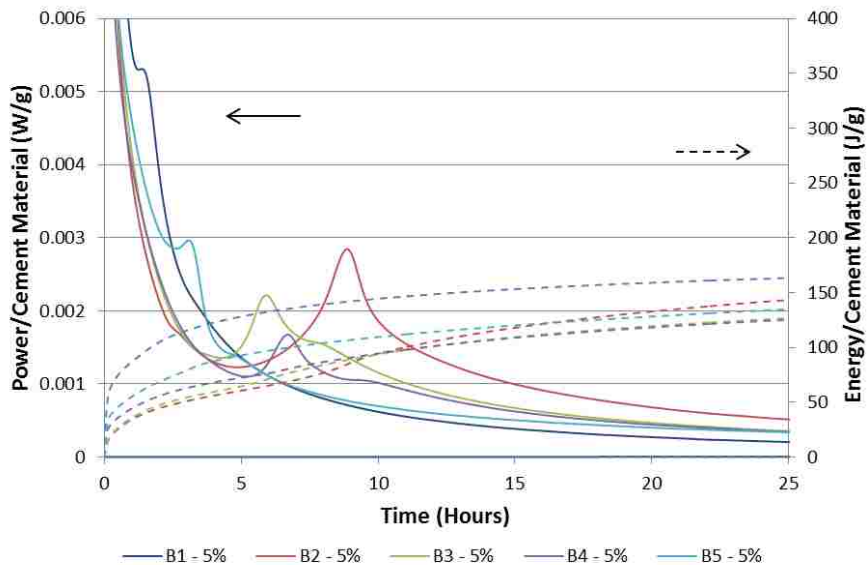


Figure 5-4: Calorimeter analyses for every large batch with 5% of gypsum by weight for the first 25 hours (zoom of the top right graph in Figure 5-3)

For all cements containing more than 10 wt. % of gypsum, another pattern was witnessed as three peaks were now clearly identified. The first peak still occurred within the first minutes of the hydration process for every clinker, while the second peak took place between 5 and 15 hours, and its intensity seemed to decrease from clinkers #1 to #5. The third and last peak appeared after 15 hours and its occurrence depended on the clinker composition. Its intensity seemed to decrease from clinkers #5 to #1.

When more than 25 wt. % gypsum was introduced into each clinker (clinkers with 30%, 40% and 50% gypsum are shown in Appendix F), only two peaks were observed during the 300 hour-test. They were the same as previously described with the 10 wt. % gypsum samples with the first of the two peaks occurring during the first few minutes of the hydration process and the second between 5 and 15 hours. The third peak was missing.

From these calorimeter experiments, the hydration processes were not identical between the clinkers with a given amount of gypsum. With up to 10 wt. % gypsum added, no clear pattern was observed between the clinkers. When more than 10 wt. % gypsum was added, the second peak always occurred between 5 and 15 hours, and its intensity decreased from clinkers #1 to #5. The third peak occurred first within clinker #5, followed by #4 and #3 (or #3 then #4) and always clinker #2 at the end. The third peak of the batch #1 occurred randomly, but never the last. Furthermore, the intensity of this third peak seemed to decrease from clinkers #5 to #1. With more than 25 wt. % gypsum, the hydration reactions occurred similarly to clinkers with 10-20 wt. % gypsum, but the third hydration peak was missing.

As the amounts of calcium sulfoaluminate remains constant in all clinkers, the total amount of silicate (alite and belite) and ferrite phases seems to influence the hydration processes. The influence of each phase on the hydration process is discussed in Section 5.2.2. with the XRD and TGA data performed on the hydration pastes. The evolution of the hydration process also depends on the amount of gypsum introduced in each composition and is detailed in Section 5.2.1.2.

#### ***5.2.1.2. Influence of gypsum in each batch***

The data on the influence of gypsum are similar for all batches, and the results on batch #3 are representative of the other batches. Calorimeter data for the other batches are shown in Appendix G.

As displayed in Figures 5-5 and 5-6, three different patterns were noticeable in batch #3 and the other batches, depending on the amount of gypsum incorporated into the clinkers.

With 0 wt. % and 5 wt. % gypsum introduced into clinker #3, two peaks were observable. The first peak occurred after few minutes into the hydration process for both 0% and 5%

of gypsum. The second peak occurred after around 250 hours with 0% gypsum, and after 5-15 hours with 5% of gypsum. An exception was observed for the clinker #1 with 5% gypsum with its second peak appearing after 100 hours. (Appendix G)

With 10 wt. % gypsum, three peaks were noticeable. The first peak still took place within the first few minutes into the hydration process. The second peak occurred at around 5-15 hours and the last peak emerged after 25 hours into the hydration process.

As the power per cement material is related to the total amount of energy released per cement material, this value is calculated and displayed in Figure 5-6. The relationship between the occurrence of the third peak (Figure 5-5) and the quick increase in the total energy released (Figure 5-6) is obvious, as the curves in Figure 5-5 are the first derivatives of the curves in Figure 5-6. When the energy released curve becomes constant, the hydration process is at its maximum and complete. In Figure 5-6, no curve seems to remain constant after 300 hours of hydration. So for this research work, the total energy released graph is only useful to confirm the apparition of the third exothermic peak, but not to confirm the total energy released.

When more than 10 wt. % gypsum was incorporated into clinker #3, the first and second peaks remained unchanged and constant over time. However, the third and last peak moved later in time with the addition of more gypsum, until its disappearance with more than 25 wt. % gypsum.

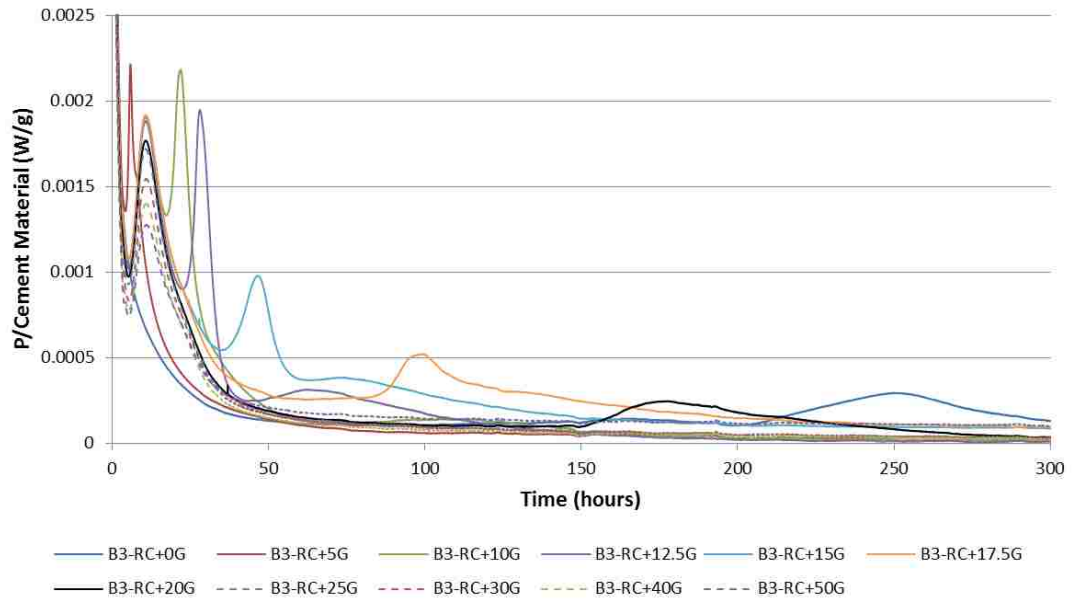


Figure 5-5: Calorimeter data of the power per cement material for the batch #3 from reagent chemicals (RC) with different amounts of gypsum (G) by weight

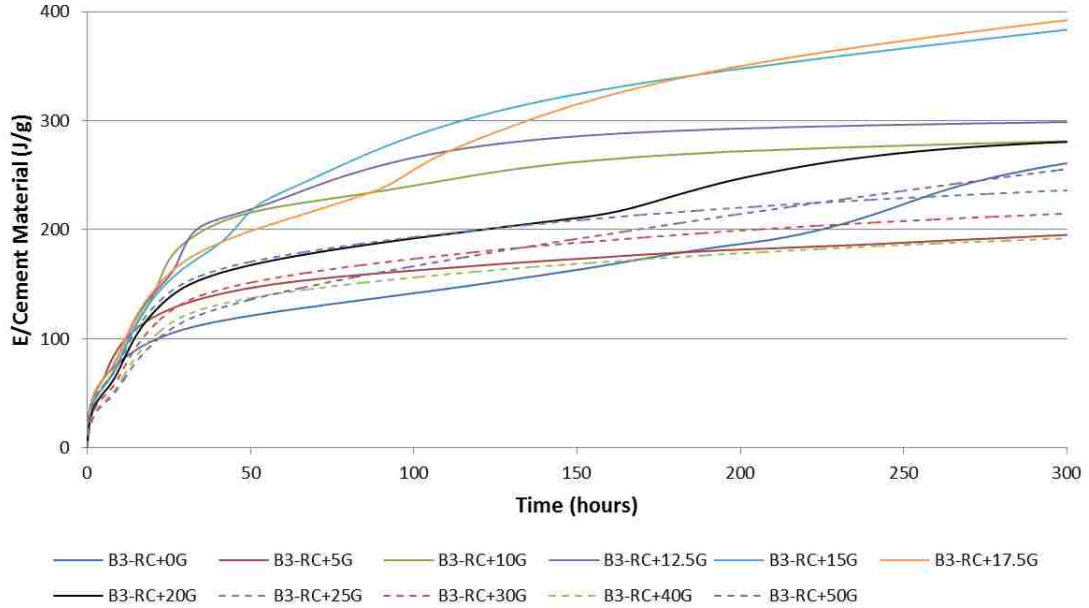


Figure 5-6: Calorimeter data of the energy per cement material for the batch #3 from reagent chemicals (RC) with different amounts of gypsum (G) by weight



**5.2.1.3. Physical aspect of the inside of the calorimeter samples**

Following the 300-hour calorimeter test, a qualitative observation was done to evaluate the physical aspect of cement pastes inside each plastic vial for each tested composition.

Table 5-3 shows all physical information from every tested composition in Section 5.2.1.

Three different physical states were observed:

- Hard cement pastes (H) and not easily “scratchable”, were observed when low amounts of gypsum were incorporated into the clinkers (Figure 5-7 – left picture);
- Moderately hard/soft (H/S) and easily “scratchable” cement pastes were noticeable as significant amounts of gypsum were added, such as 15 wt. % for batch #2, and 20 wt. % for batches #3, #4 and #5. (Figure 5-7 – middle picture);
- Expanded, swelled, or completely “decomposed” cement pastes (Ex) were identified when large amounts of gypsum were introduced into the clinkers (Figure 5-7 – right picture).

Table 5-3: Description of the physical aspect of cement pastes inside the plastic vials after the calorimeter tests were completed (H=hard cement paste, H/S=hard/soft cement paste, Ex=expanded cement paste into powder and a “dome”) of samples produced from reagent chemicals (RC)

<b>% Gypsum (by weight)</b>	<b>0</b>	<b>5</b>	<b>10</b>	<b>12.5</b>	<b>15</b>	<b>17.5</b>	<b>20</b>	<b>25</b>	<b>30</b>	<b>40</b>	<b>50</b>
<b>B#1-RC</b>	H	H	H	H	H	H	H	Ex	Ex	Ex	Ex
<b>B#2-RC</b>	H	H	H	H	H/S	H/S	H/S	Ex	Ex	Ex	Ex
<b>B#3-RC</b>	H	H	H	H	H	H	H/S	Ex	Ex	Ex	Ex
<b>B#4-RC</b>	H	H	H	H	H	H	H/S	Ex	Ex	Ex	Ex
<b>B#5-RC</b>	H	H	H	H	H	H	H/S	H/S	Ex	Ex	Ex



Figure 5-7: Images of several cement pastes from the inside of plastic vials, following the end of the calorimetric tests. Left image: B#3-RC+15G defined as hard cement paste (H); middle image: B#5-RC+25G defined as moderately hard/soft cement paste (H/S) and easily “scratchable”; right image: B#3-RC+50G defined as completely expanded cement paste (Ex), turned into powder-like aspect

This qualitative observation demonstrated the effect of the addition of gypsum to clinkers #1 to #5. Thereby, a low to moderate amount of gypsum, up to 17.5% for almost all clinkers, did not influence their physical aspects, as they remained hard at the touch. With more than 20% gypsum, the cement pastes became softer and easily “scratchable”. And with more than 25% gypsum by weight, all the cement pastes were completely soft and decomposed, back to a powdery aspect.

#### **5.2.1.4. Discussion**

From the study on the influence of the clinker composition with gypsum (Section 5.2.1.1.), the clinker mineralogical composition seems to affect the hydration processes. At low amounts of gypsum (0% and 5 wt. %), two peaks are observed in every clinker and no trend is clearly identified. However, with more than 10% gypsum, the second peak of every clinker occurs in the same time range of 5-15 hours and its intensity decreases from clinkers #1 to #5. Their third peak moves further away in time, with clinker #5 the closest to the second peak, followed by clinkers #4, #3 (or #3 and #4) and #2, the furthest away in time, while its intensity decreases from clinkers #5 to #1.

From the study of the influence of the amount of gypsum in each clinker (Section 5.2.1.2.), gypsum is unmistakably identified as retarding the hydration processes of every clinker. With up to 10% by weight of gypsum, two peaks are observed with the first one occurring within few minutes from the beginning of the hydration process, while the

second peak emerges after more than 100 hours for 0 wt. % gypsum and between 3 and 9 hours for 5 wt. % gypsum. With an amount greater than 10 wt. % of gypsum, three peaks were identified. The second peak remains constant in time, while the third peak moves further away in time with the addition of more gypsum. An excess of 25 wt. % gypsum forces the third peak off the graph (more than 300 hours), or makes it disappear or too weak to be detected.

The qualitative observation of the physical aspect of cement pastes following the calorimeter tests contributes to the comprehension of the influence of gypsum. As clearly observed in Section 5.2.1.3., with up to 20 wt. % of gypsum, the cement paste looks hard but begins to soften as soon as the amount of gypsum reaches 25 wt. %. With more than 25 wt. % gypsum, the cement pastes completely decompose.

By gathering all these information, three different stages can be identified depending on the amount of gypsum added.

The first stage is observed when low amounts of gypsum (0% and 5%) are introduced into clinkers. As the calorimeter tests suggested, no pattern is visible and the cement pastes set very quickly.

As soon as a sufficient amount of gypsum is incorporated, a pattern is identified as the second stage. In fact, three main reactions occur:

- a first peak within the first minutes into the hydration process;
- a second peak between 5 and 15 hours, depending on the clinker composition and independent on the amount of gypsum, as it remains in the same time range with addition of gypsum while its intensity decreases with the clinker composition (highest with clinker #1 and lowest with #5);
- and a third and last peak occurring at different times depending on both their clinker composition and the amount of gypsum. From Figure 5-3, the intensity of the third peak seems to decrease from clinkers #5 to #1. Also, the third peak occurs later in time with the addition of gypsum, until the mixture becomes soft with more than 25% by weight of gypsum.

The third stage is observed when cement pastes begin to soften when more than 25% of gypsum is introduced into the clinkers, which also corresponds to the great delay or disappearance of the third peak in Figure 5-5 and an extreme retardation of the hydration process.

From these calorimetric experiments, different compositions were selected for hydration paste studies. After 5 hours, 1, 7, 28, 90 and 180 days, the hydration process was halted for each sample, as described in Section 3.2.3.2., and XRD and TGA analyses were performed to determine the actual phases formed and consumed.

### **5.2.2. Hydration pastes for large batches of clinkers #1, #3 and #5 produced from reagent chemicals (RC)**

Only clinkers #1, #3 and #5 were selected for hydration paste studies, as clinkers #2 and #4 were considered intermediate clinkers due to their mineralogical compositions. Moreover, the hydration paste of clinker #3 is first described to explain the procedure followed by the interpretation of XRD and TGA results for all the other compositions.

#### **5.2.2.1. Clinker #3 (25 wt. % $C_4AF$ )**

The clinker #3 with 15 wt. % gypsum is selected as an example of the procedure followed to identify the hydrated phases formed and the clinker phases consumed during the hydration process through XRD and TGA tests. All the other XRD and TGA results of the clinker #3 with 0%, 5%, 20% and 30% gypsum are summarized in Appendices H and I.

##### **5.2.2.1.1. XRD analyses**

XRD analyses were performed to identify all clinker phases consumed and all hydrated phases formed as described in Figure 5-8 for clinker#3 with 15 wt. % gypsum. Ettringite was the only hydrated phase formed during the first 5 hours of the hydration process. After 24 hours, portlandite formed, followed by the formation of monosulfate and hemicarboaluminate after 7 days. Regarding the clinker phases, gypsum and alite were completely consumed after 7 days, and  $C_4A_3\bar{S}$  between 7 and 28 days. However, ferrite remained present even after 180 days within the hydration process.

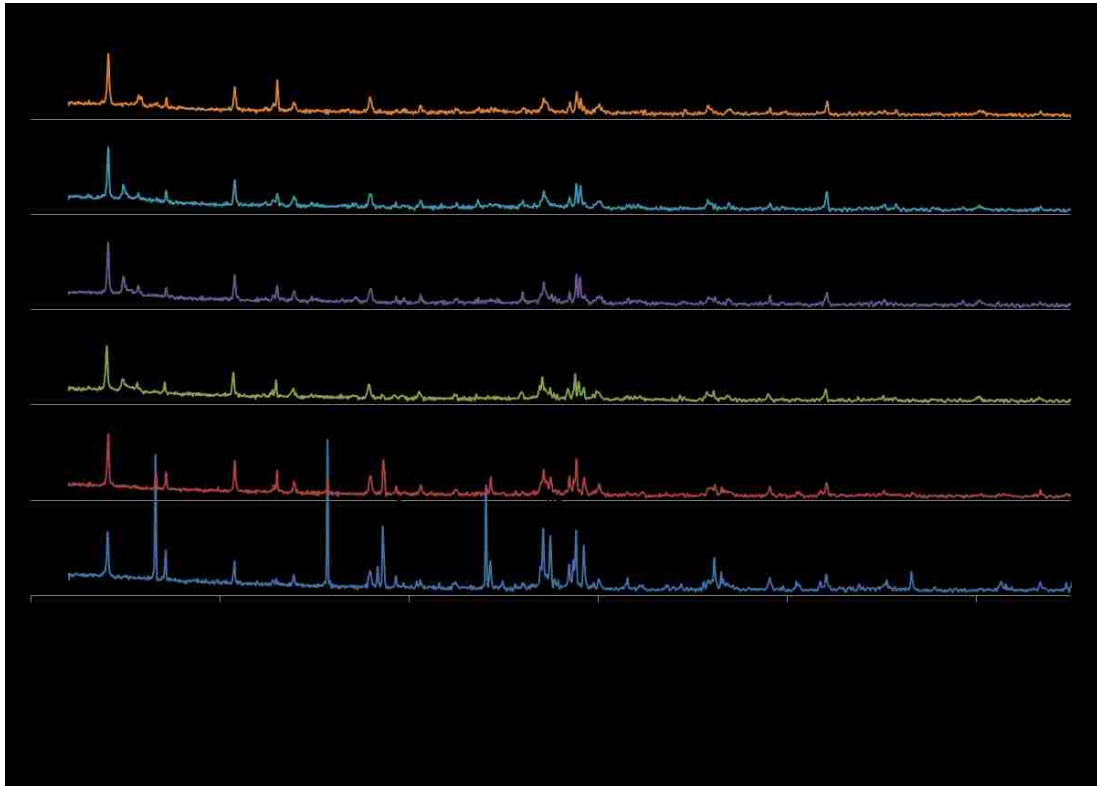


Figure 5-8: XRD analyses of the hydration paste of the clinker #3 with 15 wt. % gypsum, halted after 5 hours, 1, 7, 28, 90 and 180 days

#### **5.2.2.1.2. TGA Analyses**

Following the XRD tests, TGA analyses were performed to identify only the hydrated phases. Table 5-4 displays the major exothermic peaks for each hydrated phase appearing in TGA graphs. Some exothermic peaks corresponding to different hydrated phases occur at the same range of temperatures, such as ettringite and monosulfate at around 100-150°C, as they both lose water molecules.

Table 5-4: Temperatures of decomposition for different hydrates observed in TGA analyses [6, 87-89]

<b>Hydrated Phases</b>	<b>Temperature Range of Endothermic Peaks (°C)</b>
<b>C-S-H</b>	115-125
<b>Ettringite (AFt)</b>	120-130
<b>Gypsum</b>	140-170
<b>Monosulfate (AFm)</b>	180-200
<b>Portlandite</b>	450-500
<b>Hemicarboaluminate (AFm)</b>	≈150 / 250-300 / ≈450 / ≈650 / 800-850
<b>Monocarboaluminate (AFm)</b>	≈150 / 250-300 / ≈650 / 800-850
<b>AH<sub>3</sub></b>	250-300
<b>Hydrogarnet</b>	250-310

The TGA data, displayed in Figure 5-9, confirm the previous XRD results. Ettringite formed between 0 and 5 hours, followed by the formation of portlandite between 5 and 24 hours. Between 1 and 7 days, gypsum was completely consumed while monosulfate formed, which describes perfectly the hydration reaction of  $C_4A_3\dot{S}$  mentioned in Chapter 3. A small peak around 300°C was detected after 7 days and could correspond to the formation of hydrogarnet, or aluminum hydroxide AH<sub>3</sub>, as the hydration of calcium sulfoaluminate forms ettringite and aluminum hydroxide, or it could also correspond to a carbonated phase (hemicarboaluminate or monocarboaluminate) as another peak around 900°C was detected.

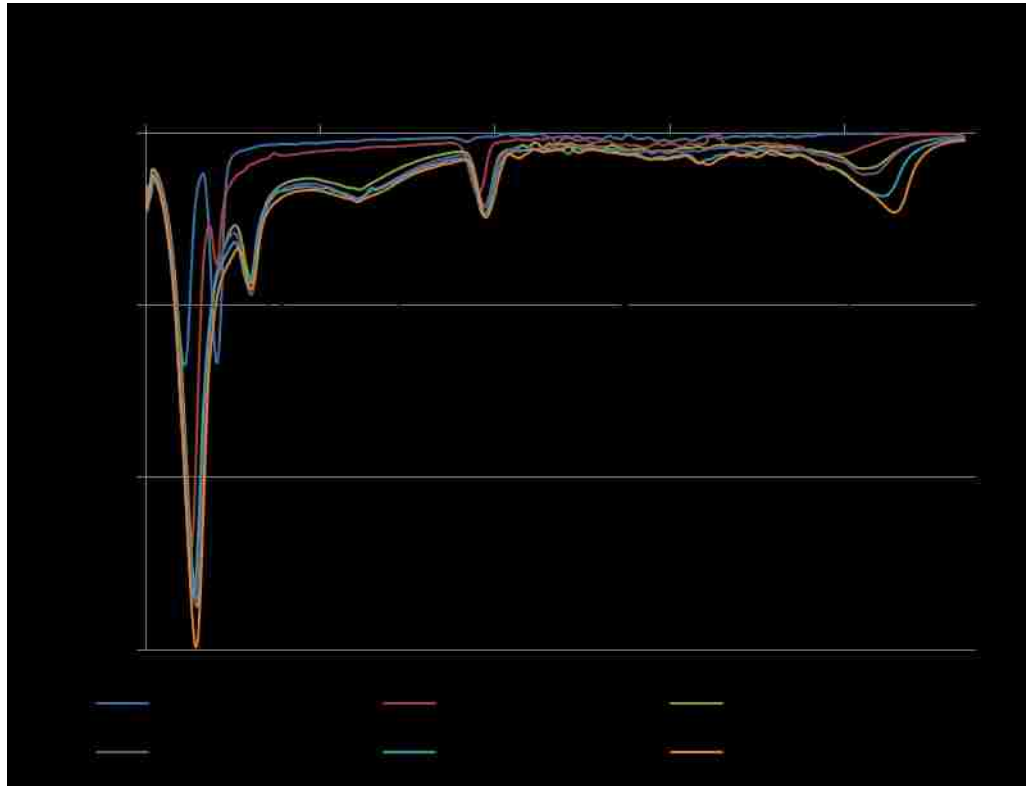


Figure 5-9: TGA graph of the hydrated cement paste of clinker #3 with 15% gypsum stopped after 5 hours, 1, 7, 28, 90 and 180 days

#### 5.2.2.1.3. “Stellerite” phase

An unexpected phase was identified for all clinkers with 0 wt. % and 5 wt. % gypsum. As displayed in Figure 5-10, a XRD peak occurred at around  $10\text{-}11^{\circ}\text{-}2\theta$  for clinker #3 with no gypsum at 5 hours, and with 5 wt. % gypsum at 24 hours. The peak was “curved”, which corresponds to a poorly crystalline or nearly amorphous phase. Also from Figure 5-11, small peaks in the TGA results are present in the same samples and as the XRD analyses (Figure 5-10) around  $140^{\circ}\text{C}$ . While comparing the ICDD files to identify the XRD peaks, “stellerite” was the best match. This aluminosilicate mineral has for chemical formula  $\text{CaAl}_2\text{Si}_7\text{O}_{18.7}(\text{H}_2\text{O})$ , or  $\text{CAS}_7\text{H}_7$  in cement chemistry. The hypothesis is that at low amounts of gypsum (0 wt. % and 5 wt. %), a “stellerite”-like phase forms, composed of aluminosilicate, or a phase crystallographically close to this phase (for example, an aluminum substitute silicate phase or a hydrated calcium silicate phase

without Al is also possible). This may happen as the chemical reactions occur too quickly and the silicate phases  $C_2S$  and  $C_3S$  may not be able to hydrate entirely.

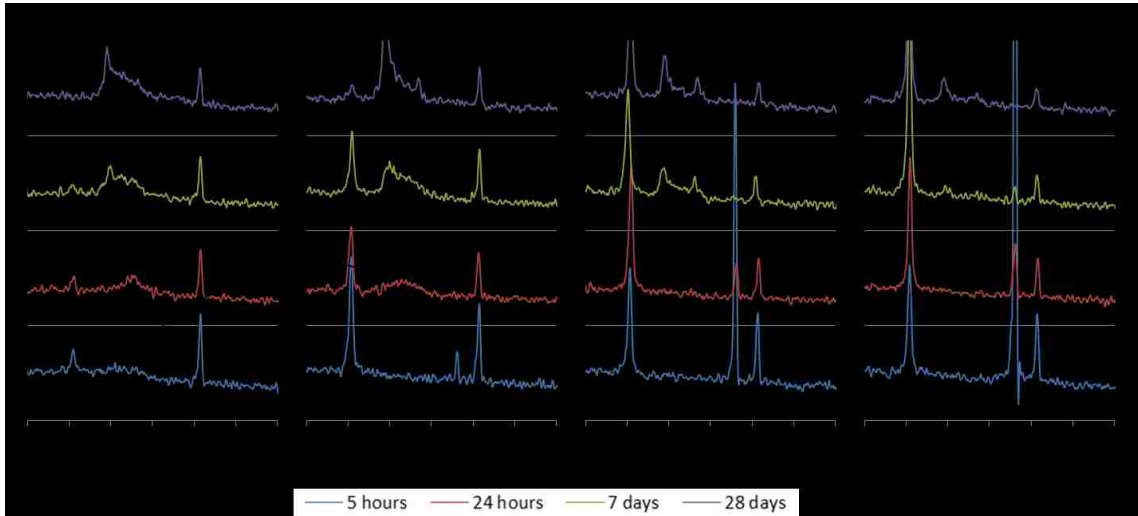


Figure 5-10: XRD graphs illustrating the evolution of "stellerite" "rounded-peak" (between 10 and 11°-2 $\theta$ ) through sample #3 with addition of gypsum

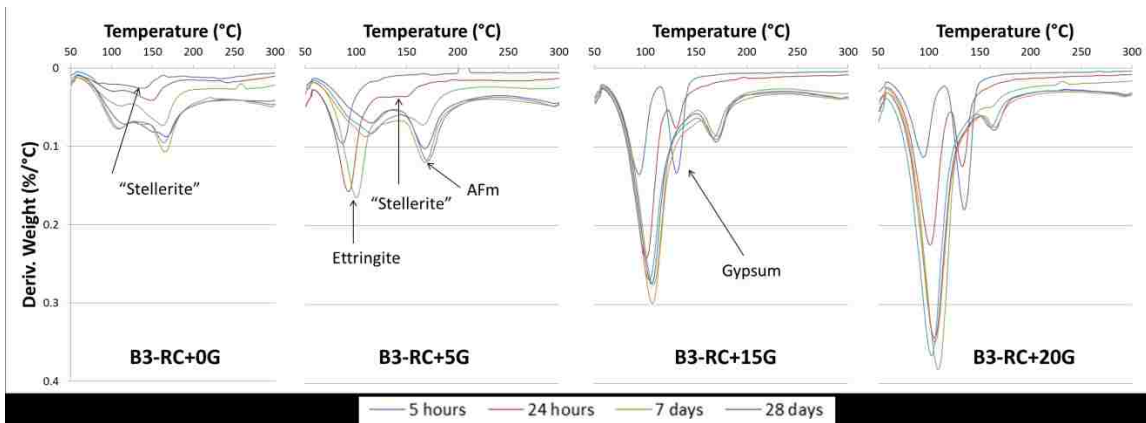


Figure 5-11: TGA graphs illustrating the evolution of the "stellerite" peak through sample #3 with addition of gypsum



**5.2.2.1.4. Summary of all XRD and TGA analyses from the study of hydration pastes of clinker #3**

All data retrieved from XRD and TGA analyses are shown in Table 5-5, indicating a time range for each clinker phase being consumed and each hydrate being formed.

Table 5-5: XRD and TGA data showing the clinker phases consumed and the hydrates formed from the hydration paste of clinker #3 with various amounts of gypsum (sign + means that this phase remained in the cement paste even after 180 days of hydration and “time/time” means “formation/consumption”)

% Gyp	Consumption				Formation							
	Gyp	C <sub>4</sub> A <sub>3</sub> S̄	C <sub>3</sub> S	C <sub>4</sub> AF	Ett	Stell	MonoS	Ca(OH) <sub>2</sub>	% of Ca(OH) <sub>2</sub> H <sub>2</sub> O at 180d	Hydro	HemiC	MonoC
0	0-5h	7-28d	7-28d	+	0-5h/7-28d	0-5h	1-7d/90-180d	7-28d	1.8	-	90-180d	-
5	5h-1d	7-28d	7-28d	+	0-5h	5h-1d	1-7d/90-180d	7-28d	1.4	-	90-180d	-
15	1-7d	7-28d	1-7d	+	0-5h	-	1-7d/90-180d	5h-1d	1.4	-	1-7d	-
20	7-28d	7-28d	1-7d	+	0-5h	-	1-7d/90-180d	5h-1d	1.5	-	7-28d	-
30	28-90d	28-90d	1-7d	+	0-5h	-	7-28d	5h-1d	1.0	-	-	-

MonoS = Monosulfate; Hydro = Hydrogarnet; HemiC = Hemicarboaluminate, MonoC = Monocarboaluminate, Ett = Ettringite, Stell = “Stellerite”, Gyp = Gypsum

The data from Table 5-5 were compared with the calorimeter data from clinker #3, displayed in Figure 5-12, and the peaks were associated with specific reactions to understand the hydration process during the first 300 hours. To organize the data, the analysis of the hydration process is divided into time ranges.

From 0 to 5 hours into the hydration process, a high hydration peak occurred within few minutes in all batches and corresponds to the dissolution of the clinker phases and to the formation of ettringite. “Stellerite” was also detected in clinker #3 without gypsum.

Between 5 and 24 hours, no hydrated phase was formed in clinker #3 without gypsum. However, “stellerite” was formed in clinker #3 with 5 wt. % gypsum, and portlandite was detected in clinker #3 with 15%, 20% and 30 wt. % gypsum. The presence of portlandite implies that the silicate phases hydrated into C-S-H and Ca(OH)<sub>2</sub>.

Between 1 and 7 days, no peak was visible for clinker #3 with 0% and 5 wt. % gypsum, even if the presence of monosulfate was detected. Yet, a third peak for clinker #3 with 15 and 20 wt. % gypsum occurred between 1 and 7 day and monosulfate formed, as well as hemicarboaluminate in the composition with 15 wt. % gypsum. Nothing formed in clinker #3 with 30% gypsum, and no peak appeared.

Because the calorimetric test was only conducted for 300 hours, data at 28 days were not obtained. Yet, from TGA analyses, portlandite formed in clinker #3 with 0% and 5% gypsum, and monosulfate in clinker #3 with 30 wt. % gypsum.

After 90 days of hydration, monosulfate was completely consumed in clinker #3 with 0% and 5 wt. % gypsum, while hemicarboaluminate formed.

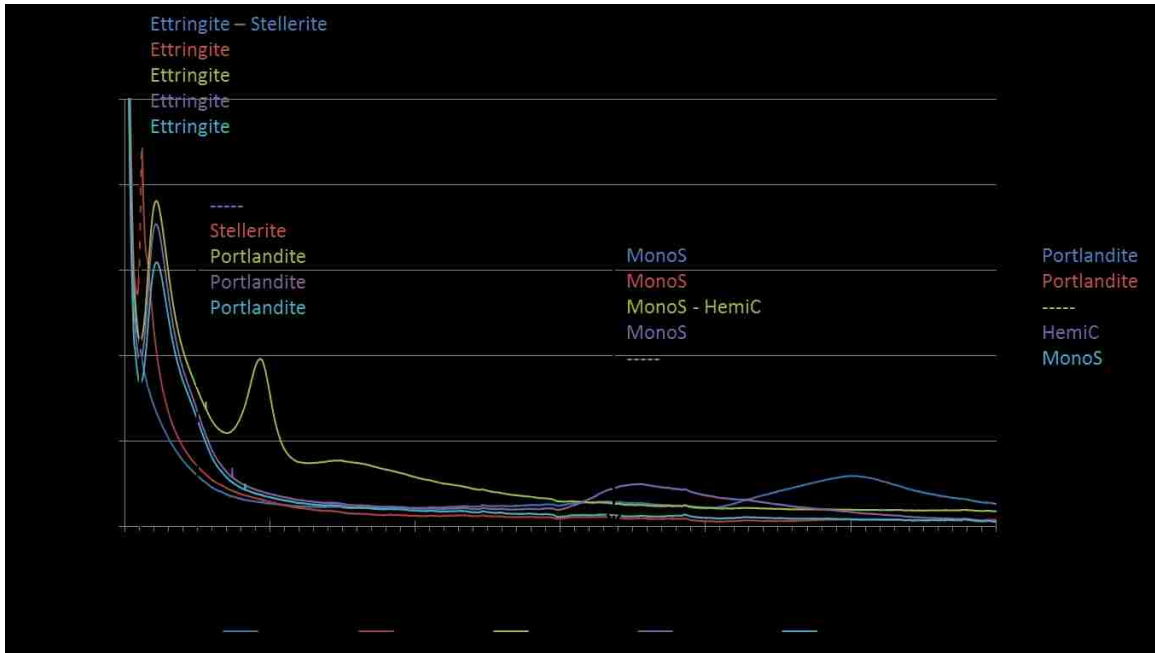


Figure 5-12: Calorimeter data of hydration paste of clinker #3 with various amounts of gypsum combined with XRD and TGA results from hydration pastes, halted after 5 hours, 1, 7 and 28 days. The 90 and 180-day measurements are not included in this graph.

By combining all the information retrieved from calorimeter, XRD and TGA analyses, a hypothesis of the hydration process can be derived. As previously described in Section 5.2.1.4., three stages were identified depending on the amount of gypsum added to the clinker sample. The first stage occurs at low amounts of gypsum incorporated, such as 0% and 5% by weight, and the hydration reactions occur instantly as ettringite and stellerite formed during the first 5-6 hours. The next stage occurs with the addition of 15% and 20% by weight of gypsum, and the rate of the hydration reactions slows down. No stellerite is detected, but instead portlandite forms at around 5-15 hours. As observed earlier, the second peak decreases from the batch #1 to #5, which can be explained by the

amount of silicate phases decreasing from 72% in clinker #1 to 32% in clinker #5. The hydration of the silicate phases is then followed by the conversion of ettringite to monosulfate as it occurs after the appearance of the third peak at 50 hours for 15% gypsum, and 150 hours for the 20 wt. % gypsum. The last stage is observed with an excess of gypsum, such as 30 wt. % gypsum, where the same first two hydration reactions occur (ettringite and portlandite), but the last reaction (ettringite to monosulfate) occurs after 300 hours into the hydration process, giving the cement paste a powder-like aspect.

In conclusion for clinker #3, the optimization of the hydration process is evaluated by optimizing the amount of gypsum, which is here identified as from 10% to 20% gypsum. If not enough gypsum is added, the reactions occur too quickly, preventing the silicate phases from hydrating completely and forming “stellerite” instead. Also, if too much gypsum is added, the hydration reactions occur too slowly, and the cement paste decomposes.

#### **5.2.2.2. Clinker #1 (5% $C_4AF$ )**

The same set of experiments with clinker #3 in Section 5.2.2.1 was followed for clinker #1. All XRD diffractograms and TGA graphs are shown in Appendix H and I, respectively, and a summary of these data are displayed in Table 5-6. This information was then compiled with the calorimeter data retrieved from clinker #1, as done previously for clinker #3 in Section 5.2.2.1., and displayed in Figure 5-13. The same hypothesis derived for clinker #3 is also applied to clinker #1.

During the first stage, at low amounts of gypsum (0% and 5 wt. %), both ettringite and “stellerite” form very rapidly inside the cement pastes. This was followed by the hydration of the silicate phases and the conversion of ettringite to monosulfate after 100 hours.

The second stage occurred with 15-20 wt. % gypsum, and ettringite was the only hydrate to form after 5 hours of hydration. Contrary to the first stage, silicate phases hydrated earlier than 100 hours, in this case between 5 and 15 hours, and silicate hydration took place at the same time range with gypsum exceeding 15 wt. %. The third peak of clinker

#1 with 15 and 20 wt. % gypsum, present during the 300 hour-test, corresponded to the conversion of ettringite to monosulfate.

Whereas for the clinker #1 with 30 wt. % gypsum, representing the third stage, the hydration process was identical to the second stage, with the exception of the third peak missing related to monosulfate formation, making the cement paste completely soft.

The consumption of ferrite in clinker #1 was complete after only 7 days, indicating that the low amount of ferrite, only 5 wt. % in clinker #1, completely reacted.

Table 5-6: XRD and TGA data presenting the clinker phases consumed and the hydrates formed from the hydration paste of clinker #1 with various amounts of gypsum (sign + means that this phase remained in the cement paste even after 180 days of hydration; and time/time means formation/consumption)

% Gyp	Consumption				Formation								
	Gyp	C <sub>4</sub> A <sub>3</sub> S	C <sub>3</sub> S	C <sub>4</sub> AF	Ett	Stell	MonoS	Ca(OH) <sub>2</sub>	% of Ca(OH) <sub>2</sub> H <sub>2</sub> O at 180d	Hydro	HemiC	MonoC	
0	0-5h	1-7d	7-28d	1-7d	0-5h/7-28d	0-5h	1-7d	1-7d	3.2	-	-	-	
5	0-5h	7-28d	7-28d	1-7d	0-5h	0-5h	1-7d	1-7d	2.5	-	-	-	
15	7-28d	7-28d	28-90d	1-7d	0-5h	-	1-7d	5h-1d	2.4	-	-	-	
20	28-90d	7-28d	7-28d	1-7d	0-5h	-	7-28d	5h-1d	2.1	-	-	-	
30	28-90d	28-90d	7-28d	1-7d	0-5h	-	-	5h-1d	1.9	-	-	-	

MonoS = Monosulfate; Hydro = Hydrogarnet; HemiC = Hemicarboaluminate, MonoC = Monocarboaluminate, Ett = Ettringite, Stell = "Stellerite", Gyp = Gypsum

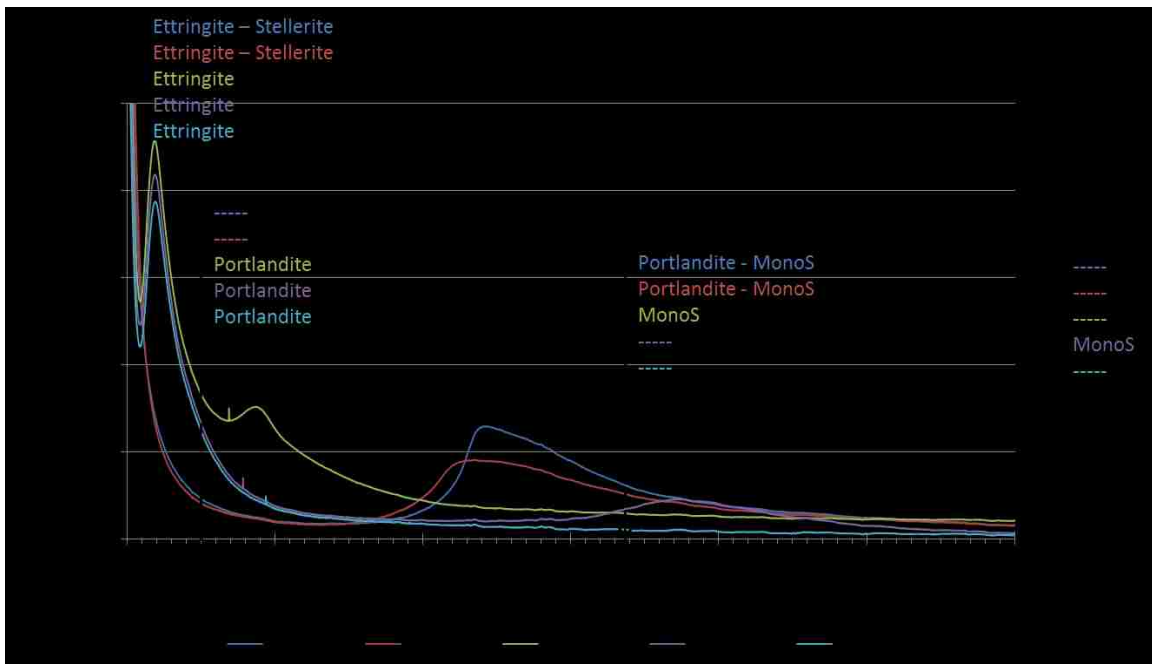


Figure 5-13: Calorimeter data of hydration paste of clinker #1 with different amounts of gypsum stopped after 5 hours, 1, 7 and 28 days. The 90 and 180-day measurements are not included in this graph.

### 5.2.2.3. *Clinker #5 (45% C<sub>4</sub>AF)*

The same procedure that was used with clinkers #3 and #1, in Sections 5.2.2.1. and 5.2.2.2., was followed for clinker #5. All the XRD diffractograms and TGA graphs are shown in Appendix H and I respectively, and a summary of these data are displayed in Table 5-7. This information was then compiled with the calorimeter data retrieved from clinker #5 and displayed in Figure 5-14.

Three different stages were clearly identified during the hydration of clinker #5 with gypsum, like those observed with clinkers #1 and #3.

The first stage occurred at low amounts of gypsum (0 wt. % and 5 wt. %). Stellerite first formed between 0 and 5 hours, followed by the formation of hydrogarnet between 1 and 7 days when no gypsum was present. With 5 wt. % gypsum, ettringite first formed, followed by stellerite, monosulfate, hemicarboaluminate and hydrogarnet.

The second stage occurred with gypsum between 15-20 wt. % with the formation of ettringite before 5 hours. Silicate phases hydrated between 5 and 24 hours, followed by the formation of monosulfate and hemicarboaluminate.

The third and last stage occurred when an excess of gypsum was added to clinker #5, where only ettringite and portlandite were formed, and the cement paste appeared completely soft with a powder-like aspect.

The consumption of ferrite in this clinker was incomplete even after 180 days into the hydration process. Furthermore, the formation of hydrogarnet was first noticed in this clinker, and may result from the large amount of ferrite initially present in the clinker. As explained in Chapter 3, the hydration of ferrite without gypsum produces hydrogarnet. The formation of hydrogarnet was thus retarded with the addition of gypsum, and hydrogarnet was formed when all sulfates were consumed and a lot of unreacted ferrite remained in clinker #5.

Table 5-7: XRD and TGA data presenting the clinker phases consumed and the hydrates formed from the hydration paste of clinker #5 with various amounts of gypsum (sign + means that this phase remained in the cement pastes even after 180 days of hydration; and time/time means formation/consumption)

% Gyp	Consumption				Formation								
	Gyp	C <sub>4</sub> A <sub>3</sub> S̄	C <sub>3</sub> S	C <sub>4</sub> AF	Ett	Stell	MonoS	Ca(OH) <sub>2</sub>	% of Ca(OH) <sub>2</sub> H <sub>2</sub> O at 180d	Hydro	HemiC	MonoC	
0	0-5h	7-28d	7-28d	+	-	0-5h	90-180d	28-90d	n.d.	1-7d	28-90d	90-180d	
5	0-5h	7-28d	1-7d	+	0-5h/90-180d	5h-1d	1-7d	28-90d	0.7	7-28d	1-7d	-	
15	1-7d	28-90d	1-7d	+	0-5h	-	1-7d	5h-1d	0.5	28-90d	1-7d	90-180d	
20	7-28d	28-90d	1-7d	+	0-5h	-	1-7d	5h-1d	0.4	28-90d	1-7d	90-180d	
30	28-90d	28-90d	1-7d	+	0-5h	-	-	5h-1d	n.d.	-	28-90d	-	

MonoS = Monosulfate; Hydro = Hydrogarnet; HemiC = Hemicarboaluminate, MonoC = Monocarboaluminate, Ett = Ettringite, Stell = "Stellerite", Gyp = Gypsum, n.d. = not determined

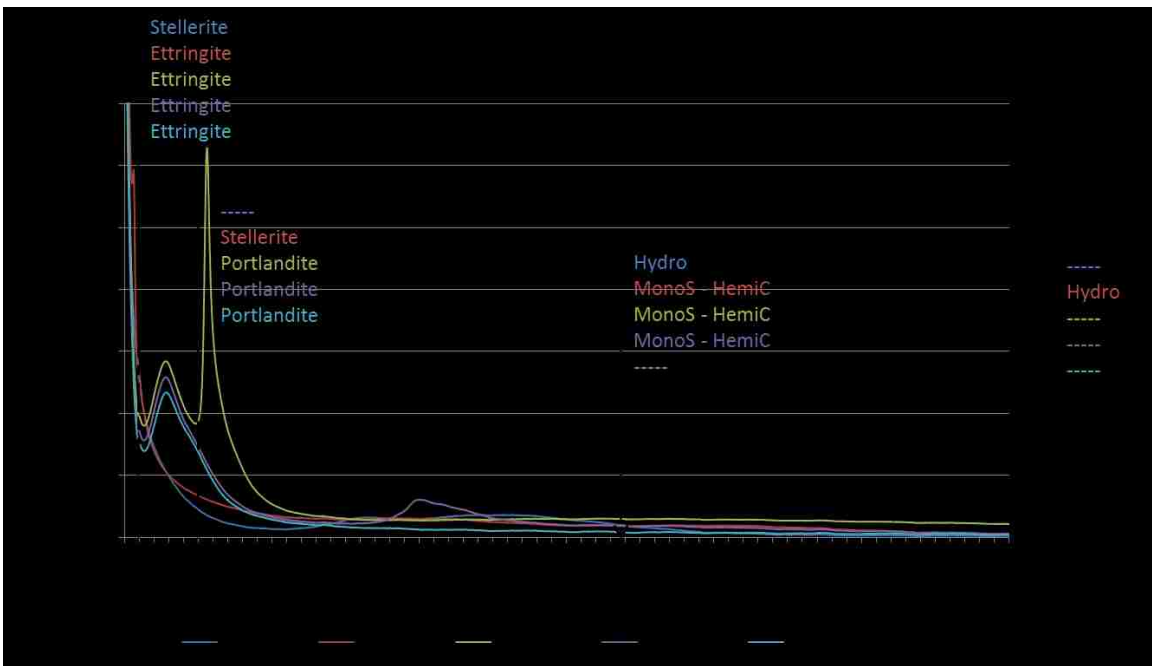


Figure 5-14: Calorimeter data of hydration paste of clinker #5 with different amount of gypsum stopped after 5 hours, 1, 7 and 28-day. The 90 and 180-day measurements are not included in this graph.

### 5.2.3. Summary of the findings

Several conclusions may be drawn from all of these hydrated pastes studies through calorimeter, XRD and TGA analyses:

- The more ferrite in a clinker, the more difficult ferrite hydrates. In clinker #1 with 5 wt. % C<sub>4</sub>AF, all ferrite is consumed, whereas in clinkers #3 and #5, ferrite is still present even after 180 days of hydration.

- Three hydration stages are discerned depending on the amount of gypsum introduced into the clinkers. The first stage occurs with gypsum up to 10 wt. %, the second stage between 10 wt. % and 25 wt. % gypsum, and the third stage above 25% by weight of gypsum. In each stage, the hydration process differs slightly. During the first stage, the clinker is “under-sulfated”, meaning there is not enough gypsum to slow down the hydration reactions. Due to this, ettringite and “stellerite” first form, followed by the formation of AFm phases and portlandite. During the second stage, when an appropriate amount of gypsum is added, only ettringite first forms, and no “stellerite” is present. Also, the silicate phases hydrate just after the formation of ettringite, producing portlandite. This is followed by the formation of AFm phases. During the third stage, the conversion from ettringite to AFm phases occurs too late, producing a powdery cement paste. Gypsum is therefore identified as an important additive for these clinkers, as an inappropriate amount of it can strongly affect the hydration reactions and the physical aspect of the cement pastes.

- The optimum amount of gypsum for each clinker is identified between 10% and 20% by weight through the Lerch method. As explained in Section 3.2.3.1., Lerch [77] established a method to evaluate the optimum amount of gypsum required for OPC as: “A properly retarded cement is defined on the basis of the shape of the heat-liberation curve during the first 30 [hours] of hydration. A properly retarded cement is one that contains the minimum quantity of gypsum required to give a heat-liberation curve that shows two cycles of ascending and descending rates and that shows no appreciable change with larger additions of gypsum. The results of the physical tests show that when considering cements ground from a given clinker, those containing the proper amount of gypsum to give this type of curve will develop the highest strength and the lowest contraction.” If his method is followed for these high-iron alite-calcium sulfoaluminate-alite cements, the amounts of gypsum required for clinkers #1 to #5 from the calorimeter graphs (Appendix G) are respectively 15%, 12.5%, 15%, 15% and 17.5% by weight.

### **5.3. Mechanical tests**

#### **5.3.1. Preparation and testing**

As explained in Section 3.2.4., the preparation of the compressive strength samples was modified from ASTM C109 [4] as not enough material was available for this test and thus “mini-mortar cubes” of 2.54 cm were produced.

To evaluate and compare these new materials, OPC samples were prepared in the same way as alite-calcium sulfoaluminate-ferrite samples. The cement consisted of clinker mixed with gypsum, and the cement:graded sand ratio by weight was kept at 1:2 for all samples, as well as the water:cement ratio at 0.45.

Two OPC type I, from two fresh and commercially available Type I OPC, were evaluated at two different sizes, 2.5 and 5 cm, to evaluate the influence of the cube size during the compressive strength test.

As discussed in Section 5.2.3., clinkers #1 to #5 have an optimum amount of gypsum of 10-20 wt. %. Two amounts of 10 wt. % and 15 wt. % gypsum were also tested for each clinker to observe the influence of gypsum.

#### **5.3.2. Results**

Figure 5-15 shows all of the data on each sample and several conclusions are stemmed from these results.

First of all, the change in the cube size, from 5 to 2.5 cm with OPC, affected its compressive strength with lower cube size. Moreover, the two tested OPC (2.5 cm) presented similar data after 7 and 28 days of hydration.

The influence of gypsum was not really obvious through these results, as the compressive strengths for each clinker with 10 wt. % and 15 wt. % gypsum were very similar to each other.

However, the influence of the clinker composition strongly affected the compressive strength. As the quantity of calcium sulfoaluminate remained constant in each composition and the ferrite content increased while silicates content decreased through clinkers #1 to #5, the compressive strength lowered for the five clinkers. This can be



explained by the reduced amount of silicate phases, which are responsible for the early strength of the cement, especially alite. As mentioned in Section 5.2.2. during the hydration paste studies, the ferrite phase does not hydrate completely, except in clinker #1 due to its low concentration. Thus the decreasing compressive strength is mainly due to the lowering of the amount of alite combined with the non-reactivity of the ferrite phase.

The physical aspect of the cement pastes following the calorimeter tests (Section 5.2.1.3.) demonstrated that an excess of gypsum caused cement pastes to weaken and to completely decompose, clinkers with high amounts of gypsum were not realized.

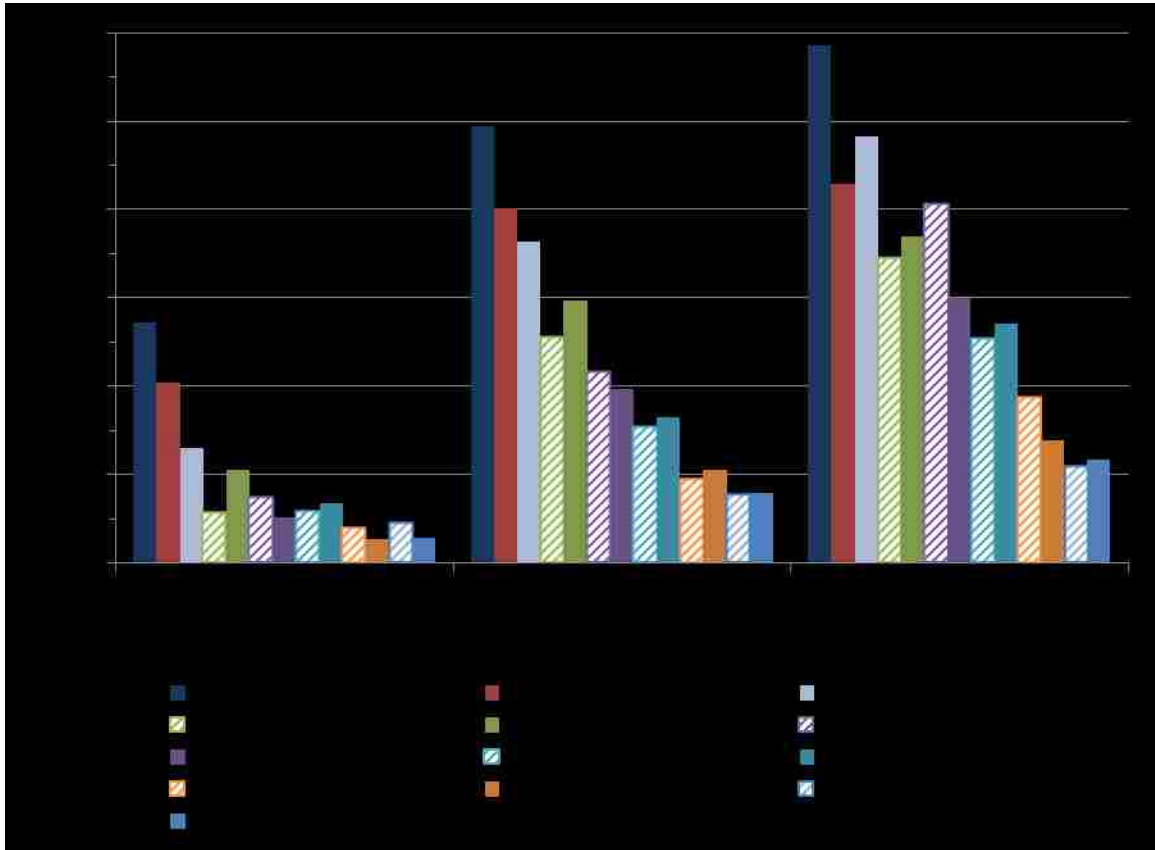


Figure 5-15: Comparison of compressive strength measurements of OPC with clinkers made from reagent chemicals (RC) with 10% and 15% of gypsum

#### 5.4. Summary of the hydration process

Several conclusions can be drawn from all of the experiments on hydration processes and mechanical properties. As described previously, three stages are observed during the hydration process of the clinkers depending on the amount of gypsum introduced in low, appropriate or excess amounts. These stages greatly affect the hydration processes and the physical properties of the clinkers. The main hypothesis is that increasing the amount of gypsum above the optimal quantity decreases the compressive strength, as the cement paste starts to harden, then becomes easily scratchable before completely desintegrating above 25 wt. % gypsum. In fact, an appropriate addition of gypsum slows down the hydration reactions, allowing the silicate phases to completely hydrate, instead of “blocking” their reactions when there is no gypsum present.

Clinker compositions also affect the hydration processes as well as the mechanical properties. As the amount of silicates phases decreases and ferrite phase increases through clinkers #1 to #5, the compressive strength decreases. Even with addition gypsum, as the quantity of silicate phases decreases, the early strength decreases too, and the ferrite phase is unable to completely hydrate.

The solution to improve the mechanical properties of these materials is to compensate the strength lost from the decreasing amount of silicates by finding a way to completely hydrate the ferrite phase. A question arises on determining how to hydrate the ferrite phase. With the use of an additive to hydrate C<sub>4</sub>AF, more gypsum will then be required to react with the now reactive ferrite, previously unreacted, to produce ettringite. A theoretical amount of gypsum can be estimated, as gypsum only reacts with the aluminate phases (C<sub>4</sub>A<sub>3</sub>Ŝ and C<sub>4</sub>AF) to produce ettringite.

An equation is then derived in Appendix J and is:

$$\text{Gypsum required} = \frac{100 * 1.26 * (0.45 C_4A_3\hat{S} + 0.84 C_4AF - C\hat{S})}{100 + [1.26 * (0.45 C_4A_3\hat{S} + 0.84 C_4AF - C\hat{S})]}$$

Gypsum required, C<sub>4</sub>A<sub>3</sub>Ŝ, C<sub>4</sub>AF and CŜ are expressed in weight percentages in this equation.

By using this equation with the theoretical and Rietveld clinker compositions from Chapter 3, the quantities of gypsum determined from Lerch and this equation were compared and the data are displayed in Table 5-8. For clinkers #1 and #2, the optimum amount of gypsum determined from Lerch and the equation were close to each other. However, for clinker #3, #4 and #5, richer in ferrite than #1 and #2, the results differed greatly with the increasing amount of ferrite.

Table 5-8: Comparison between the amounts of gypsum required for each clinker to completely react, determined from Lerch method and from the equation of gypsum required with the theoretical and Rietveld results

Clinkers from RC	Lerch method	Equation of gypsum required	
		Theory	Rietveld
#1	15	7	10
#2	12.5	15	20
#3	15	22	25
#4	15	28	30
#5	17.5	33	35

As these high-iron alite-calcium sulfoaluminate-ferrite cements are novel and differ from OPC by their mineralogical composition, Lerch method needs to be modified, and a new method for the sulfate optimization of these high-iron cements needs to be developed.

The following experiments, presented in Section 5.5., evaluate the influence of triisopropanolamine (TIPA) in high-iron cements produced from reagent chemicals.

### **5.5. Improvement of the mechanical properties with the utilization of triisopropanolamine (TIPA)?**

To improve the mechanical properties of a cement, several admixtures have long been investigated, especially alkanolamines, as grinding agents and enhancers of cement strength. Triisopropanolamine (TIPA) is a strong additive capable of increasing compressive strength after 7 and 28 days in high-iron cements. The literature on this chemical compound is detailed in Section 5.5.1.

### 5.5.1. Effects of Triisopropanolamine – Literature Review

Triisopropanolamine, or TIPA, is an aminoalcohol which belongs to the alkanolamine group. TIPA consists of hydroxyl and amino functional groups, as seen in Figure 5-16. In this study, the TIPA came from Acros Organics, with a purity of 98%. This chemical is white to light yellow with a texture similar to wax and is completely soluble in water. [90]

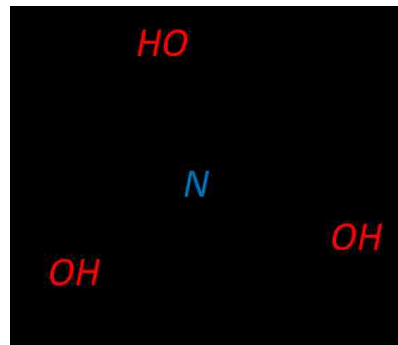


Figure 5-16: Chemical structure of triisopropanolamine (TIPA)

The influence of TIPA on cement was first discovered by Myers and Gartner [91] in the late 1980's. Their patent presents a method to enhance the strength of cement (containing at least 4 wt. % of  $C_4AF$ ) after 7 and 28 days by incorporating an admixture (TIPA) up to 0.2 wt. %. This admixture is also used as a grinding agent in cements to reduce the compaction of finished cement during the milling process.

In 1993, Gartner and al. [92, 93] proposed a mechanism explaining the influence of TIPA (named CB100 in his paper [93]) on ferrite. Their hypothesis is that TIPA acts as a catalyst to accelerate the formation of AFm phases by forming a complex iron-TIPA which increases the iron solubility and accelerates the hydration reactions of iron-bearing phases. This hypothesis lies on the facilitated transport processes mechanism [92], represented in Figure 5-17, [94] As a complex iron-TIPA forms, the iron barrier “breaks” around the silicate phases, making it possible for all of the clinker phases to hydrate, hence increasing the compressive strength of cement. Ichikawa et al. found that TIPA promoted the hydration of ferrite as well as alite, which correlates with the conclusions in Gartner et al. [95] They also noticed that the addition of TIPA increased the optimum amount of  $SO_3$  in cement after 28 days.

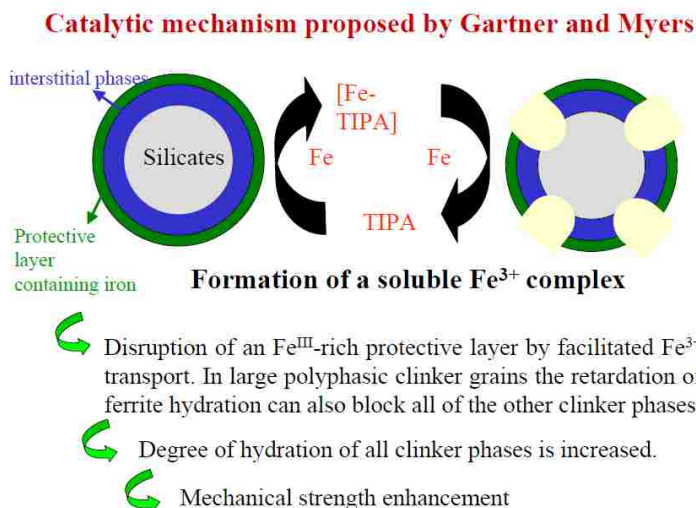


Figure 5-17: Schema displaying the influence of TIPA with ferrite, proposed by Gartner and Myers [94]

This mechanism is questioned by some results showing that the amount of portlandite, resulting from the hydration of silicate phases, remains constant with or without addition of TIPA. [96] This would mean that TIPA does not influence the hydration of the silicate phases, hence contradicting the Gartner et al. mechanism.

Even if the mechanism of TIPA on the hydration process is not completely understood, its advantages on the mechanical properties are well known. Indeed, several studies report great enhancement of the compressive strength of cements with addition of TIPA. [97-99] In these studies, the maximum content of C<sub>4</sub>AF in cements was 14 wt. %, and TIPA was 0.1 wt. %. The goal of this study is to analyze the effect of TIPA on high-iron alite-calcium sulfoaluminate-ferrite cements with C<sub>4</sub>AF up to 45 wt. %.

### 5.5.2. Effect of TIPA on selected compositions

The effect of TIPA was investigated on clinkers containing large quantities of ferrite, such as clinkers #3 and #5. Calorimeter analyses were first performed on both clinkers with various amounts of gypsum and TIPA. Hydration pastes and mechanical tests were only performed on specific samples from clinker #5, as this composition contained the highest amount of ferrite. Through all of the following experiments, the addition of TIPA was correlated to the mass of cement material (clinker with gypsum), for example 1.0% by weight of TIPA to 2.0g of cement was in fact 0.02g of added TIPA.

### **5.5.2.1. Calorimeter Tests**

During calorimeter measurements, TIPA was introduced in two ways, depending on its amount, to minimize the error from the weighting step. When TIPA was added at 0.1% by weight of the cement (2.0g), 0.002g has to be added to the 0.9g of DI water (w/c=0.45). As this quantity was too small, 0.1g of TIPA was first dissolved in 45g of deionized water and 0.9g of TIPA dissolved in water was transferred into a plastic vial for the calorimeter test, followed by the addition of 2.0g of cement material. When the amount of TIPA exceeded 0.1 wt. %, TIPA was directly added to the 0.9g of water, followed by the addition of cement, which was stirred with water for approximately 30 seconds before the plastic vial was placed in the TAM Air instrument.

#### **5.5.2.1.1. Clinker #3 (25% C<sub>4</sub>AF)**

Figures 5-18 and 5-19 display the calorimeter data for clinker #3 produced from RC with 20% and 30% by weight of gypsum and various amounts of TIPA.

The third peak from clinker #3 with 20 wt. % gypsum shifted to short times with the increasing amounts of added TIPA (Figure 5-18). Furthermore, the energy/cement material released increased with the addition of TIPA. No third peak occurred in clinker #3 with 30 wt. % gypsum with addition of TIPA. The second peak, however, altered with TIPA.

From the description of the physical appearance of the samples following the calorimeter analyses (Table 5-9), the influence of TIPA was not obvious as the clinker #3 with 20% by weight of gypsum stayed hard with addition of TIPA, while clinker #3 with 30% by weight of gypsum remained soft.

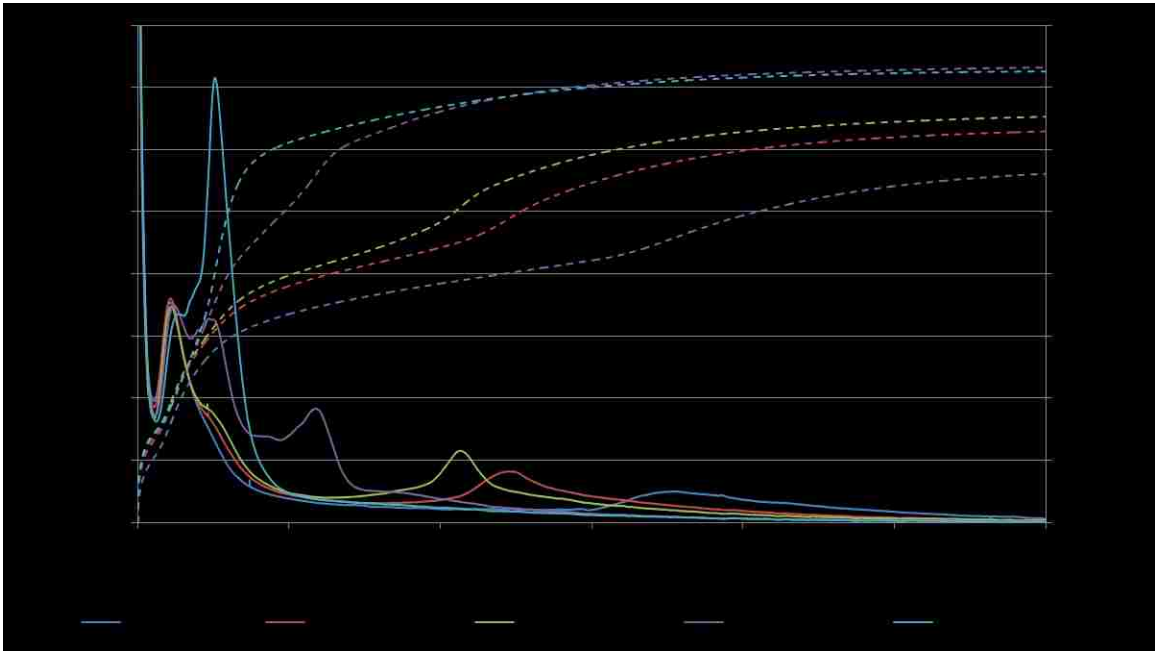


Figure 5-18: Calorimeter results of clinker #3 produced from RC with 20 wt.% gypsum (G) and different amounts of TIPA (T) for 145 hours

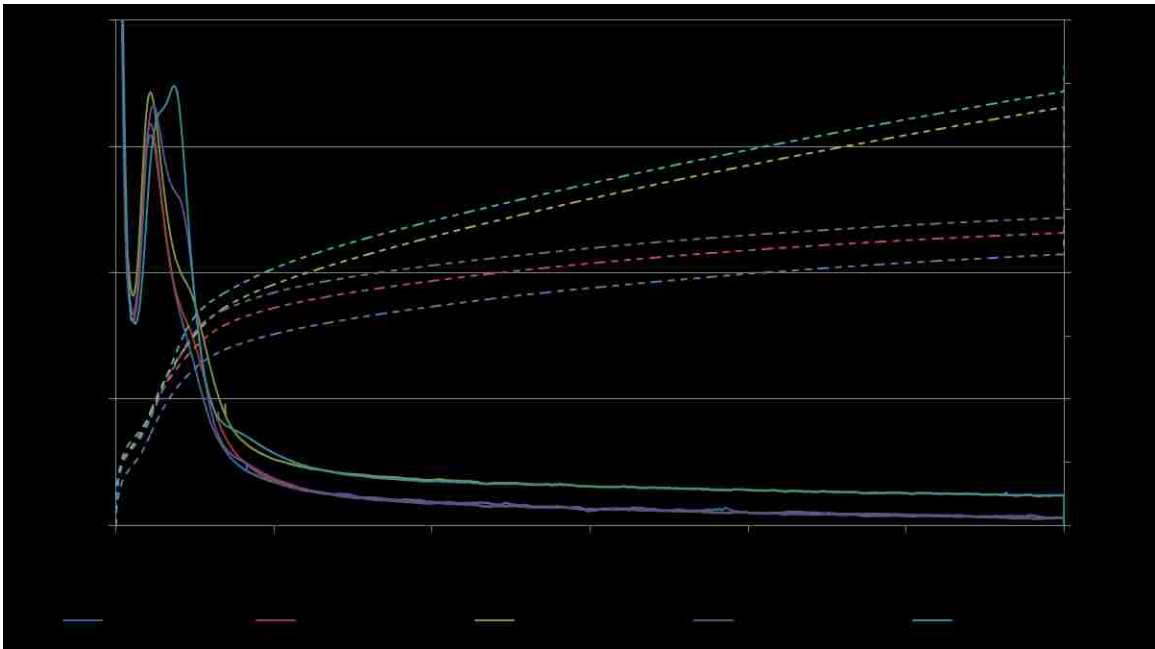


Figure 5-19: Calorimeter results of clinker #3 produced from RC with 30 wt. % gypsum (G) and different amounts of TIPA (T) for 145 hours

Table 5-9: Visual appearance of the cement paste from clinker #3 inside each plastic vials after the end of the calorimeter test (H=hard, S=scratchable, Ex=expanded)

<b>% TIPA</b>	<b>0</b>	<b>0.05</b>	<b>0.1</b>	<b>0.5</b>	<b>1.0</b>
<b>B#3-RC+20G</b>	H	H/S	H/S	H	H
<b>B#3-RC+30G</b>	Ex	Ex	Ex	Ex	Ex

**5.5.2.1.2. Clinker #5 (45% C<sub>4</sub>AF)**

Figures 5-20 to 5-24 display the calorimeter data for clinker #5 produced from RC with various amounts of gypsum and TIPA.

From Figures 5-20 to 5-22, the same pattern is observed. The third peak, appearing after 17, 120 and more than 300 hours for the compositions with 10, 20 and 30 wt. % of gypsum, respectively, was the only peak affected by the addition of TIPA. Indeed, the addition of TIPA caused the third peak to shift to shorter times.

A maximum amount of TIPA was identified for each composition as the third peak appeared constant for a TIPA content of 0.5, 0.5 and 2.0 wt. % for clinker #5 with respectively 10, 20 and 30 wt. % of gypsum.

With the addition of TIPA, the power/cement material for the third peak was ten times higher than without TIPA, and the energy/cement material released nearly doubled with the addition of TIPA.

When 40 and 50 wt. % gypsum was mixed with clinker #5 and TIPA, the third peak did not move to shorter times, under 300 hours, except for clinker #5 with 40 wt. % gypsum and 5.0 wt. % TIPA occurring after 250 hours.

An excess of TIPA introduced in any composition also disturbed the silicate peak (second peak), causing its deformation and/or disappearance.



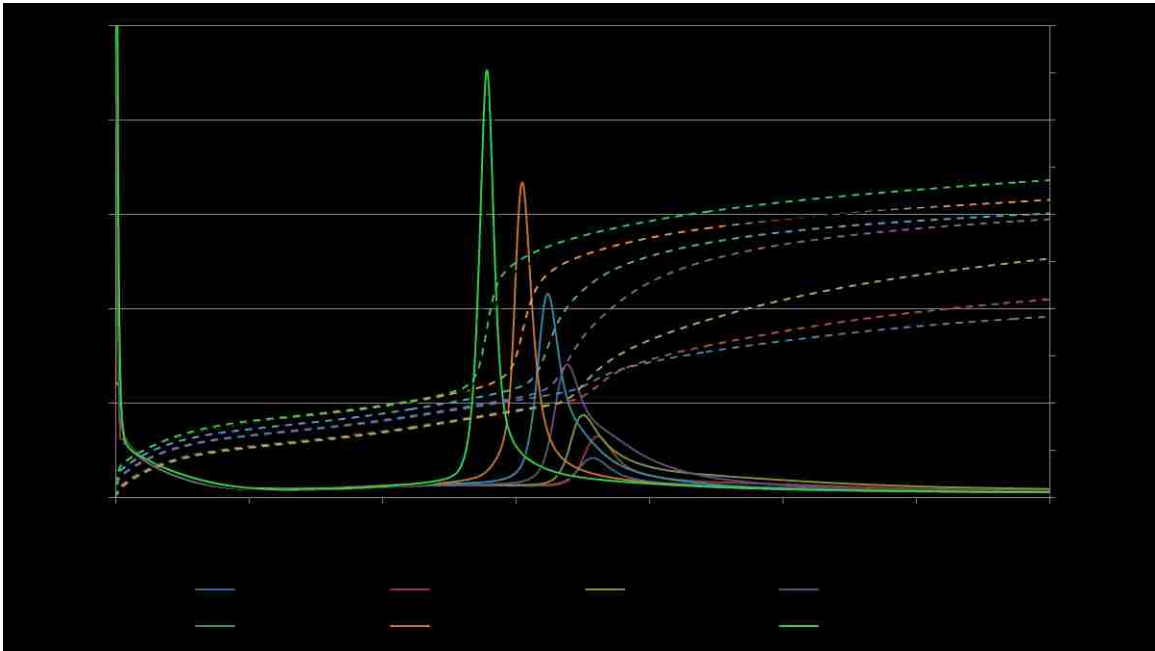


Figure 5-20: Calorimeter results of clinker #5 produced from RC with 10 wt. % gypsum (G) and different amounts of TIPA (T) for 35 hours (second peak after 10 hours is present but too weak to be detected here, refer to Figure 5-4)

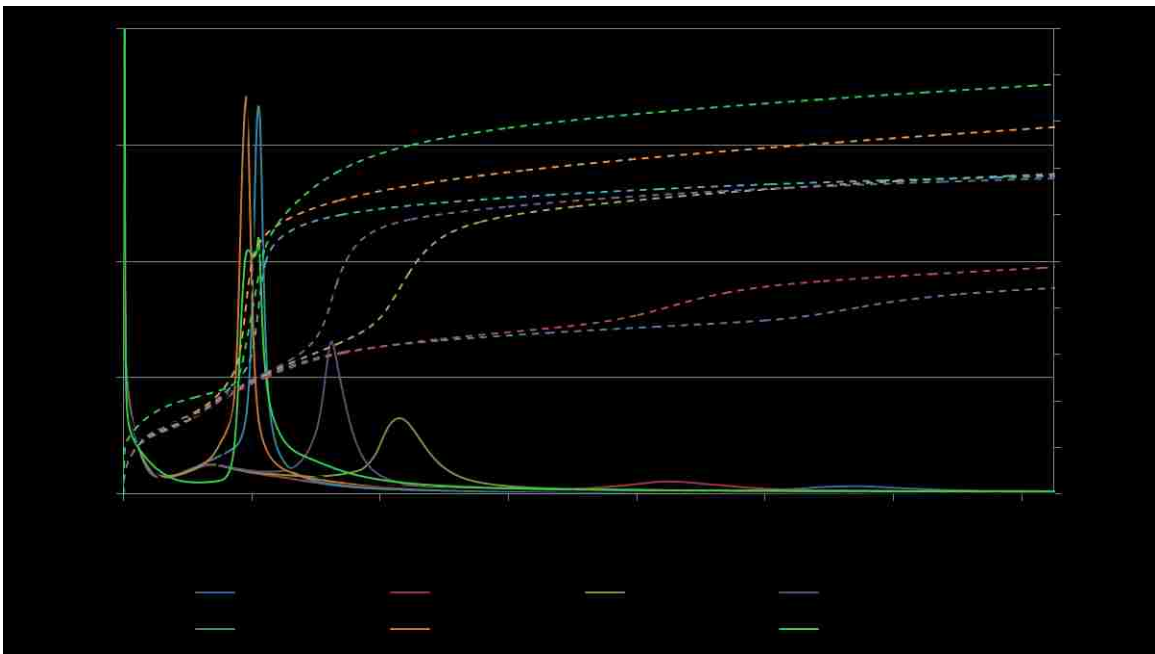


Figure 5-21: Calorimeter results of clinker #5 produced from RC with 20 wt. % gypsum (G) and different amounts of TIPA (T) for 145 hours

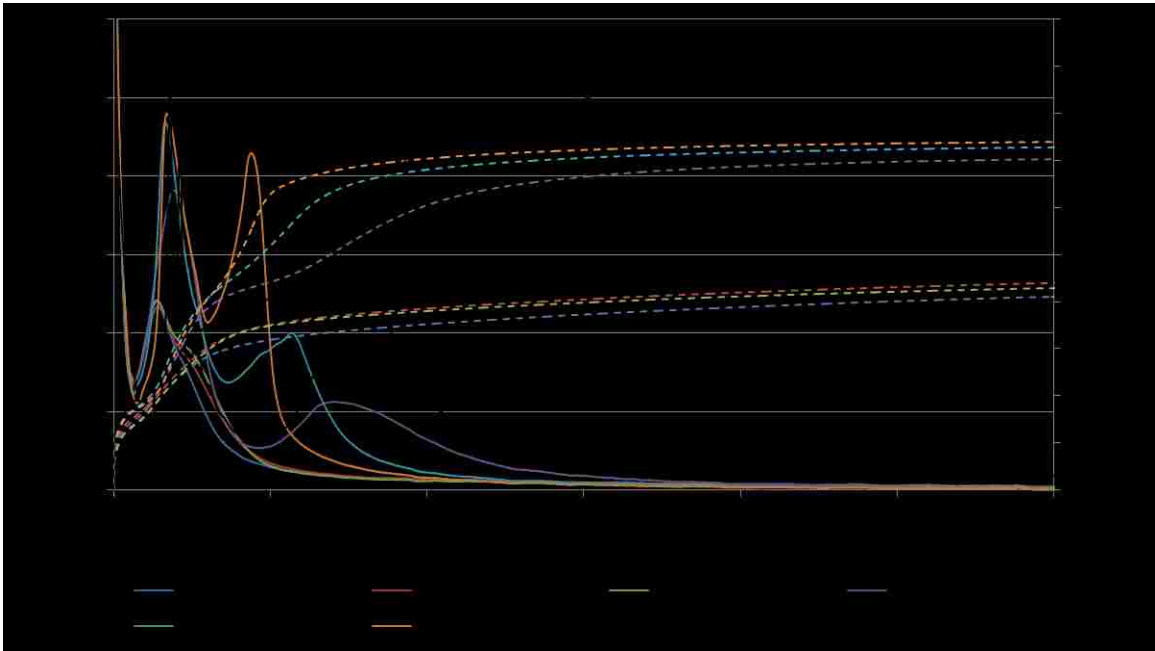


Figure 5-22: Calorimeter results of clinker #5 produced from RC with 30 wt. % gypsum (G) and different amounts of TIPA (T) for 300 hours

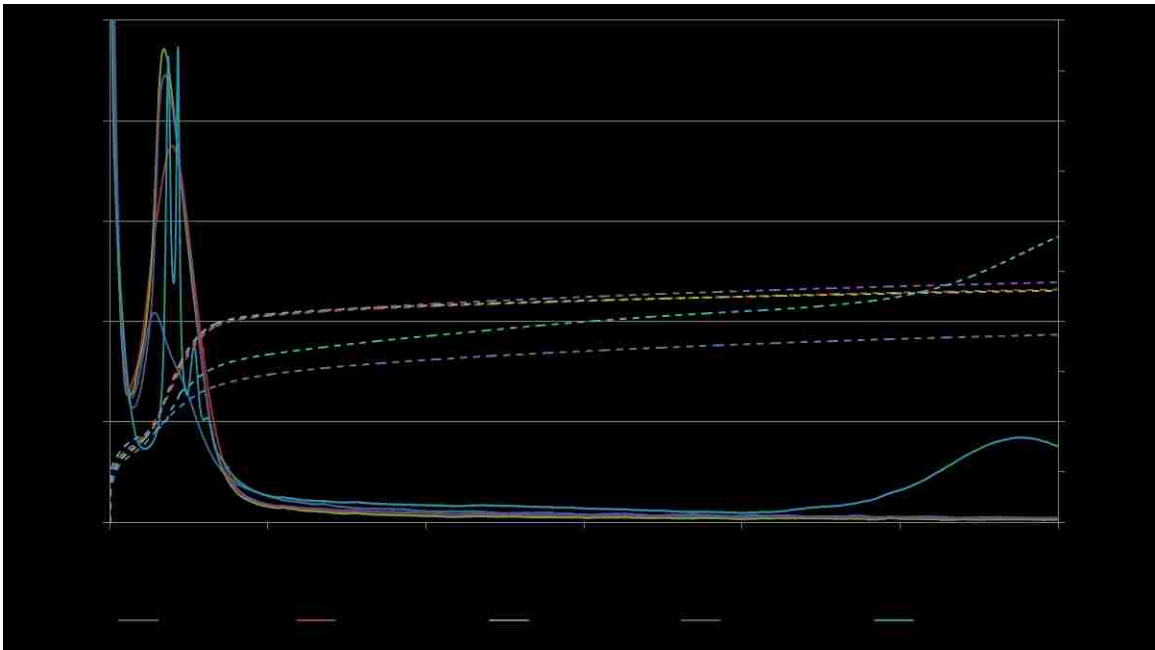


Figure 5-23: Calorimeter results of clinker #5 produced from RC with 40 wt. % gypsum (G) and different amounts of TIPA (T) for 300 hours

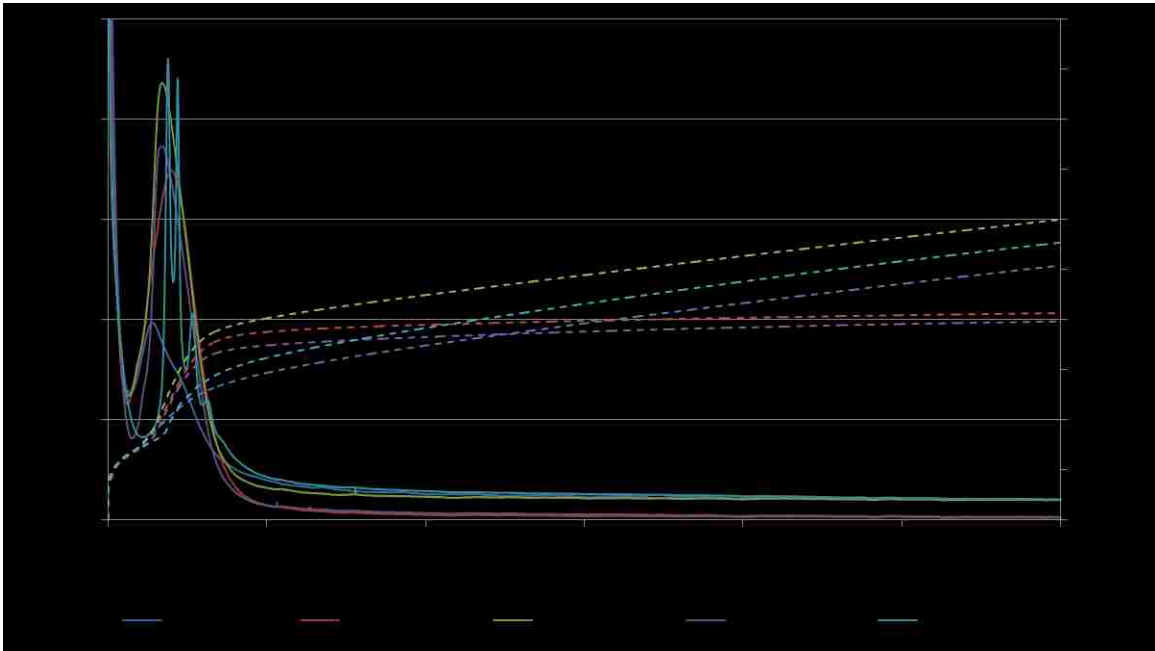


Figure 5-24: Calorimeter results of clinker #5 produced from RC with 50 wt. % gypsum (G) and different amounts of TIPA (T) for 300 hours

After the end of the calorimeter study, each cement paste was visually studied to evaluate the physical appearance of each cement paste and any effect of TIPA on them.








Two effects from the addition of gypsum and TIPA were identified and are shown in Table 5-10. Without any TIPA added, clinker #5 with more than 20 wt. % of gypsum began to decompose. With the addition of TIPA for clinker #5 with 30 wt. % gypsum, the setting was enhanced and the cement paste hardened better, depending on the amount of TIPA introduced. Also, the effect of the addition of TIPA on the clinker #5 had limitations as clinker #5 with 40 and 50 wt. % gypsum remained in a powdery condition.

The influence of TIPA is well demonstrated in Table 5-11, as clinker #5+30G+0T was very soft, domed and could be easily broken. As soon as TIPA was introduced, the cement became hard and yellowed.

Table 5-10: Visual aspect of the cement paste from clinker #5 inside each plastic vials after the end of the calorimeter test (H=hard, S=scratchable, Ex=expanded)

% TIPA	0	0.01	0.02	0.05	0.1	0.2	0.5	1.0	2.0	5.0
B#5-RC+10G	H	H	H	H	H/S	H/S				
B#5-RC+20G	H	H		H	H		H	H	H/S	H/S
B#5-RC+30G	Ex			Ex	Ex		H	H	H	H/S
B#5-RC+40G	Ex						Ex	Ex	Ex less	Ex less
B#5-RC+50G	Ex						Ex	Ex	Ex	Ex

Table 5-11: Pictures of clinker #5 with 30 wt. % gypsum with different additions of TIPA inside plastic vials after the end of the calorimeter test

% TIPA	0	0.05	0.1	0.5	1.0	2.0	5.0
B#5-RC +30%G							

### 5.5.2.1.3. Summary of the calorimetric analyzes

From these tests, TIPA effectively “accelerates” the hydration processes of clinker #5 with gypsum and also affects the mechanical properties of the material. An appropriate amount of TIPA promotes the reaction of gypsum in the clinker. Hence, more gypsum can be introduced into the clinker producing more ettringite, and thus a stronger cement. Furthermore, the energy/cement material increases with the addition of TIPA.

Hydration pastes of clinker #5 with 20 wt. % and 30 wt. % gypsum were performed to identify the hydrates formed at specific times and the results are presented in Section 5.5.2.2.

### 5.5.2.2. Hydration Pastes on clinker #5 produced from RC

The effect of TIPA was studied on compositions selected from the calorimetric tests, just after specific hydration reactions were identified from the hydration peaks in the calorimeter data. All XRD and TGA data used to compile the following information are gathered in Appendix K. Several conclusions were drawn from Figures 5-25 and 5-26 and Table 5-12.

The first conclusion was that the addition of TIPA modified the shape of the second peak, corresponding to the hydration of the silicate phases. In addition, with the alteration of this second peak, the hydration products were modified as well, and “stellerite” formed instead of portlandite.

Furthermore, a large addition of TIPA assisted in the formation of hydrogarnet. This is consistent as TIPA assists the reaction of ferrite and gypsum, which then encourages the hydration of ferrite with water only, to form hydrogarnet.

Besides, TIPA contributed to the total consumption of ferrite after 7 days, as shown in Table 5-12 in all samples with TIPA.

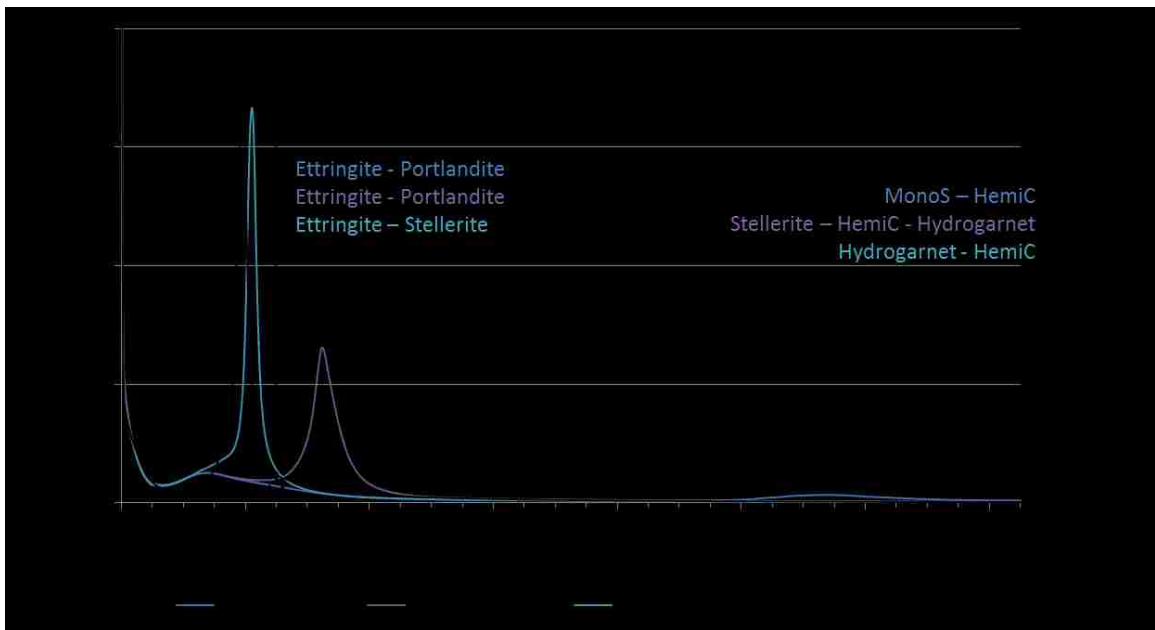


Figure 5-25: Calorimeter data of hydration paste of clinker #5 with 20 wt. % gypsum and TIPA stopped after 1, 7 and 28 days. The 28-day measurement is not shown in this graph.

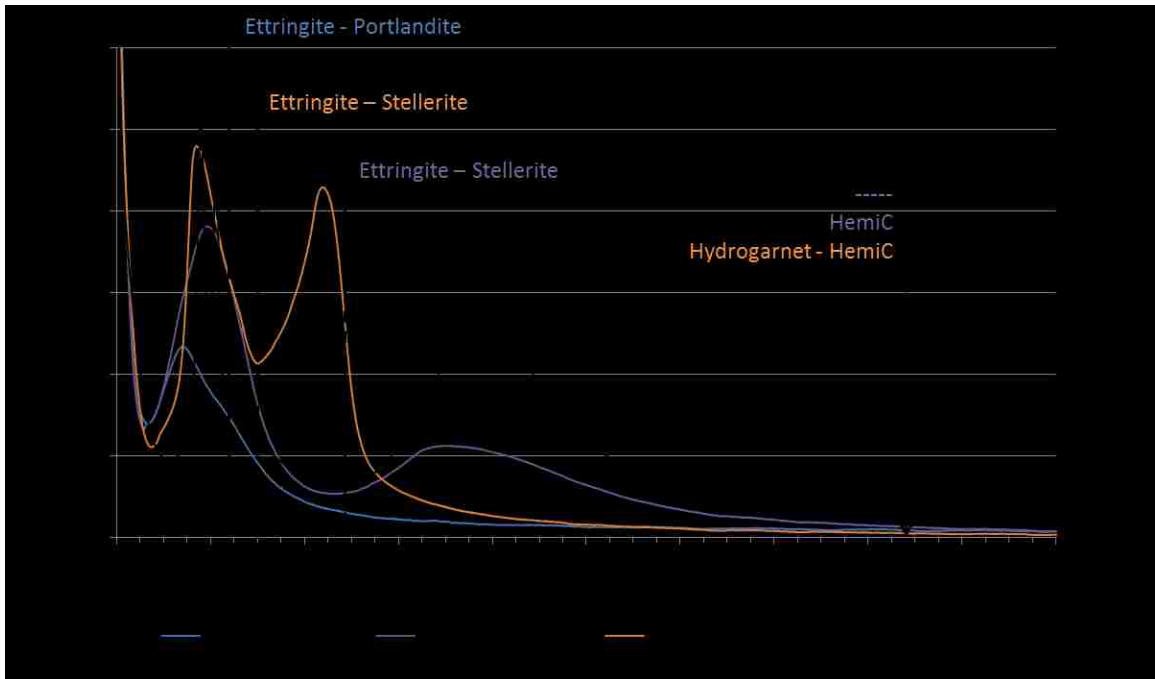


Figure 5-26: Calorimeter data of hydration paste of clinker #5 with 30 wt. % gypsum and TIPA stopped after 24, 30, 48 hours, 7 and 28 days. The 28-day measurement is not shown in this graph.

Table 5-12: XRD and TGA data presenting the clinker phases consumed and the hydrates formed from the hydration paste of clinker #5 with 20 wt. % and 30 wt. % gypsum with various amounts of TIPA (sign “+” means that this phase remains in the sample after 28 days of hydration)

% Gyp	% TIPA	Consumption				Formation							
		Gyp	C <sub>4</sub> A <sub>3</sub> S	C <sub>3</sub> S	C <sub>4</sub> AF	Ett	Stell	MonoS	Ca(OH) <sub>2</sub>	Hydro	HemiC	MonoC	
20	0	7-28d	28-90d	1-7d	+	0-5h	-	1-7d	5h-1d	28-90d	1-7d	90-180d	
	0.1	1-7d	7-28d	1-7d	1-7d	0-1d	1-7d	-	0-1d	1-7d	1-7d	-	
	0.5	1-7d	+	1-7d	1-7d	0-1d	0-1d	-	-	1-7d	1-7d	-	
	5.0	1-7d	+	1-7d	1-7d	0-1d	0-1d	-	-	1-7d	1-7d	-	
30	0	28-90d	28-90d	1-7d	+	0-5h	-	-	5h-1d	-	28-90d	-	
	0.5	2-7d	+	2-7d	2-7d	0-2d	0-2d	-	-	7-28d	2-7d	-	
	2.0	1.25-7d	+	1.25-7d	1.25-7d	0-1.25d	0-1.25d	-	-	1.25-7d	1.25-7d	-	
	5.0	7-28d	7-28d	2-7d	2-7d	0-2d	2-7d	-	-	2-7d	2-7d	-	
	5.0	7-28d	7-28d	2-7d	2-7d	0-2d	2-7d	-	-	2-7d	2-7d	-	

MonoS = Monosulfate; Hydro = Hydrogarnet; HemiC = Hemicarboaluminate, MonoC = Monocarboaluminate, Ett = Ettringite, Stell = “Stellerite”, Gyp = Gypsum

### 5.5.2.3. Mechanical tests on clinker #5 produced from RC

Using the data retrieved from calorimeter analyses, specific compositions were selected for compressive strength tests, and are shown in Figure 5-27.

The addition of TIPA strongly affected the mechanical properties after one day of hydration. Indeed, the compressive strength was actually two to five times higher with TIPA than without.

After 7 and 28 days of hydration, TIPA negatively affected the properties of clinker #5 with 10 wt. % and 15 wt. % gypsum, whereas it still enhanced compressive strength with 20 wt. % gypsum. As a consequence, TIPA enhances the strength of cement where an optimal amount of gypsum is first selected. As 10 wt. % and 15 wt. % gypsum were not adequate, 20 wt. % gypsum was however sufficient for the TIPA to enhance the strength even after 28 days of hydration.

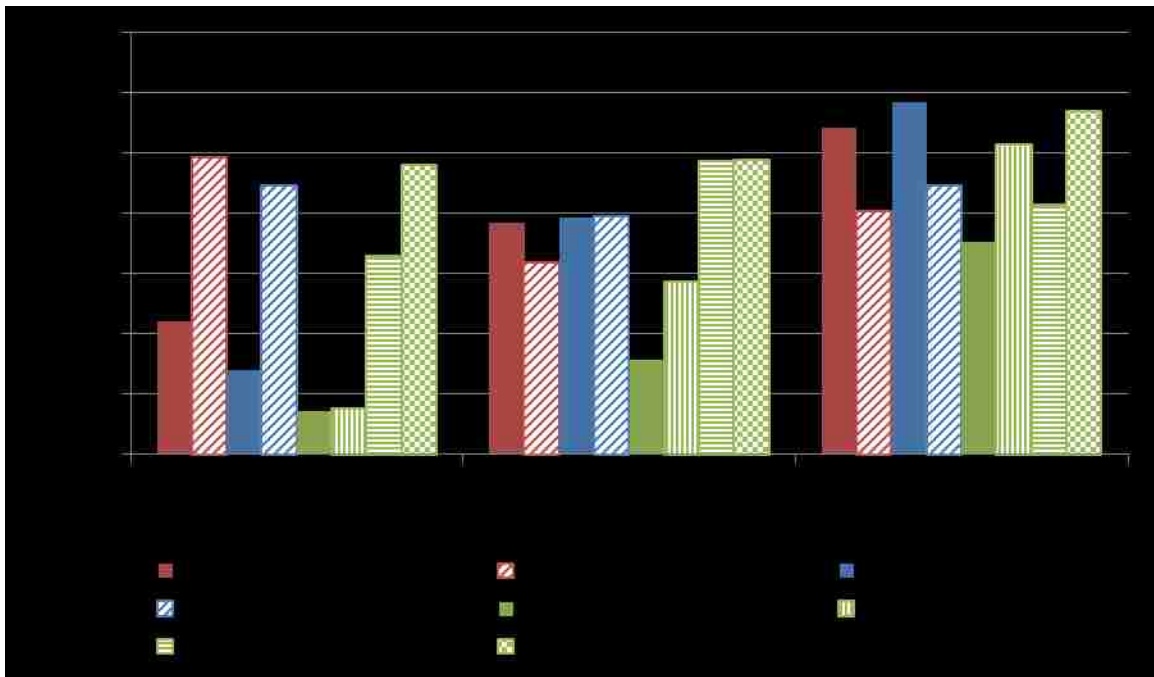


Figure 5-27: Compressive strength results of clinker #5 with 10, 15 and 20 wt. % gypsum, with addition of TIPA

### **5.5.3. Summary of the influence of TIPA on high-iron alite-calcium sulfoaluminate-ferrite cement**

Triisopropanolamine (TIPA) is generally used as a grinding agent and as an admixture to enhance the mechanical properties of cements. Even if the actual chemical mechanism of TIPA is still debated, its influence on the mechanical properties is unquestionable.

The addition of TIPA affects the chemical and mechanical properties of high-iron alite-calcium sulfoaluminate-ferrite cements. As determined through all of these tests, ferrite does not seem to completely hydrate. Besides, if a solution is found to resolve this issue, the addition of gypsum has to be optimized to react with  $C_4A_3\dot{S}$ , as well as with  $C_4AF$ , to obtain the highest compressive strength.

The described method to highly improve the compressive strength of these novel cements is to first calculate the theoretical amount of gypsum necessary for  $C_4A_3\dot{S}$  and  $C_4AF$  to completely react with and form ettringite. Lerch method is suitable for low-iron cements, but inefficient for high-iron cements. The optimum amount of TIPA is then selected through calorimeter experiments, and is chosen as the second peak (silicates hydration) remains constant in time, and the third peak occurs just after the second peak without disturbing it.



## **Chapter 6 : From By-Products Materials**

This chapter discusses the chemical and physical studies of clinkers #1, #3 and #5 produced from modified by-products (MBP), as described in Chapter 4. As industrial by-products are greatly available, large batches of clinkers of 2000g were produced with the similar mineralogical compositions than with the small batches of clinkers from MBP in Chapter 4. Therefore, the same procedure than in Chapter 5 was followed for the production of the large batches, except for the utilization of large pellets and different grinding times.

This chapter is divided in three sections. The first one focuses on the characterization of clinkers made from MBP to ensure that the new procedure with the large pellets did not affect their mineralogical compositions. The second section presents calorimeter studies performed on clinkers from MBP and compared with the clinkers made from RC. The influences of gypsum and TIPA were identified for each clinker produced from MBP. The last section presents mechanical data on samples selected from calorimeter analyses.

### **6.1. Characterization tests**

Characterization tests were performed to ensure that the mineralogical compositions of the large batches of clinkers were not different from the small batches of clinkers produced previously in Chapter 4.

#### **6.1.1. XRD/Rietveld**

As before, Rietveld analyses were performed to determine the clinker composition of each batch. The XRD and Rietveld analyses are shown in Figure 6-1 and Table 6-1. The results showed that the reproduction of the small batches of clinkers from Chapter 4 into large batches of clinkers was possible. This was demonstrated by the similar Rietveld values between the small and large batches of clinkers in Table 6-1. Hence, neither free lime determinations, nor SEM/EDS analyses were performed as the XRD/Rietveld data were sufficient.

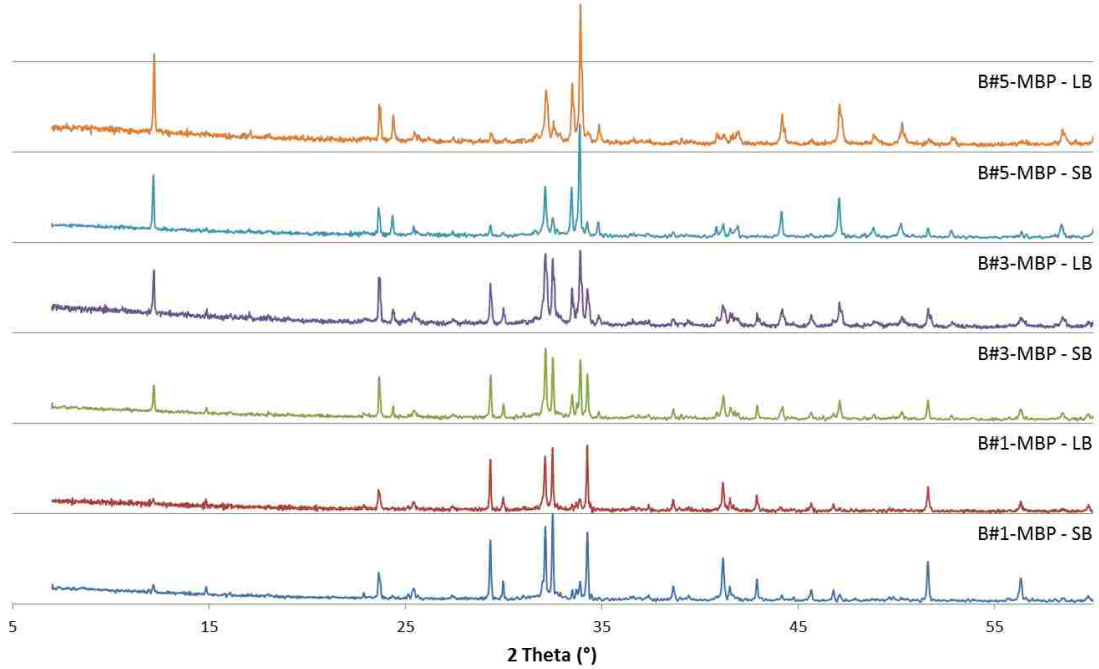


Figure 6-1: Comparison of XRD diffractograms of the small batches of clinkers (SB) from Chapter 4, and the large batches of clinkers (LB) from this chapter, made from modified by-products (MBP)

Table 6-1: Comparison of the Rietveld values for each small (Chapter 4) and large (this Chapter) batches of clinkers produced from modified by-products (MBP)

<b>Batches</b>		<b>C<sub>3</sub>S</b>	<b>C<sub>2</sub>S</b>	<b>C<sub>4</sub>A<sub>3</sub>S</b>	<b>C<sub>4</sub>AF</b>	<b>C<sub>S</sub></b>	<b>Fl*</b>	<b>C<sub>3</sub>A</b>	<b>f<sub>CaO</sub></b>	<b>MgO</b>
<b>#1</b>	Small Ch4	50.4	20.5	8.0	7.8	2.9	1.4	0.0	0.3	5.9
<b>MBP</b>	Large Ch6	54.6	15.5	8.7	7.8	2.9	1.4	0.2	0.3	5.6
<b>#3</b>	Small Ch4	37.0	17.7	10.5	22.2	1.9	2.4	1.2	0.3	3.7
<b>MBP</b>	Large Ch6	33.2	16.3	11.4	28.0	2.4	3.7	0.9	0.1	3.6
<b>#5</b>	Small Ch4	15.4	11.5	9.4	53.0	2.2	4.3	1.1	0.4	0.4
<b>MBP</b>	Large Ch6	10.7	12.1	9.8	58.0	2.0	6.2	0.9	0.1	0.1

Fl\*=Fluorellestadite

### 6.1.2. Particle Size Distribution

As shown in Figure 6-2 and Table 6-2, the data confirm that the particle size distributions of each clinker were close to each other. Indeed, all of the d(0.5) were all in the same range of about 12-22 $\mu$ m, and hence the particle size should not influence the hydration process.

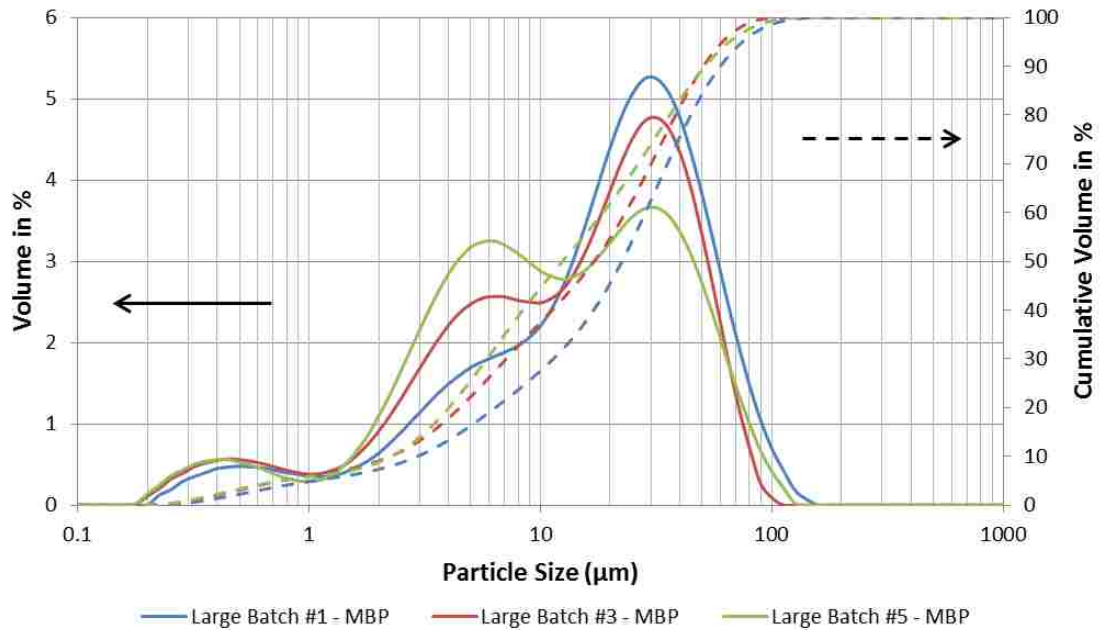


Figure 6-2: Particle size distributions of each large batch of clinker produced from MBP

Table 6-2: Particle sizes  $d(0.1)$ ,  $d(0.5)$  and  $d(0.9)$  for each large batch produced from MBP, in  $\mu\text{m}$

Large Batches #	#1-MBP	#3-MBP	#5-MBP
<b>d(0.1)</b>	2.936	2.247	2.263
<b>d(0.5)</b>	22.494	17.033	12.442
<b>d(0.9)</b>	59.815	50.561	51.395

## 6.2. Calorimetric Analyses

### 6.2.1. Calorimetric tests

The influence of the addition of gypsum into clinkers produced from MBP was studied through calorimeter analyses and the results were compared with the data from clinkers made from RC. In addition, the influence of TIPA was tested on selected compositions.

#### 6.2.1.1. Influence of gypsum

As explained in Section 3.2.3.1., the hydration processes occurring in clinkers made from MBP and RC were monitored through calorimeter studies and the results were compared for clinkers #1, #3 and #5. All the complete calorimeter data for each clinker from MBP

are gathered in Appendix L, while Figures 6-3 to 6-5 display the calorimeter data of clinkers from both RC and MBP as a comparison.

First of all, the addition of gypsum in clinkers #1, #3 and #5 from MBP affected their hydration processes. Like the observations in Chapter 5 with the clinkers produced from RC, the addition of gypsum in the clinkers produced from MBP retarded the hydration processes. Indeed, the first and second hydration peaks from Figures 6-3 to 6-5 remained unchanged, whereas the third peak shifted to the right, to longer times.

The calorimeter results were not identical between the clinkers produced from RC and MBP with similar additions of gypsum. The first two hydration reactions occurring during the first few minutes and after 10 hours for both clinkers made from RC and MBP were in the same time range; however, their third hydration peak was not. In fact, the third peak of clinker #3-RC+10G occurred at the same time as clinker #3-MBP+5G (Figure 6-4). The same phenomenon occurred between clinker #3-RC+15G and clinker #3-MBP+10G. These changes were also observed with clinker #5 in Figure 6-5. From this observation, clinkers from MBP required less gypsum than clinkers from RC to obtain almost identical hydration results.

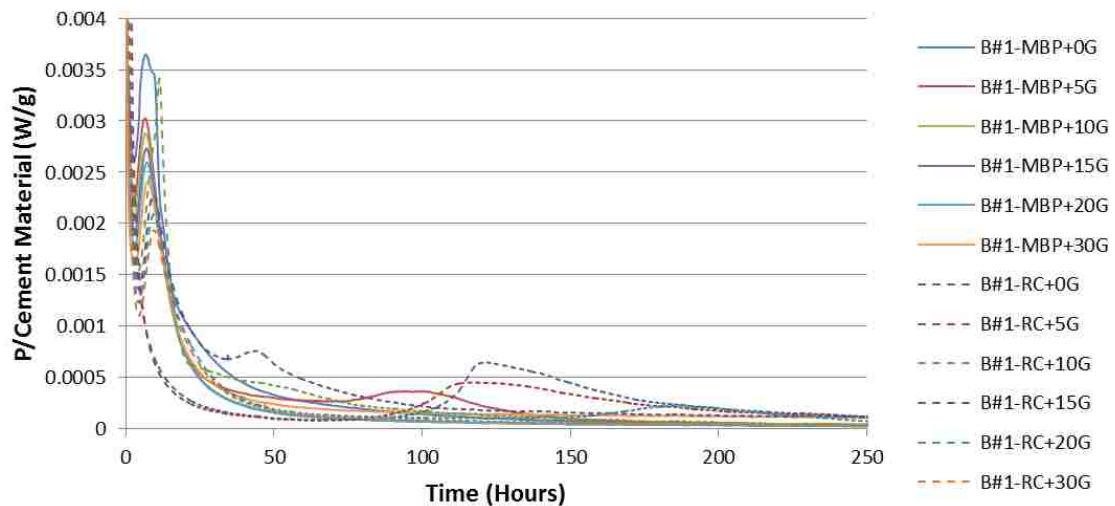


Figure 6-3: Calorimeter data from clinker #1 produced from modified by-products (MBP) and reagent chemicals (RC) with addition of gypsum (G)

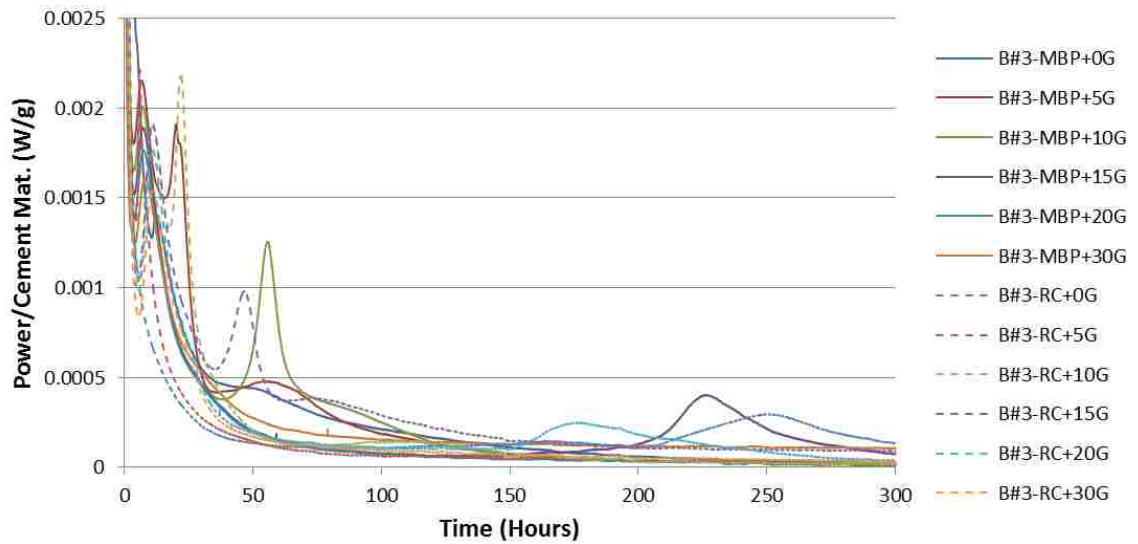


Figure 6-4: Calorimeter data from clinker #3 produced from modified by-products (MBP) and reagent chemicals (RC) with addition of gypsum (G)

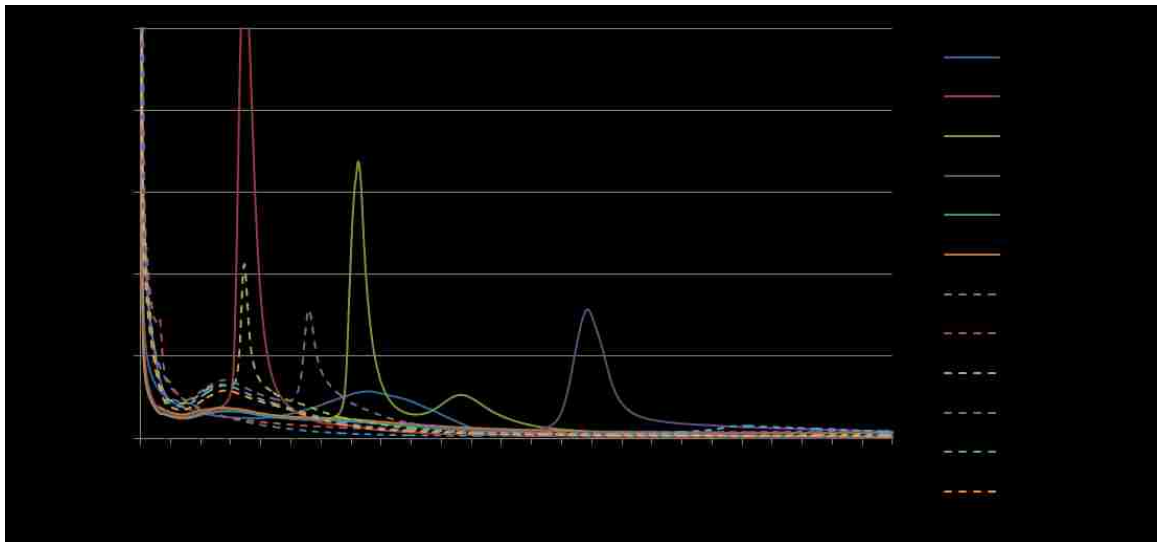


Figure 6-5: Calorimeter data from clinker #5 produced from modified by-products (MBP) and reagent chemicals (RC) with addition of gypsum (G)

The lower requirements of gypsum for the MBP clinkers may be due to the presence of impurities, such as  $\text{TiO}_2$  and  $\text{MgO}$ . Another possibility could be the differences in the mineralogical composition between the clinkers produced from RC and MBP, as clinkers produced from MBP may contain less calcium sulfoaluminate.

### **6.2.1.2. Influence of TIPA**

The addition of TIPA in clinkers #3-MBP (Figure 6-6) and #5-MBP (Figure 6-7) caused the third hydration peak to increase and move to shorter times.

As observed in Figure 6-7, the addition of gypsum in clinker #5-MBP caused the third peak to decrease, for the same addition of TIPA, such as 0.5% and 1.0% by weight.

The influence of TIPA on both clinkers #3 and #5 produced from MBP was the same as with clinkers from RC. The addition of TIPA both accelerated and increased the power per cement material for the third hydration peak, related to the conversion of ettringite to AFm phases. Whether the clinkers were produced from RC or MBP, they reacted in similar ways with addition of both gypsum and TIPA. The only difference observed was that the presence of impurities in industrial by-products may have affected the optimum amount of gypsum for each MBP clinker, and may also have been caused by the amount of calcium sulfoaluminate, which is lower in the MBP clinkers.

All data regarding the influence of the addition of gypsum on the MBP clinkers #1, #3 and #5 summarized in Figures 6-6 and 6-7 are shown in Appendix L.

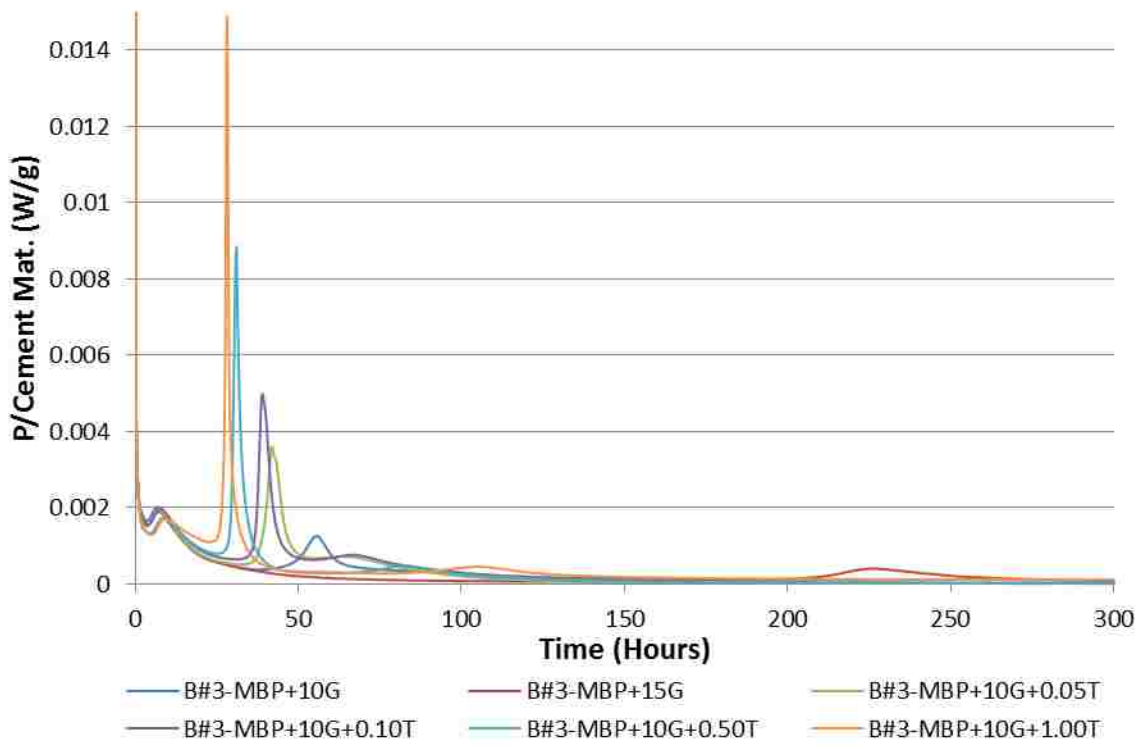


Figure 6-6: Calorimeter data of clinker#3-MBP with addition of gypsum (G) and TIPA (T)

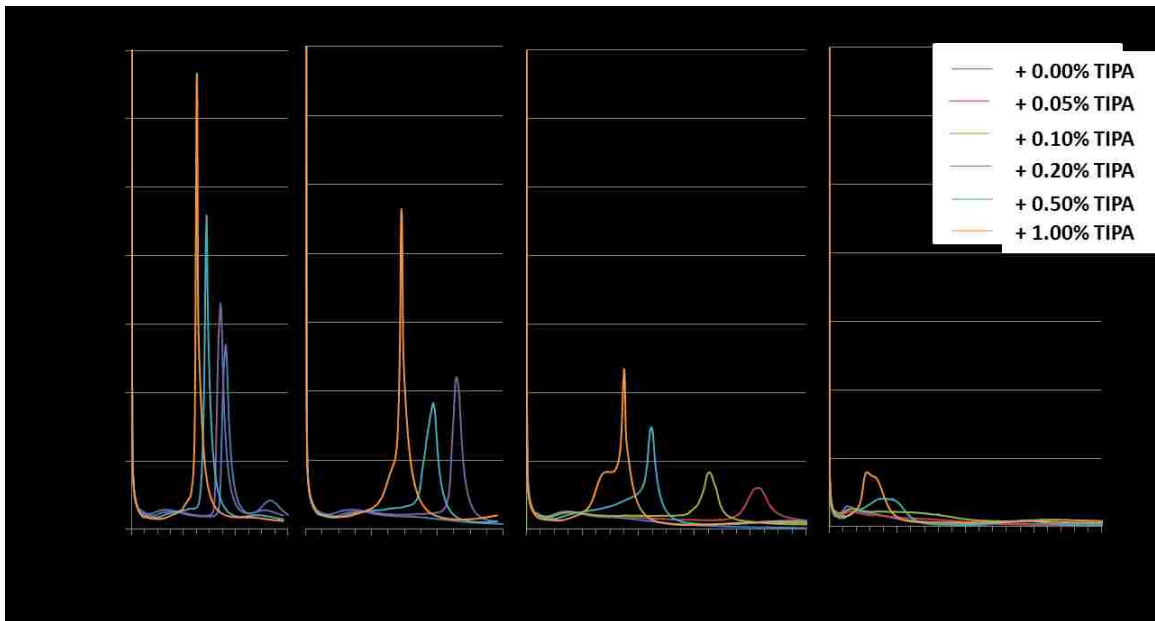


Figure 6-7: Calorimeter data of clinker#5-MBP with addition of gypsum (G) and TIPA (T)

### 6.3. Mechanical tests

From all of the calorimeter analyses performed in Section 6.2., some compositions were selected for compressive strength tests to compare with both the influence of gypsum and TIPA in clinkers #3 and #5 produced from RC and MBP. The compositions chosen for these additional experiments had to demonstrate an early and high third hydration peak from the calorimeter data in Figures 6-6 and 6-7 to be selected for further tests. As a consequence, clinkers #3 and #5 with 5, 10 and 15 wt. % gypsum with 0.0 to 1.0 wt. % TIPA were selected.

Several conclusions can be derived from Figure 6-8. First of all, the compressive strengths between clinkers #3-RC+10G and #3-MBP+10G were very similar at all days, which was not the case for clinkers #3-RC+15G and #3-MBP+15G. While clinker #3-RC+15G became stronger over time, up to 27MPa at 28-day, clinker #3-MBP+15G remained weak over time, with a compressive strength of about 3MPa at 28 days. In addition, “mini-mortar cubes” of clinker #3-MBP+15G began to crack after only 7 days of hydration and a picture of these samples after 28 days is shown in Figure 6-9. As mentioned previously in Section 6.2., MBP clinkers require less gypsum for hydration, which may be the cause for the formation of cracks in clinker #3-MBP+15G because it may have been “over-sulfated”.

The addition of TIPA increased the compressive strength of clinker #3-MBP+10G after 7 days of hydration from about 18 to 22MPa, and for clinker #3-MBP+15G after 7 and 28 days of hydration from 2-3MPa to 17-27MPa. From a physical point of view, “mini-mortar cubes” of clinker #3+15G were completely broken after 28 days (Figure 6-9), while the same samples with the addition of 1.0 wt. % TIPA remained intact during the same period of time (Figure 6-10).



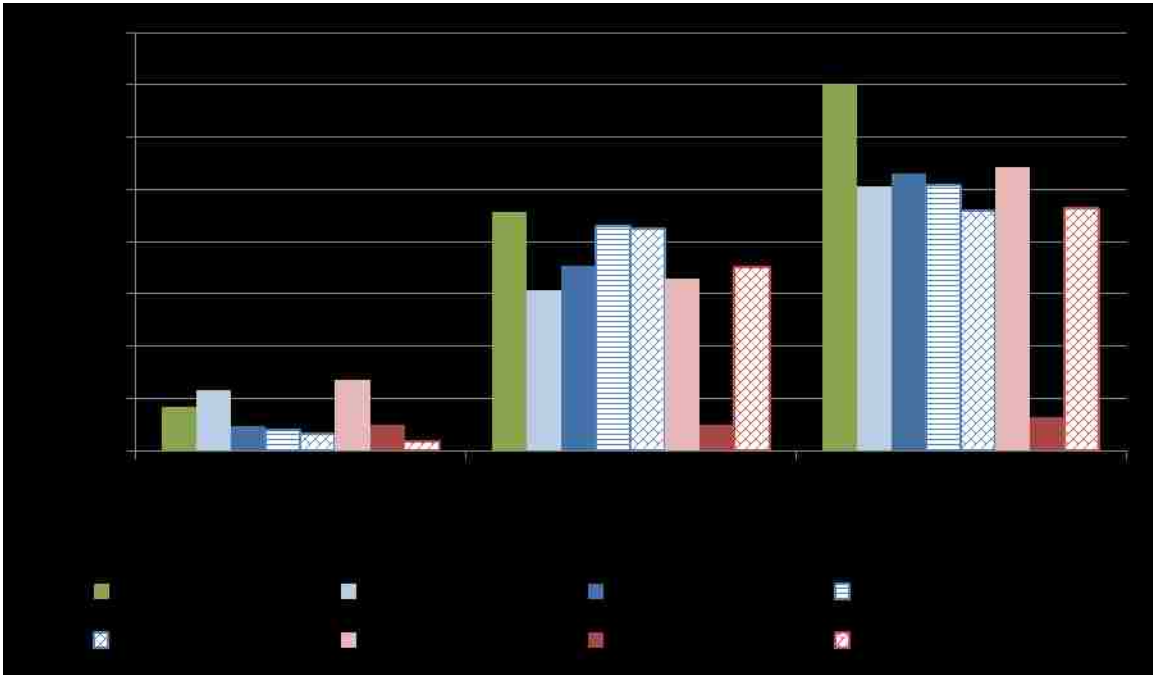


Figure 6-8: Compressive strength data for clinker#3 produced from RC and MBP with the additions of gypsum (G) and TIPA (T)



Figure 6-9: Mini mortar cube of clinker#3-MBP+15G after 28 days of hydration



Figure 6-10: Mini mortar cubes of clinker#3-MBP+15G+1.0T, #3-MBP+10G+0.5/1.0T after 28 days of hydration

Concerning clinker #5-MBP, several observations can be made. The compressive strengths of clinker #5-RC was higher than the ones from clinker #5-MBP at all curing times. As presumed earlier, impurities in the by-products and small differences in the mineralogical compositions could be the cause for the strength differences. They also may have been over-sulfated.

The addition of TIPA was not visible after one day of hydration in both clinkers #5-MBP+10/15G, but it did affect the 7 and 28-day tests, depending on the quantity added. In fact, the compressive strength of clinker #5-MBP+15G increased with the addition of TIPA, from 7 to 9, 13 and 14.5MPa at 0 to 0.2, 0.5 and 1.0 wt. % TIPA respectively at 28-day. Clinker #5-MBP+15G also benefited more from the addition of TIPA than clinker #5-MBP+10G as the compressive strength was higher for the clinker with more gypsum.

As noticed with clinker #3-MBP, “mini-mortar cubes” of clinker #5-MBP+15G were cracking after 28 days (Figure 6-12), whereas the cubes from the same clinker, but with TIPA, were intact (Figures 6-13 and 6-14).

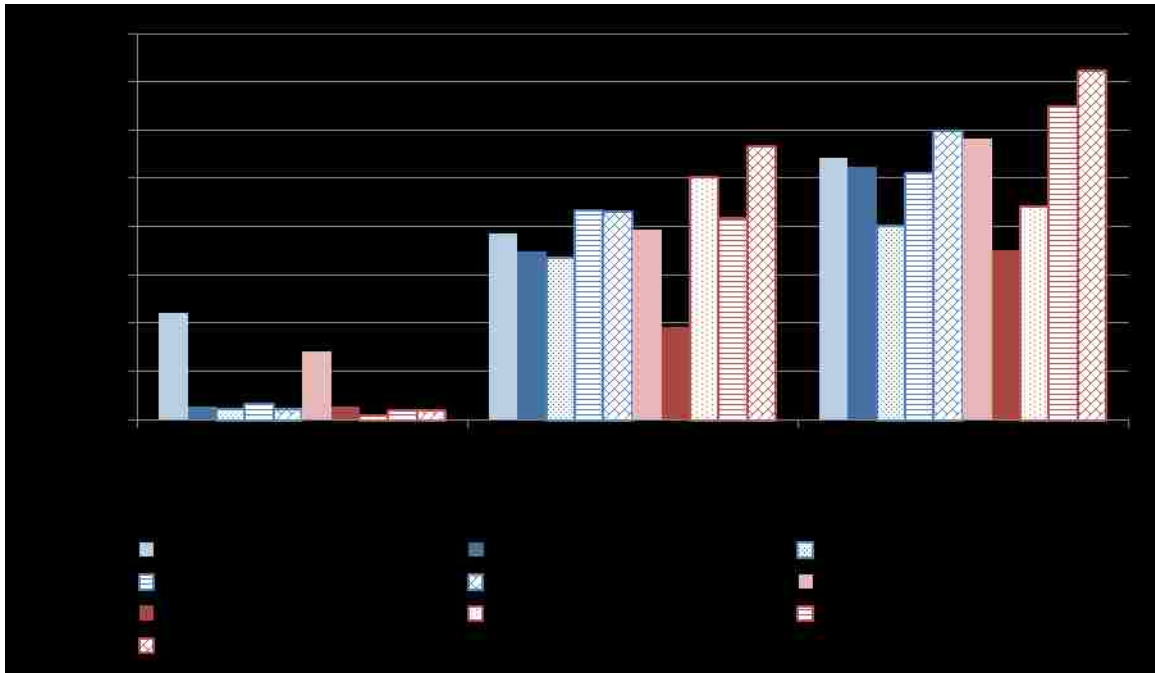


Figure 6-11: Compressive strength data for clinker#5 produced from RC and MBP with the additions of gypsum and TIPA



Figure 6-12: Mortar cubes of clinker#5-MBP+10/15G after 28 days of hydration



Figure 6-13: Mortar cubes of clinker#5-MBP+10/15G+0.2T after 28 days of hydration



Figure 6-14: Mortar cubes of clinker-MBP#5+10/15G+0.5/1.0T after 28 days of hydration

Both the additions of gypsum and TIPA positively affect the mechanical properties of clinkers #3 and #5 produced from MBP. The influence of TIPA seems to be optimal with an increase amount of gypsum, especially observed for clinker #5-MBP. Triisopropanolamine does not only affect the mechanical performance of these high-iron cements, it also contributes to the physical aspect as the addition of this admixture ensures a better cohesion inside the mortar cement and prevents cracking from happening.

## **Chapter 7 : Conclusions and Future Work**

### **7.1. Reminder of the general problem**

The main goal of this research project was to identify, formulate and investigate a novel cement with improved properties compare to OPC or CSAC, by emitting less CO<sub>2</sub>, using more industrial by-products (“green” material) and having lower costs.

As explained in the introduction, different directions can be pursued to achieve these goals, but the path followed during this project was to combine both beneficial clinker phases, alite and calcium sulfoaluminate from OPC and CSAC, into one and unique cement. The purpose of substituting iron for aluminum in these novel clinkers was to utilize as much red mud and other industrial by-products as possible instead of expensive bauxite.

The plan followed during this research was the following. First, preliminary experiments were performed to confirm the modified Bogue equations established by Zhou [2]. The clinker compositions selected for this project contained 15 wt. % of calcium sulfoaluminate, 5 wt. % of anhydrite, 33 to 73 wt. % of silicates (alite and belite) and 5 to 45 wt. % of ferrite, and were produced from both reagent chemicals and industrial by-products to study the influence of the raw materials sources. As calcium sulfoaluminate and anhydrite contents were fixed, only the influence of the addition of ferrite was then studied, while the amount of silicates decreased. Different parameters, such as firing temperatures and dwelling times, were evaluated and tested on compositions produced from both reagent chemicals and industrial by-products. Many characterization methods were employed to identify the optimal parameters for each clinker. Following this step, hydration pastes studies were performed to understand the reactions occurring during the hydration processes. Mechanical tests were also conducted to identify the optimal parameters for each composition, such as the optimal amounts of gypsum and admixtures (triisopropanolamine).

## 7.2. General Conclusions

Through all of the experiments performed in this dissertation, several conclusions can be drawn.

Chapter 4 was focused on the feasibility, production and characterization of high-iron alite-calcium sulfoaluminate-ferrite cements. The establishment of modified Bogue equations by Zhou to formulate these novel cements was tested and confirmed. High-iron alite-calcium sulfoaluminate-ferrite cements can be produced at lower firing temperatures of 1250-1275°C for 60 minutes, depending on the raw materials used, reagent chemicals or industrial by-products.

Chapter 5 was centered on the hydration processes taking place in these high-iron cements made from reagent chemicals. The hydration processes were dependent on the amounts of gypsum incorporated into the clinkers, and on the clinker composition, as three main stages were identified. Clinkers with low amounts of gypsum, up to 10 wt. %, demonstrated a very rapid hydration process, with the formation of ettringite, followed by “stellerite”, and later on by portlandite and AFm phases. With an appropriate quantity of gypsum introduced into the clinkers, the hydration processes slowed down, with the formation of first ettringite and portlandite, followed by AFm phases. For the first two stages, the cement pastes were hard at the touch. However, during the third and last stage, with an excessive amount of gypsum, the cement pastes decomposed into powders. The hydration was similar to the second stage hydration, except that the conversion of ettringite to AFm phases was too retarded over time and decomposed the material. Concerning the mechanical properties, the compressive strength decreased with the decreasing amount of silicates (especially alite as this phase hydrates quicker than belite) and the increasing amount of ferrite. Besides, in clinkers with large amounts of iron, the ferrite never completely hydrated, even after 180 days of hydration, which caused the low compressive strength related with the low amount of alite.

Chapter 6 was concentrated on producing clinkers made from industrial by-products with the same mineralogical compositions as the clinkers produced from reagent chemicals, and on studying their hydration processes. In general, their hydration processes were the same as the ones observed in clinkers produced from reagent chemicals, with the three

stages depending on the gypsum content and clinker composition. Few differences were also visible between them. From calorimeter results, the hydration of MBP clinkers required less gypsum than RC clinkers to acquire the same hydration profiles. Impurities in industrial by-products or small differences in the mineralogical composition (less CSA than anticipated from MBP – 10 wt. % instead of 15 wt. %) between clinkers made from RC and MBP may be the cause of these differences in the amount of optimal gypsum.

Moreover, Chapters 5 and 6 dealt with the influence of triisopropanolamine (TIPA) as this was tested on both clinkers produced from RC and MBP to enhance their compressive strengths through the hydration of ferrite. As observed in clinkers with high amounts of iron, ferrite did not fully hydrate as this phase was still unreacted even after 6 months into the hydration process. However, through the additions of TIPA, ferrite did react completely in a matter of a few days and the mechanical properties were also enhanced.

From all of this research, the production of high-iron alite-calcium sulfoaluminate-ferrite cement from reagent chemicals and industrial by-products was successful. These clinkers remained stable and their hydration processes were in general the same between the two sources of materials (RC and MBP). They demonstrated promising mechanical properties, but a lot of work could still be accomplished to improve this material.

### **7.3. Future Work**

After having successfully producing and testing high-iron alite-calcium sulfoaluminate-ferrite cements, more research needs to be done to improve these materials.

Additional research would include:

- Produce clinkers from industrial by-products in considerable quantities of about 10kg by modifying the production process. Instead of making large pellets individually through one pellet mold, pelletization of the raw materials would be produced as small rounded pellets, which would then be fired in a rotary kiln. This process would then need to be validated by ensuring that the clinker compositions were not modified during the new industrial process.

- The production of considerable large batches of clinkers would then be followed by testing mortar cubes of 5-cm following ASTM C109. A comparison with OPC mortar cubes would be more realistic and the compressive strength of these high-iron cements should be higher and easier to compare with. Moreover, the influence of gypsum and TIPA would also be more accurate with 5-cm mortar cubes.
- Study the hydration pastes from clinkers produced made from industrial by-products and identify if and where the chemical impurities, such as MgO and TiO<sub>2</sub>, may be located.
- Test different water/cement ratios and introduce supplementary cementitious materials (SCMs), such as fly ash or slag, into these high-iron alite-calcium sulfoaluminate-ferrite cements to improve their mechanical properties.
- Formulate all the clinkers with a quantity of liquid phase (QLP) of 0.12 instead of 0.10. This may increase the amount of alite and decrease the amount of less-reactive belite formed during the firing process.
- Do more compressive strength tests on clinkers #3-MBP and #5-MBP+30/40/50% gypsum with an excessive amount of TIPA.
- Use anhydrite as a calcium sulfate source instead of gypsum during the hydration process.
- Confirm the existence of the stellerite-like phase, investigate its aluminum and silicate contents and identify the hydration reactions that produced it.

Appendices

Appendix A: XRD patterns for clinker and hydrated phases

Clinker Phase	Mineral Name	Chemical Abbreviation	PDF Files	Significant Peaks 2 Theta in ° (Intensity in %)
Alite	Hatruite	C <sub>3</sub> S	01-086-0402	29.357 (87.6); 29.414 (85.2); 32.193 (100); 32.504 (87.4); 34.355 (77)
Belite	Larnite	C <sub>2</sub> S	00-049-1673	32.007 (100); 32.149 (89); 32.570 (98); 34.345 (61); 41.030 (64)
			01-077-0420	31.095 (68.1); 32.060 (100); 39.336 (24.8); 45.267 (34.4)
Ferrite	Brownmillerite	C <sub>4</sub> AF	01-070-2765	12.181 (46.3); 32.203 (35.8); 33.543 (46.4); 33.917 (100); 47.184 (42.2)
Calcium Sulfoaluminate	Yeelimite	C <sub>4</sub> A <sub>3</sub> S	00-033-0256	23.643 (100); 33.797 (25); 41.664 (20)
Anhydrous Calcium Sulfate	Anhydrite	C $\bar{S}$	01-072-0503	25.461 (100); 31.380 (30.1); 38.646 (17.4); 40.822 (18.9)
Calcium Sulfate Dihydrate	Gypsum	C $\bar{S}$ H <sub>2</sub>	00-033-0311	11.589 (100); 20.722 (100); 29.111 (75); 31.104 (45); 33.344 (35)
Tricalcium Aluminate		C <sub>3</sub> A	00-002-0920	33.280 (100); 47.835 (70); 59.179 (80); 79.870 (70)
Calcium Fluoride Silicate Sulfate	Fluorellestadite	3C <sub>2</sub> S.3C $\bar{S}$ .CaF <sub>2</sub>	00-045-0009	31.658 (100); 32.826 (55); 49.150 (49)
Calcium Oxide	Lime	C	00-037-1497	37.347 (100); 53.856 (54)
Calcium Carbonate	Calcite	C $\bar{C}$	00-005-0586	29.406 (100)
Magnesium Oxide	Periclase	M	00-045-0946	42.917 (100); 62.304 (39)

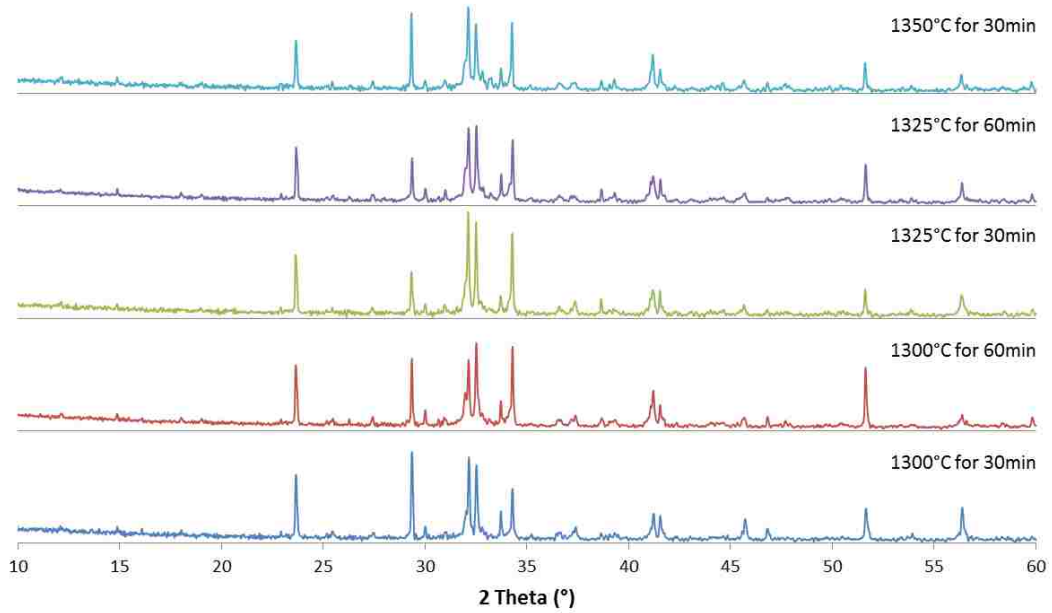
Appendix A 1: ICDD Files for clinker phases [63]



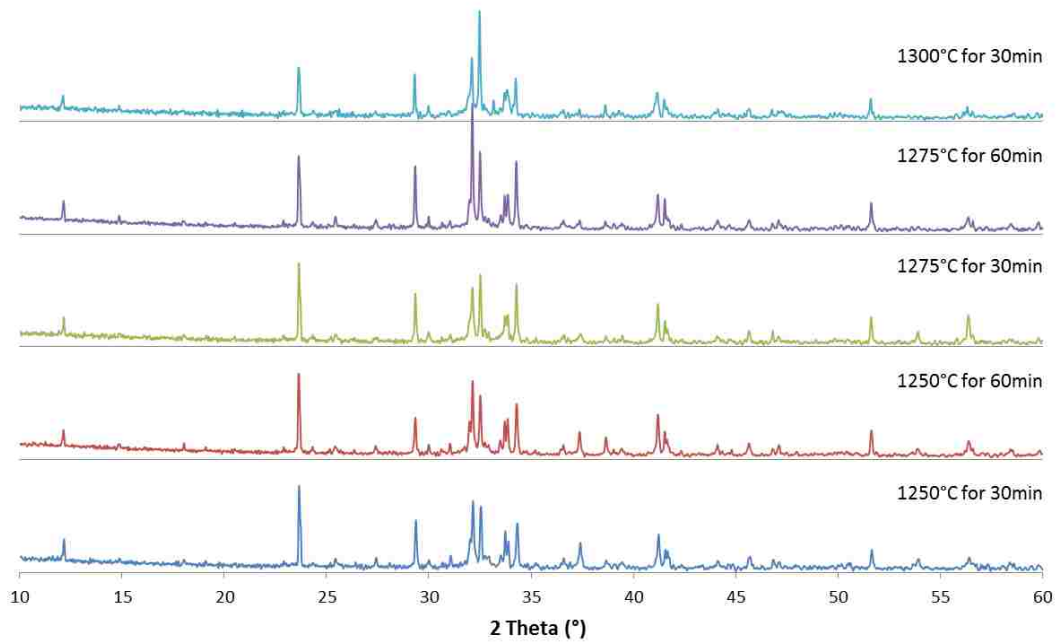
Hydrated Phase	Mineral Name	Chemical Formula	PDF Files	Significant Peaks 2 Theta in ° (Intensity in %)
Calcium Aluminum Silicate Hydrate	Stellerite B	$\text{Ca}_{6.4}\text{Al}_{15.9}\text{Si}_{56.1}\text{O}_{142.4}\text{O}_{4.16}\text{H}_{8.24}$	01-071-1874	9.835 (30.6); 10.303 (100); 10.598 (38.7)
			00-036-0129	10.781 (100); 21.674 (90)
Hemicarboaluminate		$\text{C}_4\text{A}\dot{\text{C}}_{0.5}\text{H}_{12}$	00-041-0221	10.781 (100); 21.661 (90)
			00-041-0219	11.671 (100); 23.491 (90); 35.562 (50)
Monocarboaluminate		$\text{C}_4\text{A}\dot{\text{C}}\text{H}_{11}$	00-054-0848	11.733 (100); 23.591 (25); 36.739 (10)
Monosulfate	Kuzelite	$\text{C}_4\text{A}\dot{\text{S}}\text{H}_{12}$	01-083-1289	9.895 (100); 19.865 (21.2); 22.205 (19.4); 31.035 (14.2); 37.122 (15.2)
Ettringite		$\text{C}_6(\text{Al}(\text{OH})_6)_2(\text{SO}_4)_3(\text{H}_2\text{O})_{25.7}$	01-072-0646	9.061 (100); 15.728 (41.4); 18.850 (22.5); 22.867 (30.8); 34.911 (20.4)
Calcium Hydroxide	Portlandite	CH	01-076-0571	18.066 (74.1); 34.101 (100); 47.144 (39.3); 50.798 (26.1)
Hydrogarnet	Hydrogarnet	$\text{Al}_2\text{C}_3\text{D}_{12}\text{O}_{12}$	01-084-1350	17.309 (100); 26.578 (51.0); 31.893 (76.3); 39.325 (94.3); 44.506 (89.7);
	Hydrogrossularite	$\text{C}_3\text{A}\text{H}_6$	00-002-1124	17.238 (90); 31.937 (90); 39.492 (100); 44.600 (100); 54.865 (80)
	Hydroandradite	$\text{C}_3\text{Fe}_2\text{H}_{7.4}\text{O}_{12}\text{Si}_{1.15}$	01-075-0553	20.092 (90.9); 28.564 (82.6); 32.021 (88.2); 35.172 (96.2); 54.970 (100)

Appendix A 2: ICDD Files for hydrated phases [63]

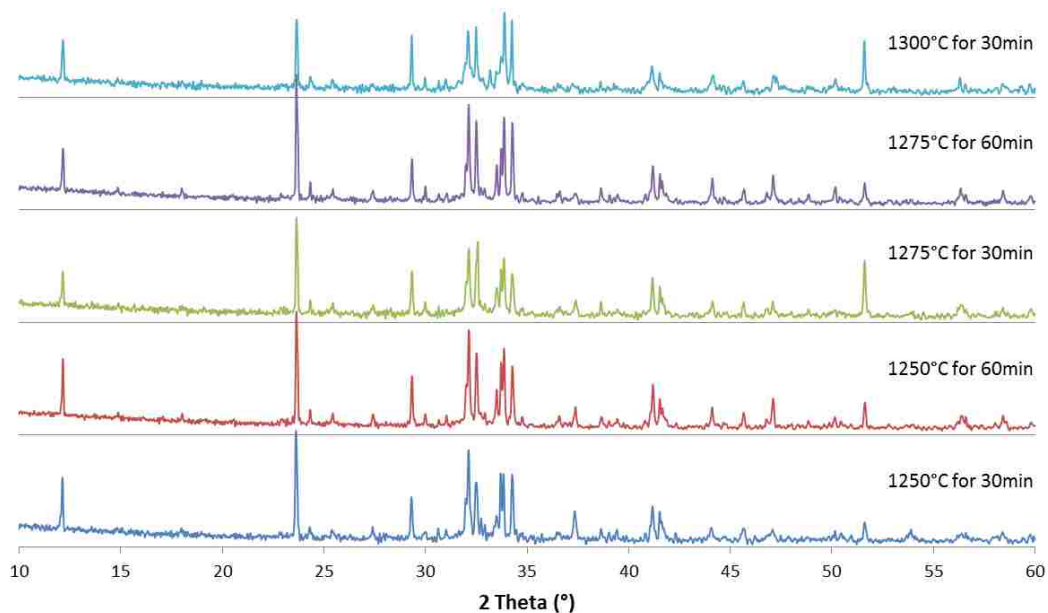
Appendix B: XRD diffractograms for batches #1 through #5 produced from reagent chemicals (RC) fired at different temperatures and dwelling times



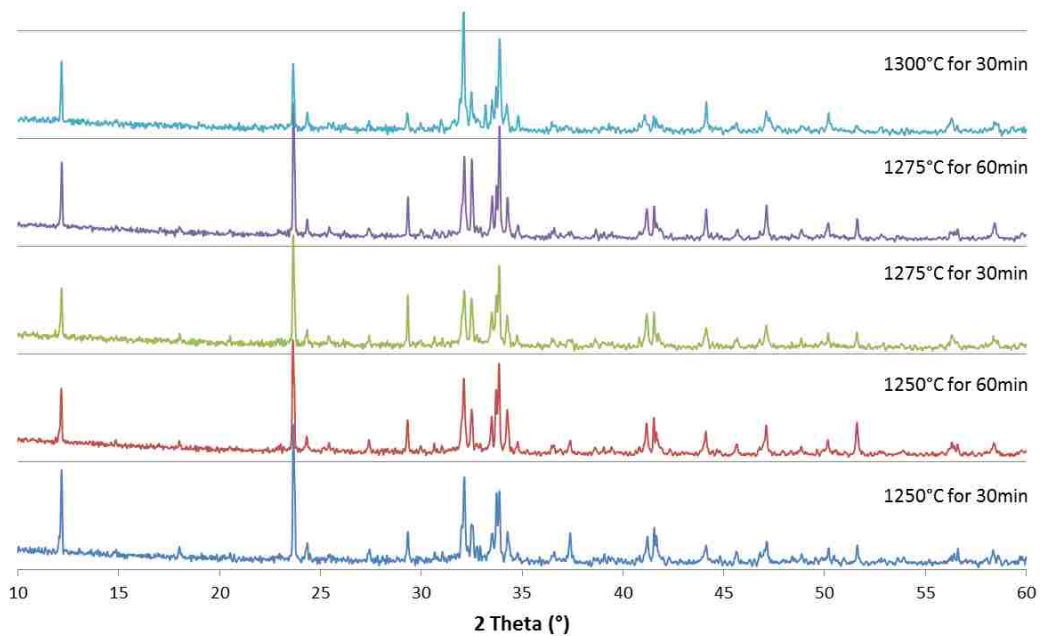
Appendix B 1: Clinker #1 produced from RC fired at different temperatures for 30-60min



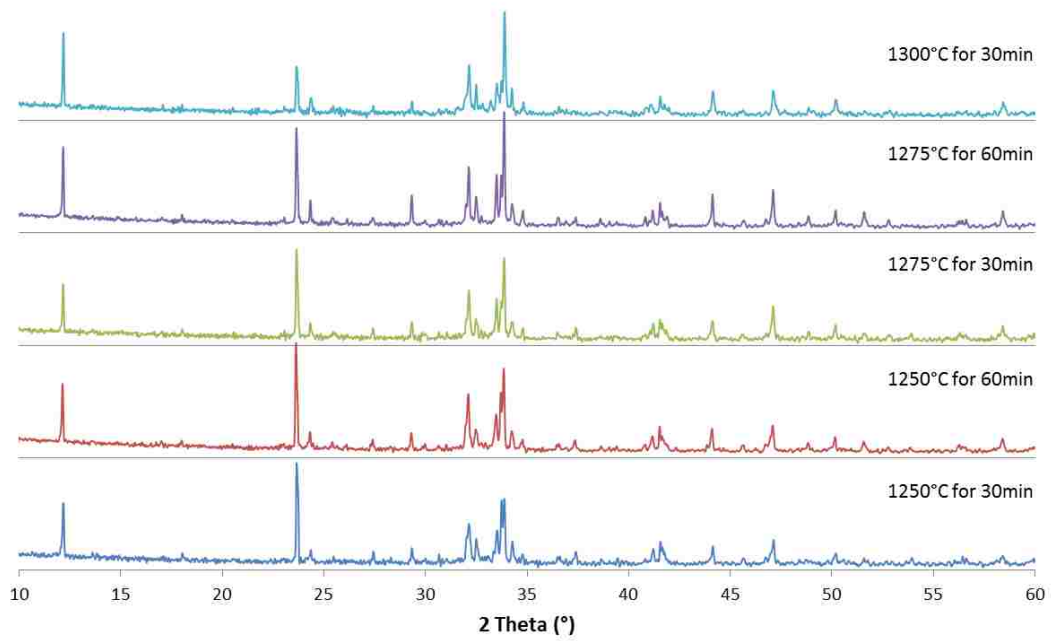
Appendix B 2: Clinker #2 produced from RC fired at different temperatures for 30-60min



Appendix B 3: Clinker #3 produced from RC fired at different temperatures for 30-60min

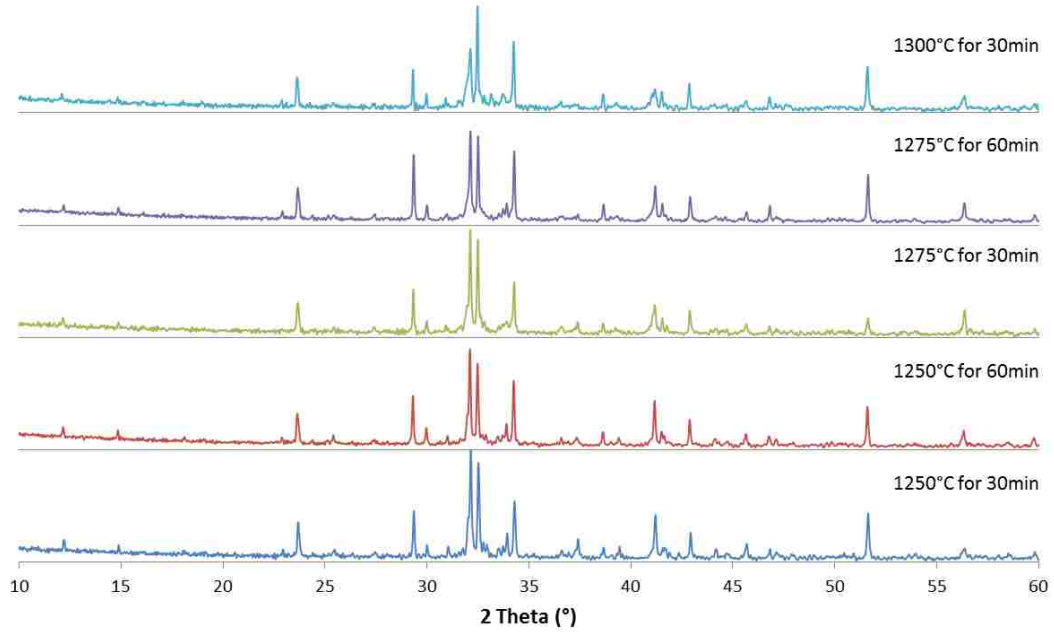


Appendix B 4: Clinker #4 produced from RC fired at different temperatures for 30-60min

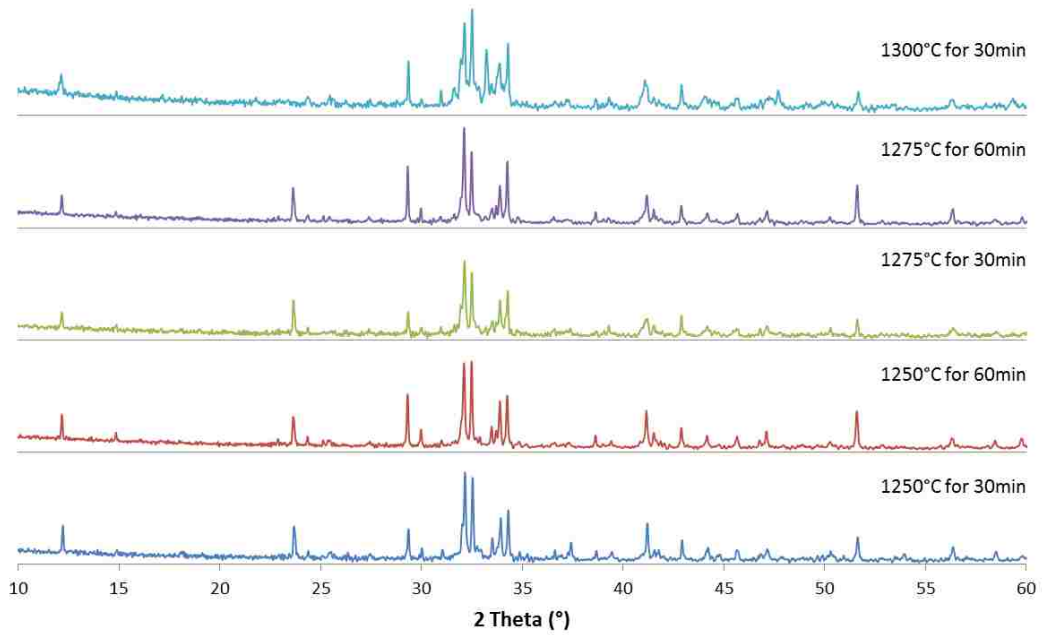


Appendix B 5: Clinker #5 produced from RC fired at different temperatures for 30-60min

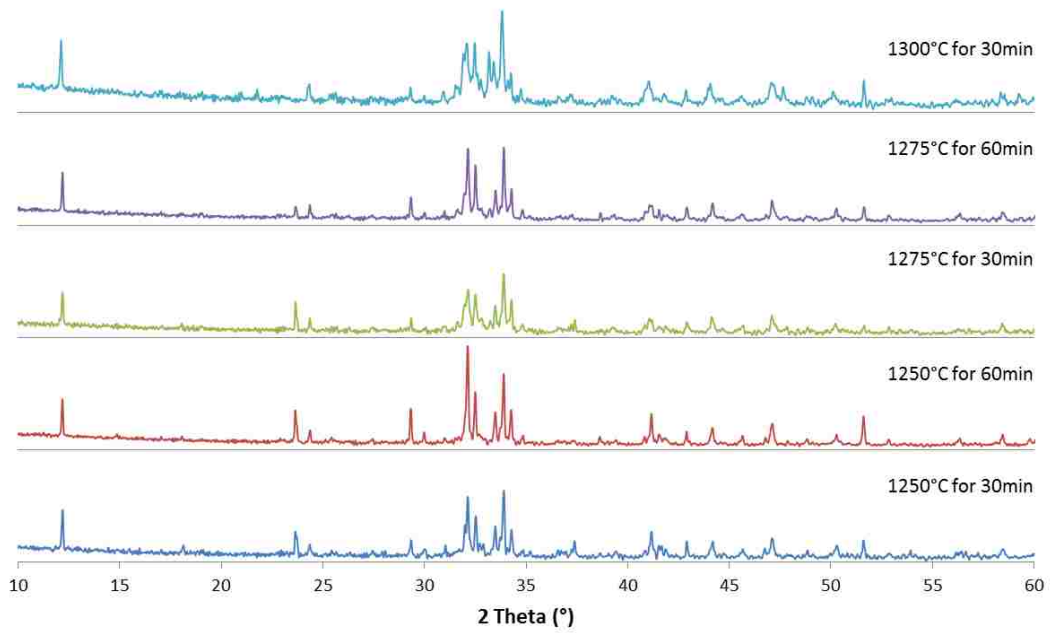
Appendix C: XRD diffractograms for batches #1 through #5 produced from by-products (BP), fired at different temperatures and dwelling times



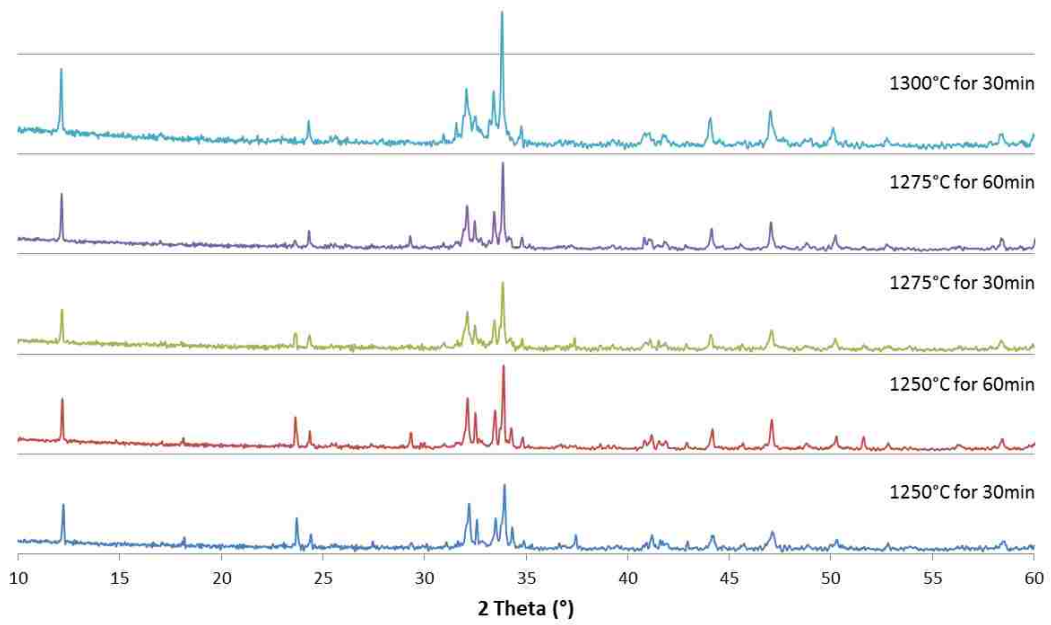
Appendix C 1: Clinker #1 produced from BP fired at different temperatures for 30-60min



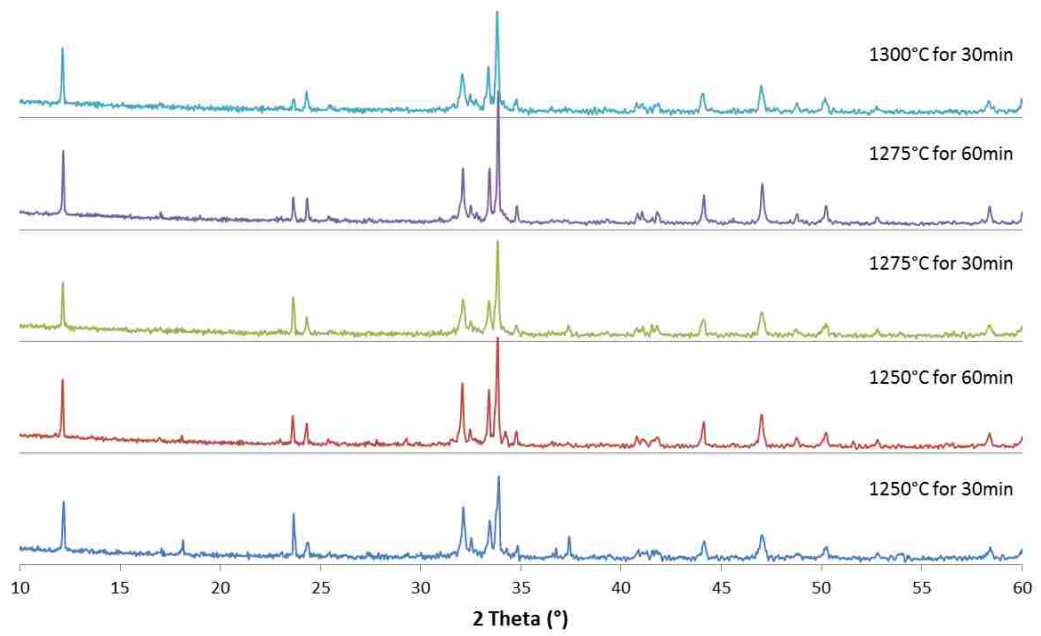
Appendix C 2: Clinker #2 produced from BP fired at different temperatures for 30-60min



Appendix C 3: Clinker #3 produced from BP fired at different temperatures for 30-60min



Appendix C 4: Clinker #4 produced from BP fired at different temperatures for 30-60min



Appendix C 5: Clinker #5 produced from BP fired at different temperatures for 30-60min

Appendix D: Calculation of the amount of iron oxide underestimated in red mud (RM) from XRF

As explained in Chapter 4, compositions formulated from by-products (BP) showed higher amounts of ferrite than expected. This means that the iron may have been underestimated by XRF and the problem is discussed here.

In order to identify the error from the standard used in XRD analyses, red mud (RM) was mixed with pure silica at different percentages and the error is determined at a specific level.

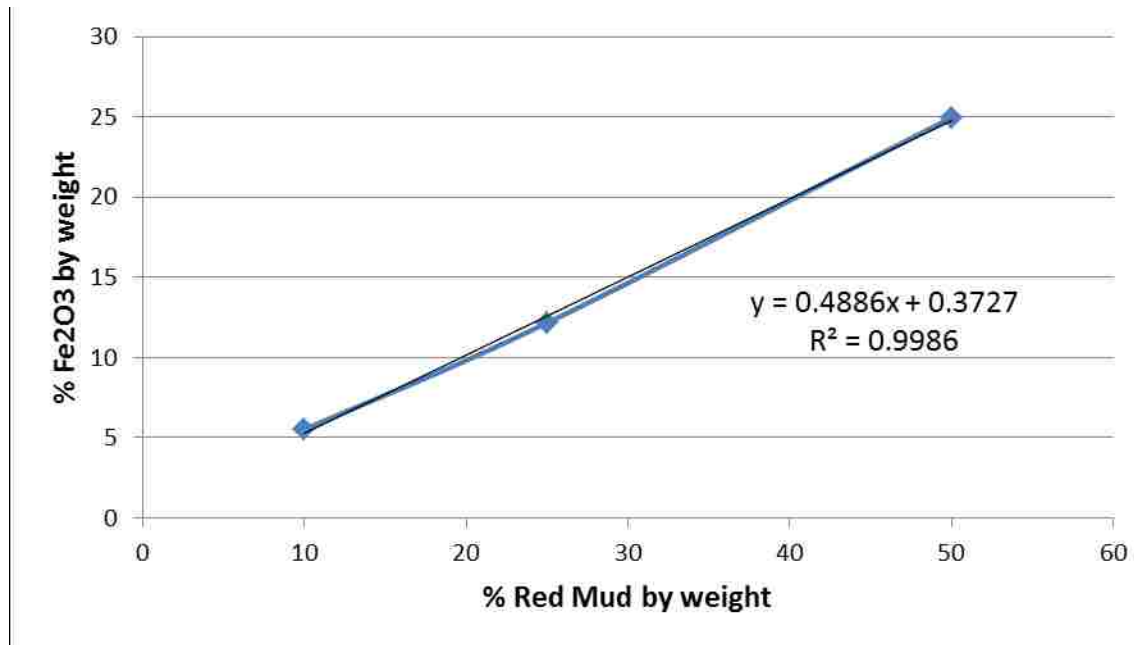
% RM / % SiO <sub>2</sub>		100/0	50/50	25/75	10/90
Major Oxides	CaO	7.64	3.56	1.56	0.64
	SiO <sub>2</sub>	10.17	57.47	78.64	90.91
	Al <sub>2</sub> O <sub>3</sub>	17.42	9.62	5.62	3.28
	Fe <sub>2</sub> O <sub>3</sub>	<b>46.07</b>	<b>24.96</b>	<b>12.17</b>	<b>5.52</b>
	SO <sub>3</sub>	0.02	<0.01	<0.01	<0.01
	MgO	0.56	0.24	0.11	0.02
	TiO <sub>2</sub>	6.26	2.95	1.49	0.7
	Na <sub>2</sub> O	1.63	0.65	0.24	<0.01
	K <sub>2</sub> O	0.2	0.13	0.08	0.05
	P <sub>2</sub> O <sub>5</sub>	0.82	0.35	0.16	0.05
	%Ash	86.27	92.68	95.96	97.98
	<b>Sum</b>	<b>90.79</b>	<b>99.94</b>	<b>100.08</b>	<b>101.19</b>

Appendix D 1: Chemical compositions of mixtures of red mud mixed with pure silica, by weight percentages

The sums of all oxides in each mixture are close to 100% for up to 50wt. % red mud mixed with silica, whereas the sum of the oxide of pure red mud is 90.79%.

By plotting these three points of iron oxide in red mud related to 50/50, 25/75 and 10/90, we obtain the plot in Appendix D2.





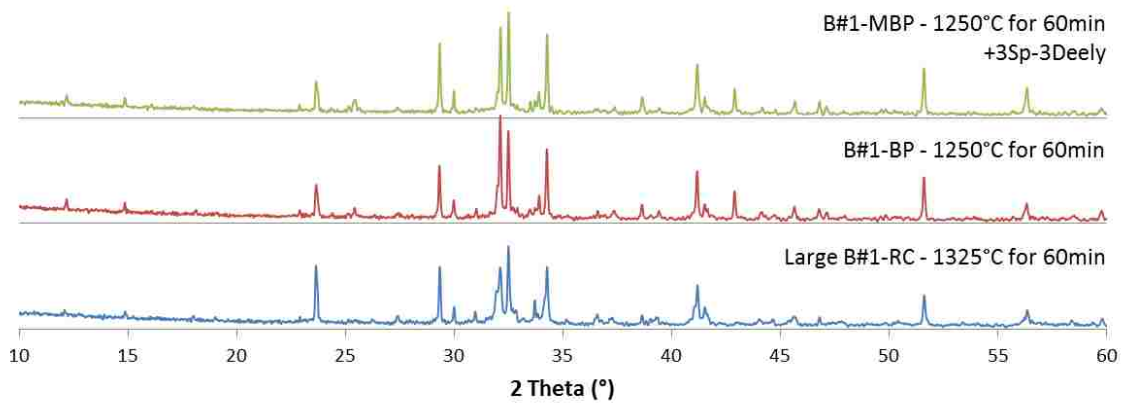
Appendix D 2: Plot of iron oxide in red mud in weight percentages in mixtures 50/50, 75/25 and 10/90

By adding the trend line of this graph, we obtain this equation:  $y=0.4886x+0.3727$ . By replacing “y” with 100, we can estimate the actual iron oxide contained in red mud and supposed to be 49.232%.

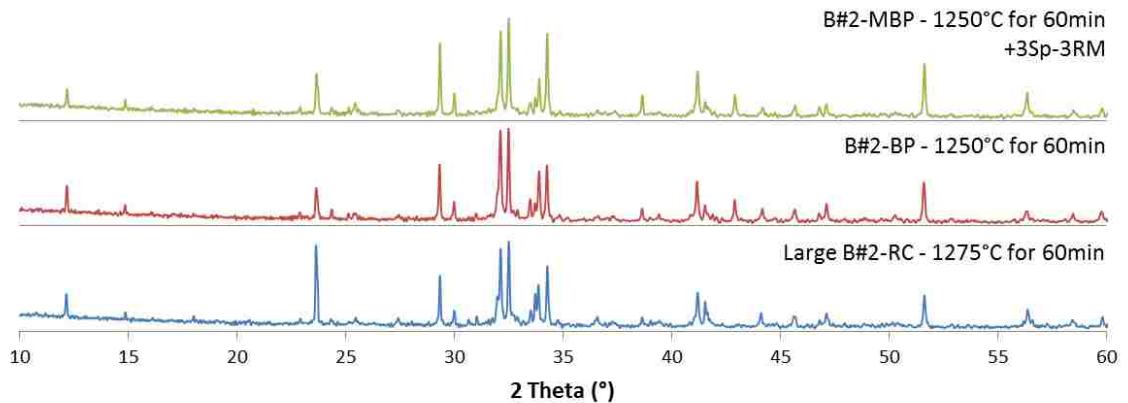
As a result, the amount of iron oxide in red mud has been underestimated, which explains the high amounts of ferrite in clinkers from BP.

The next batches of clinkers produced from MBP (Modified By-Products) were close to the mineralogical compositions of the same clinkers produced from BP with reduced amount of red mud in them.

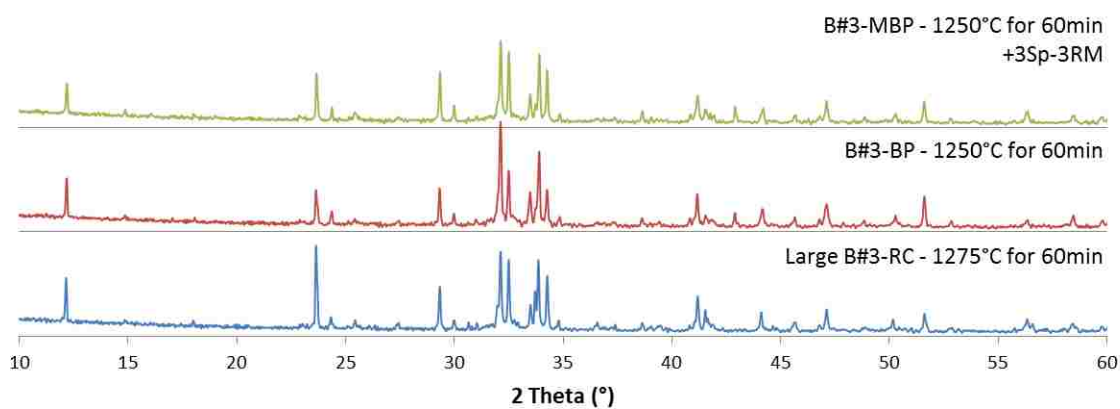
Appendix E: XRD diffractograms for batches #1 to #5 produced from different processes (reagent chemicals (RC), by-products (BP) and modified by-products (MBP)), fired at different temperatures and dwelling times



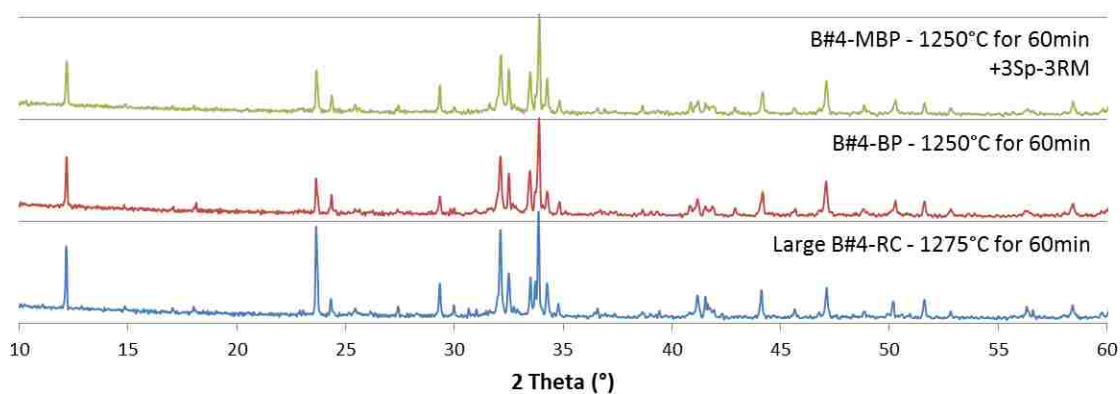
Appendix E 1: Comparison of XRD data from clinker #1 made from different processes



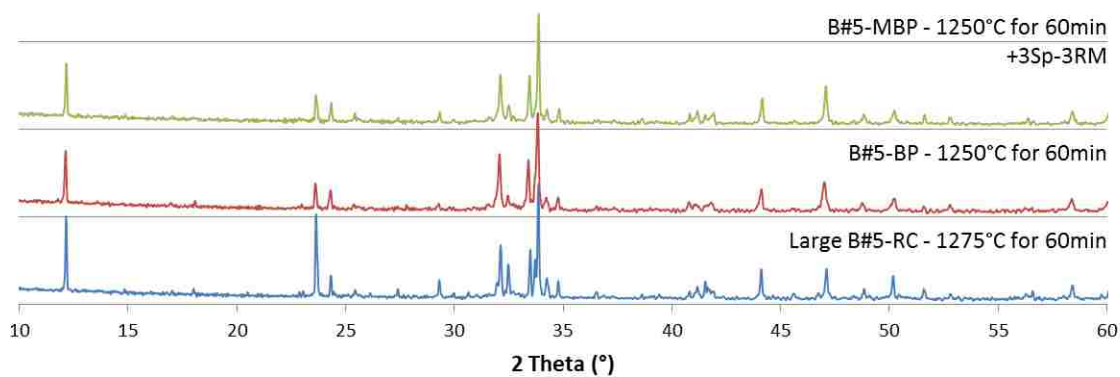
Appendix E 2: Comparison of XRD data from clinker #2 made from different processes



Appendix E 3: Comparison of XRD data from clinker #3 made from different processes

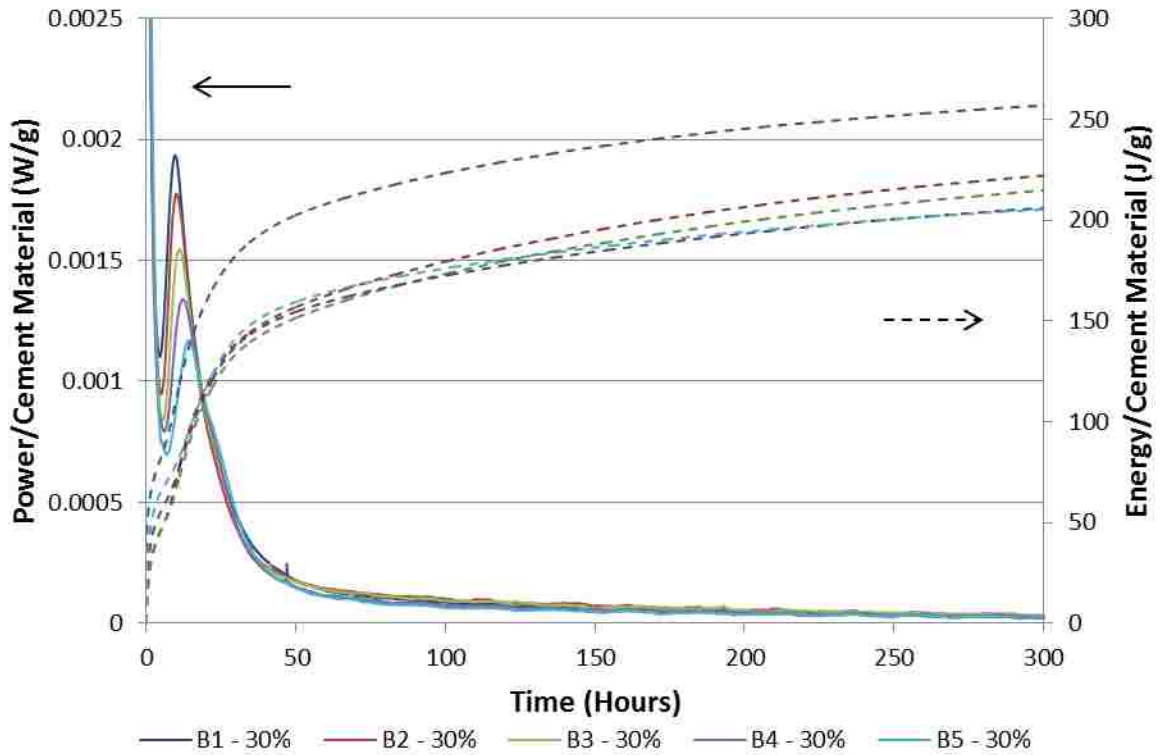


Appendix E 4: Comparison of XRD data from clinker #4 made from different processes

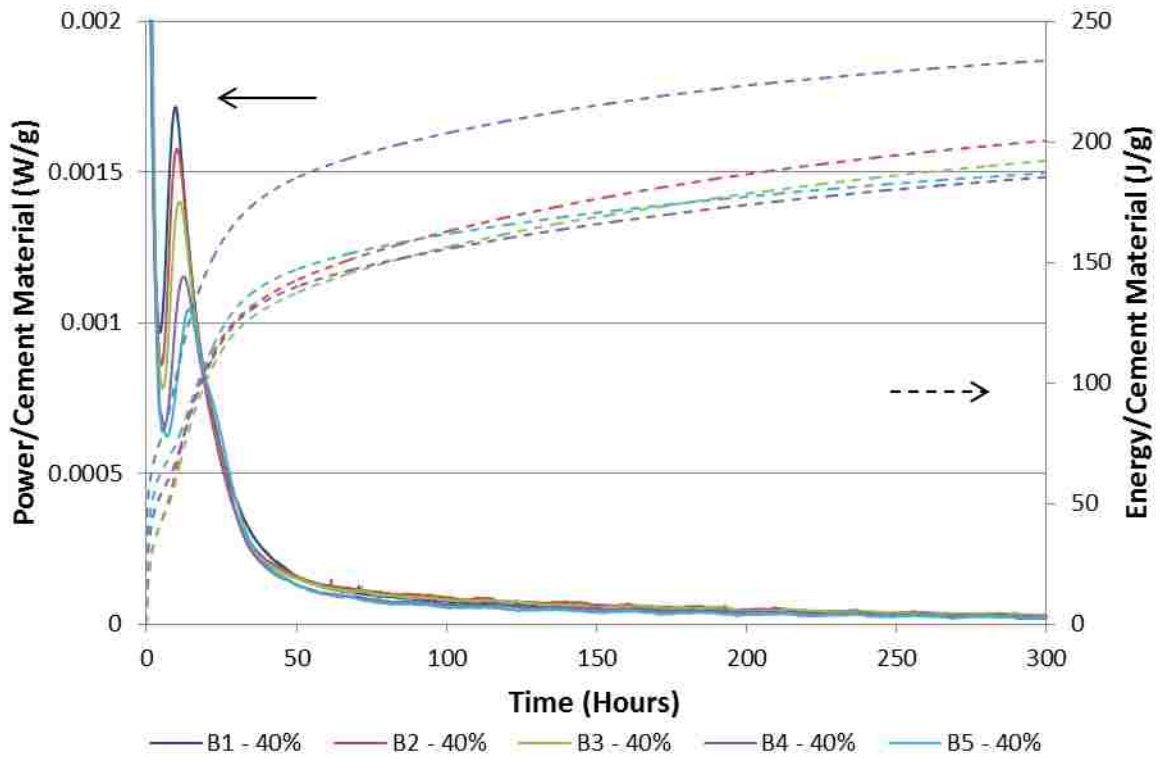


Appendix E 5: Comparison of XRD data from clinker #5 made from different processes

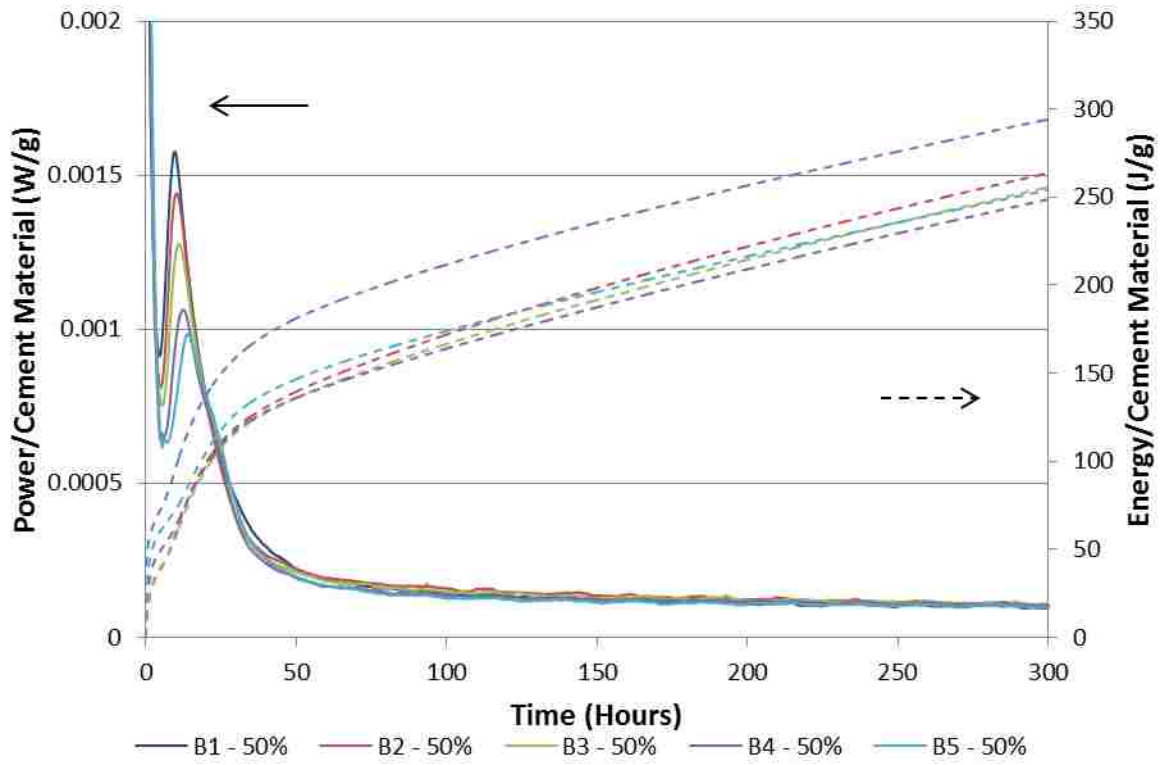
Appendix F: All calorimeter data for batches #1 to #5 with 30%, 40% and 50% gypsum, all produced from reagent chemicals (RC)



Appendix F 1: Calorimeter data of batches #1 to #5 produced from RC with 30% of gypsum by weight for the first 300 hours into the hydration process

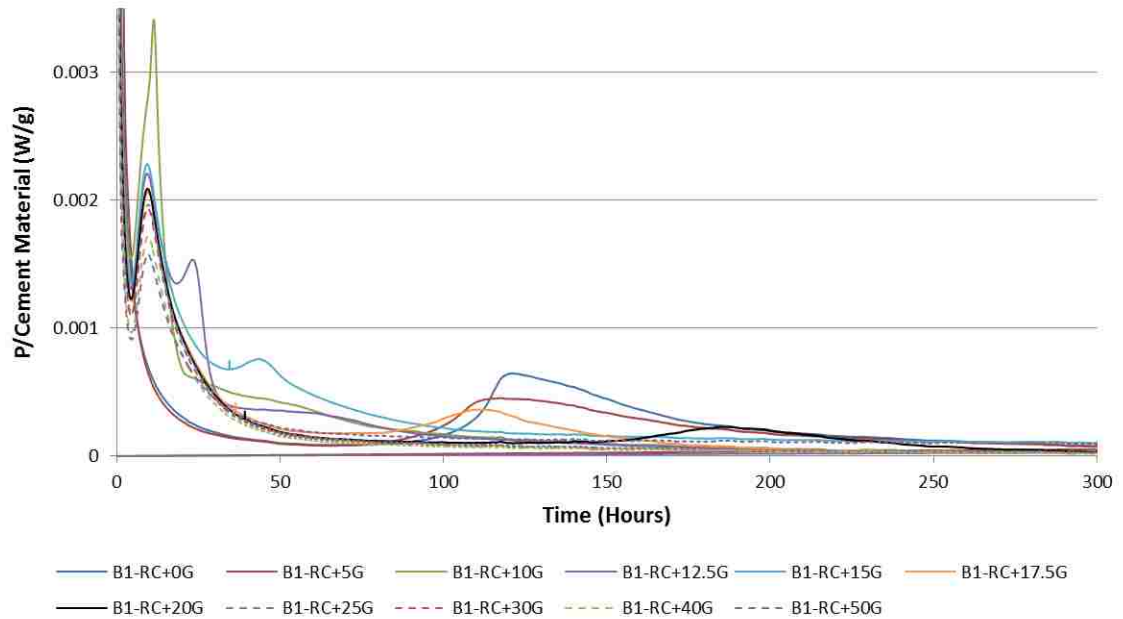


Appendix F 2: Calorimeter data of batches #1 to #5 produced from RC with 40% of gypsum by weight for the first 300 hours into the hydration process

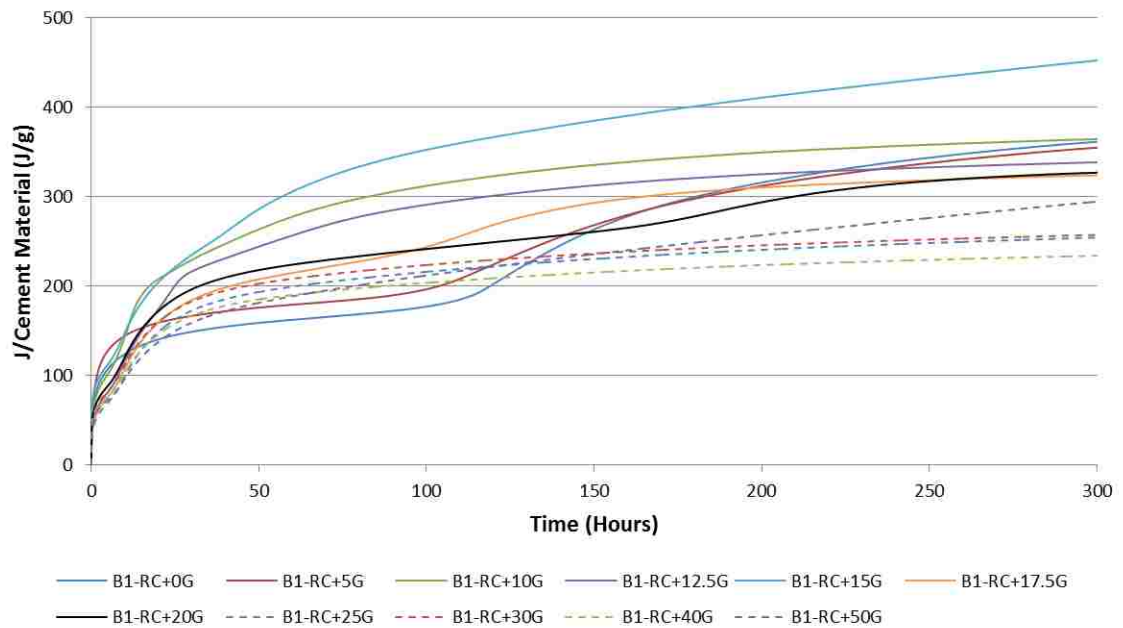


Appendix F 3: Calorimeter data of batches #1 to #5 produced from RC with 50% of gypsum by weight for the first 300 hours into the hydration process

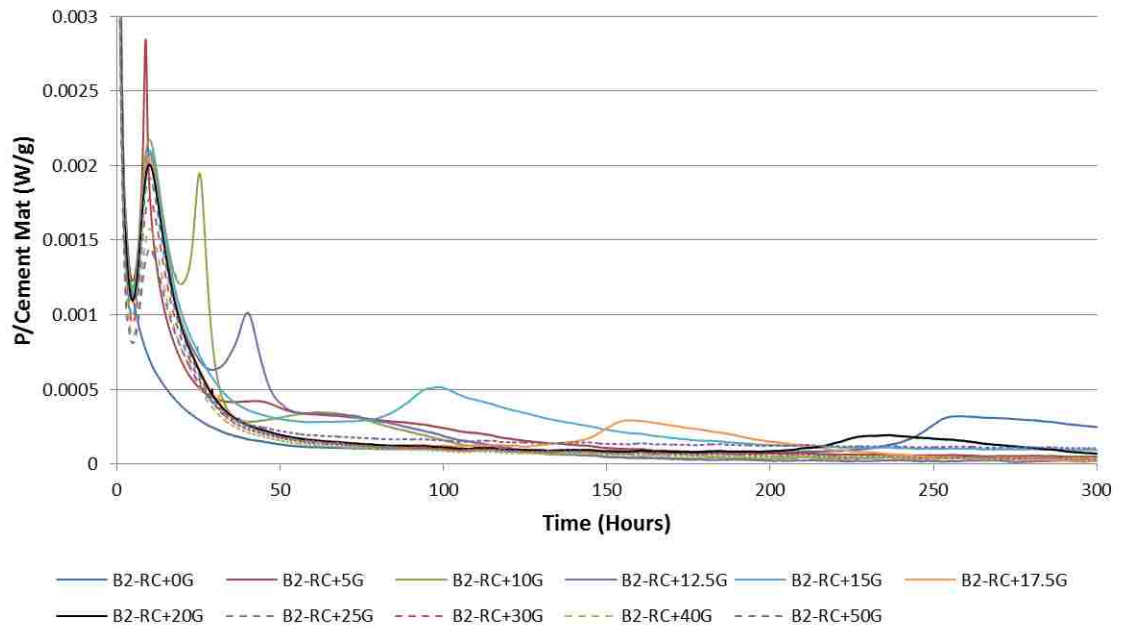
Appendix G: Calorimeter data for each batch produced from reagent chemicals (RC) with different amounts of gypsum introduced



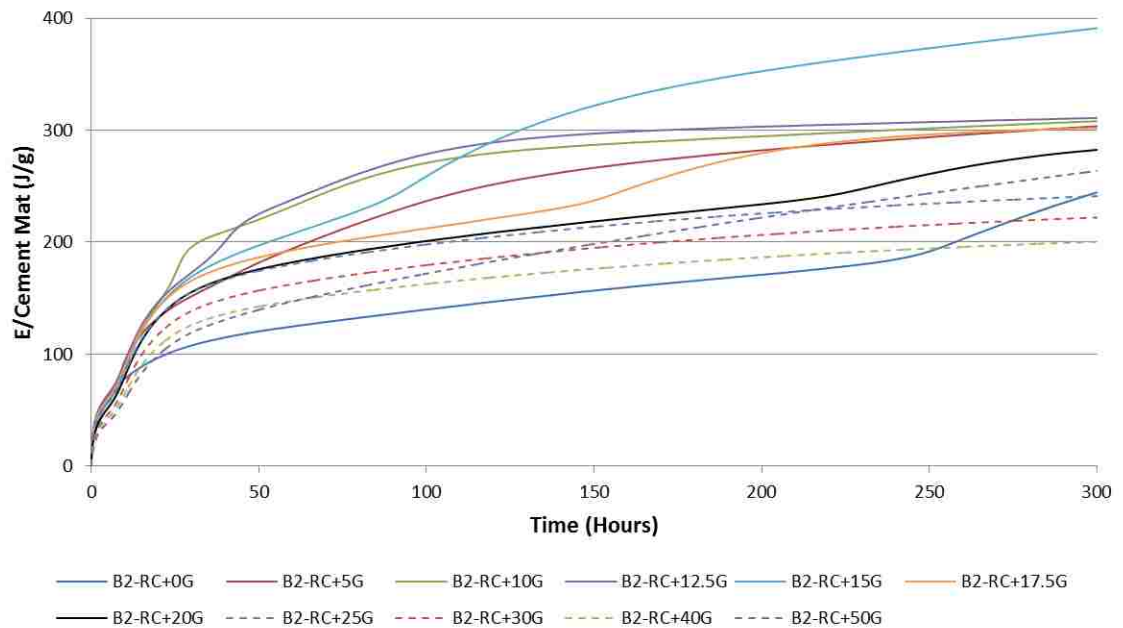
Appendix G 1: Calorimeter data of batch #1 produced from RC with different amounts of gypsum, from 0% to 50% by weight



Appendix G 2: Calorimeter data of the total energy released for batch #1 produced from RC with different amounts of gypsum, from 0% to 50% by weight

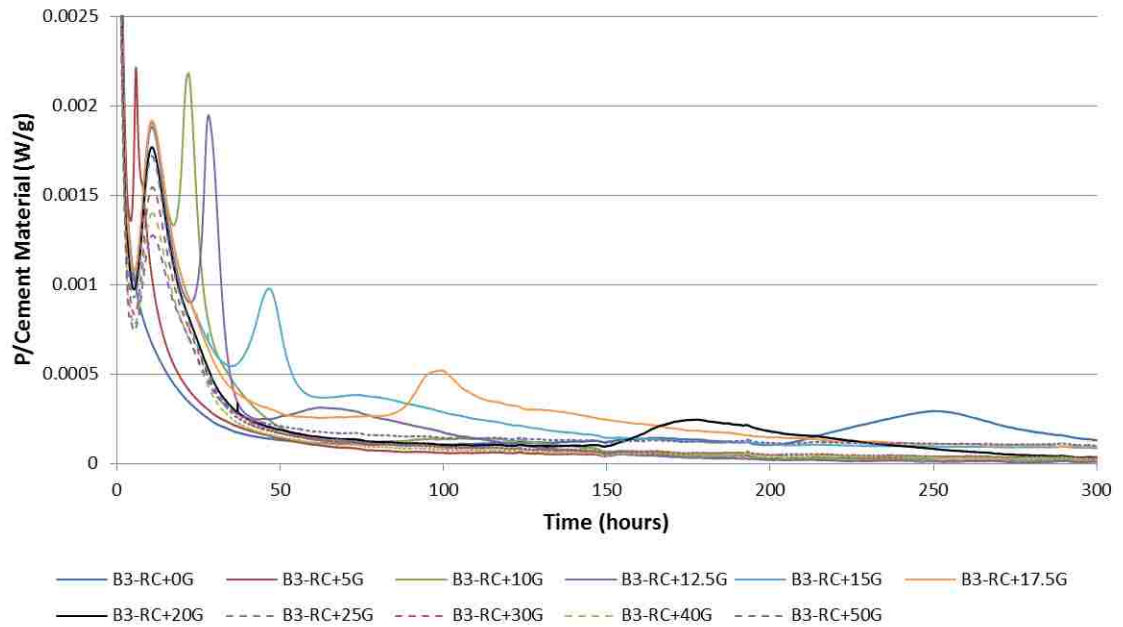


Appendix G 3: Calorimeter data of batch #2 produced from RC with different amounts of gypsum, from 0% to 50% by weight

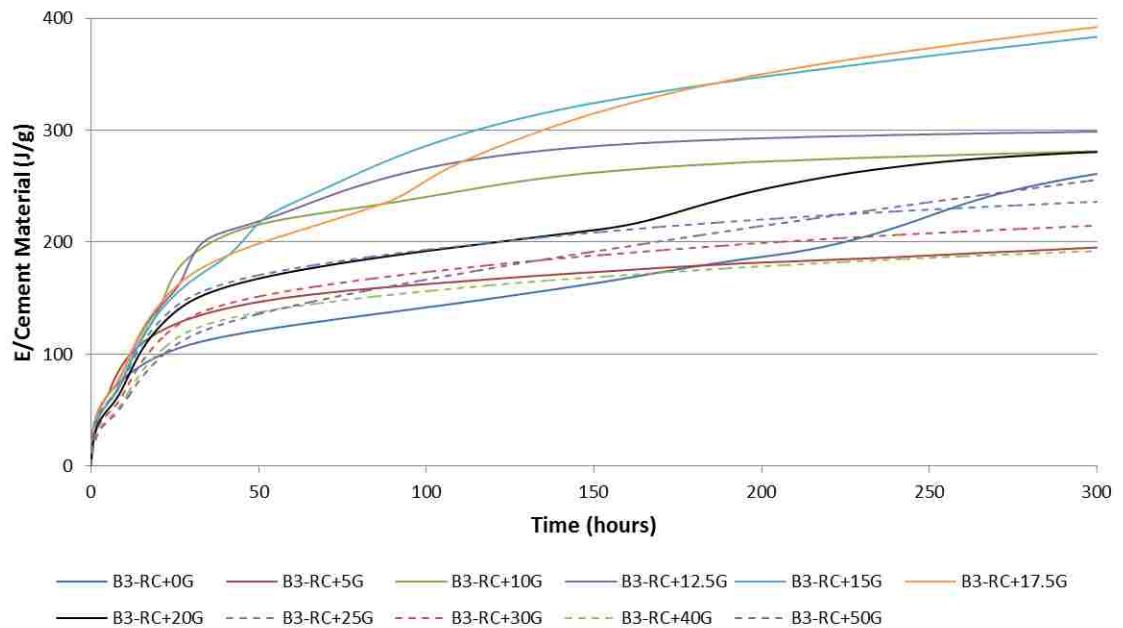


Appendix G 4: Calorimeter data of the total energy released for batch #2 produced from RC with different amounts of gypsum, from 0% to 50% by weight

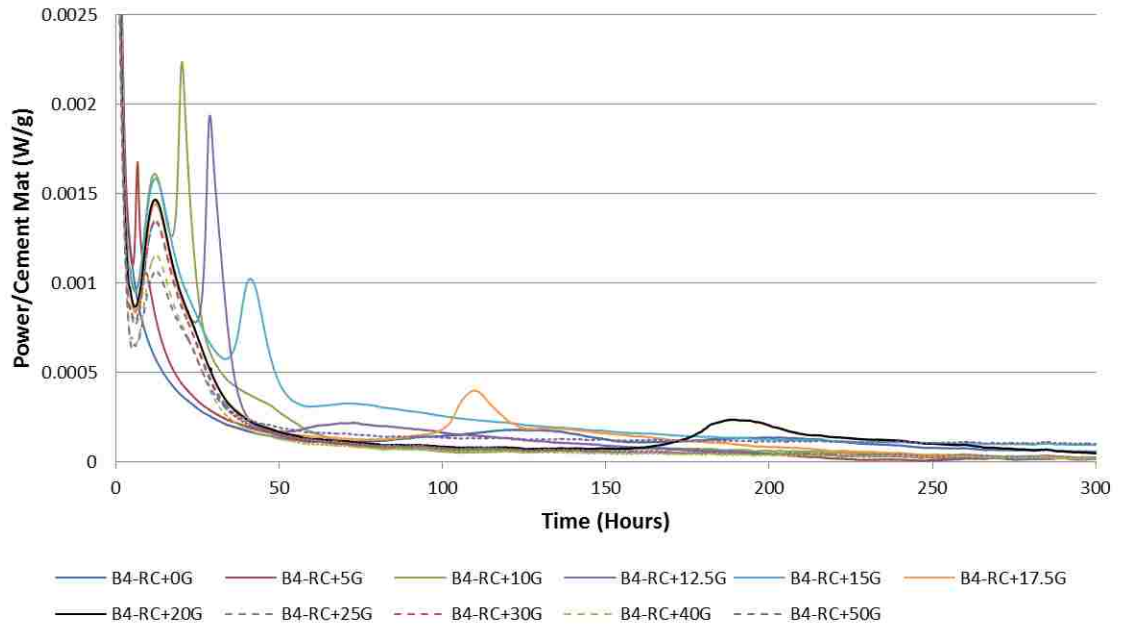




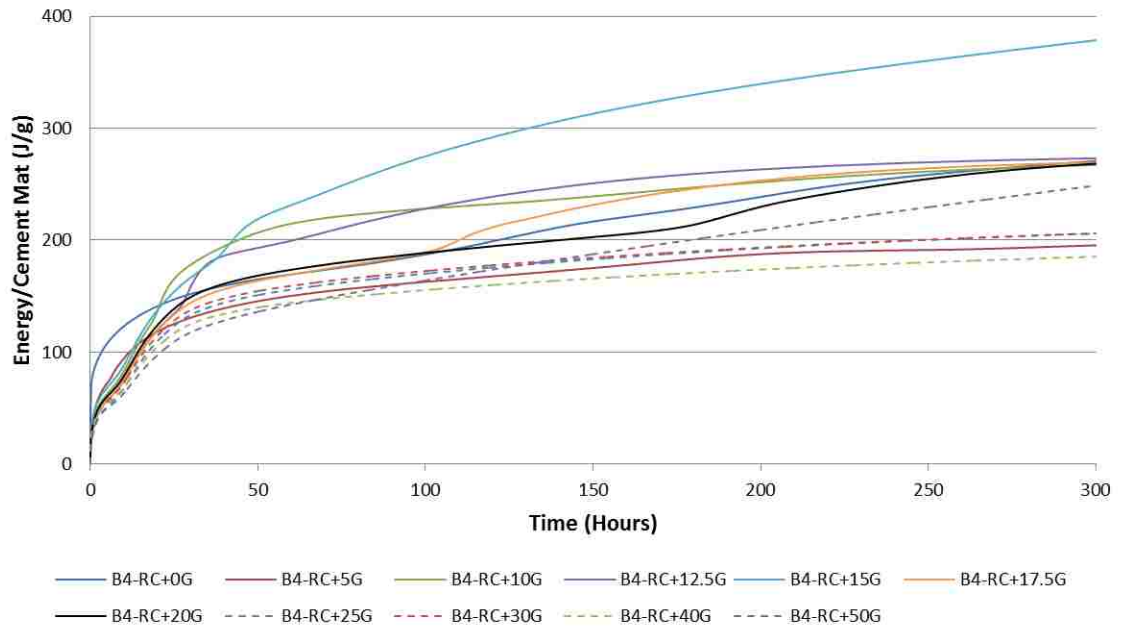
Appendix G 5: Calorimeter data of batch #3 produced from RC with different amounts of gypsum, from 0% to 50% by weight



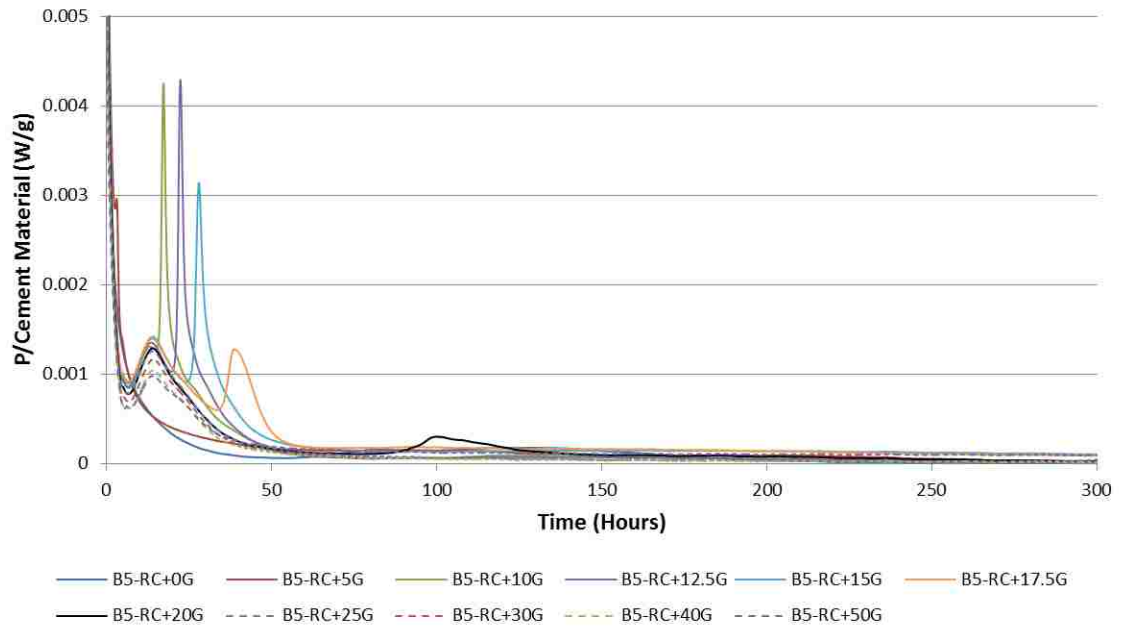
Appendix G 6: Calorimeter data of the total energy released for batch #3 produced from RC with different amounts of gypsum, from 0% to 50% by weight



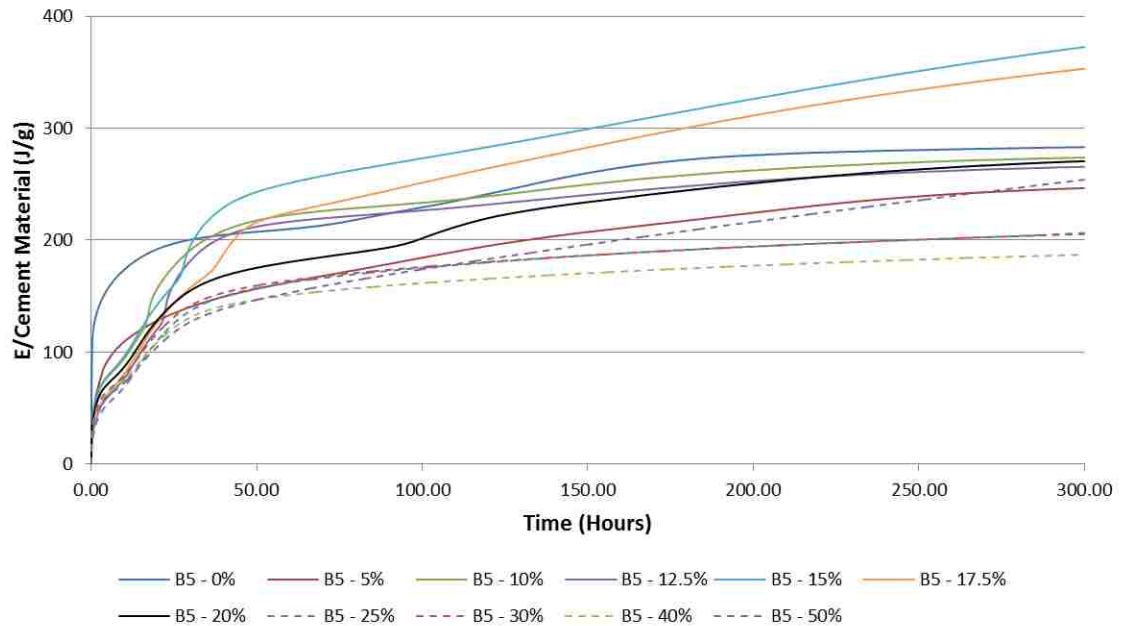
Appendix G 7: Calorimeter data of batch #4 produced from RC with different amounts of gypsum, from 0% to 50% by weight



Appendix G 8: Calorimeter data of the total energy released for batch #4 produced from RC with different amounts of gypsum, from 0% to 50% by weight

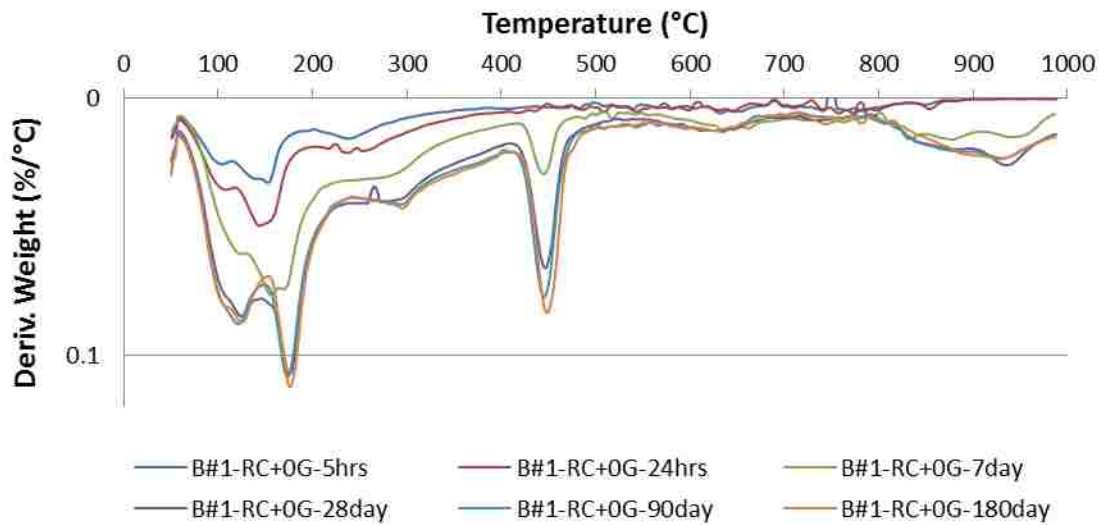


Appendix G 9: Calorimeter data of batch #5 produced from RC with different amounts of gypsum, from 0% to 50% by weight

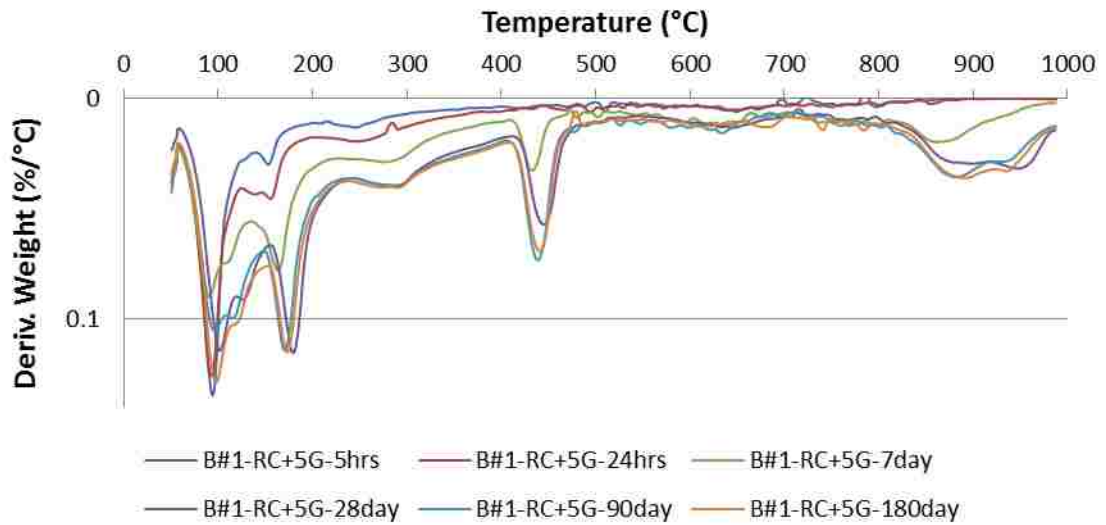


Appendix G 10: Calorimeter data of the total energy released for batch #5 produced from RC with different amounts of gypsum, from 0% to 50% by weight

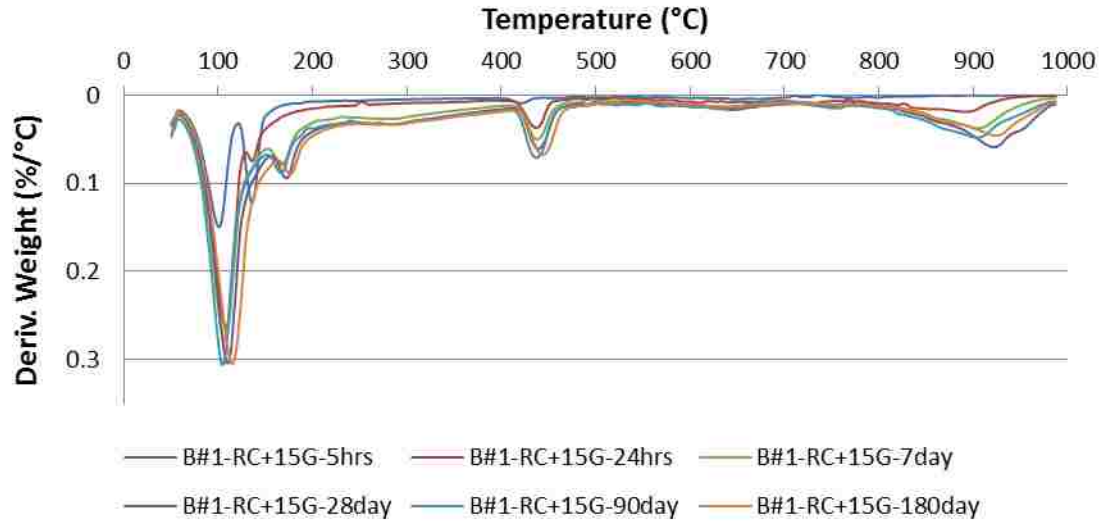
Appendix H: TGA data for all batches produced from Reagent Chemicals (RC)



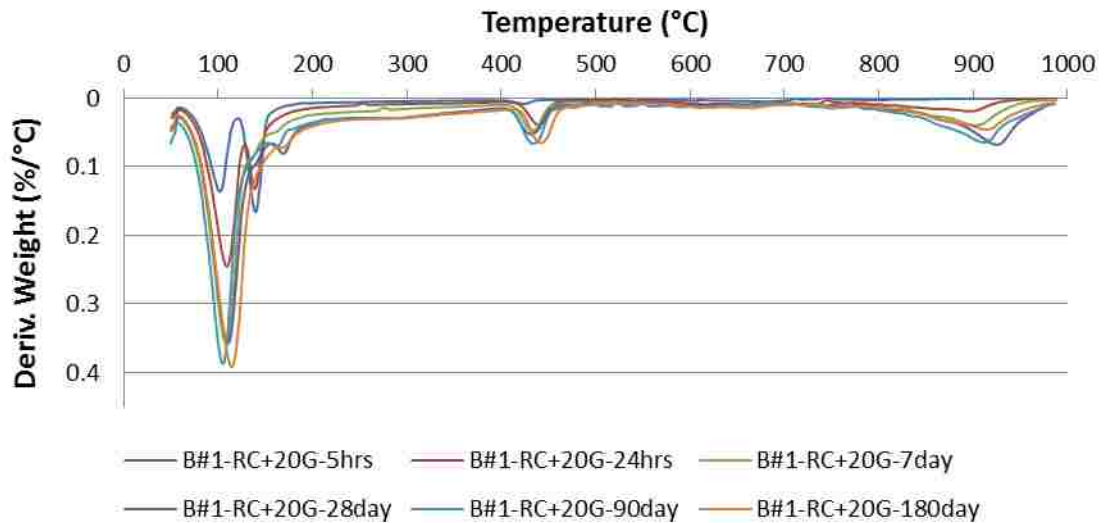
Appendix H 1: TGA analysis of the cement paste of batch #1 produced from RC with 0% gypsum by weight, after 5 hours, 1, 7, 28, 90 and 180 days into the hydration process



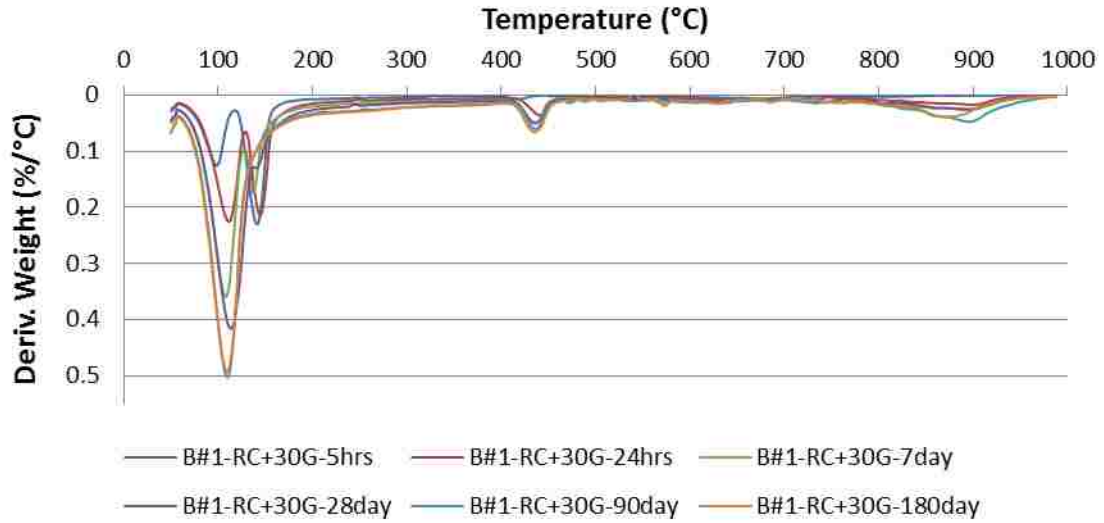
Appendix H 2: TGA analysis of the cement paste of batch #1 produced from RC with 5% gypsum by weight, after 5 hours, 1, 7, 28, 90 and 180 days into the hydration process



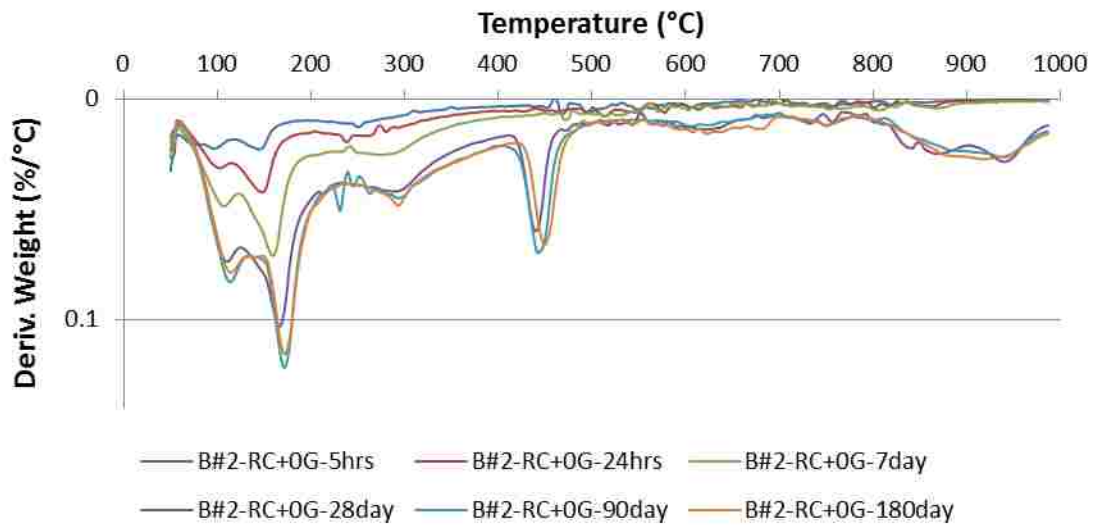
Appendix H 3: TGA analysis of the cement paste of batch #1 produced from RC with 15% gypsum by weight, after 5 hours, 1, 7, 28, 90 and 180 days into the hydration process



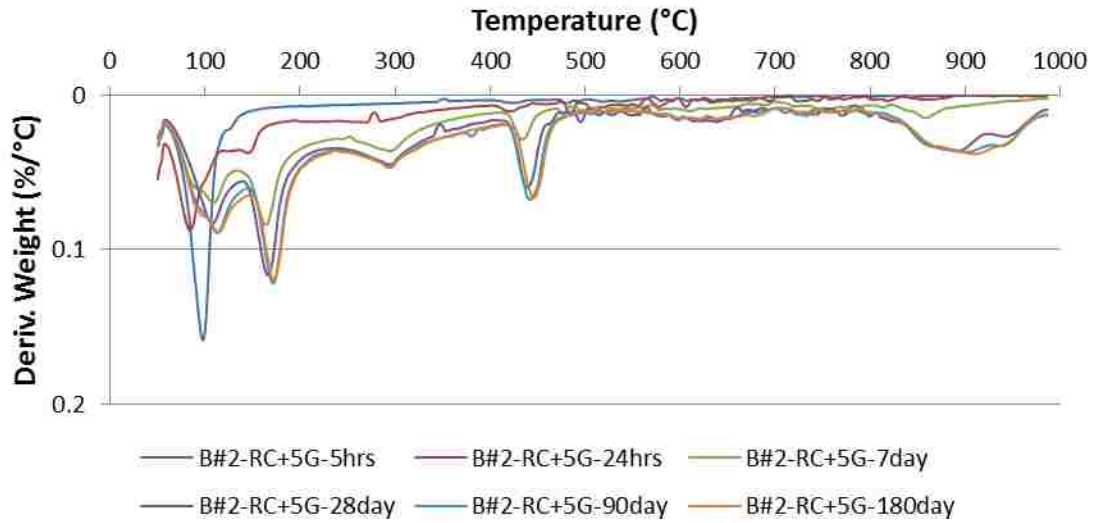
Appendix H 4: TGA analysis of the cement paste of batch #1 produced from RC with 20% gypsum by weight, after 5 hours, 1, 7, 28, 90 and 180 days into the hydration process



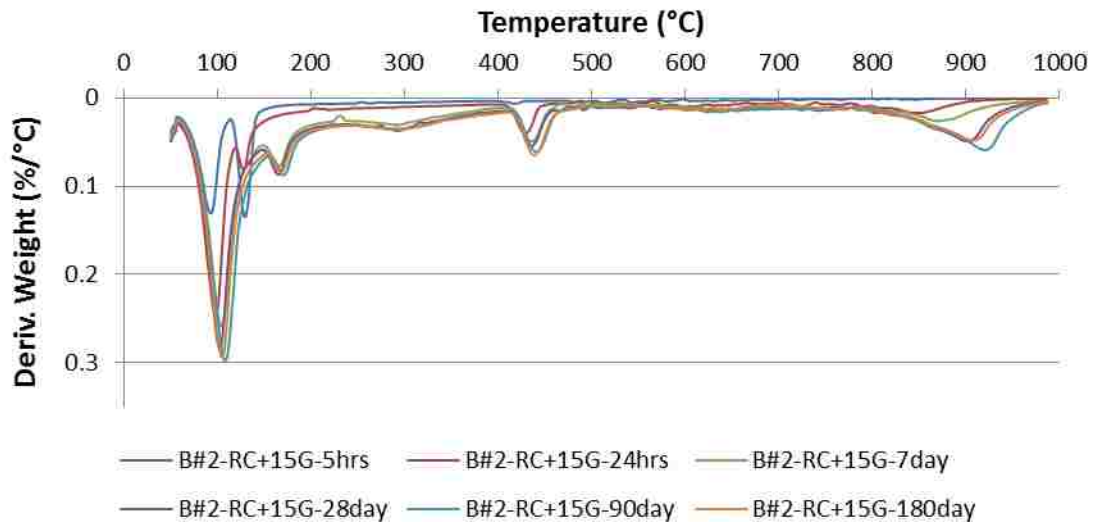
Appendix H 5: TGA analysis of the cement paste of batch #1 produced from RC with 30% gypsum by weight, after 5 hours, 1, 7, 28, 90 and 180 days into the hydration process



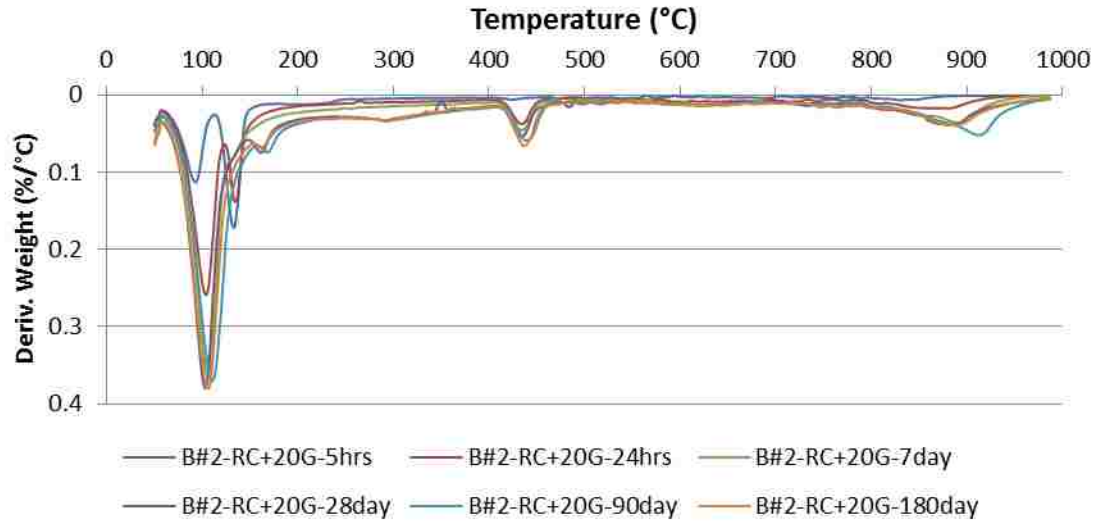
Appendix H 6: TGA analysis of the cement paste of batch #2 produced from RC with 0% gypsum by weight, after 5 hours, 1, 7, 28, 90 and 180 days into the hydration process



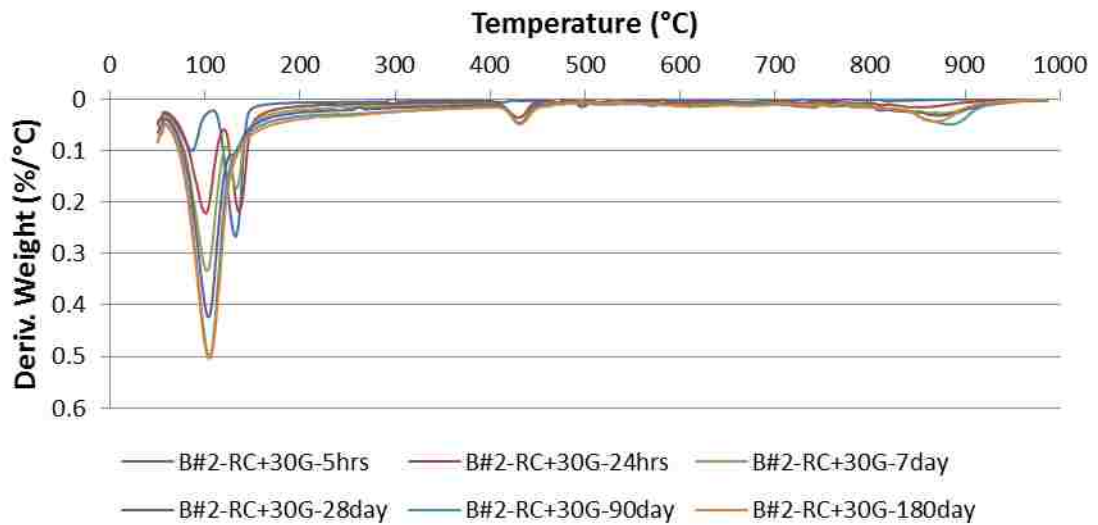
Appendix H 7: TGA analysis of the cement paste of batch #2 produced from RC with 5% gypsum by weight, after 5 hours, 1, 7, 28, 90 and 180 days into the hydration process



Appendix H 8: TGA analysis of the cement paste of batch #2 produced from RC with 15% gypsum by weight, after 5 hours, 1, 7, 28, 90 and 180 days into the hydration process

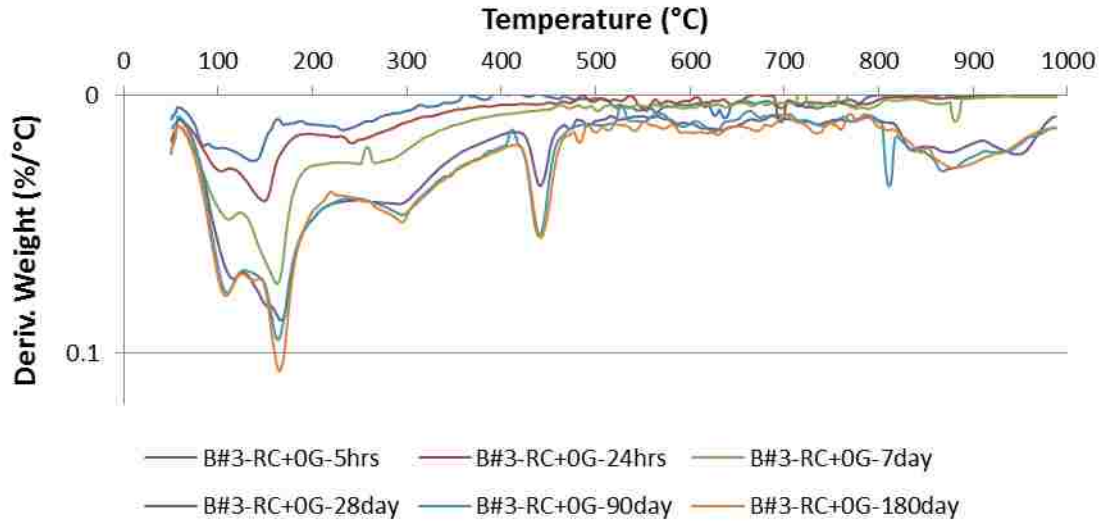


Appendix H 9: TGA analysis of the cement paste of batch #2 produced from RC with 20% gypsum by weight, after 5 hours, 1, 7, 28, 90 and 180 days into the hydration process

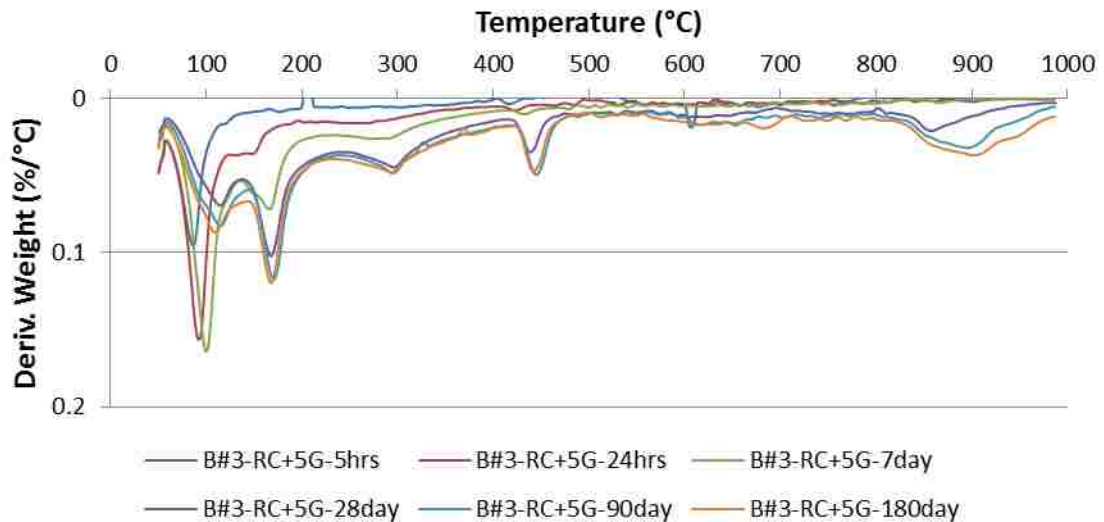


Appendix H 10: TGA analysis of the cement paste of batch #2 produced from RC with 30% gypsum by weight, after 5 hours, 1, 7, 28, 90 and 180 days into the hydration process

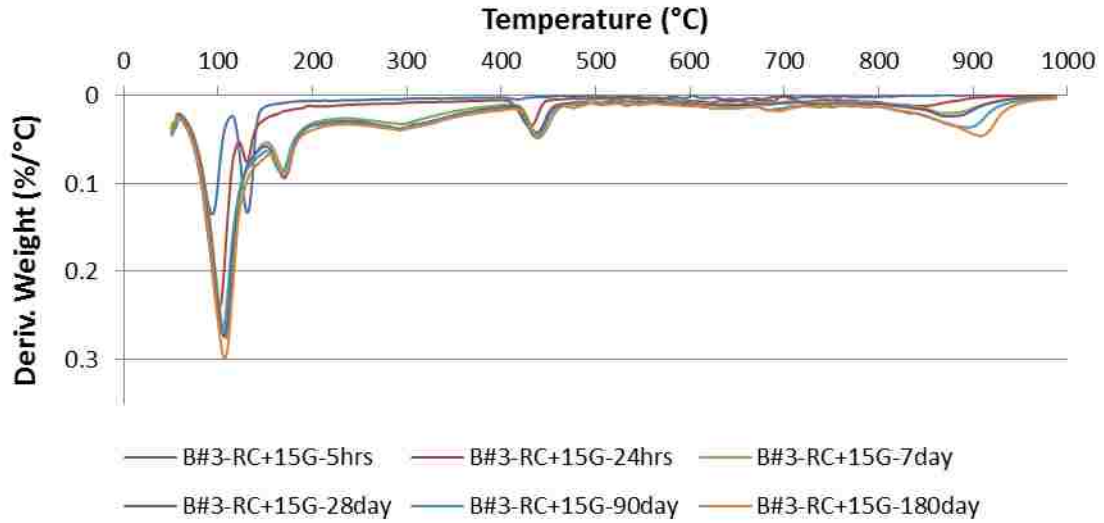




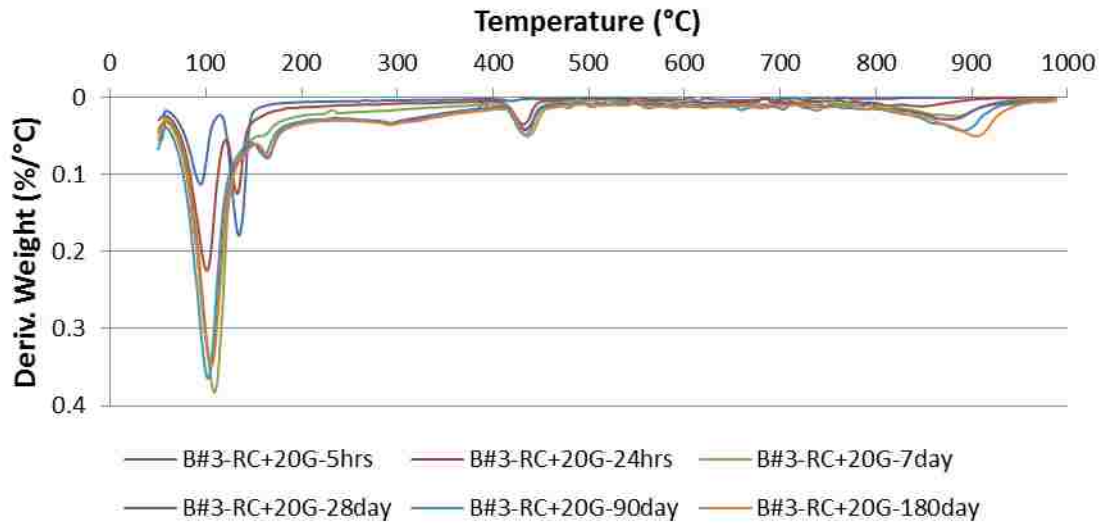
Appendix H 11: TGA analysis of the cement paste of batch #3 produced from RC with 0% gypsum by weight, after 5 hours, 1, 7, 28, 90 and 180 days into the hydration process



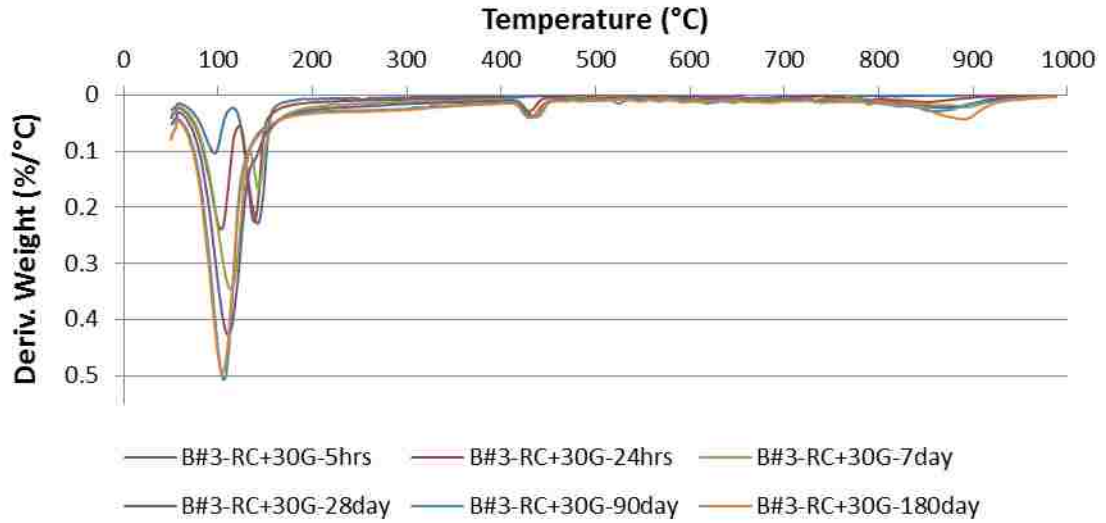
Appendix H 12: TGA analysis of the cement paste of batch #3 produced from RC with 5% gypsum by weight, after 5 hours, 1, 7, 28, 90 and 180 days into the hydration process



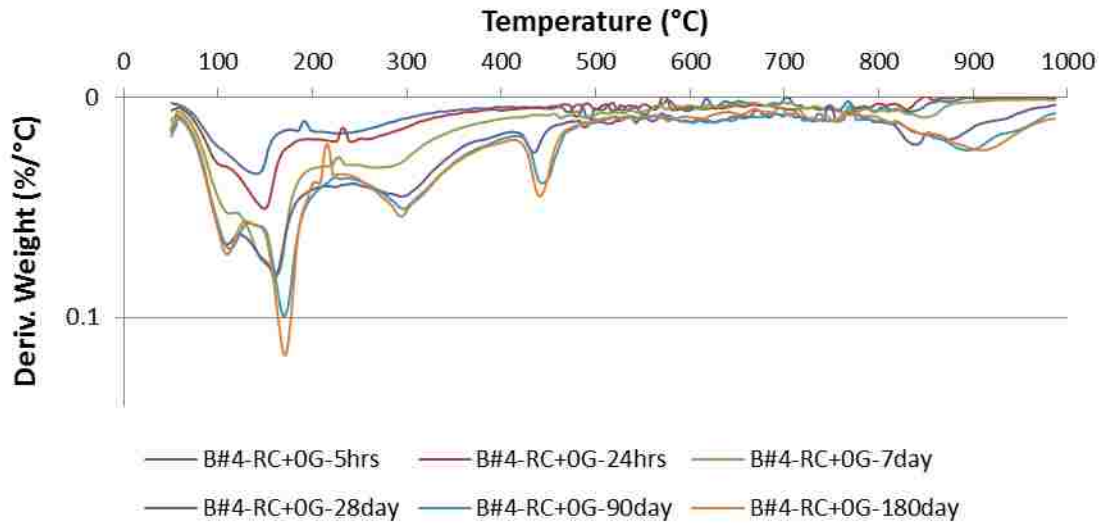
Appendix H 13: TGA analysis of the cement paste of batch #3 produced from RC with 15% gypsum by weight, after 5 hours, 1, 7, 28, 90 and 180 days into the hydration process



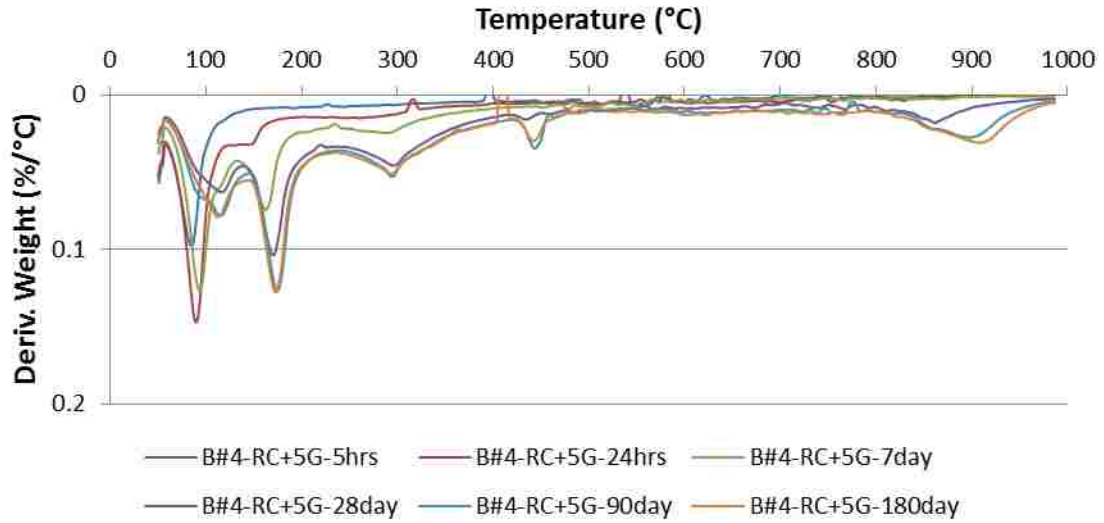
Appendix H 14: TGA analysis of the cement paste of batch #3 produced from RC with 20% gypsum by weight, after 5 hours, 1, 7, 28, 90 and 180 days into the hydration process



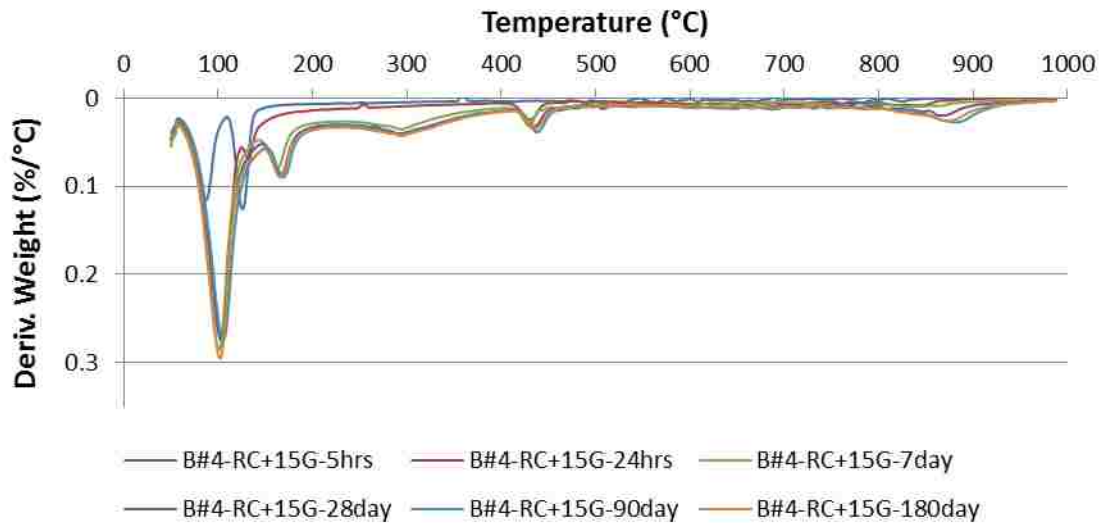
Appendix H 15: TGA analysis of the cement paste of batch #3 produced from RC with 30% gypsum by weight, after 5 hours, 1, 7, 28, 90 and 180 days into the hydration process



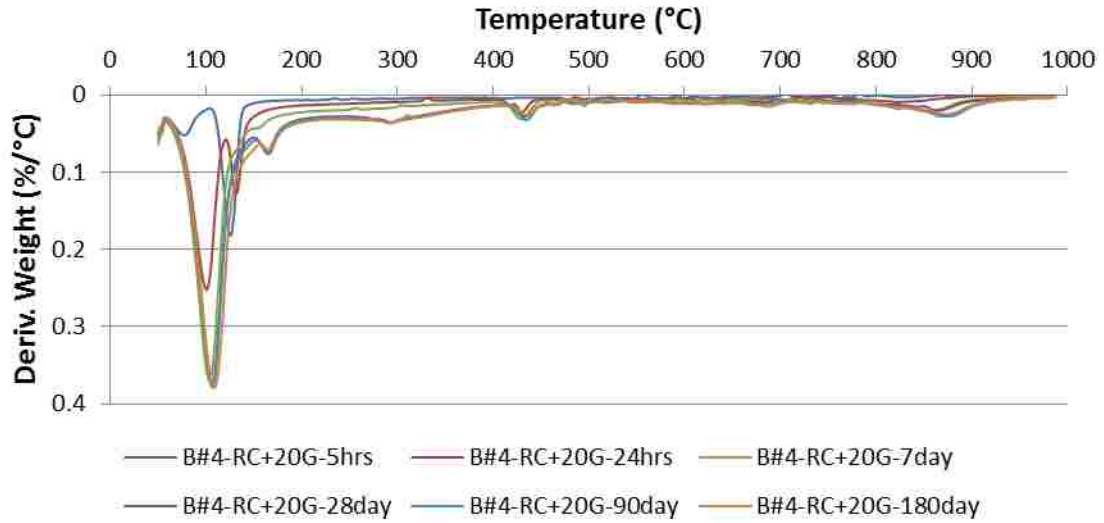
Appendix H 16: TGA analysis of the cement paste of batch #4 produced from RC with 0% gypsum by weight, after 5 hours, 1, 7, 28, 90 and 180 days into the hydration process



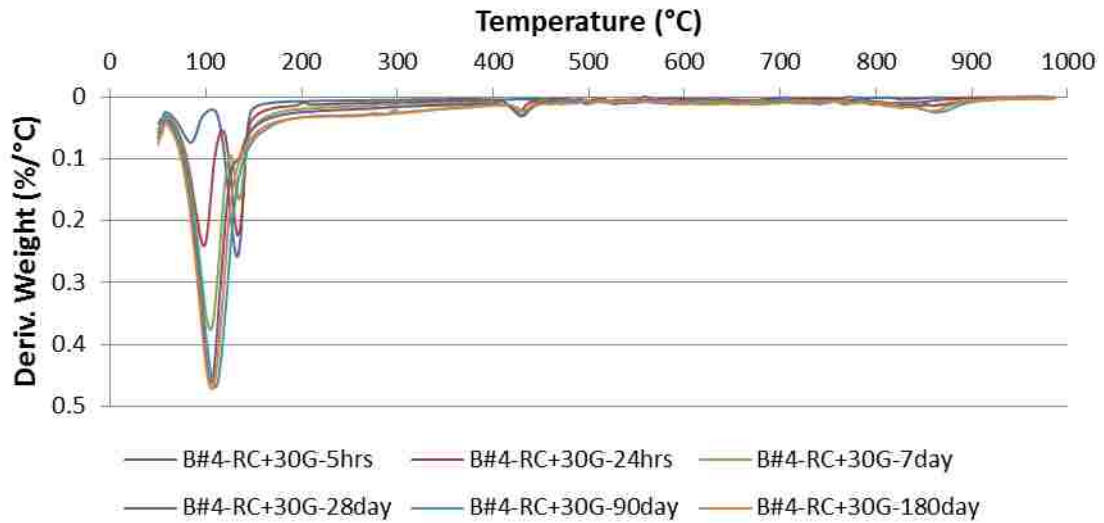
Appendix H 17: TGA analysis of the cement paste of batch #4 produced from RC with 5% gypsum by weight, after 5 hours, 1, 7, 28, 90 and 180 days into the hydration process



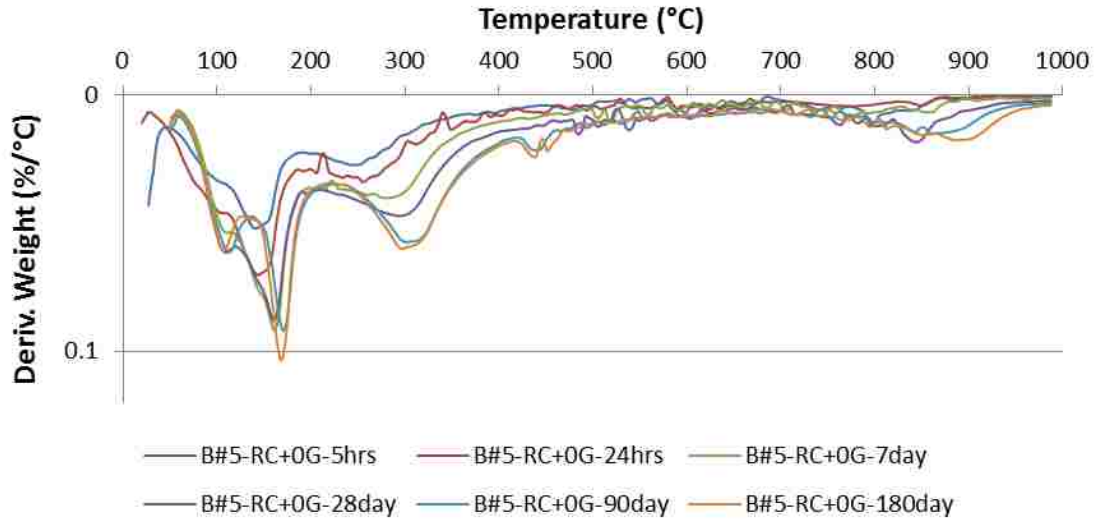
Appendix H 18: TGA analysis of the cement paste of batch #4 produced from RC with 15% gypsum by weight, after 5 hours, 1, 7, 28, 90 and 180 days into the hydration process



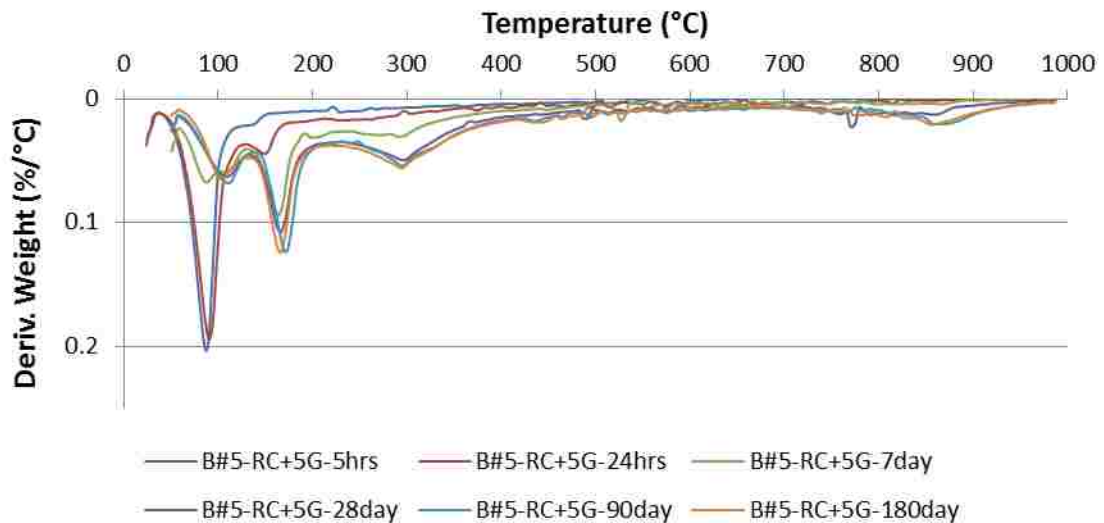
Appendix H 19: TGA analysis of the cement paste of batch #4 produced from RC with 20% gypsum by weight, after 5 hours, 1, 7, 28, 90 and 180 days into the hydration process



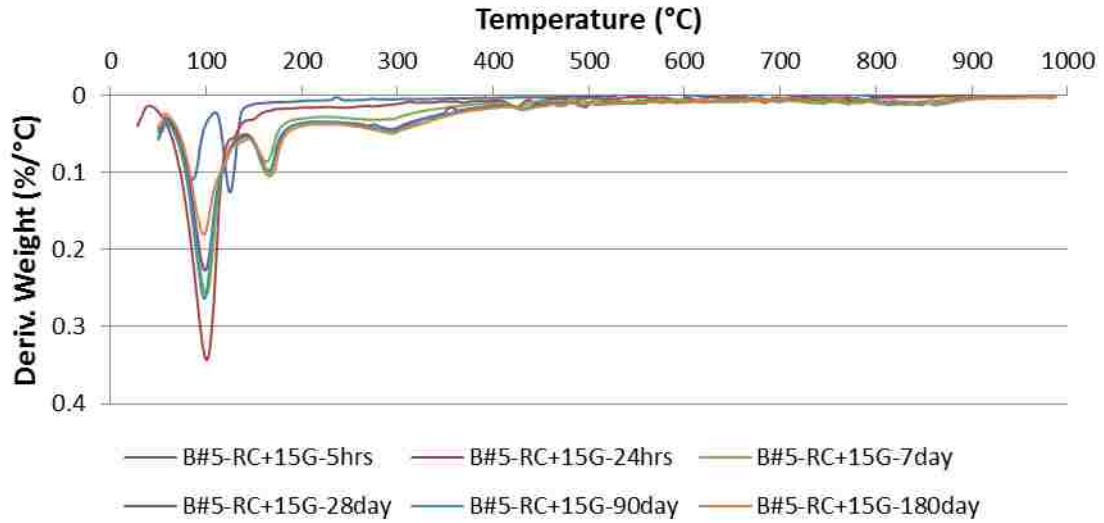
Appendix H 20: TGA analysis of the cement paste of batch #4 produced from RC with 30% gypsum by weight, after 5 hours, 1, 7, 28, 90 and 180 days into the hydration process



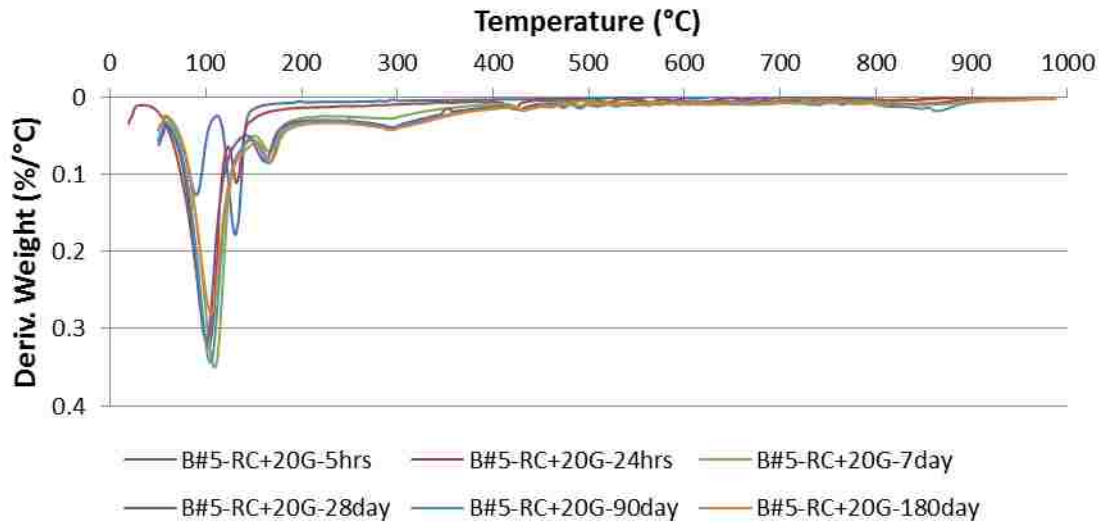
Appendix H 21: TGA analysis of the cement paste of batch #5 produced from RC with 0% gypsum by weight, after 5 hours, 1, 7, 28, 90 and 180 days into the hydration process



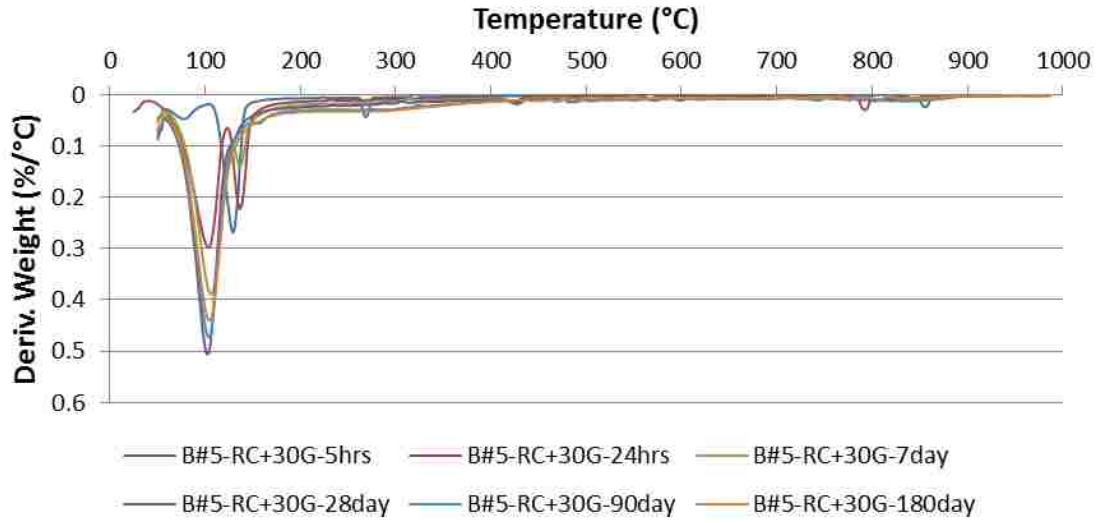
Appendix H 22: TGA analysis of the cement paste of batch #5 produced from RC with 5% gypsum by weight, after 5 hours, 1, 7, 28, 90 and 180 days into the hydration process



Appendix H 23: TGA analysis of the cement paste of batch #5 produced from RC with 15% gypsum by weight, after 5 hours, 1, 7, 28, 90 and 180 days into the hydration process



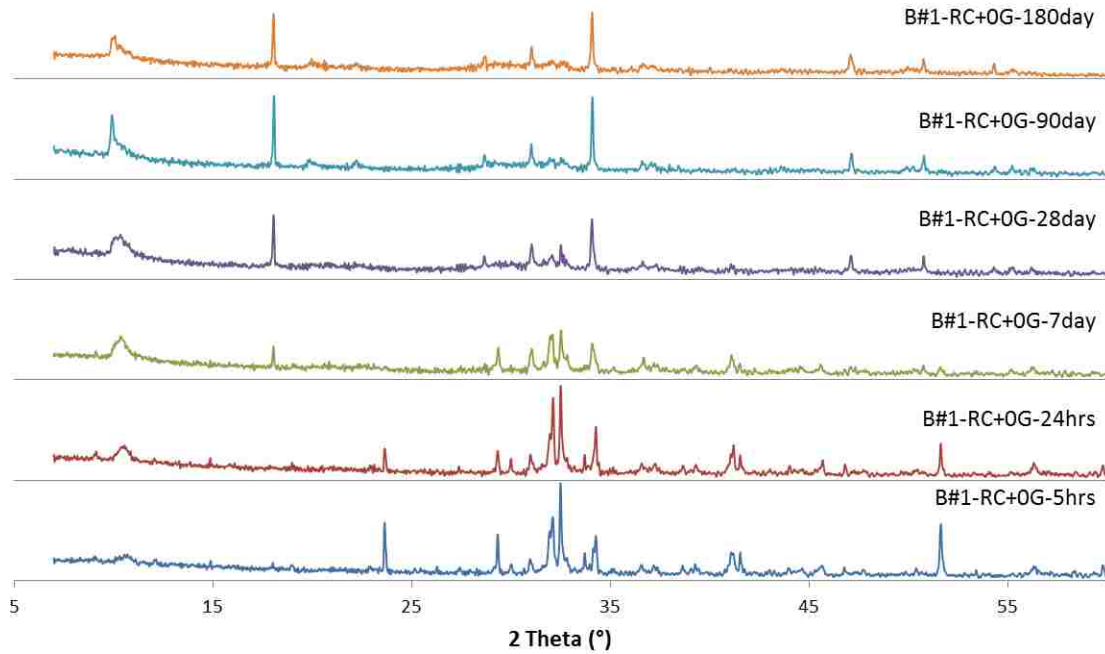
Appendix H 24: TGA analysis of the cement paste of batch #5 produced from RC with 20% gypsum by weight, after 5 hours, 1, 7, 28, 90 and 180 days into the hydration process



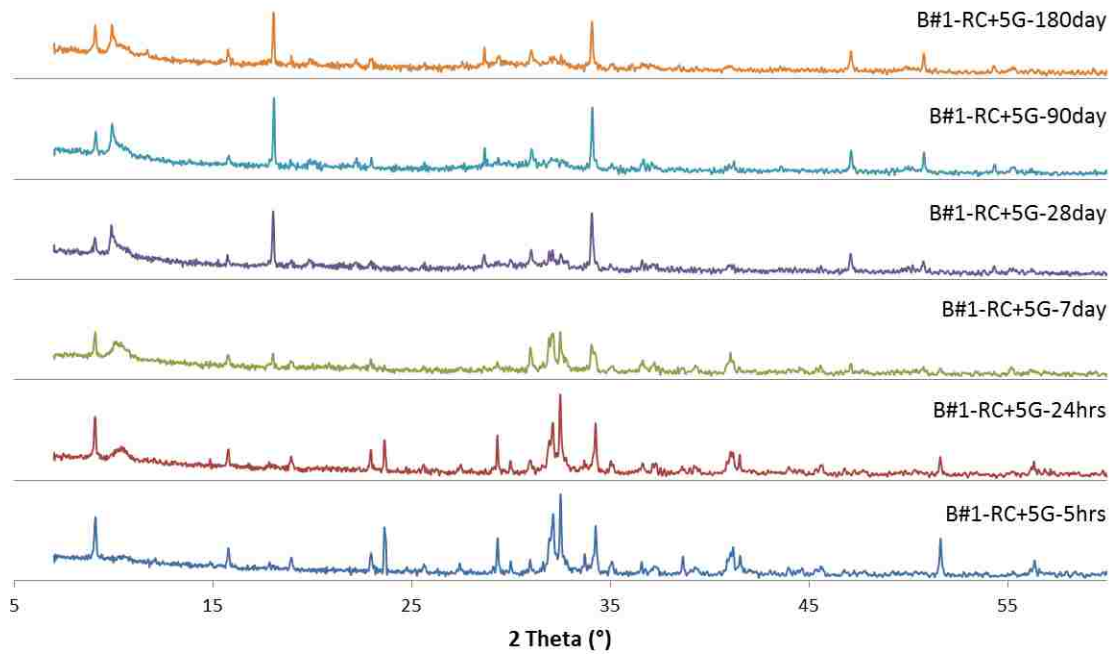
Appendix H 25: TGA analysis of the cement paste of batch #5 produced from RC with 30% gypsum by weight, after 5 hours, 1, 7, 28, 90 and 180 days into the hydration process



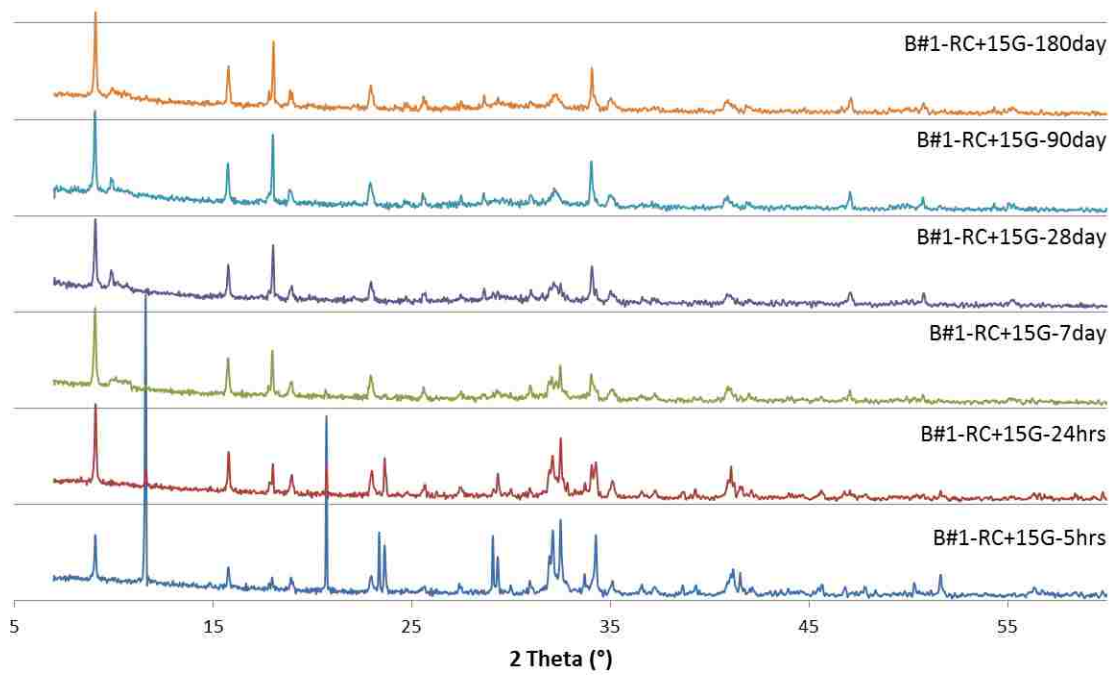
Appendix I: XRD diffractograms of hydration of cement pastes from batches #1, #3 and #5 produced from reagent chemicals (RC) with different amounts of gypsum, stopped at different times (after 5 hours, 1, 7, 28, 90 and 180 days of hydration)



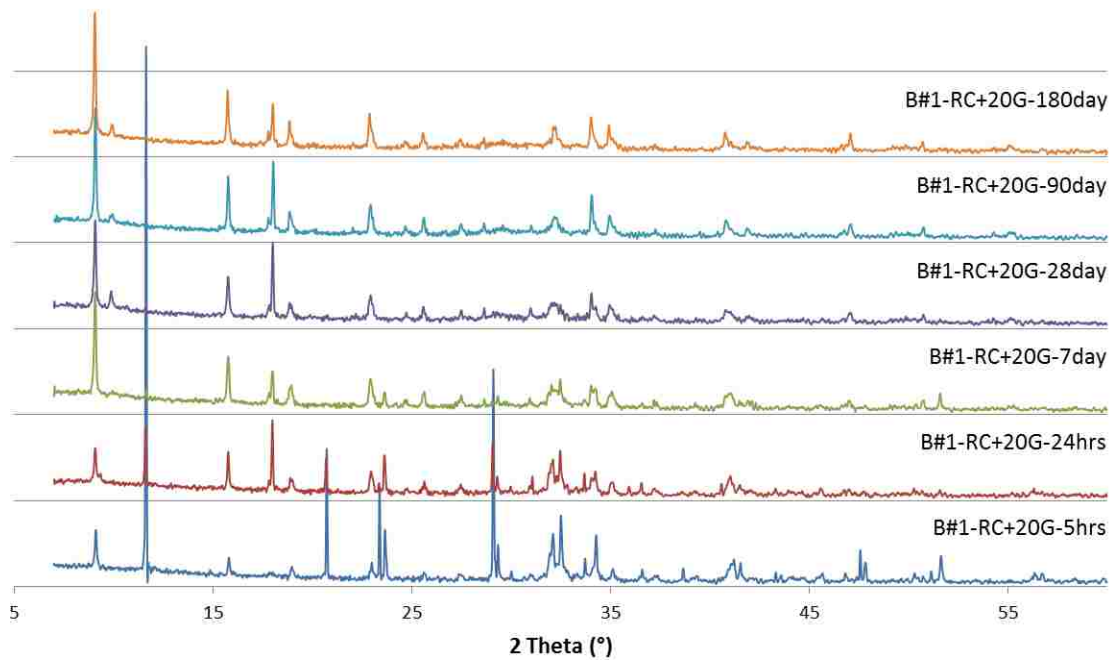
Appendix I 1: XRD diffractograms of cement paste of batch #1 produced from RC with 0% gypsum by weight, after 5 hours, 1, 7, 28, 90 and 180 days into the hydration process



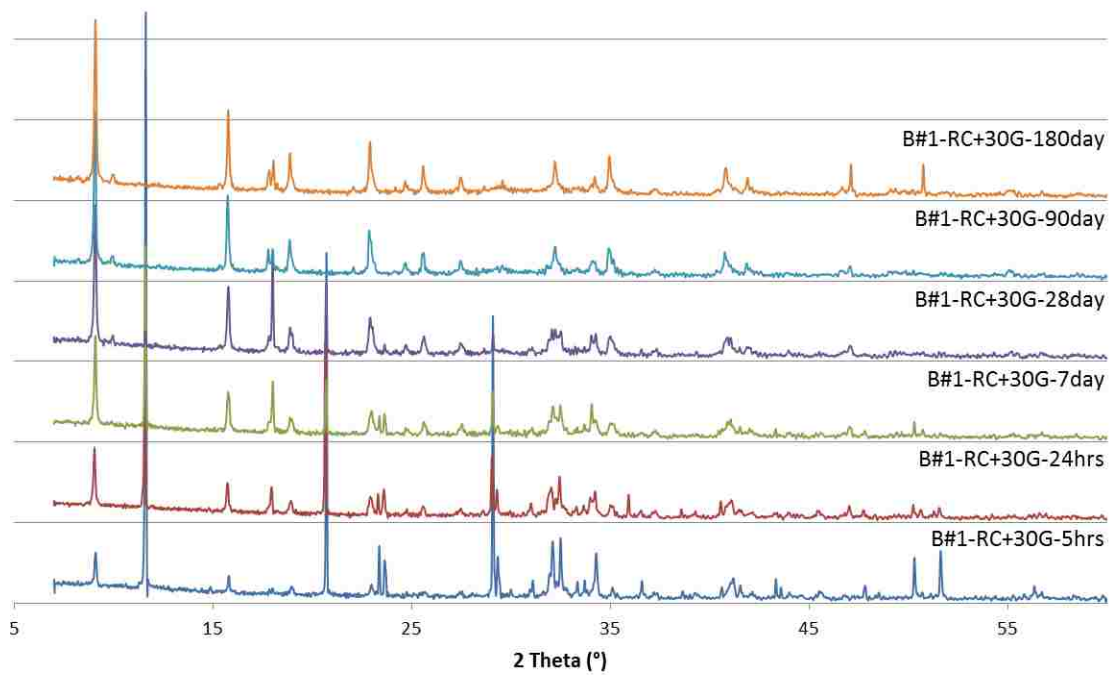
Appendix I 2: XRD data of cement paste of batch #1 produced from RC with 5% gypsum by weight, after 5 hours, 1, 7, 28, 90 and 180 days into the hydration process



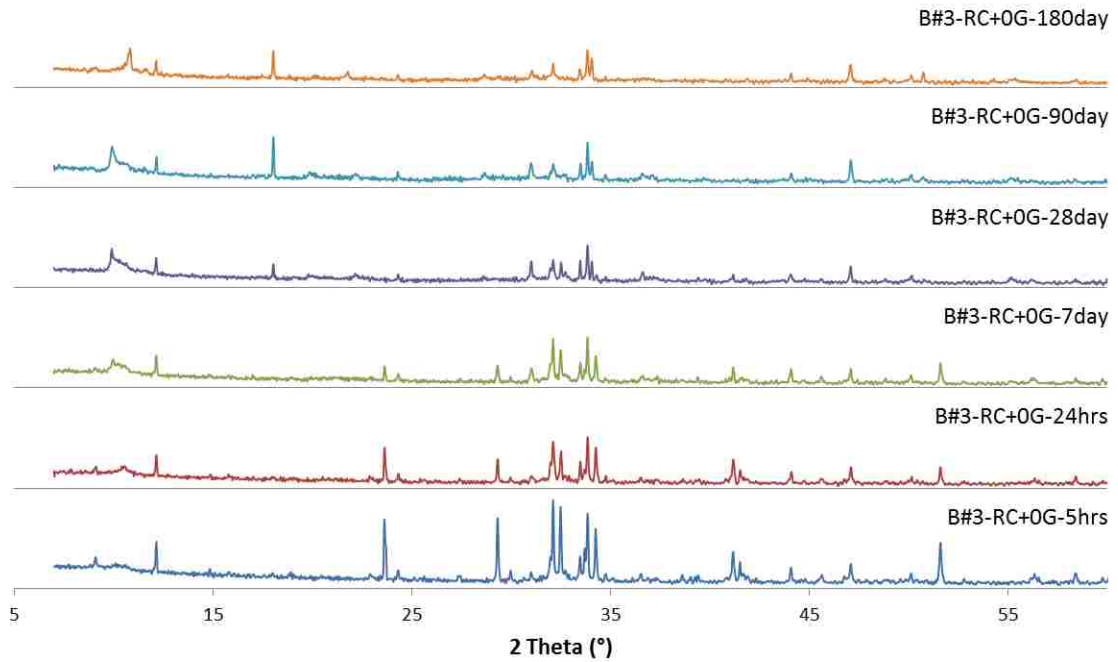
Appendix I 3: XRD data of cement paste of batch #1 produced from RC with 15% gypsum by weight, after 5 hours, 1, 7, 28, 90 and 180 days into the hydration process



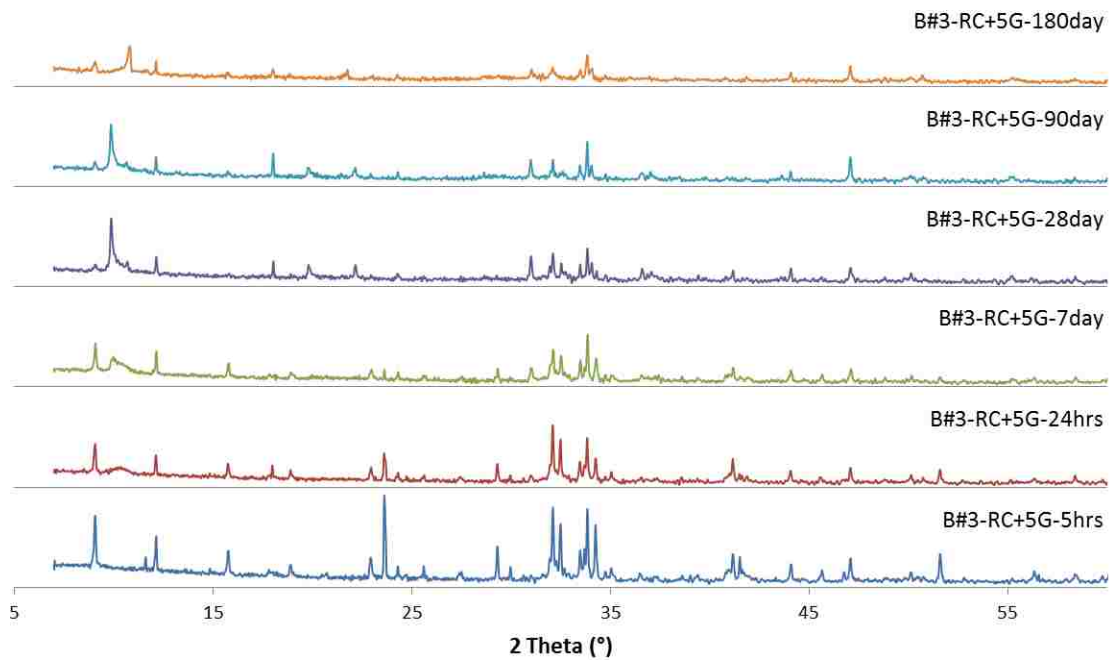
Appendix I 4: XRD data of cement paste of batch #1 produced from RC with 20% gypsum by weight, after 5 hours, 1, 7, 28, 90 and 180 days into the hydration process



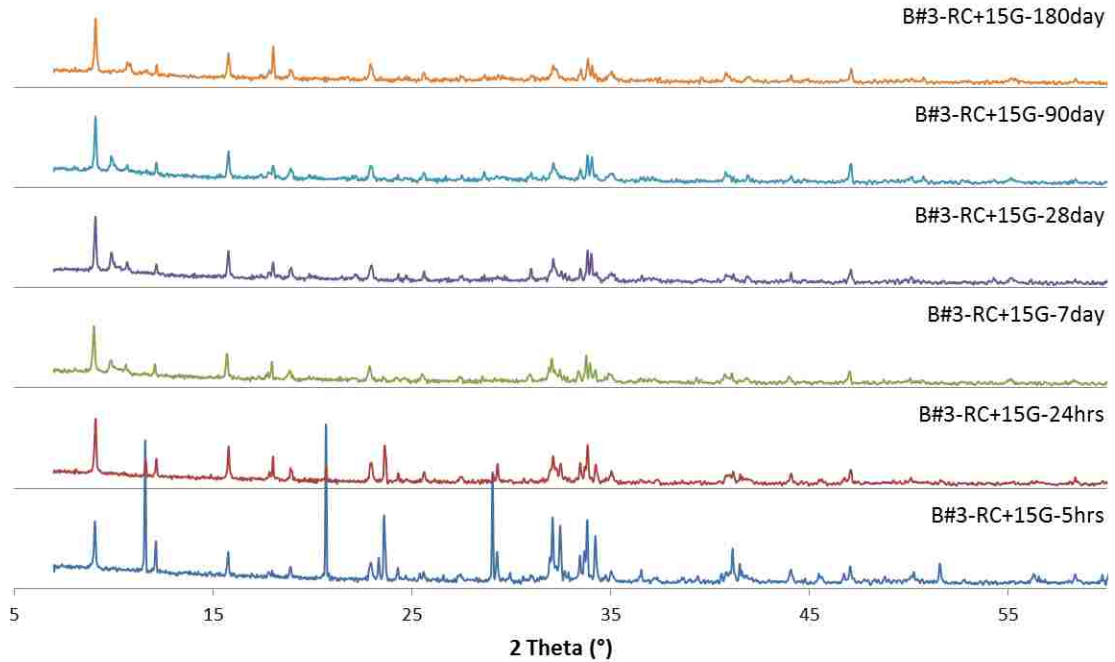
Appendix I 5: XRD data of cement paste of batch #1 produced from RC with 30% gypsum by weight, after 5 hours, 1, 7, 28, 90 and 180 days into the hydration process



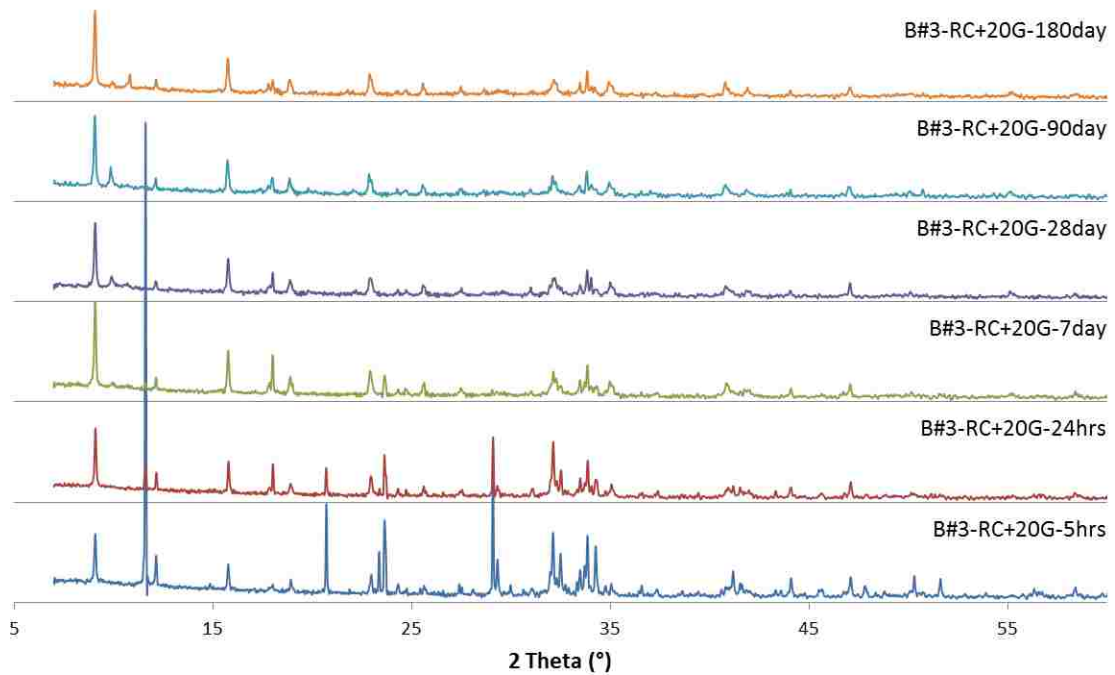
Appendix I 6: XRD data of cement paste of batch #3 produced from RC with 0% gypsum by weight, after 5 hours, 1, 7, 28, 90 and 180 days into the hydration process



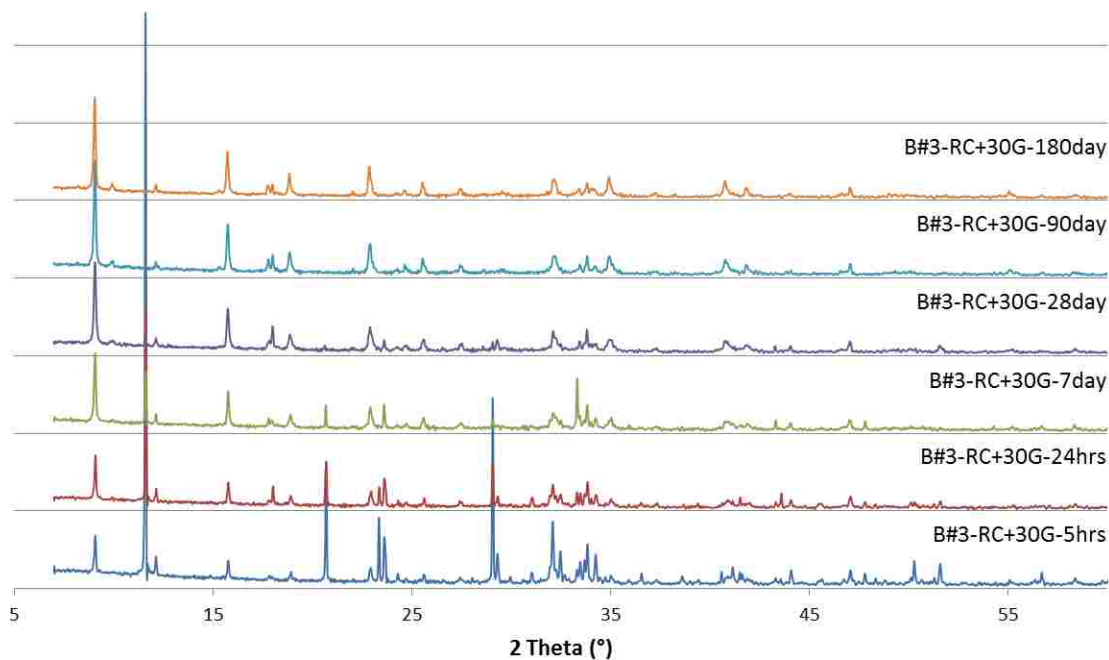
Appendix I 7: XRD data of cement paste of batch #3 produced from RC with 5% gypsum by weight, after 5 hours, 1, 7, 28, 90 and 180 days into the hydration process



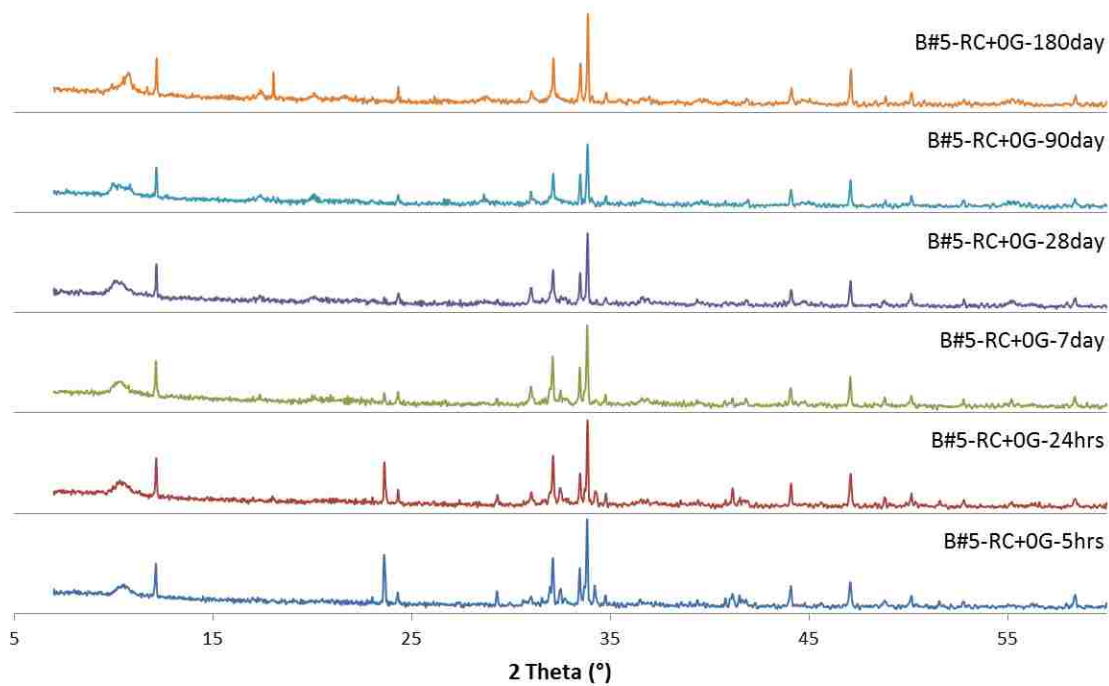
Appendix I 8: XRD data of cement paste of batch #3 produced from RC with 15% gypsum by weight, after 5 hours, 1, 7, 28, 90 and 180 days into the hydration process



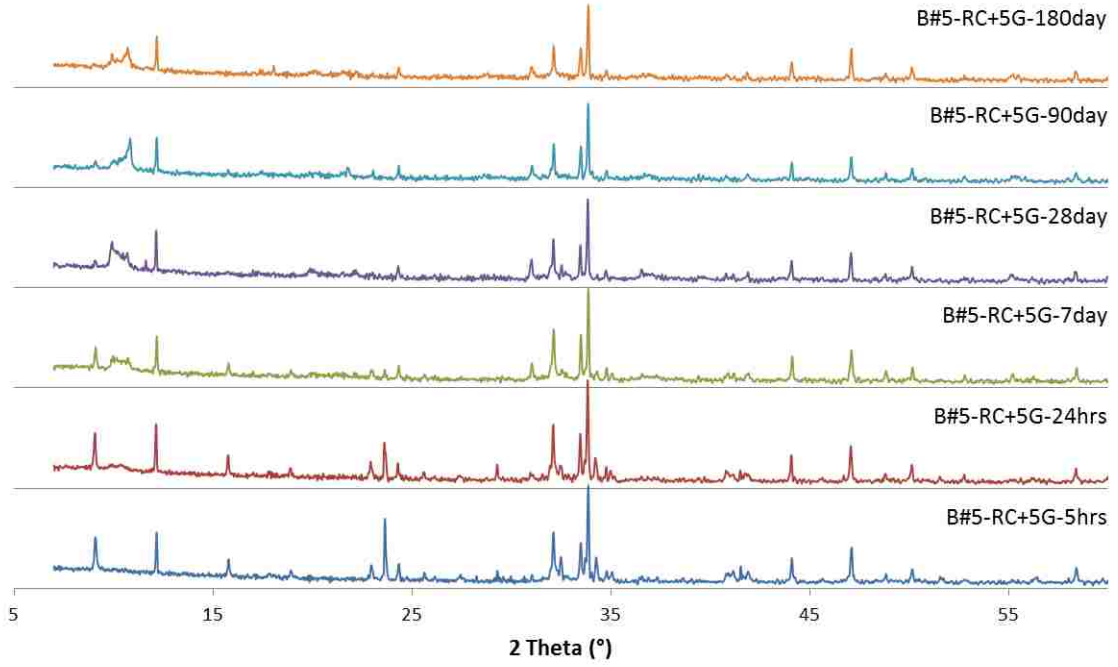
Appendix I 9: XRD data of cement paste of batch #3 produced from RC with 20% gypsum by weight, after 5 hours, 1, 7, 28, 90 and 180 days into the hydration process



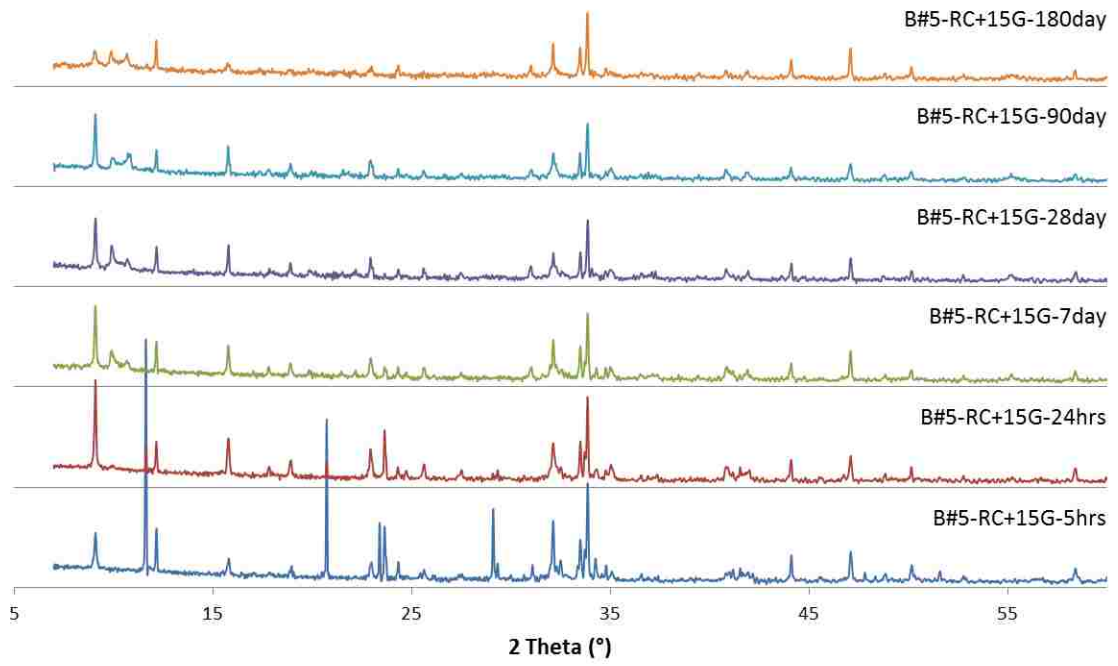
Appendix I 10: XRD data of cement paste of batch #3 produced from RC with 30% gypsum by weight, after 5 hours, 1, 7, 28, 90 and 180 days into the hydration process



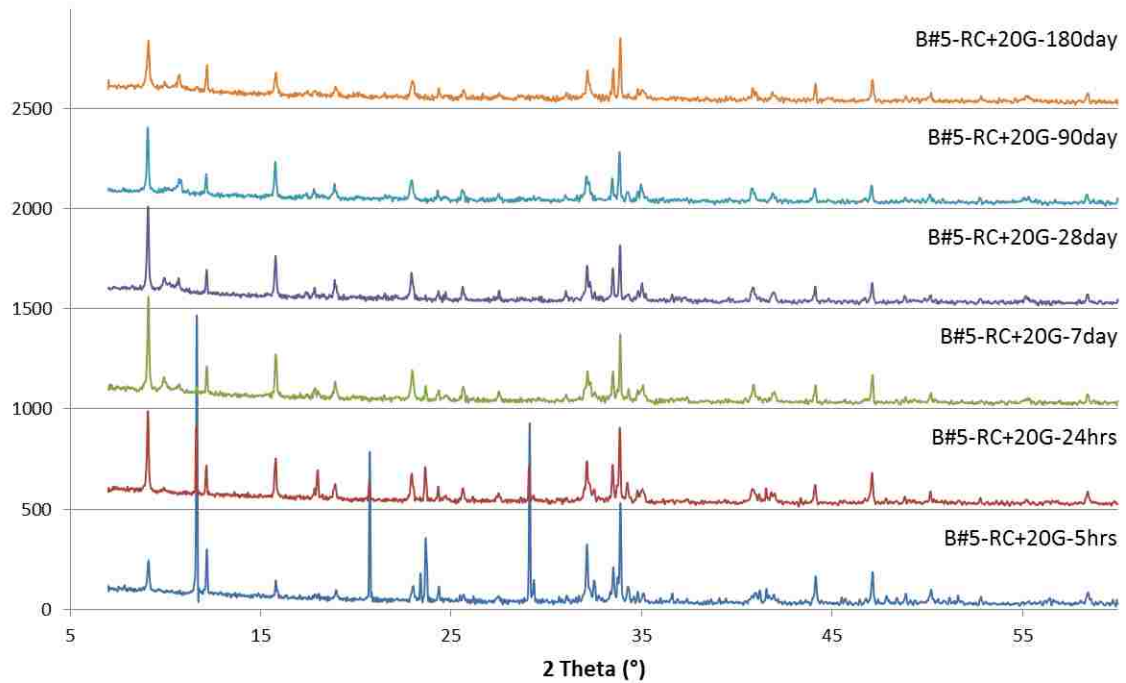
Appendix I 11: XRD data of cement paste of batch #5 produced from RC with 0% gypsum by weight, after 5 hours, 1, 7, 28, 90 and 180 days into the hydration process



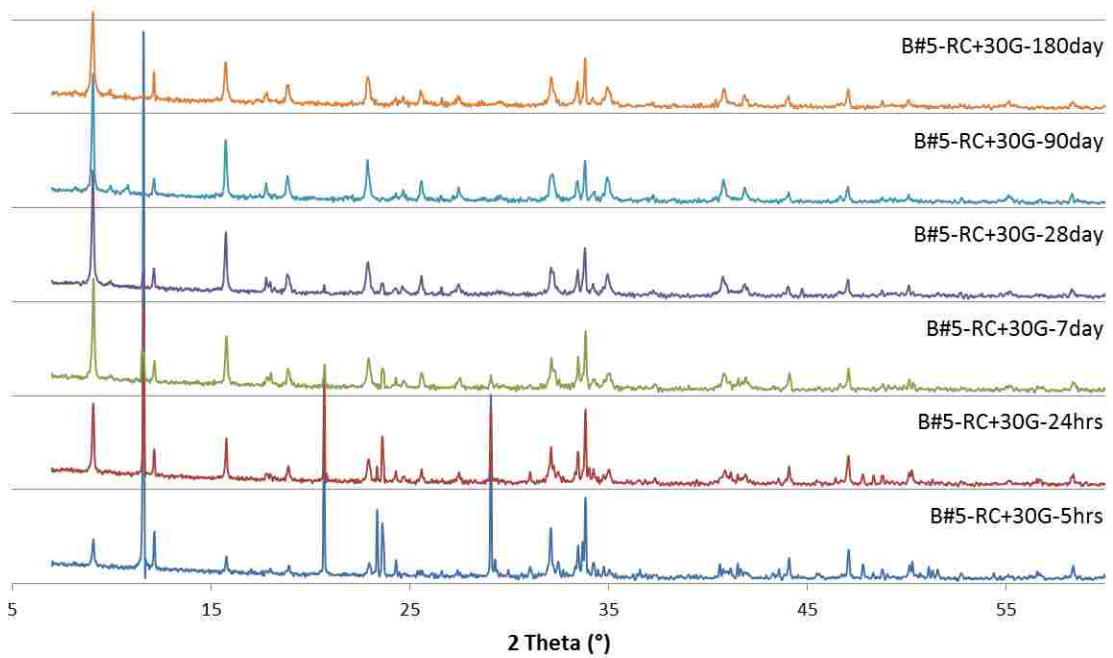
Appendix I 12: XRD data of cement paste of batch #5 produced from RC with 5% gypsum by weight, after 5 hours, 1, 7, 28, 90 and 180 days into the hydration process



Appendix I 13: XRD data of cement paste of batch #5 produced from RC with 15% gypsum by weight, after 5 hours, 1, 7, 28, 90 and 180 days into the hydration process



Appendix I 14: XRD data of cement paste of batch #5 produced from RC with 20% gypsum by weight, after 5 hours, 1, 7, 28, 90 and 180 days into the hydration process



Appendix I 15: XRD data of cement paste of batch #5 produced from RC with 30% gypsum by weight, after 5 hours, 1, 7, 28, 90 and 180 days into the hydration process

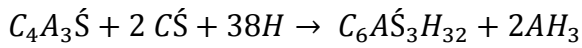


Appendix J: Derivation of the theoretical amount of gypsum required to completely react with  $C_4A_3\dot{S}$  and  $C_4AF$

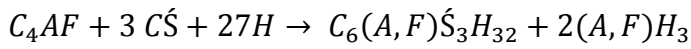
Chemical	CaO	Al <sub>2</sub> O <sub>3</sub>	Fe <sub>2</sub> O <sub>3</sub>	SO <sub>3</sub>	H <sub>2</sub> O
Molecular Mass (g.mol <sup>-1</sup> )	56	102	160	80	18

Appendix J 1: Molecular mass in g.mol<sup>-1</sup> for each oxide

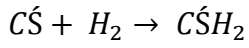
The hydration reactions for calcium sulfoaluminate and ferrite are as follows.



$$610 + 272 + 684 \text{ g.mol}^{-1}$$



$$486 + 408 + 486 \text{ g.mol}^{-1}$$



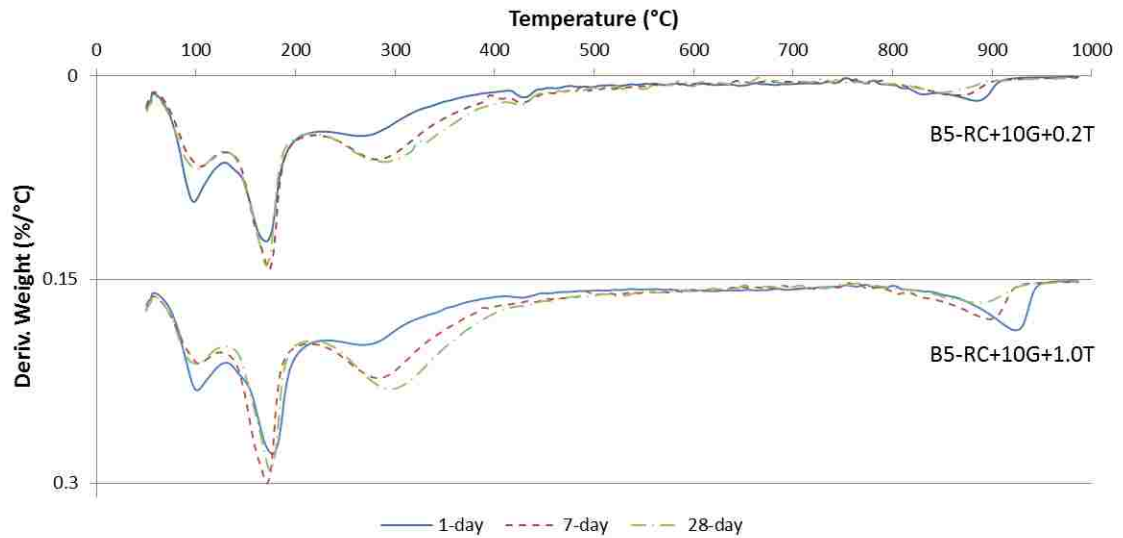
$$136 + 36 \text{ g.mol}^{-1}$$

As we want to know the theoretical amount of gypsum, anhydrite is converted to gypsum.

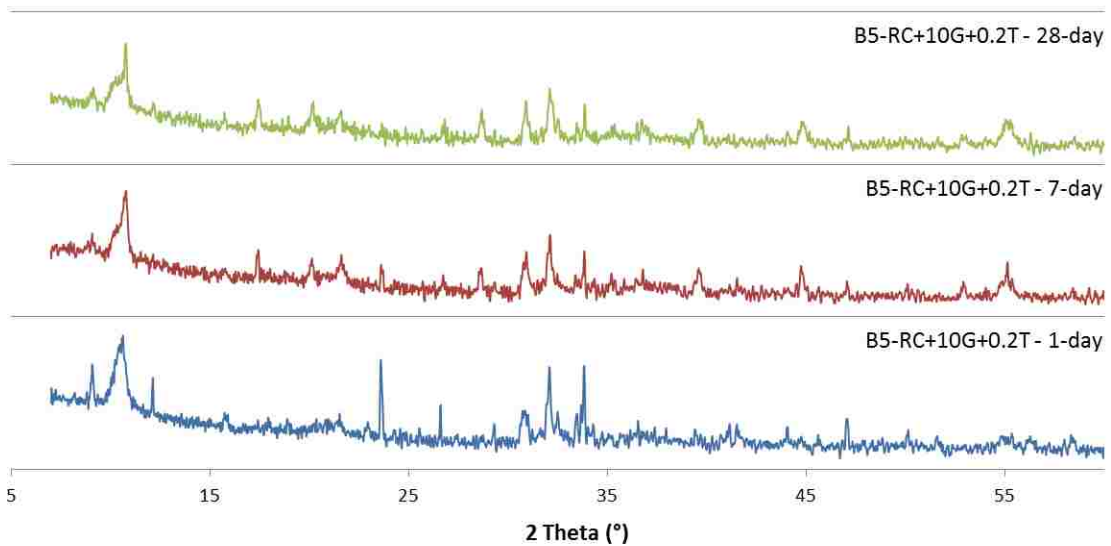
The gypsum required is then equal to:

$$Gypsum\ required = \frac{100 * 1.26 * (0.45 C_4A_3\dot{S} + 0.84 C_4AF - C\dot{S})}{100 + [1.26 * (0.45 C_4A_3\dot{S} + 0.84 C_4AF - C\dot{S})]}$$

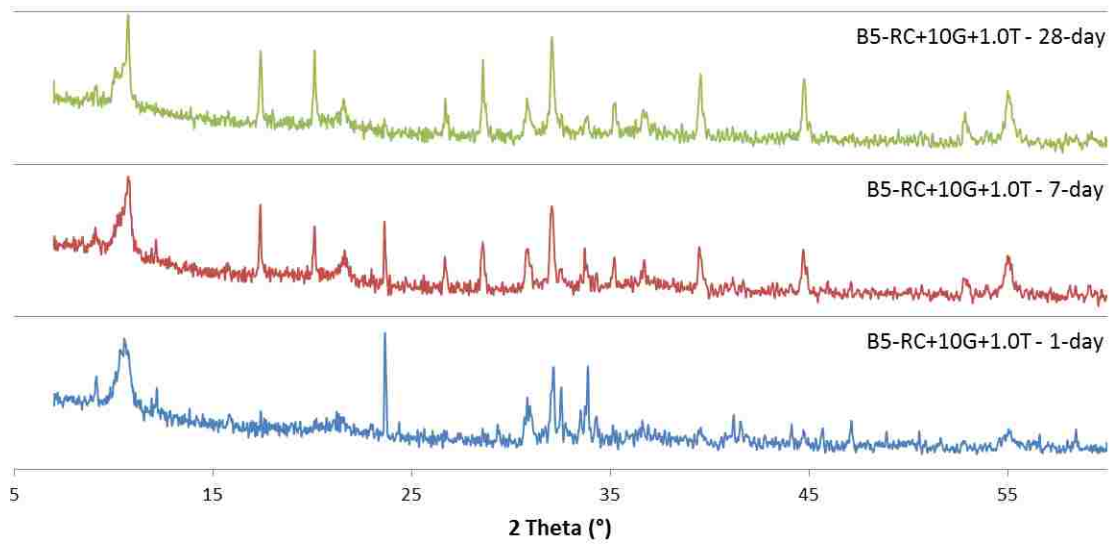
Appendix K: Influence of addition of TIPA to batch #5 produced from RC with 10%, 20% and 30% gypsum by weight



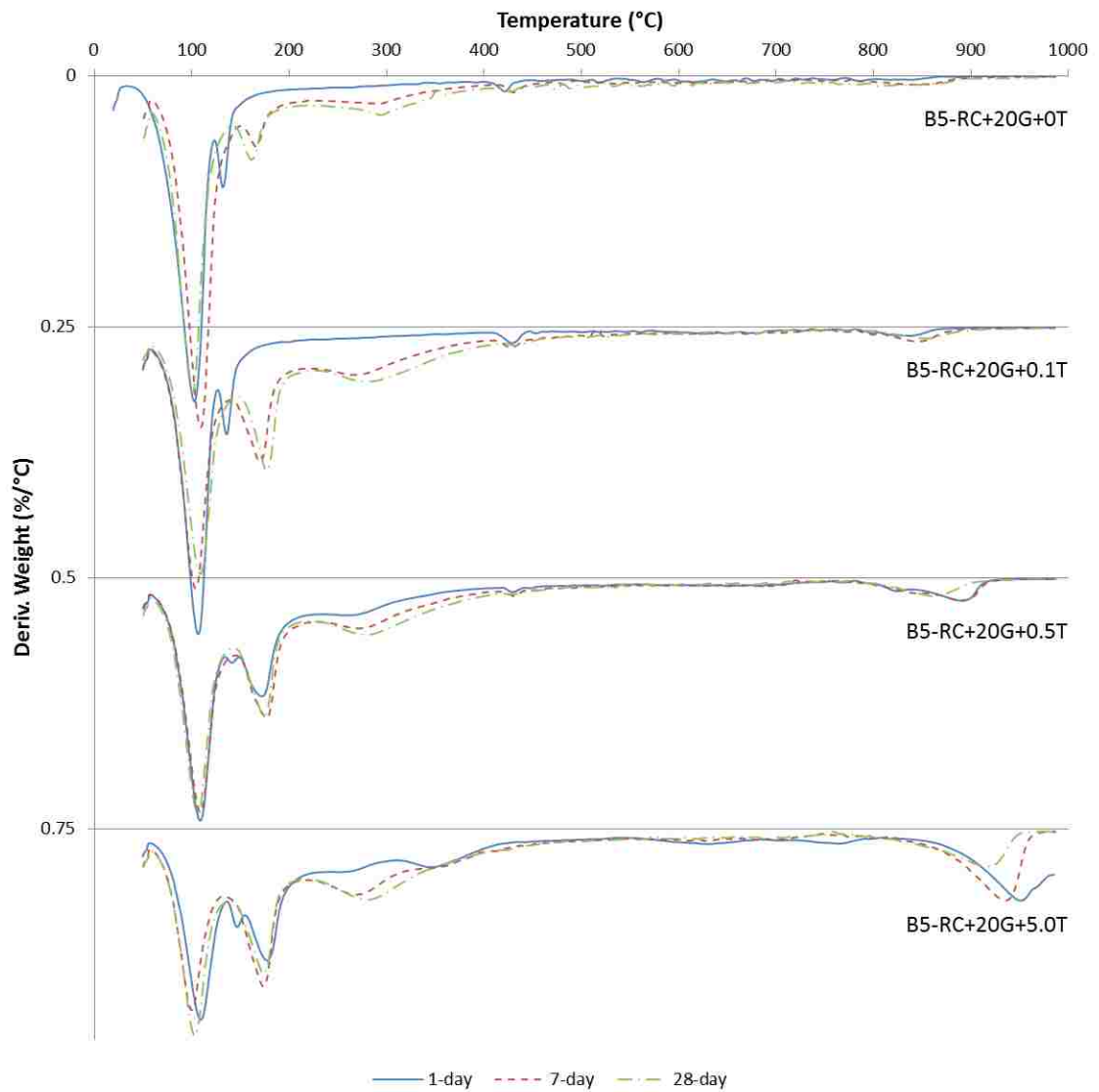
Appendix K 1: TGA analysis of the cement paste of batch #5 produced from RC with 10% gypsum by weight and 0.2% and 1.0 % TIPA, after 1, 7 and 28 days into the hydration process



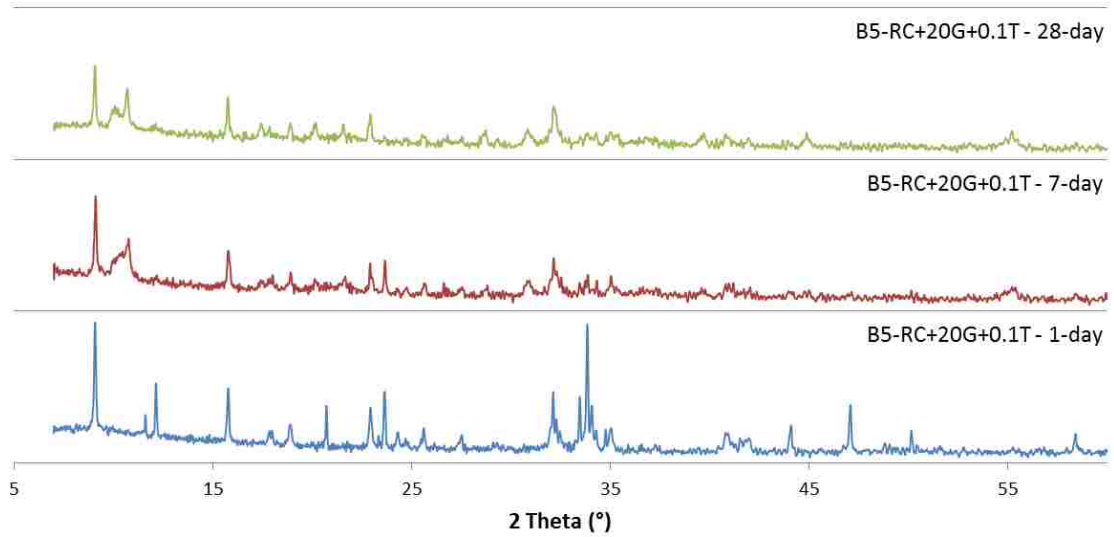
Appendix K 2: XRD diffractograms of cement paste of batch #5 produced from RC with 10% gypsum by weight and 0.2% TIPA, after 1, 7 and 28 days into the hydration process



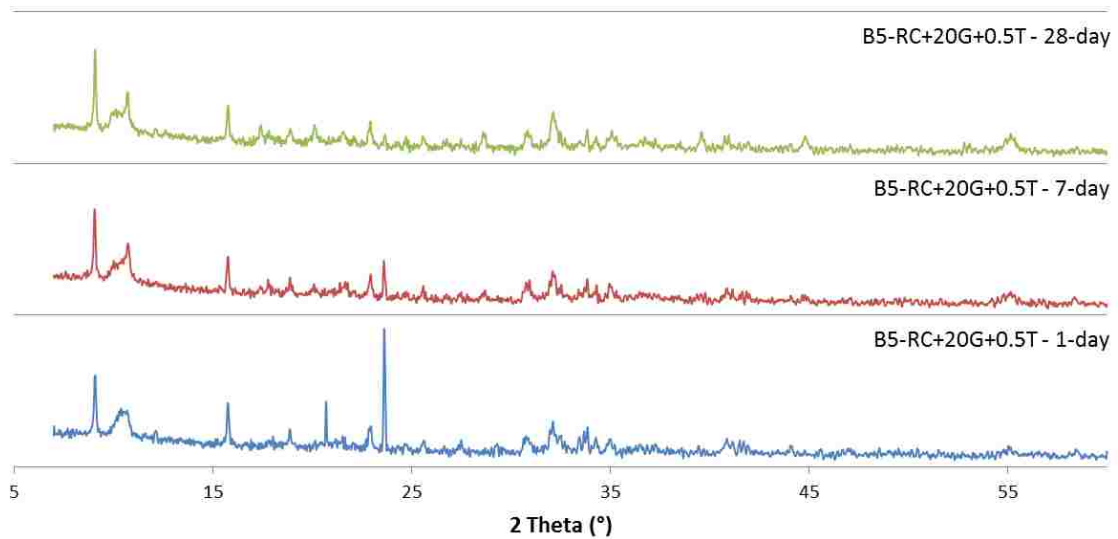
Appendix K 3: XRD diffractograms of cement paste of batch #5 produced from RC with 10% gypsum by weight and 1.0% TIPA, after 1, 7 and 28 days into the hydration process



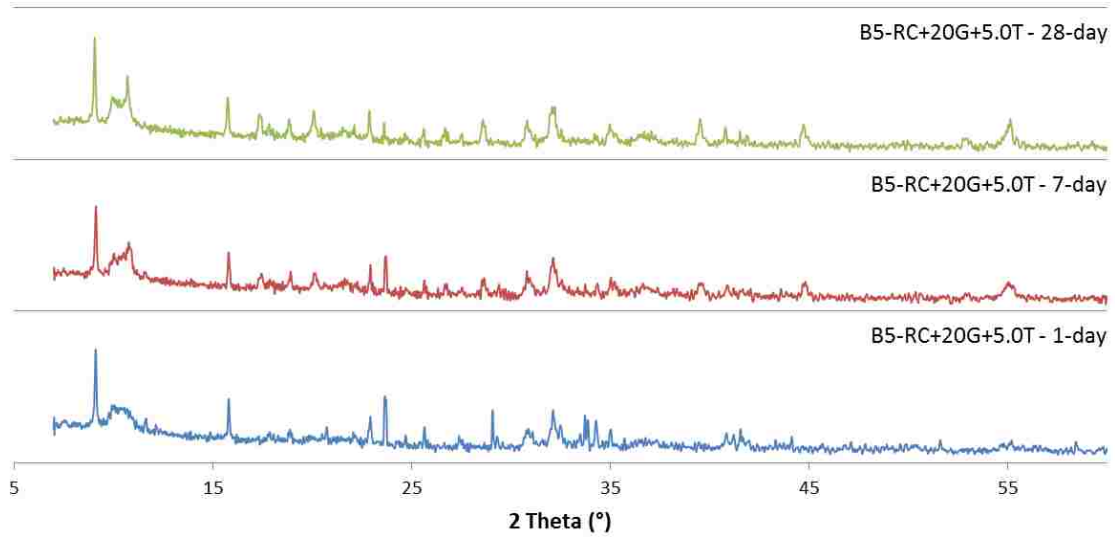
Appendix K 4: TGA analysis of the cement paste of batch #5 produced from RC with 20% gypsum by weight and 0%, 0.1%, 0.5% and 5.0 % TIPA, after 1, 7 and 28 days into the hydration process



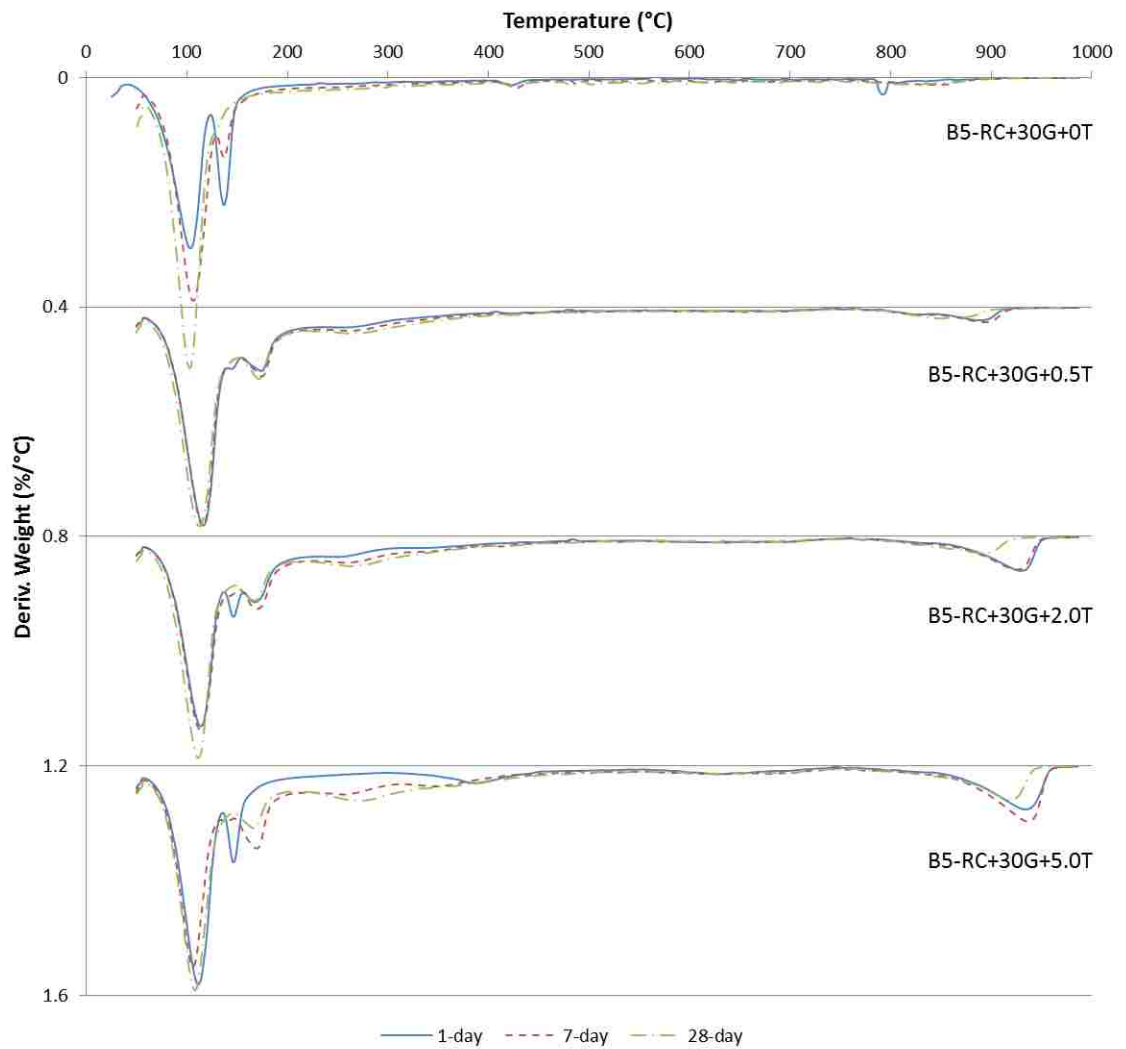
Appendix K 5: XRD diffractograms of cement paste of batch #5 produced from RC with 20% gypsum by weight and 0.1% TIPA, after 1, 7 and 28 days into the hydration process



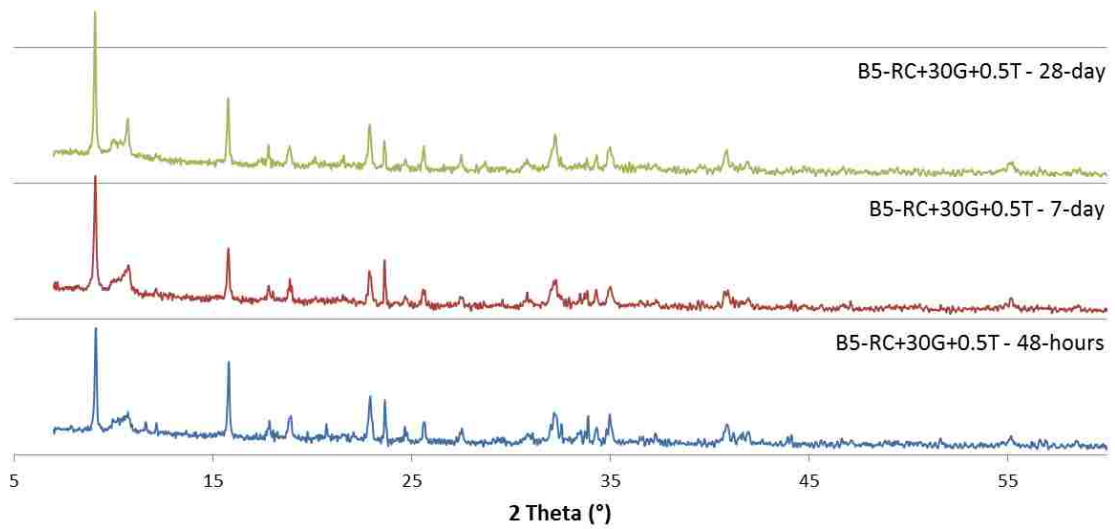
Appendix K 6: XRD diffractograms of cement paste of batch #5 produced from RC with 20% gypsum by weight and 0.5% TIPA, after 1, 7 and 28 days into the hydration process



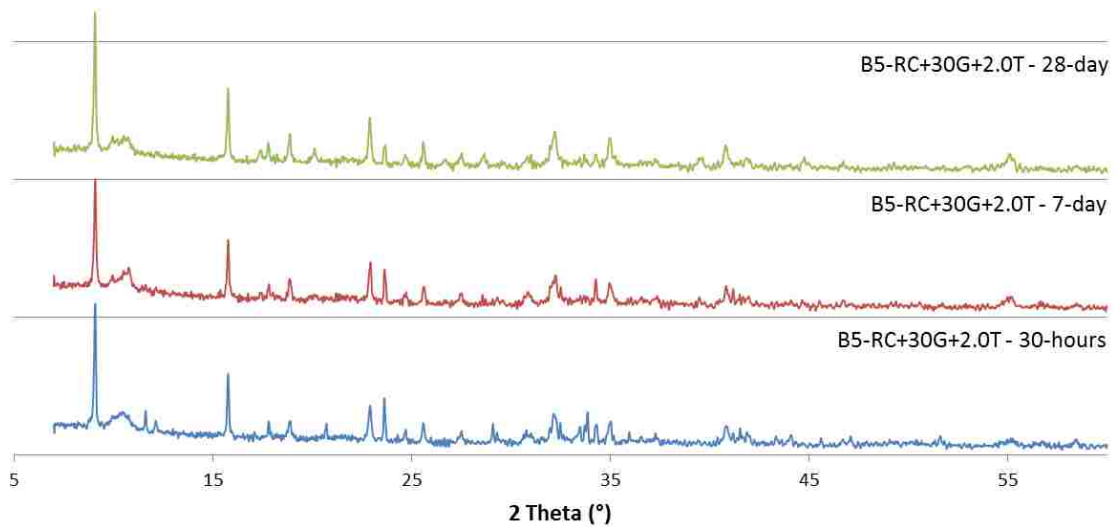
Appendix K 7: XRD diffractograms of cement paste of batch #5 produced from RC with 20% gypsum by weight and 5.0% TIPA, after 1, 7 and 28 days into the hydration process



Appendix K 8: TGA analysis of the cement paste of batch #5 produced from RC with 30% gypsum by weight and 0%, 0.5%, 2.0% and 5.0 % TIPA, after 1, 7 and 28 days into the hydration process

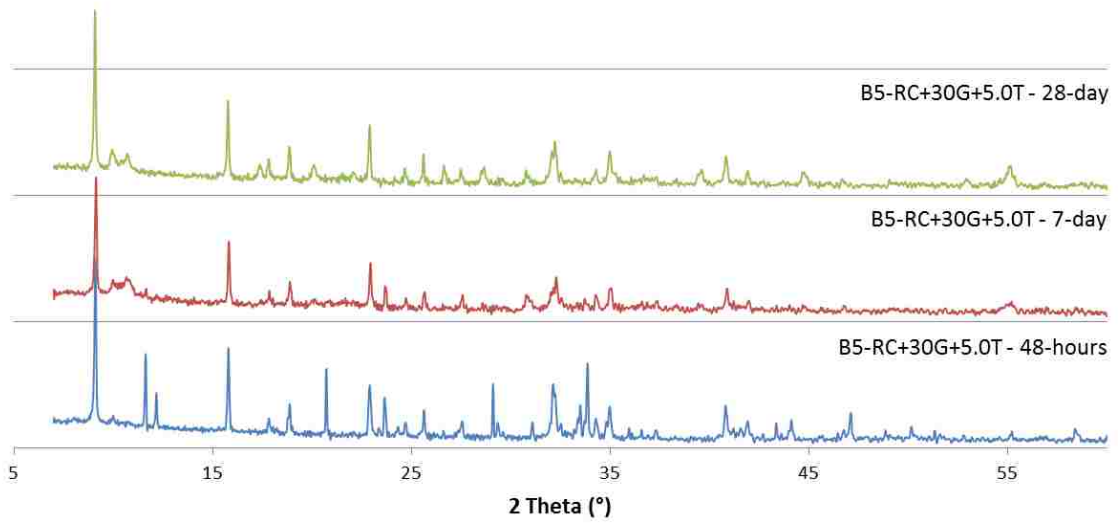


Appendix K 9: XRD diffractograms of cement paste of batch #5 produced from RC with 30% gypsum by weight and 0.5% TIPA, after 1, 7 and 28 days into the hydration process



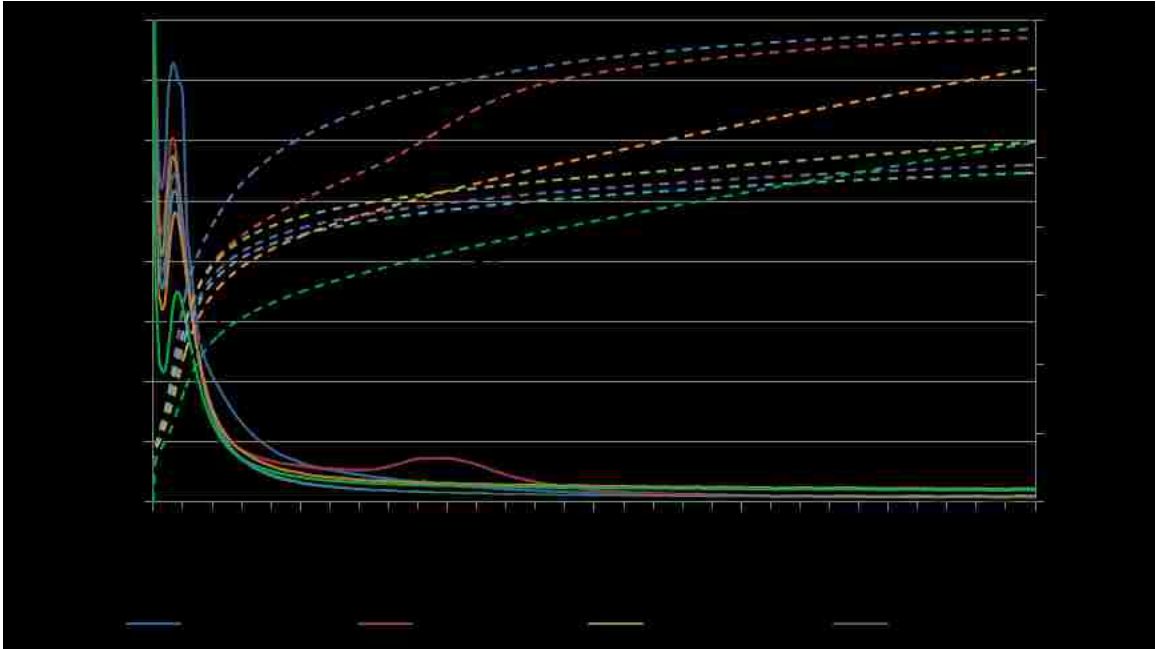
Appendix K 10: XRD diffractograms of cement paste of batch #5 produced from RC with 30% gypsum by weight and 2.0% TIPA, after 1, 7 and 28 days into the hydration process



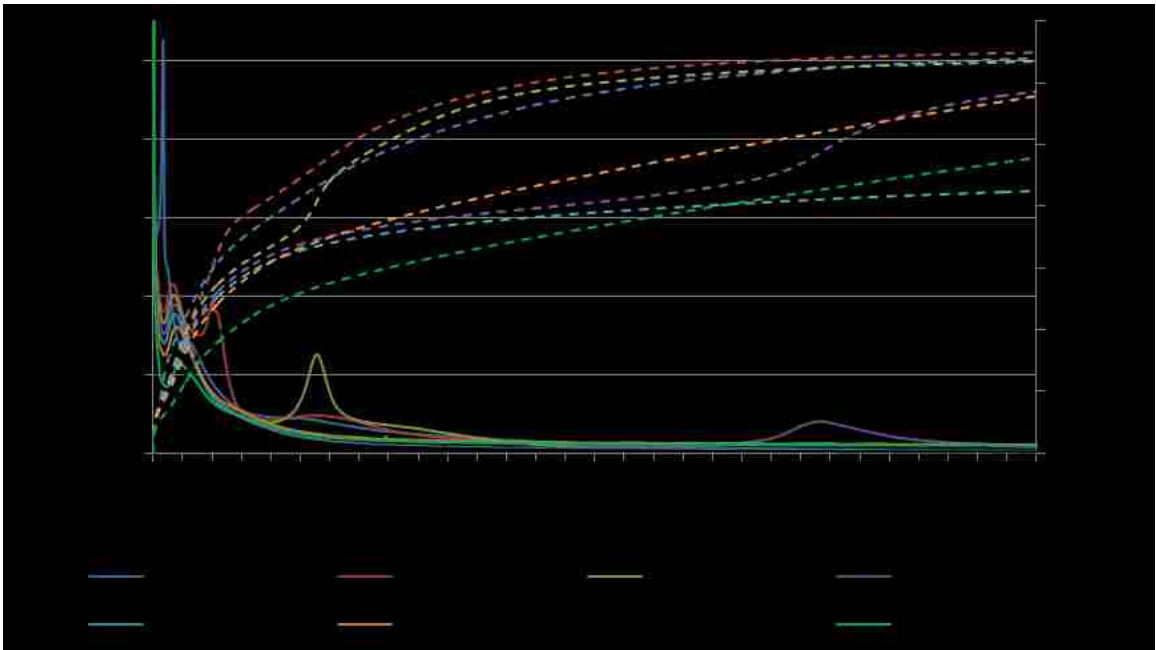


Appendix K 11: XRD diffractograms of cement paste of batch #5 produced from RC with 30% gypsum by weight and 5.0% TIPA, after 1, 7 and 28 days into the hydration process

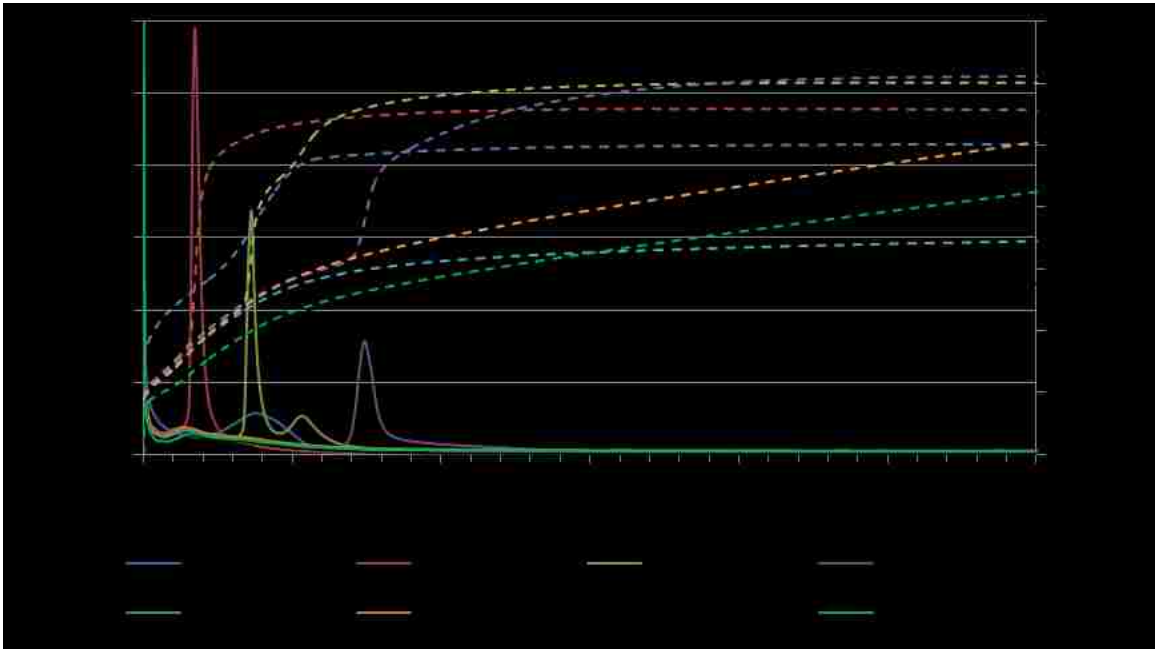
Appendix L: Influence of addition of gypsum to clinkers #1, #3 and #5 produced from Modified By-Products (MBP)



Appendix L 1: Calorimeter data of batch #1 produced from modified by-products (MBP) with different amounts of gypsum, from 0% to 15% by weight



Appendix L 2: Calorimeter data of batch #3 produced from modified by-products (MBP) with different amounts of gypsum, from 0% to 50% by weight



Appendix L 3: Calorimeter data of batch #5 produced from modified by-products (MBP) with different amounts of gypsum, from 0% to 50% by weight

## References

- [1] K.L. Scrivener, R.J. Kirkpatrick, Innovation in use and research on cementitious material, *Cement and Concrete Research*, 38 (2008) 128-136.
- [2] Y. Zhou, Study on System of CSA/I Cement Clinker, in, Center for Applied Energy Research, University of Kentucky, Lexington, KY, 2010, pp. 126.
- [3] ASTM Standard C1679, 2009, "Standard Practice for Measuring Hydration Kinetics of Hydraulic Cementitious Mixtures Using Isothermal Calorimetry", ASTM International, West Conshohocken, PA, in.
- [4] ASTM Standard C109/C109M, 2012, "Standard Test Method for Compressive Strength of Hydraulic Cement Mortars (Using 2-in. or [50-mm] Cube Specimens)", ASTM International, West Conshohocken, PA, in.
- [5] E. Gartner, Industrially interesting approaches to "low-CO<sub>2</sub>" cements, *Cement and Concrete Research*, 34 (2004) 1489-1498.
- [6] H.F.W. Taylor, *Cement chemistry*, 2nd ed., T. Telford, London, 1997.
- [7] C.A. Hendricks, E. Worrell, D. de Jager, K. Blok, P. Riemer, Emission reduction of Greenhouse Gases from the Cement Industry, in: *Proceedings of the 4th International Conference on Greenhouse Gas Control Technologies*, Interlaken, 1998.
- [8] J.B. Newman, B.S. Choo, *Advanced Concrete Technology: Constituent Materials*, in, Butterworth-Heinemann, 2003, pp. 288.
- [9] R.H. Bogue, Calculation of the compounds in Portland cement, *Industrial and Engineering Chemistry*, 1 (1929) 192-197.
- [10] A.M. Harrison, H.F.W. Taylor, N.B. Winter, Electron-optical analyses of the phases in a portland cement clinker, with some observations on the calculation of quantitative phase composition, *Cement and Concrete Research*, 15 (1985) 775-780.
- [11] P.C. Hewlett, *Lea's Chemistry of Cement and Concrete*, 1998.
- [12] J. Bensted, P. Barnes, *Structure and performance of cements*, 2nd ed. ed., 2002.
- [13] D. Damidot, S. Stronach, A. Kindness, M. Atkins, F.P. Glasser, Thermodynamic investigation of the CaO · Al<sub>2</sub>O<sub>3</sub> · CaCO<sub>3</sub> · H<sub>2</sub>O closed system at 25°C and the influence of Na<sub>2</sub>O, *Cement and Concrete Research*, 24 (1994) 563-572.

- [14] H.J. Kuzel, H. Pöllmann, Hydration of  $C_3A$  in the presence of  $Ca(OH)_2$ ,  $CaSO_4 \cdot 2H_2O$  and  $CaCO_3$ , *Cement and Concrete Research*, 21 (1991) 885-895.
- [15] R. Fischer, H.J. Kuzel, Reinvestigation of the system  $C_4A.nH_2O \cdot C_4A.CO_2.nH_2O$ , *Cement and Concrete Research*, 12 (1982) 517-526.
- [16] T. Matschei, B. Lothenbach, F.P. Glasser, The AFm phase in Portland cement, *Cement and Concrete Research*, 37 (2007) 118-130.
- [17] I. Jawed, S. Goto, R. Kondo, Hydration of tetracalcium aluminoferrite in presence of lime and sulfates, *Cement and Concrete Research*, 6 (1976) 441-453.
- [18] AASHTO M 85, "Standard Specification for Portland Cement", American Association of State Highway and Transportation Officials, in.
- [19] ASTM Standard C150/C150M, 2011, "Standard Specification for Portland Cement", ASTM International, West Conshohocken, PA, in.
- [20] P.K. Mehta, Investigations on energy-saving cements, *World Cement Technology*, 11 (1980) 166-177.
- [21] L. Zhang, M. Su, Y. Wang, Development of the use of sulfo- and ferroaluminate cements in China, *Advances in Cement Research*, 11 (1999) 15-21.
- [22] H. Zhang, F.P. Glasser, in *Modern Concrete Materials: Binders, Additions and Admixtures*, in: e. R. K. Dhir and T. D. Dyer (Ed.) *Proceedings of the International Conference held at the University of Dundee, Dundee, Scotland, September 1999*, pp. 261-274.
- [23] K. Quillin, Performance of belite-sulfoaluminate cements, *Cement and Concrete Research*, 31 (2001) 1341-1349.
- [24] L. Zhang, F.P. Glasser, New concretes based on calcium sulfoaluminate cement, *Proceedings of the International Conference on Modern Concrete Materials: Binders, Additions and Admixtures*, (1999) 261-274.
- [25] F.P. Glasser, L. Zhang, High-performance cement matrices based on calcium sulfoaluminate-belite compositions, *Cement and Concrete Research*, 31 (2001) 1881-1886.
- [26] M.M. Ali, S. Gopal, S.K. Handoo, Studies on the formation kinetics of calcium sulphoaluminate, *Cement and Concrete Research*, 24 (1994) 715-720.

- [27] J.H. Sharp, C.D. Lawrence, R. Yang, Calcium sulfoaluminate cements - Low-energy cements, special cements or what?, *Advances in Cement Research*, 11 (1999) 3-13.
- [28] M. Marroccoli, M. Nobili, A. Telesca, G.L. Valenti, Early hydration of calcium sulfoaluminate-based cements for structural applications, in: *International Conference on sustainable construction materials and technologies*, Coventry, 2007, pp. 389-395.
- [29] G. Sudoh, T. Ohta, H. Harada, High strength cement in the  $\text{CaO-Al}_2\text{O}_3\text{-SiO}_2\text{-SO}_3$  system, *7th Int Congr Chem Cem*, 3 (1980) 152-157.
- [30] F. Winnefeld, B. Lothenbach, Hydration of calcium sulfoaluminate cements — Experimental findings and thermodynamic modelling, *Cement and Concrete Research*, 40 (2010) 1239-1247.
- [31] S. Sahu, J. Havlica, V. Tomková, J. Majling, Hydration behaviour of sulphoaluminate belite cement in the presence of various calcium sulphates, *Thermochimica Acta*, 175 (1991) 45-52.
- [32] K. Quillin, *Calcium Sulfoaluminate Cements - CO<sub>2</sub> reduction, concrete properties and applications*, IHS - BRE Press; Spi Edition, 2010.
- [33] J. Péra, J. Ambroise, New applications of calcium sulfoaluminate cement, *Cement and Concrete Research*, 34 (2004) 671-676.
- [34] C. Cau Dit Coumes, S. Courtois, S. Peysson, J. Ambroise, J. Pera, Calcium sulfoaluminate cement blended with OPC: A potential binder to encapsulate low-level radioactive slurries of complex chemistry, *Cement and Concrete Research*, 39 (2009) 740-747.
- [35] Q. Zhou, N.B. Milestone, M. Hayes, An alternative to Portland Cement for waste encapsulation—The calcium sulfoaluminate cement system, *Journal of Hazardous Materials*, 136 (2006) 120-129.
- [36] S. Peysson, J. Péra, M. Chabannet, Immobilization of heavy metals by calcium sulfoaluminate cement, *Cement and Concrete Research*, 35 (2005) 2261-2270.
- [37] X. Tang, L. Lu, Review on the hydration and hardening of alite-sulphoaluminate cement, *Jinan University Science and Technology*, 20 (2006) 202-205.
- [38] H. Guo, J. Xie, Thermodynamics and kinetics of calcium sulphoaluminate, *Journal of Wuhan University of Technology--Materials Science Edition*, 26 (2011) 719-722.

- [39] M.T. Blanco-Varela, A. Palomo, F. Gates, T. Vazquez, Influence of the joint incorporation of  $\text{CaF}_2$  and  $\text{CaSO}_4$  in the clinkerization process. Obtainment of new cements, *Construction Materials*, 45 (1995) 21-39.
- [40] D. Herfort, G.K. Moir, V. Johansen, F. Sorrentino, H. Bolio Arceo, The chemistry of Portland cement clinker, *Advances in Cement Research*, 22 (2010) 187-194.
- [41] I. Odler, Portland cement clinker and portland cement, in, 1994.
- [42] O. Dominguez, A. Torres-Castillo, L.M. Flores-Velez, R. Torres, Characterization using thermomechanical and differential thermal analysis of the sinterization of Portland clinker doped with  $\text{CaF}_2$ , *Materials Characterization*, 61 (2010) 459-466.
- [43] M.T. Blanco-Varela, A. Palomo, T. Vázquez, Effect of fluorspar on the formation of clinker phases, *Cement and Concrete Research*, 14 (1984) 397-406.
- [44] K. Raina, L.K. Janakiraman, Use of mineralizer in black meal process for improved clinkerization and conservation of energy, *Cement and Concrete Research*, 28 (1998) 1093-1099.
- [45] M.T. Blanco-Varela, T. Vázquez, A. Palomo, A study of a new liquid phase to obtain low-energy cements, *Cement and Concrete Research*, 16 (1986) 97-104.
- [46] V. Johansen, N.H. Christensen, Rate of formation of  $\text{C}_3\text{S}$  in the system  $\text{CaO-SiO}_2\text{-Al}_2\text{O}_3\text{-Fe}_2\text{O}_3\text{-MgO}$  with addition of  $\text{CaF}_2$ , *Cement and Concrete Research*, 9 (1979) 1-5.
- [47] S. Giménez-Molina, M.T. Blanco-Varela, Solid state phases relationship in the  $\text{CaO-SiO}_2\text{-Al}_2\text{O}_3\text{-CaF}_2\text{-CaSO}_4$  system, *Cement and Concrete Research*, 25 (1995) 870-882.
- [48] K. Kolovos, P. Loutsi, S. Tsvivilis, G. Kakali, The effect of foreign ions on the reactivity of the  $\text{CaO-SiO}_2\text{-Al}_2\text{O}_3\text{-Fe}_2\text{O}_3$  system: Part I. Anions, *Cement and Concrete Research*, 31 (2001) 425-429.
- [49] I. Odler, H. Zhang, Investigations on high  $\text{SO}_3$  Portland clinkers and cements I. Clinker synthesis and cement preparation, *Cement and Concrete Research*, 26 (1996) 1307-1313.
- [50] H. Zhang, I. Odler, Investigations on high  $\text{SO}_3$  Portland clinkers and cements II. Properties of cements, *Cement and Concrete Research*, 26 (1996) 1315-1324.

- [51] Y. Hou, W. Cao, B. Wang, R. Zhao, Y. Fu, High-activity alite-sulphoaluminate cement and its hydration reaction, Beijing Keji Daxue Xuebao/Journal of University of Science and Technology Beijing, 26 (2004) 631-636.
- [52] X. Liu, Y. Li, Effect of MgO on the composition and properties of alite-sulphoaluminate cement, Cement and Concrete Research, 35 (2005) 1685-1687.
- [53] J. Li, H. Ma, H. Zhao, Preparation of sulphoaluminate-alite composite mineralogical phase cement clinker from high alumina fly ash, in, 2007, pp. 421-424.
- [54] X.C. Liu, B.L. Li, T. Qi, X.L. Liu, Y.J. Li, Effect of TiO<sub>2</sub> on mineral formation and properties of alite-sulphoaluminate cement, Materials Research Innovations, 13 (2009) 92-97.
- [55] X. Song, S. Yang, B. Tian, Trial production of alite-sulphoaluminate cement, Cement, 2 (2003) 24-25.
- [56] P.K. Mehta, High iron oxide hydraulic cement, in, 1977.
- [57] W. Kurdowski, F. Sorrentino, Waste Materials Used in Concrete Manufacturing, William Andrew Publishing/Noyes, 1997.
- [58] ASTM Standard C114, 2006, "Standard Test Methods for Chemical Analysis of Hydraulic Cement", ASTM International, West Conshohocken, PA in.
- [59] H. Rietveld, A profile refinement method for nuclear and magnetic structures, Journal of Applied Crystallography, 2 (1969) 65-71.
- [60] G. Malmros, J.O. Thomas, Least-squares structure refinement based on profile analysis of powder film intensity data measured on an automatic microdensitometer, Journal of Applied Crystallography, 10 (1977) 7-11.
- [61] R.A. Young, P.E. Mackie, R.B. von Dreele, Application of the pattern-fitting structure-refinement method of X-ray powder diffractometer patterns, Journal of Applied Crystallography, 10 (1977) 262-269.
- [62] G. Walenta, T. Fullmann, Advances in Quantitative XRD Analysis for Clinker Cements, and Cementitious Additions, International Centre for Diffraction Data 2004, Advances in X-ray Analysis, 47 (2004) 287-296.
- [63] I.C.f.D.D. (ICDD), Powder Diffraction Files (PDF), in, System X'Pert System Philips, 2004.



- [64] ASTM Standard D 4326, 1997, "Standard Test Method for Major and Minor Elements in Coal and Coke Ash By X-Ray Fluorescence", ASTM International, West Conshohocken, PA, in.
- [65] P.E. Stutzman, Scanning electron microscopy imaging of hydraulic cement microstructure, *Cement and Concrete Composites*, 26 (2004) 957-966.
- [66] P.E. Stutzman, J.R. Clifton, Specimen Preparation for Scanning Electron Microscopy, in: *Twenty-First International Conference on Cement Microscopy*, Las Vegas, Nevada, 1999, pp. 10-22.
- [67] D.H. Campbell, *Microscopical Examination and Interpretation of Portland Cement and Clinker*, Portland Cement Association, 1986.
- [68] R.T. Chancey, Characterization of crystalline and amorphous phases and respective reactivities in a class F fly ash, in: *Civil Engineering*, The University of Texas at Austin, Austin, 2008.
- [69] I.A. Chen, Synthesis of portland cement and calcium sulfoaluminate-belite cement for sustainable development and performance, in: *Materials Science and Engineering*, The University of Texas at Austin, Austin, 2009.
- [70] R.T. Chancey, P. Stutzman, M.C.G. Juenger, D.W. Fowler, Comprehensive phase characterization of crystalline and amorphous phases of a Class F fly ash, *Cement and Concrete Research*, 40 (2010) 146-156.
- [71] W.S. Rasband, ImageJ, in, National Institutes of Health, Bethesda, Maryland, USA, 1997-2014.
- [72] D. Landgrebe, L. Biehl, MultiSpec, in, Purdue University, West Lafayette, IN, 2003.
- [73] J.W. Lydon, The measurement of the modal mineralogy of rocks from SEM imagery: the use of MultiSpec © and ImageJ freeware, in, Geological Survey of Canada, Open File 4941, 2005, pp. 37.
- [74] P. Stutzman, Scanning electron microscopy imaging of hydraulic cement microstructure, *Cement and Concrete Composites*, 26 (2004) 957-966.
- [75] S. Schorn, E. Hock, C. Linde, P. Blümner, D. Lunau, Thomas, V. Annacker, A. Brand, N. Kirchhoff, G. Diether, S. Koch, J. Wachsmuth, G. Frenz, O. Schmitsberger, M. Gäbelein, *Fluorellestadite Mineral Description*, in.

- [76] D. Barthelmy, Periclase Mineralogical Description, in.
- [77] W. Lerch, The influence of gypsum on the hydration and properties of Portland cement pastes, in: Proceedings of the American Society for Testing Materials, 1946.
- [78] N.C. Collier, J.H. Sharp, N.B. Milestone, J. Hill, I.H. Godfrey, The influence of water removal techniques on the composition and microstructure of hardened cement pastes, *Cement and Concrete Research*, 38 (2008) 737-744.
- [79] J. Zhang, G.W. Scherer, Comparison of methods for arresting hydration of cement, *Cement and Concrete Research*, 41 (2011) 1024-1036.
- [80] E. Knapen, O. Cizer, K. Van Balen, D. Van Gemert, Comparison of solvent exchange and vacuum drying techniques to remove free water from early age cement-based materials, in: Proceedings of the 2nd International RILEM Symposium on Advances in Concrete through Science and Engineering, Quebec, Canada, 2006.
- [81] H. Hornain, M. Regourd, Cracking and Grindability of Clinker, *Fissuration et bryabilite du clinker*, (1980) 354-361.
- [82] B.R. Lawn, D.B. Marshall, Hardness, Toughness, and Brittleness: An Indentation Analysis, *Journal of the American Ceramic Society*, 62 (1979) 347-350.
- [83] K. Velez, S. Maximilien, D. Damidot, G. Fantozzi, F. Sorrentino, Determination by nanoindentation of elastic modulus and hardness of pure constituents of Portland cement clinker, *Cement and Concrete Research*, 31 (2001) 555-561.
- [84] X. Liu, Y. Li, N. Zhang, Influence of MgO on the formation of  $\text{Ca}_3\text{SiO}_5$  and  $3\text{CaO}\cdot 3\text{Al}_2\text{O}_3\cdot \text{CaSO}_4$  minerals in alite-sulphoaluminate cement, *Cement and Concrete Research*, 32 (2002) 1125-1129.
- [85] J.I. Bhatti, Effect of Minor Elements on Clinker and Cement Performance: A Laboratory Analysis, in, Portland Cement Association, Skokie, Illinois, U.S.A., 2006, pp. 99.
- [86] T. Duvallet, T.L. Robl, F.P. Glasser, The Effect of Titanium Dioxide on the Structure and Reactivity of Ferrite, in: 8th International Conference: Concrete in the Low Carbon Era, Dundee, UK, 2012.
- [87] V.S. Ramachandran, R.M. Paroli, J.J. Beaudoin, A.H. Delgado, Handbook of Thermal Analysis of Construction Materials, 1st ed., William Andrew, 2002.

- [88] O. Chowaniec, Limestone Addition in Cement, in: Science et Genie des Materiaux, Ecole Polytechnique Federale de Lausanne (EPFL), 2012, pp. 242.
- [89] Z.D. Belay, Poster: Application of thermogravimetric method in cement science, in, EMPA.
- [90] A. Organics, MSDS of triisopropanolamine, 98% from Acros Organics, in, 2013.
- [91] D.F. Myers, E.M. Gartner, Strength enhancing additive for certain portland cements, in: U.S. Patent (Ed.), W. R. Grace & Co.-Conn, New York, N.Y., United States, 1991.
- [92] E. Gartner, D. Myers, Influence of Tertiary Alkanolamines on Portland Cement Hydration, Journal of the American Ceramic Society, 76 (1993) 1521-1530.
- [93] E. Gartner, R. Hu, J.H. Cheung, Influence of tertiary alkanolamines on rates of reaction of C<sub>3</sub>A and C<sub>4</sub>AF with calcite under conditions typical of Portland cement hydration in concrete, World Cement Research and Development, (1998) 17.
- [94] E. Gartner, Catalysis of cement hydration by chemical admixtures, in: The COE Workshop on Material Science in 21st Century for the Construction Industry - Durability, Repair and Recycling of Concrete Structures, Hokkaido University Conference Hall, Sapporo, Japan, 2005.
- [95] M. Ichikawa, M. Kanaya, S. Sano, Effect of triisopropanolamine on hydration and strength development of cements with different character, in: Proceedings of the 10th International Congress on the Chemistry of Cement, Gothenburg, Sweden, 1997, pp. 8.
- [96] J.-P. Perez, A. Nonat, S. Garrault, P. Sylvie, M. Martin, Influence of Triisopropanolamine on the Physico-Chemical and Mechanical Properties of Pure Cement Pastes and Mortars, Ann Chim Sci Mat, 28 (2003) S35-S42.
- [97] N. Chikh, M. Cheikh-Zouaoui, S. Aggoun, R. Duval, Effects of calcium nitrate and triisopropanolamine on the setting and strength evolution of Portland cement pastes, Materials and Structures, 41 (2008) 31-36.
- [98] P.J. Sandberg, F. Doncaster, On the mechanism of strength enhancement of cement paste and mortar with triisopropanolamine, Cement and Concrete Research, 34 (2004) 973-976.
- [99] E.M. Gartner, D.F. Myers, J.M. Gaidis, Processing additives for blended cements, in: U.S. Patent (Ed.), W.R. Grace & Co.-Conn, New York, N.Y., United States, 1990, pp. 11.

## Vita

Tristana Yvonne Françoise Duvallet

Born in Châteaudun, France

## EDUCATION

- 2008-2014    **PhD Candidate**, Materials Science and Engineering, University of Kentucky, Lexington, KY
- 2005-2008    **Engineer's Diploma**, Materials Science, ESIREM, Dijon, France
- 2003-2005    **Preparatory School (CPGE)**, Chemistry and Physics, Lycée Pothier, Orléans, France

## PROFESSIONAL POSITIONS

- 2009-2014    **Research Assistant**, Materials Science and Engineering Department and the Center for Applied Energy Research (CAER), Lexington, KY
- 2008-2008    **Engineer's Internship**, Center for Applied Energy Research, Lexington, KY
- 2007-2007    **Technician Internship**, LKT Lehrstuhl für Kunststofftechnik (Institute of Polymer Technology), Friedrich-Alexander-Universität, Erlangen-Nürnberg

## PENDING PATENT

Thomas L. Robl, **Tristana Duvallet**, Robert Rathbone, Yongmin Zhou, "Hybrid Cement Clinker and Cement Made from that Clinker", Application No. 14180619, filed on February 14<sup>th</sup>, 2014

## PUBLICATIONS

**Tristana Duvallet**, Thomas L. Robl, “Effect of Titanium Dioxide on the System Brownmillerite-Gypsum”, under review at Cement and Concrete Research

**Tristana Duvallet**, Thomas L. Robl, Rodney Andrews, “Synthesis, characterization, hydration process and mechanical properties of iron-rich alite-calcium sulfoaluminate-ferrite cements”, following patent submission

**Tristana Duvallet**, Thomas L. Robl, Rodney Andrews, “Synthesis and Characterization of High-Iron Alite-Calcium Sulfoaluminate-Ferrite Cements produced from Industrial By-products”, following patent submission

## PRESENTATIONS

**Tristana Duvallet**, Thomas L. Robl, “Production of Alite-Calcium Sulfoaluminate-Ferrite Cements from Coal and Other Industrial By-products.” Presented at the 2013 World Of Coal Ash conference, Lexington, KY, USA, 22-25 April 2013

**Tristana Duvallet**, T. L. Robl, F. P. Glasser, “The Effect of Titanium Dioxide on the Structure and Reactivity of Ferrite.” Presented at the 8th International Conference: Concrete in the Low Carbon Era, Dundee, UK, July 2012

**Tristana Duvallet**, Robert F. Rathbone, Kevin Henke and Robert B. Jewell, “Low-energy, low CO<sub>2</sub>-emitting cements produced from coal combustion by-products and red mud.” Presented at the 2009 World Of Coal Ash conference, Lexington, Kentucky, 4-7 May 2009.